High-frequency geodetic positioning of terrestrial and maritime gnss networks

Stavros A. Melachroinos

MINISTERE DE L'ENSEIGNEMENT SUPERIEURE ET DE LA RECHERCHE

OBSERVATOIRE DE PARIS

ECOLE DOCTORALE

D'ASTRONOMIE et D'ASTROPHYSIQUE ILE DE FRANCE

DOCTORAT

ASTRONOMIE et ASTROPHYSIQUE

SPECIALITE : GEODESIE SPATIALE

Stavros A. MELACHROINOS

« POSITIONNEMENT GEODESIQUE A HAUTE FREQUENCE DE RESEAUX GNSS TERRESTRES ET MARINS »

Soutenue à l'Observatoire Midi-Pyrénées le 02 Octobre 2007 devant le jury composé de :

Daniel GAMBIS	(Observatoire de Paris)	*Président*
Urs HUGENTOBLER	(Technische Universität München)	*Rapporteur*
Ilias TZIAVOS	(Αριστοτέλειο Πανεπιστήμιο Θεσσαλονίκης) (Université d'Aristote de Thessaloniki)	*Rapporteur*
Muriel LLUBES	(Université Paul Sabatier)	*Examinatrice*
Philippe ESCUDIER	(Collecte Localisation Satellites)	*Examinateur*
Françoise DUQUENNE	(Institut Géographique National)	*Examinatrice*
Richard BIANCALE	(Centre National d'Etudes Spatiales)	*Directeur de thèse*
Mireille BOUGEARD	(Université Lyon 1)	*Directrice de thèse*
Felix PEROSANZ	(Centre National d'Etudes Spatiales)	*Invité*

MINISTERE DE L'ENSEIGNEMENT SUPERIEURE ET DE LA RECHERCHE

OBSERVATOIRE DE PARIS

ECOLE DOCTORALE

D'ASTRONOMIE et D'ASTROPHYSIQUE ILE DE FRANCE

DOCTORAT

ASTRONOMIE et ASTROPHYSIQUE

SPECIALITE : GEODESIE SPATIALE

Stavros A. MELACHROINOS

« POSITIONNEMENT GEODESIQUE A HAUTE FREQUENCE DE RESEAUX GNSS TERRESTRES ET MARINS »

Soutenue à l'Observatoire Midi-Pyrénées le 02 Octobre 2007 devant le jury composé de :

Daniel GAMBIS	(Observatoire de Paris)	*Président*
Urs HUGENTOBLER	(Technische Universität München)	*Rapporteur*
Ilias TZIAVOS	(Αριστοτέλειο Πανεπιστήμιο Θεσσαλονίκης) (Université d'Aristote de Thessaloniki)	*Rapporteur*
Muriel LLUBES	(Université Paul Sabatier)	*Examinatrice*
Philippe ESCUDIER	(Collecte Localisation Satellites)	*Examinateur*
Françoise DUQUENNE	(Institut Géographique National)	*Examinatrice*
Richard BIANCALE	(Centre National d'Etudes Spatiales)	*Directeur de thèse*
Mireille BOUGEARD	(Université Lyon 1)	*Directrice de thèse*
Felix PEROSANZ	(Centre National d'Etudes Spatiales)	*Invité*

"*To my beloved wife Marie and precious daughter Estelle, to my mother Evanthia, to my brother Alexander and to my beloved father Anthony who is not present in this world with us anymore*"

"A ma femme bien aimée, Marie, et notre fille adorée, Estelle, à ma mère Evanthia, mon frère Alexander, ainsi qu'à mon père bien aimé, Antoine, qui n'est plus parmi nous "

"*Στην αξιολάτρευτη γυναίκα της ζωής μου Μαρί, στην πολύτιμη κόρουλα μας Εστέλλα, στην υπέροχη μητέρα μου Ευανθία , στον αδελφό μου Αλέξανδρο, και στον αγαπημένο μου πατέρα Αντώνη ο οποίος δεν μπορεί να είναι πια μαζί μας σε τούτον τον κόσμο*"

Stavros A. Melachroinos

- Ingénieur Géomètre et Topographe
  de l'Ecole Polytechnique de l'Université d'Aristote de Thessaloniki

- M.Sc. (DEA) : « Dynamique des systèmes Gravitationnels »
  de l'Observatoire de Paris et de l'Ecole Doctorale d'Astronomie et d'Astrophysique
  Ile de France

- PhD (Doctorat) : « Astronomie et Astrophysique », spécialité « Géodésie Spatiale »
  de l'Observatoire de Paris et de l'Ecole Doctorale d'Astronomie et d'Astrophysique
  Ile de France

First Edition 2007-09-04
Second Edition 2007-13-11

« Positionnement Géodésique à Haute Fréquence des Réseaux GNSS Terrestres et Marins »
« High-Frequency Geodetic Positioning of Terrestrial and Maritime GNSS networks »

Groupe de Recherches de Géodésie Spatiale
Laboratoire de Dynamique Terrestre et Planétaire – UMR5562
Observatoire Midi-Pyrénées
14 Av. Edouard Belin
31400, Toulouse
France

« ως ούσις της φύσεως αρχής τινός και αιτίας του κινείσθαι και ηρεμείν »
Αριστοτέλης Φυς. 1962 20-2

Table of Contents

Supporting Publications

A number of publications have been produced while undertaking this Thesis. Wherever parts from these publications have been reproduced in this Thesis, the work is my original contribution to the publication. Joëlle Nicolas, Stéphane Durand., Laurent Morel, Marie-Noëlle Bouin and Frederic Masson are acknowledged for providing the GPS data of the Brittany ocean tide loading campaign. The publications include:

- Refereed Journal Articles

De Saint-Jean B., Verdun, J., Duquenne, H., Barriot, J.-P., **Melachroinos S.**, Cali, J., 2007, Fine analysis of lever arm effects in moving gravimetry, in International Association of Geodesy Symposia, Cairns, Australia: vol. 130, 809(8), Chris Rizos (Ed.), Springer – Verlag Berlin Heidelberg.

Melachroinos S. A., Biancale, R., Llubes, M., Perosanz F., Lyard F., Vergnolle M., Bouin M.-N., Masson F., Nicolas J., Morel L., Durand S., 2007, Ocean tide loading (OTL) displacements from global and local grids : comparisons to GPS estimates over the shelf of Brittany, France, in Journal of Geodesy, doi: 10.1007/s00190-007-0185-6

Vergnolle, M., Bouin, M-N., Morel, L., Masson, F., Durand, S., Nicolas, J., **Melachroinos S.**, 2007, GPS estimates of ocean tide loading constituents and comparison with a recent ocean tide model, in Journal of Geophysical Research (in press)

- Books

Melachroinos S., 2004, The development of a strapdown system with GPS and accelerometers for moving gravimetry (in French), M.Sc. Thesis, ed. Observatoire de Paris, Paris, France

- Published Proceedings

Melachroinos S., Biancale, R., Perosanz, F., 2006a, Ocean loading effects in a high time resolution GPS analysis: Implications and artefacts with GINS software, International Global Navigation Satellite Service (IGS) Workshop proceedings, ESA European operation space center, Darmstadt, Germany.

Melachroinos S. A., Deleflie, F., Perosanz F., Biancale R., Laurain O., Exertier P., 2007a, Galileo In Orbit Validation Element-A and GPS-35/36 satellite orbits: analysis of dynamical properties based on SLR-only tracking data, 15th International Laser Ranging Workshop proceedings, Canberra, Australia.

- International Congress presentations

Biancale R., J.-M. Lemoine., **S. Melachroinos**, S. Loyer, 2006, Assessing the impact of the time-variable part of the global gravity field model EIGEN-CGL04C on Jason-1 orbit quality, Ocean Surface Topography Science Team (OSTST) meeting, Venice, Italy. (Oral Presentation)

De Saint-Jean B., **Melachroinos S.**, Verdun, J., Duquenne, H., Cali, J., Barriot, J.-P., 2005, Fine analysis of lever arm effects in moving gravimetry, EGU Vienna, Austria (Poster)

Fazilova D., Perosanz F., Ramillien , G., Cretaux, J.F., **Melachroinos S.**, Soudarin, L., 2006, Time variable vertical displacements compared from GRACE gravity models, GPS, DORIS and hydrological models, International GNSS Service workshop, Darmstadt, Germany. (Poster)

Fazilova D., Perosanz F., Ramillien G., Cretaux J.F., **Melachroinos S.**, Soudarin, L., 2006, Time-variable vertical deformations determined from GRACE and in-situ GPS data, European Geosciences Union , Vienna, Austria. (Poster)

J Cali, B. De Saint-Jean, H. Duquenne, J. Verdun, **S. Melachroinos**, J-P. Barriot, 2005, A new strapdown system for moving gravimetry, American Geosciences Union Fall Meeting, San Francisco, USA (Oral Presentation)

J. Nicolas, L. Morel, M.-N. Bouin , S. Durand , F. Masson , **S. Melachroinos** , M. Vergnolle, 2006, GPS analysis software effects on geodynamical application: Case study on ocean loading in Brittany, NW France, COSPAR meeting, Beijing, China. (Poster)

J. Nicolas, **S. A. Melachroinos**, L. Morel, M. Vergnolle, M.-N. Bouin, S. Durand, F. Masson, 2006, GPS analysis software effects on geodynamical application: Case study on ocean loading in Brittany, NW France, American Geosciences Union Fall meeting, San Francisco, USA. (Oral Presentation)

Melachroinos S. A., Biancale R., Llubes M., Perosanz F. , Lemoine, J , Loyer, S., 2006b, Diurnal, semi-diurnal, third, fourth and sixth diurnal ocean tide loading signals in Brittany, France: modelled and un-modelled displacements by GPS., American Geosciences Union Fall meeting, San Francisco, USA. (Poster)

Melachroinos S. A., Biancale, R., Sundaramoorthy, P. P., Faillot, M., Menard, Y., Perosanz, F., 2007c, Validation of the Jason-1 altimetric data based on kinematic GPS sea level measurements during the DRAKE passage, EGU general assembly, Vienna, Austria. (Poster)

Melachroinos S. A., Llubes M, Biancale, R., Lyard, F., Perosanz, F., Vergnolle, M., Nicolas, J., Bouin, M-N, Morel, L., Durand, S., Masson, F., 2007d, Ocean tide loading (OTL) displacements from global and local grids: comparison to GPS estimates, EGU general assembly, Vienna, Austria. (Oral Presentation)

Melachroinos S. A., Perosanz, F., Biancale, R., 2007b, GIOVE-A orbit determination and analysis of dynamical properties based on SLR tracking data, EGU general assembly, Vienna, Austria. (Poster)

Melachroinos S. A., Sundaramoorthy P., Faillot M., Menard Y., Biancale R., Provost C., 2007a, Validation of the Jason-1 altimetric data based on kinematic GPS sea level measurements during the DRAKE passage, Part 1: Calibration of the Floating line of the research vessel POLARSTERN and GPS-buoy water level measurements inside the Port of Puntas Arenas, Chile, Ocean Surface Topography Science Team (OSTST) meeting, Hobart 12-15 March, Australia. (Poster)

Perosanz F., **Melachroinos S.**, Rekhis S., Loyer S., Biancale R., 2007, PPP vs Double-Difference positioning: first results of the GINS CNES/GRGS software, IUGG XXIV Perugia, GS004 Positioning and Applications. (Poster)

Vergnolle, M., M.-N. Bouin, **S. Melachroinos**, L. Morel, S. Durand, J. Nicolas, F. Masson, 2006, GPS multi-software analysis applied to 3D ocean loading effects in NW France, Journées Luxembourgeoises de la Géodynamique, JLG93, Luxembourg.(Oral presentation)

Acknowledgments

Usually some words are not enough for all the people to be thanked for contributing both professionally and personally during this Thesis.

Firstly I sincerely thank Richard Biancale for his supervision, guidance and friendship that he so generously offered me through the last three years. I specially thank him for the trust that he demonstrated to me and which I will always honour.

Felix Perosanz and Sylvain Loyer also deserve special thanks for their time in showing me the basic functionalities of GINS GNSS software. I thank Felix for sharing his knowledge on GNSS as being the pioneer of GPS implementation in GINS software.

I would like to thank Muriel Llubes who so kindly explained to me the complexity of ocean tide loading predictions and for sharing her algorithms.

Especially I would like to thank Jean Michel Lemoine for his kindness and friendly advices on normal equations and people's moods and attitudes.

Sean Bruinsma is also thanked for his kind contribution in correcting my idiomatic English mistakes.

I will never forget as well the warming welcoming of Nicole Lestieu who did not stop offering us delicious house made marmalades for breakfast.

Before, giving my final acknowledgments I would like to thank as well all my Greek family, Lena, "giagia", "thia" Kaiti and cousins for the unstoppable encouragement during this difficult road. I specially thank my grandmother "giagia" for her infinite wisdom, simplicity and patience that she taught me in life and who I always have in mind when I loose my patience. Many thanks go as well to the French part of my family and especially Jean-Michel and Monique Fromion, Jean and Brigitte Fromion, Anne and Thierry Leveque and many more who were always there to support us when needed.

Finally, and as said in the cover and repeated again, I would like to express my endless love to Marie for her patience and efforts that this period represented for her and our daughter. I promise her that long waiting hours and difficult moments belong in the past and that I am looking forward for our new adventures together all three of us.

List of Figures

List of Tables

Résumé

L'équipe géodésique du GRGS, du Centre National d'Etudes Spatiales, a saisi l'importance des systèmes GNSS sur la détermination du système international de référence terrestre et la détermination des paramètres des mouvements du Pôle via le projet pilote des Centres de Recherche et des Combinaisons (CRC) de l'IERS.

L'observation des déformations surfaciques de la croûte Terrestre mesurée par des stations permanentes GNSS est un sujet que le CNES/GRGS voulait investiguer. L'impact de tels types de déformations sur les applications scientifiques de la géodésie de très haute précision ne peut plus être négligé comme c'est déjà mentionné dans les conventions de l'IERS pour 2003. En parallèle les besoins en océanographie et en altimétrie pour des mesures indépendantes de variations du niveau des océans, ainsi que leurs validations et comparaisons croisées à partir des traceurs flottants sur des bouées et des bateaux ou des marégraphes co-localisées avec des stations permanents GPS, ont imposé l'utilisation des récepteurs du système GNSS.

Dans une première partie de la thèse, je présente une recherche bibliographique sur les caractéristiques principales de quatre systèmes du positionnement global par satellites et qui constitueront le futur système global des systèmes de navigation. Les bénéfices et les complexités des futures combinaisons des multiples observables de phase et de code sont appréhendés.

Dans une deuxième partie de la thèse, je me concentre sur la définition des composantes géodésiques utilisées pour le positionnement par GNSS. Les modèles observationnels et les plus récentes évolutions en matière de précision et d'exactitude des GNSS qui ont occupé mes recherches pendant mon projet, sont simultanément présentés. Les erreurs dues à des effets systématiques qui perturbent la précision sur la détermination des positions des stations sont estimées. Ces effets se trouvent soit au niveau du prétraitement des mesures, soit en provenance des délais exercés sur la propagation des signaux, soit dues aux déplacements de la croûte terrestre sur laquelle se positionnent les stations.

Dans une troisième partie de la thèse, je présente tout d'abord le logiciel scientifique GINS qui a constitué l'outil principal de mes études ainsi que les modifications que j'ai apportées. Je présente ensuite, les différents tests de validations que j'ai effectuées pour

évaluer les modifications tells que : les comparaisons sur les positions des stations à des séries temporelles de haute fréquence avec des résultats en provenance des logiciels globalement connus dans la communauté géodésique ; les comparaisons d'orbite GINS GNSS par rapport aux orbites précises de l'IGS pour valider des nouveaux modèles de radiation de pression solaire implémentés pour les satellites GPS comme le modèle « Box-and-Wing » ; puis pour préparer les premiers pas vers l'exploitation scientifique de Galileo, l'évaluation sur la précision de l'orbite du premier satellite du système de navigation européen GIOVE-A.

Dans une quatrième partie, l'étude principale sur les paramètres de la surcharge océanique dans des régions côtières complexes, comme en Bretagne, est présentée. Les modifications récentes et validées dans la troisième partie pour le positionnement par GNSS dans GINS, sont utilisées. La méthode implémentée a pour but d'utiliser une campagne GPS destinée à évaluer/valider les modèles de marées dans la région. L'impact des déplacements verticaux non modélisés des stations géodésiques sur les paramètres troposphériques est quantifié. D'ailleurs, la stabilité du datum (système de référence) utilisé pour l'alignement des solutions GNSS sur le système de référence terrestre et ses influences sur les séries temporelles finales des coordonnées des stations sont examinées. Les effets du repliement du spectre sur des séries temporelles des stations dues aux mouvements verticaux mal or non modélisés sont démontrés. Finalement, les performances de sept modèles globaux et régionaux de marées et les différences des deux logiciels utilisés pour les prédictions des mouvements dus à la surcharge océanique, dans la région, sont quantifiées.

Dans la cinquième partie j'analyse les observations des données cinématique d'une campagne GPS dans l'océan Antarctique abord des bouées et un bateau de recherche pendant le passage du DRAKE au sud de Chili. La campagne DRAKE a été dédiée à comparer et valider les observations altimétriques et océanographiques pour l'étude du courant circumpolaire Antarctique. Les résultats sont préliminaires et se concentrent plutôt sur la définition de la ligne de flottaison du bateau par l'utilisation combiné GPS – bateau – bouées. Les perspectives et la planification pour la continuation du projet en Post-Doc sont présentées.

Summary

The impact of GNSS in the realization of the International Terrestrial Reference Frame (ITRF) and the determination of the Earth's Pole motion was seized by the geodetic team of GRGS of the French Space Agency (CNES) throughout the Centres de Recherche et des Combinaisons (CRC) IERS project.

The measurement of surface deformations sensed by permanent GNSS stations is a subject that the CNES/GRGS team wanted to investigate thoroughly. As already noted in the IERS 2003 conventions, the impact of these deformations in today's scientific applications of geodesy of high precision cannot any longer be neglected. In parallel the needs of oceanography and altimetry for independent measurements of the sea level variations by validation and cross comparison, have made the use of GNSS receivers on floating tracers (buoys, ships) or permanent GPS stations collocated with tide gauge sites, more than necessary.

In the first part of this PhD I present a bibliographic research on the main characteristics and differences of four global positioning systems that will constitute the future Global Navigation Satellite System of Systems. The benefits and complexities of future combinations from a multiple of carrier phases and code observables are presented.

In the second part, I concentrate in the definition of the basic geodetic components of GNSS used in positioning. Observational models and the most recent issues of GNSS accuracy and precision and which have occupied my research during the last time are simultaneously presented for real cases. An updated error budget of the systematic effects perturbing the accuracy and precision of the determination of position of the geodetic stations at the pre-processing level, from signal delay's and stations' displacements due to the movements of the Earth's crust are examined.

In the third part, the GINS' scientific software package the basic tool used in this PhD study is presented. Updated modifications implemented for the needs of my research are overseen. Then, validations through inter-comparisons with other well-known in the geodetic community software and through comparisons to the precise IGS sp3 orbits on the level of precise orbit determination for the GPS constellation are presented. Furthermore, a first-step implementation for the integration of the future Galileo GNSS system is evaluated.

In the fourth part, the main study of ocean loading parameters in a complex coastal area that of Brittany, in France is presented. The recently validated modifications in matters

of positioning inside GINS GNSS software are used. The implemented method aims to use a dedicated GPS campaign in the area in order to evaluate/validate the performances of ocean tide models. The impact of un-modeled vertical displacements of the geodetic stations on tropospheric parameters is quantified. Moreover, the datum stability used to align the GNSS solution to a terrestrial reference system and its impacts on the final coordinate times-series are examined. Low frequency aliasing affects in the campaign stations' time-series of unmodeled vertical displacement due to ocean tide loading are demonstrated. Finally, the performances of seven global and regional tide models and the differences between two algorithms for ocean tide loading predictions are quantified.

Finally, in the fifth and last part of my PhD dissertation, I analyze GPS kinematic data sets from a dedicated campaign (buoy and ship) in the DRAKE passage south of Chile designated to cross compare and validate altimetric and oceanographic observations and their products for the observation of the Antarctic Circumpolar Current. The results are preliminary and concern only two calibration periods for the definition of the vessel's floating line through the use of GPS-buoys. The perspectives and the planning for the future continuation on this project are presented.

Introduction

a) The Problem

According to Euclid, the geometrical distance of a point with respect to another reference point is:

$$\rho_R^S = \sqrt{\left[\mathrm{x}^S(t) - \mathrm{x}^R(t)\right]^T \left[\mathrm{x}^S(t) - \mathrm{x}^R(t)\right]} \qquad \textbf{Eq. 1}$$

Where: $\mathrm{x}^S(t)$ is the 3D coordinate vector of the point S at the time *t*; $\mathrm{x}^R(t)$ is the 3D coordinate vector of the reference point R at the time *t*. The observed distance between these points will help us determine the coordinates of the one with respect to the other in time and in space. The exact and precise knowledge of their coordinates at the mm and sub-mm level is mandatory in today's scientific applications of space geodesy.

For example, in the *International Earth Rotation Service* (IERS) standards it is mentioned that the coordinates of geodetic points attached to the solid surface are used for the realization of a *Terrestrial Reference System* (TRS) and the determination of the *Earth Orientation Parameters* (EOPs). This system is a spatial reference system co-rotating with the Earth in its diurnal motion in space. A *Terrestrial Reference Frame* (TRF) is a set of physical points with precisely determined coordinates in a specific coordinate system (IERS 2003). The connection of the TRS to the *Celestial Reference System* (CRS) is accomplished through the EOPs. The EOPs are a by-product of the positioning of a set of reference points on the Earth's surface that participate in its daily rotation, polar motion and annual revolution around the sun.

Precise point positions are also important in interdisciplinary oceanographic-geodetic-geophysical applications such as: altimeter in-situ calibration methods, determination of the dynamic topography of the sea, ocean tide model validations, tectonics, volcanology etc.

In all cases, the exact determination of the position state parameters is a problem of determining the 3D coordinates of a geodetic point on the surface of the Earth, which is subject to several types of displacements due to:

- Ocean loading (tidal and non-tidal part) ;

- Atmospheric Loading (tidal and non-tidal part) ;
- Loading caused from surface and sub-surface hydrological variations ;
- Post Glacial Rebound ;
- Effects of the Solid Earth Tides (permanent and time dependent) ;
- Rotational deformation due to Polar Motion (Pole tides) ;
- monument deformations (thermal expansions etc.).

In practice the methods used for determining the 3D positions of geodetic points, vary significantly in function with:

- the physical environment (atmospheric conditions, multi-path etc.);
- the positioning mode : static/kinematic, real-time/post-processed ;
- the method and the techniques used (SLR, GPS, DORIS, VLBI) ;
- the observational models ;

b) The context

The definition of the position of a moving target or a stable geodetic point on the surface of the Earth has been troubling geodesists since the very beginning of the Greek civilization. One of the classical methods used was the measurements of angles and distances combined with astronomical observations. The first of these measurements was done by Eratosthenes in 230 BC. He introduced the first estimation of the Earth's radius by simultaneously comparing the time of the sun's zenith during the summer solstice at local noon in the town of Syene on the Tropic of Cancer, and the time where the angle of elevation of the Sun would be 1/50 of a full circle (7°12') south of the zenith at his hometown of Alexandria. Assuming that Alexandria was due north of Syene he concluded that the distance from Alexandria to Syene must be 1/50 of the total circumference of the Earth. His estimated distance between the cities was 5000 stadia (1 stadio = 185.2 m). He rounded the result to a final value of 700 stadia per degree, which implies a circumference of 252,000 stadia. The estimated Earth's radius was calculated at 7427824.8 m 16 % too large. If Eratosthenes has used as a unit the Alexandia's stadion (158.3 m) the estimation of the Earth's radius comes to 6348945 m 0.3 % smaller. Albeit their long age and history, part of these methods are still being used nowadays.

In the early 60's with the apparition of the first radio technique such as the Transit/NNSS (*Navy Navigation Satellite System*) we have entered the era of a new

revolution in positioning applications. The principal of this system was based on measuring the Doppler effect of a moving target with respect to a stable station in order to measure the relative velocity. The Doppler technique was also developed in the 80's by the *Centre National des Etudes Spatiales* (CNES, FR) with the DORIS (*Doppler Orbitography by Radio-positioning Integrated on Satellite*) system (**Fig. 1-1**).

Fig. 1-1 : DORIS: the French space geodesy system. How does it work? Courtesy CLS (available at http://www.cls.fr/html/doris/principe_fr.html)

Measuring distances and determining coordinates has also been possible by the use of laser technology. One of the first ranging measurements has been made to the satellites BE-B (October 10 1964) of the Goddard Space Flight Centre (GSFC) with a precision of 30m, DIAPASON D-1A (February 17 1966) and DIADEM-1C and 1D (February 8 and 15 1967) of the French National Space Centre CNES, (Biancale 1997). This was the beginning of the so called *Satellite Laser Ranging* (SLR) technique. *Lunar Laser Ranging* (LLR) from powerful telescopes on the surface of the Earth became also possible, by the use of laser retro reflectors placed on the moon's surface during the first Apollo (July 11 1969, February 14 1971 and August 15 1971, USA) and Luna (November 17 1970, January 21 1973, USSR) missions. Today SLR technique is widely used for the determination of the TRF's scale, the motion of the centre of mass of the Earth system and in the *Precise Orbit Determination* (POD) of *Medium and Low Earth Orbiters* (MEO and LEO) such as:

- the STELLA, Starlette and LAGEOS satellites used for the measure of the secular perturbations of J_2 ;
- the altimetric satellites like Topex/Poseidon, Jason, Envisat, ERS, GFO etc. ;
- the GRACE satellites used for the determination of the gravity field ;

- the GPS 35 and GPS 36 satellites of the Global Positioning System (GPS);
- the first *Galileo In Orbit Validation Element* (GIOVE-A).

In 1978 the *Department of Defense* (DoD) of the United States of America has launched GPS the first Global radio-positioning system in order to replace the old and limited in coverage Transit system. Its principle is based on calculating the distances between MEO satellites, and a receiver on the Earth's surface by comparing the departure and arrival time of a radio signal. Nowadays GPS is vastly used for the determination of 3-dimentional coordinates of geodetic stations. Together with GPS the Russian *Global Navigation Satellite System* (GLONASS) is also operating. The later is based on the same principle as GPS. On the other hand, the European Community is developing its own global positioning system, Galileo, which will be fully operational by 2012. Recently the Chinese government has decided to enter the game of "public" global positioning by building its own navigation satellite system Compass/Beidou. Together all four systems form of what we call as the Global Navigation Satellite System, commonly GNSS.

The impact of GNSS on the way we determine coordinates on the Earth's surface is considerable compared to other techniques.

Inside these recent evolutions in matters of high precision positioning, the GRGS team of CNES is developing over 30 years the scientific software GINS (*Géodésie par Integrations Numériques Simultanées*). The main functions of this software are designated to problems of the adjustment and combination of data sets coming from all techniques of space geodesy like GPS, DORIS, SLR, VLBI, SLR, LLR, altimetry etc.

GNSS have gained large popularity in the domain of geodetic sciences. The exploitation and use of their data sets offers significant advantages with respect to the other space geodesy techniques such as:

- high density of observations (every receiver can simultaneously observe up to 10 satellites from a single GNSS, and even more satellites in the case of Galileo, GLONASS and Compass) ;
- continuous tracking measurements for LEO satellites ;
- extreme precision, rapidity, and low cost ;
- easy to set up ;

The scientific "GNSS activity" of the CNES/GRGS team is regrouped around three axes:

1. POD of LEO satellites (TOPEX/POSEIDON, JASON-1, ENVISAT etc.) and the determination of the gravity field from CHAMP, GRACE and GOCE ;
2. POD of MEO satellites (GPS, GIOVE-A, Galileo) and global Earth kinematic study. GRGS participates in a pilot project coordinated by the IERS called *Centres de Recherche et de Combinaison* (CRC) ;
3. Deformations of local geodetic networks observed by GNSS and kinematic positioning of floating tracers (this Thesis);

These directions are coherent with the motivations of GRGS to propose the use of GINS at laboratories around the world as an alternative to already well established scientific software such as:

- Bernese GPS software (Astronomical Institute and University of Berne, Switzerland) ;
- GAMIT/GLOBK (Massachusetts Institute of Technology/ USA) ;
- GIPSY/OASIS (Jet Propulsion Laboratory / USA) ;

c) The subject

Since the beginning of its GNSS activities the team of GRGS/CNES had invested in the research and algorithmic/software development concepts designated to problems of POD and determination of the gravity field modeling (GRIM and EIGEN gravity models series). In parallel the impact of GNSS in the realization of the *International Terrestrial Reference Frame* (ITRF) and the determination of the Earth's Pole motion was seized by GRGS through the CRC project (Biancale et al. 2007).

The geodetic software package GINS used by GRGS and unique in France, initially was not adapted for the studies of positioning and the deformations of dense geodetic networks by GNSS. The measurement of surface deformations sensed by GNSS stations is a subject that the GRGS team wants to investigate thoroughly. As already noted in the IERS 2003 conventions (McCarthy and Petit 2004), the impact of these deformations in today's geodetic applications of high precision cannot be neglected any longer. The physical causes of these crustal deformations are numerous and their time scale varies considerably. In parallel the needs of oceanography and altimetry for independent measurements of the sea surface topography by validation and cross comparison, have made the use of GNSS receivers on floating tracers (buoys, ships) more than necessary.

So, under these conditions, and for the preparation of the future European GNSS positioning system Galileo, as well, one of my missions during my PhD, was to introduce all the necessary modifications in the software and then perform high precision millimeter positioning of geodetic terrestrial and maritime GNSS networks designated to the study of geophysical deformations and the observations of the mean sea-level.

I have organized the development of this PhD project around 4 axes: 1) Initially, I had to adjust myself in the logic and the complex treatment of GPS data by the use of other scientific GPS software. For that I firstly used the GAMIT/GLOBK software package of MIT. Then for reasons of comprehension and acquisition of experience with GPS processing I studied the long term motion of GPS stations in tectonically active (Crete) and non-active regions (S-W France) and the impact on the final coordinate time-series from different strategies combinations.

2) Secondly, I concentrated in problems of POD and notably that of the impact of solar radiation pressure parameters on the GPS satellites orbits and the use of SLR for the POD of the first GIOVE-A satellite including the implementation of a box-and-wing solar radiation pressure model.

3) Thirdly, I dealt with the study of ocean tide loading parameters and the validation of tide models by the use of a dedicated GNSS campaign, in a complex coastal area, that of Brittany, in France. This part was divided into three steps. The first was dedicated to the GINS' software modifications:

- Ambiguity resolution;
- Troposphere modeling;
- Algorithmic modifications;
- New processing strategies.

The second, was the validation of GINS' results through comparisons to other software and notably GAMIT 10.21 (King and Bock 2005), GIPSY/OASIS II (Zumberge et al. 1997) and Bernese 5.0 (Dach et al. 2007) and which was treated together with the participation of several French research teams. The last part was assigned to the scientific evaluation and tide models' validation by comparisons to the estimated GPS ocean tide loading constituents in the diurnal, semi-diurnal, third, fourth, fifth and sixth-diurnal spectral bands.

4) And finally, I have processed the GPS kinematic data from a dedicated campaign (buoy and Ship) in the DRAKE passage south of Chile for the cross comparison and

calibration of altimetric and oceanographic parameters in the area. Part of this work is still in progress and the continuation should be assured hopefully by a Post-Doc grant.

d) This Thesis

A technical and historical description of all existing and future GNSS systems is given in the first chapter of this manuscript.

In the second part the geodetic components of GNSS are sub-divided into four categories: a) The terrestrial reference frame, b) the geodetic GNSS networks, c) the GNSS observational models and errors, d) the GNSS station displacements.

In the third part a general presentation of the GNSS capacities inside GINS software together with the recent modifications are presented. Validation tests of these new functionalities, through intra-software differences on the estimated time-series of geodetic stations and through POD of the GPS satellites compared to external references, are presented in the same chapter.

In the fourth part, the study of observed and predicted ocean tide loading displacements and their validations through a new dedicated GPS campaign in Brittany and Contentin at the northwestern part of France, is presented.

The fifth chapter is dedicated to the preliminary results of a GPS kinematic campaign applied to the study of the Antarctic Circumpolar Current.

Last but not least, the conclusions of my studies during this PhD and the perspectives for further research continuation are given in the sixth chapter.

« Τον άντρα τον πολύπραγο τραγούδησέ μου, ω Μούσα, που περισσά πλανήθηκε, σαν κούρσεψε τής Τροίας το ιερό κάστρο, και πολλών ανθρώπων είδε χώρες κι έμαθε γνώμες, και πολλά στα πέλαα βρήκε πάθια, για μία ζωή παλεύοντας και γυρισμό συντρόφων »

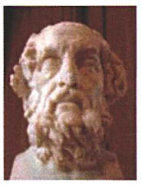
Homère

1 The GNSS System of Systems

If Ulysses had a GNSS receiver in his disposal would have he found an easier way to Ithaca?

In this chapter a description of the characteristics of GPS, Galileo, GLONASS and Compass-Beidou systems is given. GPS is currently fully developed. Galileo is at its first steps of implementation. In 2006 the first test-bed satellite of the constellation, GIOVE-A, has been launched. GLONASS is under a modernization phase. Compass, which will be the future Chinese global positioning system, is also under way and a first satellite has been placed in a MEO in April 2007. Problems, related to the interoperability and compatibility between GNSS systems, are also presented.

1.1 The GNSSes of today

Today, Russia hopes to return GLONASS to *Full Operation Capability* (FOC) with a completed constellation by 2009, and Galileo's FOC is expected now for 2012 (Hein et al. 2007). Compass-Beidou is already on the move with its successful launch on April, 14, 2007. A scenario of four global coverage satellite systems seems to be very likely in the near future.

With this increasing number of GNSS matters of interoperability come to the surface. For example, Galileo has managed to deal with problems of interoperability with its predecessor GPS, in a more successful way than GLONASS. That is because the latest system had and still has substantial differences from GPS. Nevertheless the working groups of GPS/GLONASS are working intensively towards a future interoperability of the two systems. The addition of *Code Division Multiple Access* (CDMA) signals on the third frequency and at L1 of the modernized GLONASS system will set the steps towards an easier interoperability with the other GNSS. At its present state, the Russian system employs *Frequency Division Multiple Access* (FDMA) technology in which a common code is broadcast on different *Reference Frequency* (RF) bands, unlike GPS and Galileo that use the CDMA signals that transmit different codes on the same frequency. The Compass system will be using CDMA signals thus rendering the interoperability easier with other GNSS.

1.1.1 The interoperability and compatibility of GNSSes

The new U. S. Space-Based *Positioning, Navigation and Timing* (PNT) Policy signed in December 2004, addresses the global compatibility and interoperability of future systems with GPS.

But what does the word interoperability and compatibility of GNSS mean? According to the new PNT policy (available at http://pnt.gov/policy/):

- *Compatibility* refers to the ability of U.S. and foreign space-based PNT services to be used separately or together without interfering with each other service or signals and without adversely affecting navigation warfare.
- *Interoperability* refers to the ability of civil U.S. and foreign space-based PNT services to be used together to provide better capabilities at the user level than would be achieved by relying solely on one service or signal.

The previously mentioned model to compute the level of interference is set up in the 2004 EU-US agreement.

The general term of interoperability splits into : *system interoperability* – where different GNSS provide the same answer, within the specified accuracy of each individual system, and *signal interoperability* – in which different GNSS transmit signals allowing their successful combination inside a receiver or a combined solution.

1.1.1.1 Interoperability of GPS, Galileo and GLONASS

The present signal interoperability between GPS and Galileo is unique with respect to the other two GNSS (GLONASS and Compass). In order to ensure combined use of the two systems with the highest performance possible at the user level the following requirements were considered:

- *Signals-in-Space* (SIS). Different frequencies may introduce frequency biases. Common center frequencies are needed for combined processing of observations.
- *Coordinate reference system*. Today the GPS coordinate reference system is the WGS84 and is realized by the coordinates of the GPS control stations. Differences between GPS and ITRF amount to less than two centimeters. The present goal for Galileo is to realize within less than three centimeters with respect to ITRF a *Galileo Terrestrial Reference Frame* (GTRF). This ensures independence of both GPS and Galileo systems. For the GLONASS more information is given in **§ 1.1.4.5**.
- *Time reference frame*. The *Galileo System Time* (GST), the GPS time and the GLONASS time will be different real-time realizations of the *Universal Time Coordinated* (UTC) / *Atomic Time* (TAI). The GPS – Galileo time offset will be easily determined and received at the user's level.

Moreover GLONASS is not *signal interoperable* with GPS and Galileo but mostly is *system interoperable*. More description on GST and GTRF is presented in **§ 1.1.3.4** and **§1.1.3.5**.

1.1.2 The Global Positioning System, GPS

GPS is based on a network of initially 24 active satellites placed into orbit by the US *Department of Defense* (DoD). The GPS baseline constellation of 24 satellites consists of six quasi-circular MEO planes at a nominal average orbit semi-major axis of 26559.7 km with an inclination of the orbital plane of 55 degrees with reference to the equatorial plane.

1.1.2.1 The development phase

GPS is an active program over 30 years. The history of its development phase till full operational capability is summarized in the following synopsis (Hothem 2006):

- In 1973 started the development which is an underway of separate programs;
- In 1978 the first satellites were developed and launched;
- The first operational satellites went into orbit in 1989;
- The system reached *Initial Operational Capability* (IOC) in 1993;
- And obtained FOC in 1995.

The system actually exceeds the baseline constellation with 31 orbiting satellites after the last successful launch on November 17 2006.

1.1.2.2 The modernization Plan

The current constellation of GPS satellites consists of:

- 16 II/IIA operational satellites;
- 12 IIR satellites, modernizing up to 8 Block IIR satellites ;
- 3 IIR-M satellites launched on September 25 2005, September 14 2006 and November 17 2006.

Before December 2005 the *Standard Positioning Service* (SPS) was provided by the C/A code on the L1 frequency and the *Precise Positioning Service* (PPS) provided by the P(Y)-code on L1 and L2 (**Fig. 1-1**).

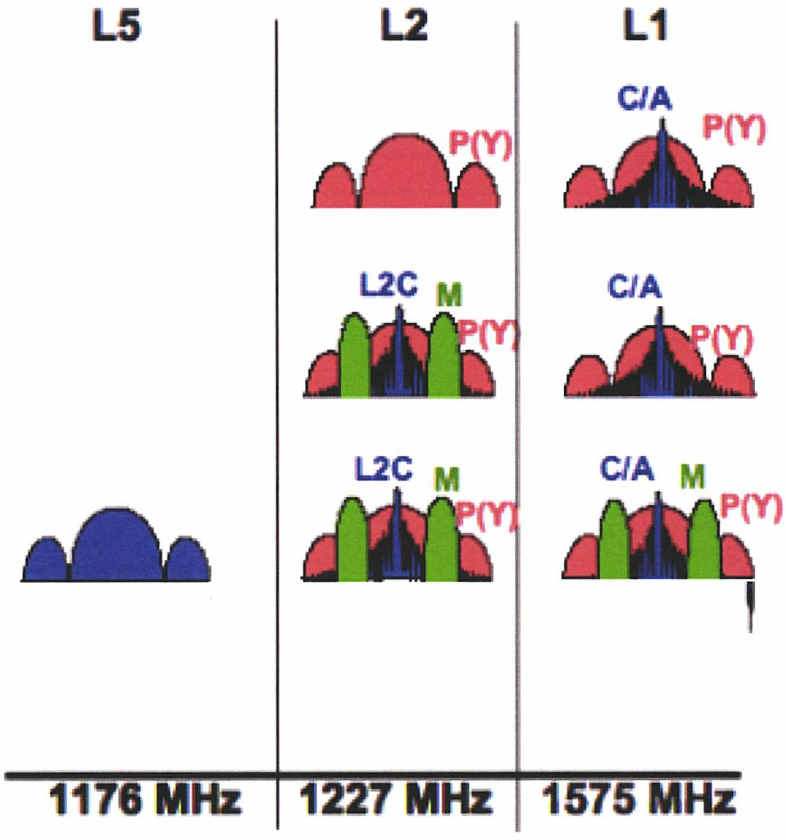

Fig. 1-1 : The GPS Signal Spectrum, present and future. (Source CNES)

1.1.2.2.1 Block IIR-M

Since the launch of the first IIR-M satellites, a second civil signal was introduced with improved services (L2C). This generation is about to reach the 24-satellite FOC around 2012 (Hein et al. 2007). For military purposes a modernized M-code will be placed on both L1 and L2. The second civil signal L2C may enable higher civilian accuracy when combined with the existing civil GPS signal L1 (C/A). L2C overcomes some limitations of L1(C/A) such as:

- Higher effective power ;
- Improved data structure ;
- It will have reduced interference and it will enable indoor use.

1.1.2.2.2 Block IIF

The third civil signal L5 (**Fig. 1-1**) will be present in the future IIF satellites. The FOC with 24 satellites is expected to be complete around 2015. The first launch of this generation is scheduled for 2008. The third civil signal L5 will have:

- New enhanced performance with higher power (higher than other GPS civil signals);
- Wider bandwidth (1176.45 MHz +/- 10 MHz) which enables more accurate tracking ability ;
- Improved resistance to narrow bandwidth interference ;
- A frequency located in an *Aeronautical Radio Navigation Service* (ARNS) band. An ARNS band has the advantage of limiting the in-band interference environment because it is regulated by stringent aviation requirements.

1.1.2.2.3 Block III

The GPS Block III phase is still under design stage. It includes significant improvements both in the ground and space segment. This will most likely include:

- Assured and improved level of integrity;
- Improved availability of accuracy with integrity;
- Backward compatibility with existing receivers;
- Support for new signals in combination with IIR-M & IIF satellites
    - L2C, L5, M-code;
    - L1C and future options for new navigation messages, flexible power levels;

The first launch is previewed for around 2013 (Hothem 2006). The new improved L1C civil signal will exist in addition to the C/A code in order to ensure backward compatibility with older receivers. During the 2006 and 2004 joint statement agreement between EU & US in matters of GNSS cooperation, L1 band was optimized as the common baseline open service signal for GPS & Galileo. The FOC of the Block III phase is expected around 2020.

The L1C will have a *pilot carrier*, which, as in the case of Galileo's L1 band, helps for better code and carrier tracking.

A preview of the four GPS satellites generations is shown in the following **Fig. 1-2**.

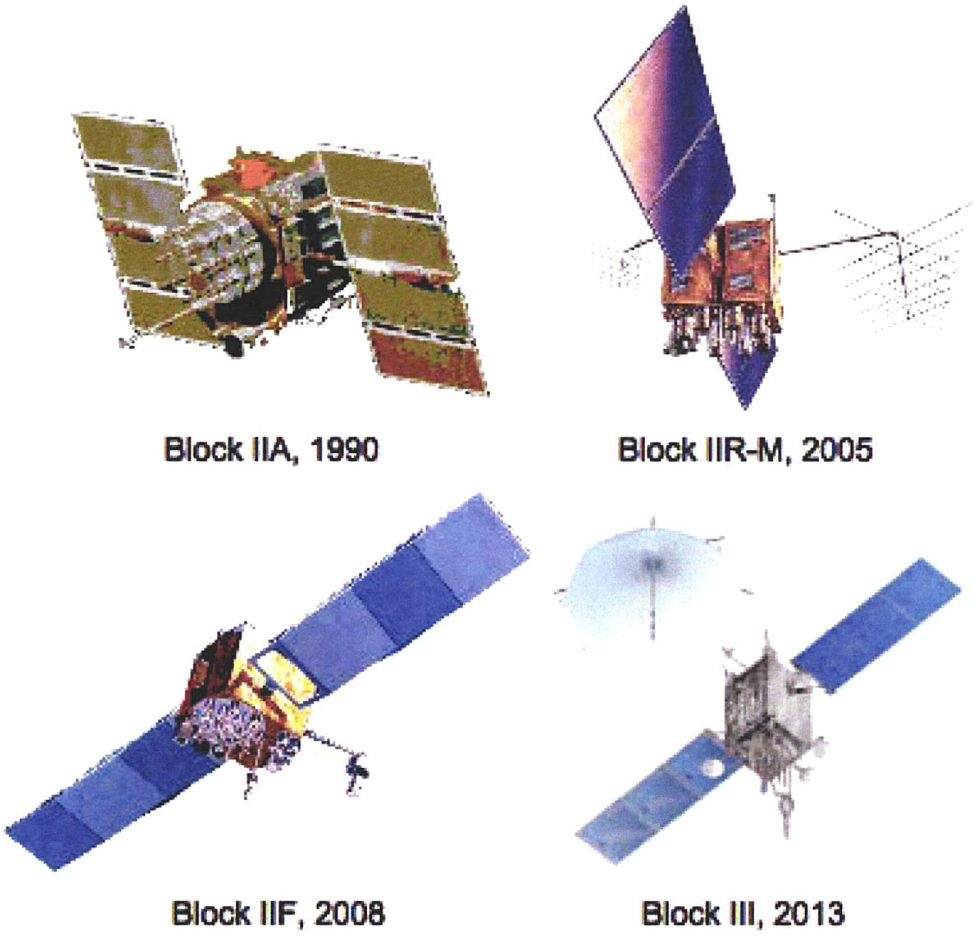

Fig. 1-2 : The GPS satellite generation, past, present and future. (Source US Department of State, DoS)

1.1.2.3 The GPS Control Segment

Currently the operational capability of the GPS control segment counts a total of 14 globally distributed stations. During the improvement plan a total of 4 more control sites is envisaged (**Fig. 1-3**). The modernization of the *Operational Control Segment* (OCS) has as goals:

- Each *Satellite Vehicle* (SV) will be tracked at least by three or more monitor stations over 99% of the time;
- The *User Range Error* (URE) will be around 1.0 m;

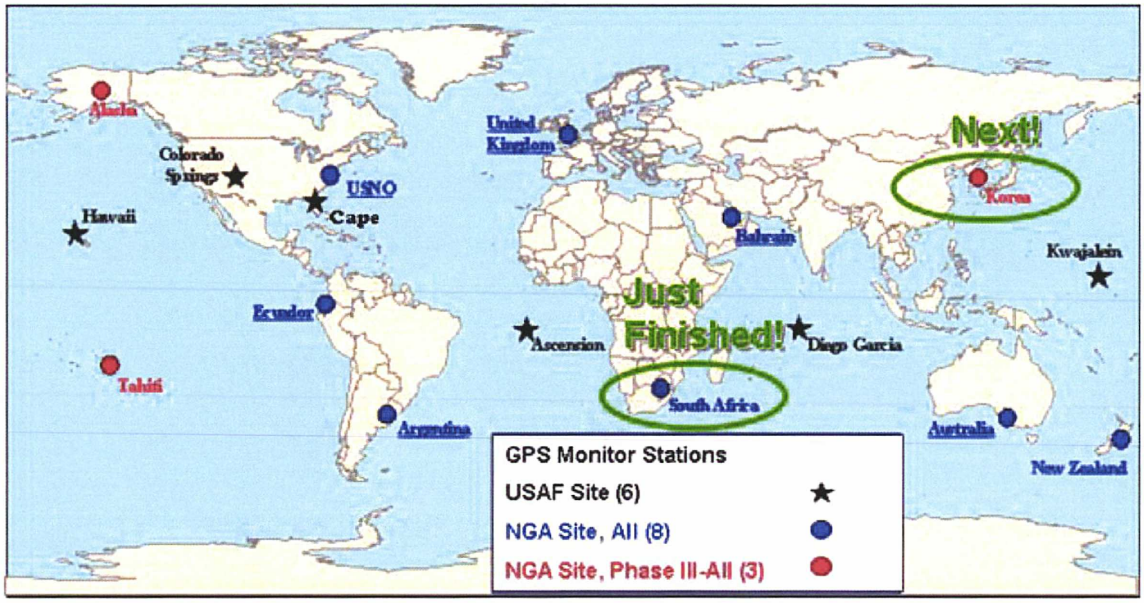

Fig. 1-3 : The GPS Operational Control Segment. (Source US DoS)

1.1.3 Galileo, the European Global Positioning System

In March 2002 the European Union decided to build Europe's future GNSS system Galileo. Nevertheless the vision of a European GNSS existed long before, since 1992. Benefits for Europe in a level of social and economic growth will be considerable. Galileo is not only another technological project but it is a key component to tomorrow's civil, commercial, scientific, industrial and defense strategic tasks of the EU and its 27 nations.

Galileo is designed to provide a highly accurate, global positioning service. According to *Galileo's Signal-In-Space Interface Control Document* (Galileo SIS-ICD) the system will be signal interoperable with GPS and, at least to some extent – excluding the real-time high-precision services of the systems – with GLONASS.

The fully deployed Galileo systems will consist of 30 Satellites (27 operational and 3 non-active spares). The system's orbit will be a quasi-circular MEO orbit of 29601.297 km semi-major axis and an inclination of the orbital planes of 56 degrees with reference to the Earth's equatorial plane.

1.1.3.1 The development phase

In December 1992, Galileo was just a glimmer in a few visionaries' eyes. That was the month that two European Commission (EC) directorates-general – those for transport and science, research and development – decided to fund a modest study of satellite navigation options for Europe. Since that epoch Galileo went through many seas and storms. Some of the past, present and future steps in its rather "wild" coarse are exposed:

- The EU Transport Council resolution on March 23 2002 puts the Galileo project in action;
- In the same year comes the creation of the *Galileo Joint Undertaking* (GJU) enterprise. The role of GJU was to coordinate and manage the *In Orbit Validation* phase (IOV) up to the selection of the system's operator during the launch of the FOC phase;
- Starting of the IOV phase beginning of 2004;
- During the final conclusions' policy of the EU Transport Council of the 10/12/2004 the 5 services of the Galileo system were defined as well as the beginning of the deployment and exploitation phase;
- Beginning of the European Geostationary Navigation Overlay Service (EGNOS);
- On October 28 2005 the first Galileo In Orbit Validation Element GIOVE-A was launched from Baikonur space center;
- On December 5 2005 the EU Transport Council has decided that the 2 Galileo Control Centers (constellation and mission) will be situated in Germany (Oberpfaffenhofen DLR) and in Italy (Fucino) and Galileo's headquarters in France (Toulouse, CNES);
- On January 12 2006 GIOVE-A started transmitting the first navigation signals near 17:30 UTC (Montenbruck et al. 2006). The signals were received with the first *Galileo TEst Receiver* (GTER, Simsky et. al 2005) and closely monitored by radio telescopes in Redu (Belgium), Chibolton (UK), Toulouse – CNES (France);
- On May 23 2006 the Galileo SIS-ICD was released on the GJU website (www.Galileoju.com);
- A technical glitch in GIOVE-B technical components has delayed Galileo's second test bed satellite to fly till late 2007;

- In February 2007 the GJU has seized to exist and the European GNSS Supervisory Agency (EGSA, formerly stated as Galileo Supervising Authority) has taken responsibility of the further development of the Galileo project. EGSA will extend the concession contract, own and oversee Galileo infrastructure and operations on behalf of the public interest. Furthermore, a variety of high-level tasks such as signal certification and system security will be duties of the EGSA.
- On March 2 2007 ESA released the GIOVE-A SIS ICD;
- On May 2007 the EU Transport council revises the *Public Private Partnership* (PPPp) in order to further finance the Galileo project;
- Launch of the first four Galileo IOV satellites is scheduled for beginning of 2009 as well as 3 more experimental spacecraft;
- FOC with the complete constellation is projected for 2012 (**Fig. 1-4**).
- On July 26 2007, the US and the EU announced their agreement to jointly adopt and provide an improved design for the respective GNSS signals. These will be implemented on the Galileo Open Service (L1F) and the GPS IIIA (L1C) new civil signals.

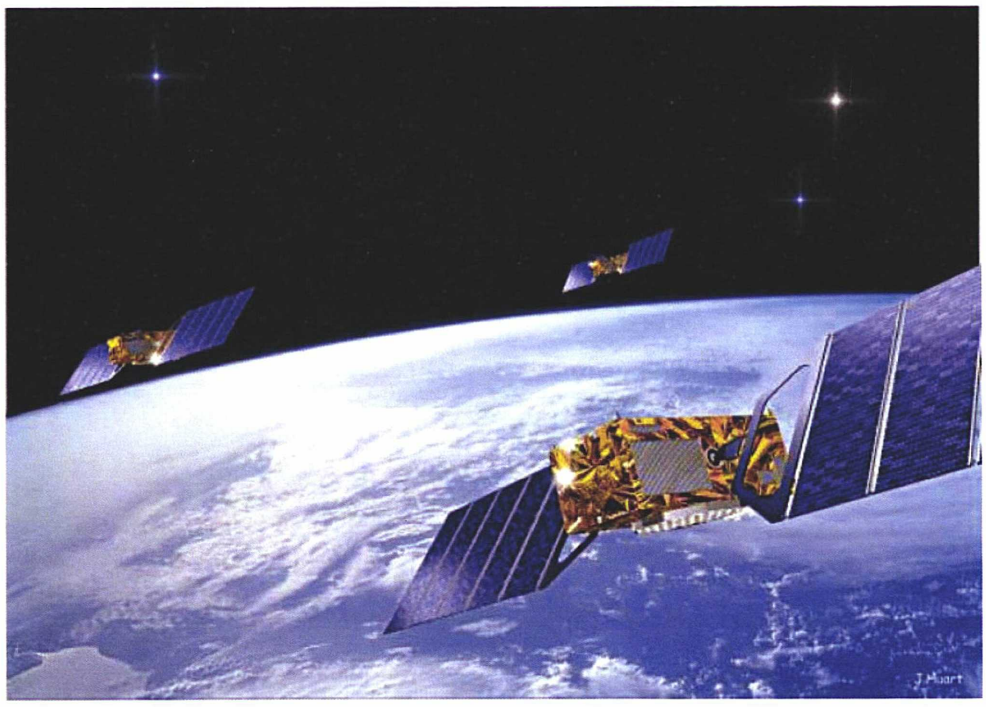

Fig. 1-4 : The Galileo constellation. Artistic view. (Source ESA)

1.1.3.2 The modernization plan

Galileo is not yet in operation but already the evolution program for the second generation Galileo II is planned to start by the middle of 2007. Galileo II could arrive somewhere around 2020 and is expected to introduce new modernization elements analogous to the steps made by its counterparts GPS and GLONASS. Inter-satellite links could be introduced at that time and aeronautical certification could be of relevance.

1.1.3.3 The Galileo services and signals

1.1.3.3.1 Services

The Galileo positioning services will be divided in 5 categories according to Galileo's SIS-ICD (D.0) edited on May 23 2006:

- An *Open Service* (OS), providing positioning, navigation and timing services, free of charge for mass market navigation applications;
- A *Safety-of-Life Service* (SoL) compliant to standards in the aeronautical, maritime and rail domain. The SoL includes integrity and authentication capability, although the activation of these possibilities will depend on the user communities;
- A *Commercial Service* (CS) whose existence according to the recent evolutions might be compromised. This service generates commercial revenue by providing added value over the OS, such as by determination of encrypted navigation related data ranging and timing for professional use – with services guarantees;
- A *Public Regulated Service* (PRS) for applications devoted to European and Member States National Security, regulated or critical applications and activities of strategic importance;
- A *Search and Rescue Support Service* (SAR) which provides assistance by detecting Emergency Beacons and forwarding Return Link Messages to the Emergency Beacons.

1.1.3.3.2 Signals

The Galileo navigation signals are transmitted in three frequency bands. These are: The E5, E6 and the E2-L1-E1 band. The frequency bands have been selected in the allocated spectrum for *Radio Navigation Satellite Services* (RNSS) and in addition the E5a, E5b and L1 signals are included in the allocated spectrum for ARNS. All Galileo transmitting satellites share the same frequency bands (CDMA). Spread spectrum signals will be transmitted including different ranging codes per signal, per frequency and per Galileo satellite.

Two of these carrier phases will be in common with GPS, the E5a and L1. In **Fig. 1-5** are illustrated the Galileo signals mapped onto the services.

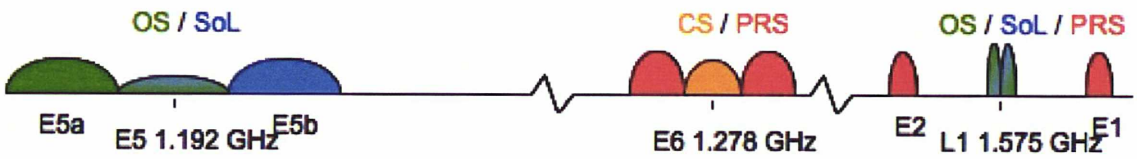

Fig. 1-5 : Galileo signals mapped onto services. (Source CNES)

Many of the signals will contain a pilot (no-data) signal for better carrier phase tracking. A summary of the main characteristics of the signals is provided in **Table 1-1**
Briefly:

- The L1 band consists of :
  - The L1F signal, which is an OS signal comprising a data channel (L1-B) and a pilot channel (L1-C). It contains integrity and encrypted commercial data;
  - The L1P signal which is a restricted access signal transmitted in L1-A signal channel. Its ranging codes and navigation data are encrypted using a governmental encryption algorithm.
- The E6 band consist of :
  - The E6C signal, which is a commercial access signal, transmitted in E6 that includes a data channel (E6-B) and a pilot channel (E6-C);

- The E6P signal, which is a restricted access signal transmitted in E6-A signal channel. Its ranging codes and navigation data are encrypted using a governmental encryption algorithm.

- The E5 band consists of :
  - The E5a signal which is an OS signal transmitted in the E5 band that includes data (E5a-I) and pilot (E5a-Q) channels;
  - The E5b signal, which is an OS signal transmitted in the E5 band and includes data (E5b-I) and pilot (E5b-Q) channels;
  - Finally the E5a and E5b signals are modulated onto a single E5 carrier using a modulation technique known as Alt-BOC.

Frequency band and channels	**Signal Components (Data, Pilots, modulations, combinations)**	**Comments, data encryption**
E5a	I+Q (data +pilot)	= GPS L5, OS/CS/SoL
E5b	I+Q (data +pilot) GIOVE-A	OS/CS/SoL
E5a+b	Alt-BOC (15,10) E5a + E5b	Low multipath and tracking noise
E6-A	Data	PRS
E6-BC	B+C (data + pilot) GIOVE-A	CS
E2 (L1-A)	Data, C1A, L1A	PRS
L1-E1 (L1-BC)	B+C (data +pilot) GIOVE-A	= GPS L1, OS/CS/SoL, PRS

Table 1-1 : The Galileo's signal caracteristics, modulations, channels, ranging codes and data encryption

1.1.3.4 The Galileo Terrestrial Reference Frame (GTRF)

A *Terrestrial Reference Frame* (TRF) is the realization of terrestrial reference systems of different observations techniques (SLR, DORIS, GNSS, and VLBI) of a set of stations' coordinates and velocities (see **§ 2.1**). The TRF of Galileo is the frame provided by the control segment of the system. The realization of the GTRF is based on a dedicated global set of geodetic stations **(Fig. 1-6)** and is one of the important keys in the realization of the Galileo system as well as in its interoperability with the other GNSS.

The GTRF implementation is part of the duties of the *Galileo Geodetic Service Provider* (GGSP) as the latest one was appointed by the 2420 call of the 6th Framework program of the *European Commission* (EC) on June 2004. The GGSP contract covers the specification, design, implementation, testing and operation of the prototype *Galileo Reference Service Provider* (GRSP) to support the Galileo IOV phase. The prototype of the Galileo Reference Service Provider is responsible for establishing the GTRF and its relation with the *International Terrestrial Reference Frame* (ITRF) (see **§ 2.1.1**) within tight specifications (http://ec.europa.eu/transport/gsa/rd/rdggsp.html). The head of the consortium is the *GeoForschungsZentrum* (GFZ) Institute at Potsdam. The kick off phase started on 2005. The main tasks and actions of the GGSP are (Söhne et al 2007):

- Definition and realisation of the GTRF ;
- Maintenance of the GTRF until the IOV phase ;
- Recommendations for the permanent service ;
- Delivery to the GRSP ;
- GTRF definition, realisation, maintenance, link to the IERS and to the *International Laser Ranging Service* (ILRS).

A stable and precise GTRF will serve as the basis for all Galileo-related services and Galileo orbits. It will be an independent reference frame made by Galileo's own observations, at least after the completion of the FOC phase. Until then the GTRF will be materialised by observations of both GPS+Galileo. One of the quality specifications is that the GTRF shall be compatible with the ITRF at 3cm (2σ). That means that the relative accuracy of the GTRF solution (station positions) with respect to the solutions of ITRF or those of the *International GNSS Service* (IGS) core stations expressed in ITRF shouldn't be more than 3cm at a 95 % confidence level (Gendt et al. 2007). The coordinates and velocities necessary for the GTRF realisation will be provided by a core network of 18 *Galileo Sensor Stations* (GSS) during the IOV phase and a total of 50 GSS including 5 *Galileo Uplink Stations* (ULS) after the kick off of the FOC phase (Söhne et al 2007). In the total number of GSS are included also stations with at-least 2 collocated techniques such as SLR and VLBI and optionally GLONASS and DORIS (Mandatory GPS) (Söhne et al 2007). **Fig. 1-6** describes the GTRF network of the GSS stations.

The realisation of the GTRF will be established by a free network adjustment (Grafarend and Schaffrin 1973, Heflin et al. 1992) in order to avoid errors in fixing the ITRF reference stations and to simultaneously determine:

- Station positions and velocities ;
- Earth Orientation Parameters (EOPs) ;
- Orbit and Clocks.

The necessary alignment to ITRF will be accomplished via an IGS core network expressed in ITRF collocated to GSS and non co-located stations. As none of the space geodesy techniques is able to provide all the necessary parameters for the TRF datum definition, SLR and VLBI stations co-located to GSS will provide independent quality check and connection to geocentre, scale and the inertial frame (earth rotation) (Söhne et al. 2007). Local and intra-technique ties must be determined with an extreme precision.

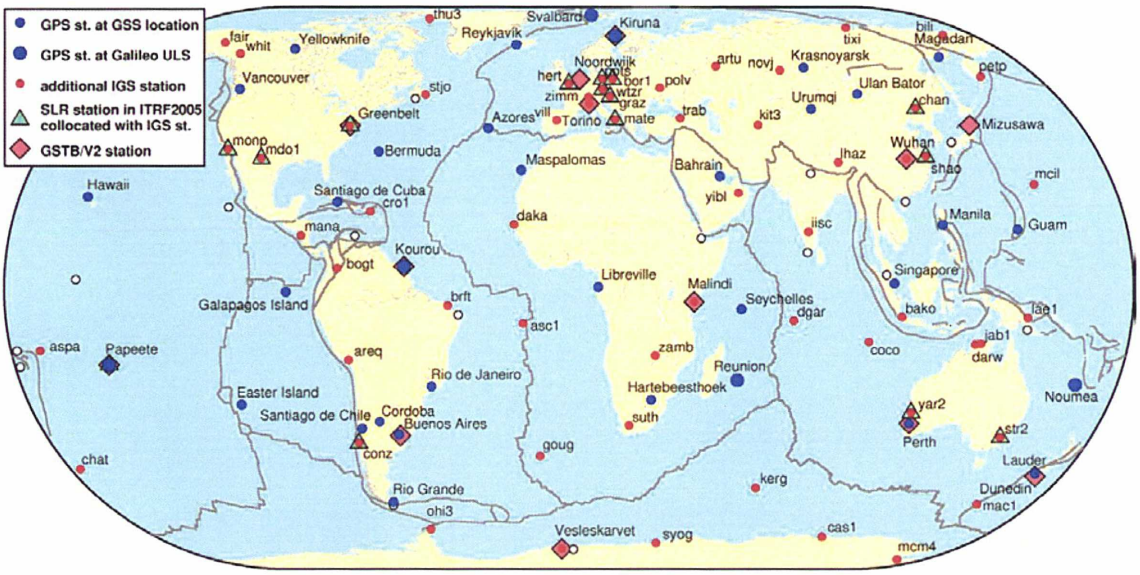

Fig. 1-6 : Initial GTRF network at the beginning of IOV, ~100 locations, (Source GGSP)

Preliminary observations from around 10 GSS stations in combination with IGS stations have been collected during the IOV phase for the determination and characterisation of GIOVE-A orbits and clocks (see **§ 3.2.2.2**).

1.1.3.5 The Galileo System Time (GST)

As stated in **§ 1.1.1.1**, an important element in combining different GNSS, apart from a geodetic reference frame, is the implementation of a reference system time (GST for Galileo). Galileo will establish a reference time scale, GST, to support system's operations. The GPS time and GST will be in general independent.

The metrological function (the accuracy in the dissemination of the *Temps Universel Coordonnée,* UTC) of the GST is the responsibility of the *Galileo Time Service Provider* (GTSP) which will cover matters related to design, implementation testing and operations during the IOV phase.

The key element in the GST architecture will be the *Precision Timing Facility* (PTF) (Hahn and Powers 2005). This element is in charge of the navigation timekeeping and will:

- Maintain a stable ensemble of clocks (2 Active Hydrogen Maser AHM, 4 Cesium clocks) in a well controlled environment;
- Measure the time offsets of all the clocks compared to the master clock through a local measurement system;
- Compute GST;
- Steer GST towards the *Temps Atomic International* (TAI), modulo one second, through the external correction provided by GTSP;
- Provide GST to the orbit determination and time synchronization process.

The PTF facility is located within the *Galileo Control Centers* (GCC).

The offset between TAI representations derived from GPS and Galileo broadcast can be expected to be around 33 ns (95%) (Moudrak et al. 2005). As of January 2006, TAI is ahead of UTC by 33 (UTC-TAI = - 33 sec) leap seconds (Bulletin C 30, http://hpiers.obspm.fr/eoppc/bul/bulc). GPS time is synchronized to UTC and is not adjusted for leap seconds (www.iers.org).

The GTSP is responsible for keeping GST aligned (steered) to TAI within tight specification and predict the time offset from UTC (leap seconds).This is achieved by conducting time transfer measurements between the Galileo PTF master clocks and the timescales within the core UTC laboratories. These UTC core laboratories are the National Metrological Institutes of France, Germany, Italy, and UK. GTSP will provide its corrections to the *Galileo Mission Segment* (GMS) which will be responsible for all ground functions related to Galileo mission implementation. Among them is the generation of the GST. GTSP, after the end of the IOV phase and beginning of FOC phase, will constitute and provide support to the full *Time Service Provider* (TSP).

Some of the essential differences and similarities between the GPS time and GST are summarized in **Table 1-2.**

	GPS Time	**GST**
Source of time	One-way	One-way
Type of time scale	Implicit mean of atomic clocks within the GPS system steered to UTC	PTF active H-maser steered to TAI
Physically implemented at	The GPS Master Control Station (MCS)	At the Galileo Precision Timing Facility (PTF)
Access outside the system	Through broadcasted corrections to satellite clocks	Either through direct time transfer or broadcasted corrections to satellite clocks
Steering to TAI/UTC	Through the US Naval Observatory	Through the GTSP combinations of several institutes
Stability over 1-day (sec)	$2x10^{-14}$ (Ray and Senior 2005)	$\sim 2.8x10^{-15}$ (requirement, 2σ) *source GJU*
Offset (Accuracy) from TAI (sec)	$\sim 4.3x10^{-9}$ (rms in 30/5/2007) *Source USNO*	$50x10^{-9}$ (requirement, 2σ) *source GJU*

Table 1-2 : GPS Time vs GST

GST will be available as a physical signal and will be fed to the *Orbit Determination and Synchronization Facility* (OSPF) which will compute the orbits of Galileo satellites and predict their clocks versus GST.

The satellite clocks which will be installed on-board of the Galileo satellites are of two kinds:

- Rubidium atomic clocks ;
- Space Passive Hydrogen Maser clocks.

The estimated offset of GST from TAI will be broadcast in the Galileo navigation message.

1.1.3.5.1 The Galileo-GPS Time Offset (GGTO)

The residual offset between GST and GPS Time, GGTO, can be expected to be about 57 ns (95%) considering today's performance of GPS Time and the required performance of Galileo.

A schematic representation of the GGTO is in **Fig. 1-7.**

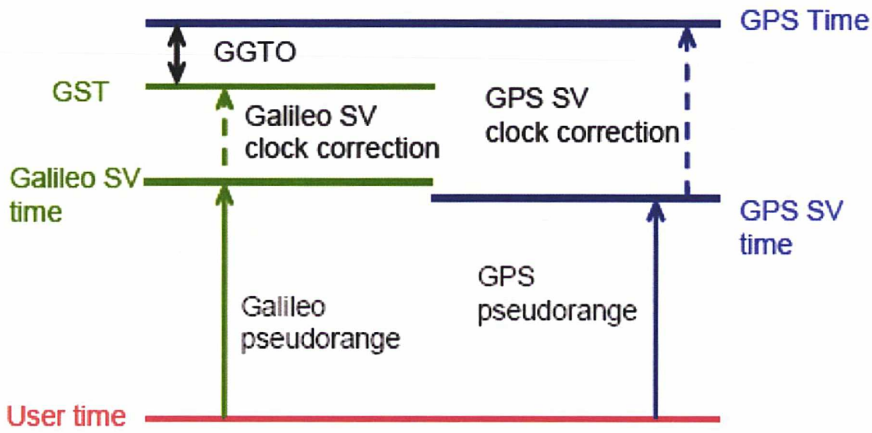

Fig. 1-7 : GPS time versus GST and the GGTO bias in the navigation solution. (Source DLR)

The GGTO will represent an important issue for GPS-Galileo interoperability, since it will cause bias between measurements in combined GPS/Galileo receivers.

1.1.3.6 Galileo Integrity

Whereas many Galileo user services benefit uniquely from the system's positioning accuracy, a rather large number of navigation applications will require the navigation information provided by the system with the highest confidence level possible. This is the case for SoL applications such as earth or air transportations. The integrity functions will be managed and executed from the *Integrity Processing Facility* (IPF) which is a real time processing of the GMS that provides the broadcast satellite navigation data based on the GSS. In this case, with known positions of the GSS the actual position of the SV and with this the maximum error on the range (*Signal-in-Space-Error*, SISE) can be estimated (Hernandez et al. 2006, Oelher et al. 2004).

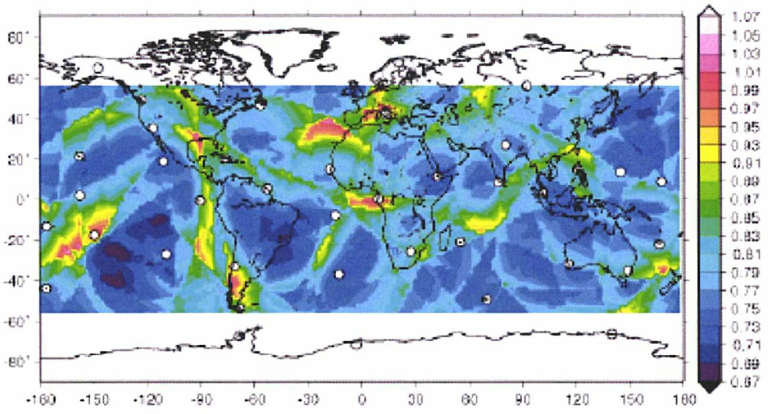

Fig. 1-8 : SISMA estimations (m) of all potential satellite positions for nominal SoL-FOC. The GSS stations are in white circles (Hernandez et al. 2006)

If the SISE is larger than a certain threshold the satellite will be flagged "Don't Use". Next, and after certain *False Alarm* (FA) verifications, the following information is disseminated to the user:

- Navigation Message: SISA values for the satellites updated every 30 sec;
- Integrity Message: the sigma of the difference of the estimated SISE and an unbiased one (*Signal-in-Space-Monitoring-Accuracy*, SISMA, **Fig. 1-8**) together with the *integrity flags* (IF) updated every 30 sec;
- Alerts and connectivity status : each alert is coded with 4-bits and 16 different states can be accessible to the user (Don't use, Not Monitored, 14 states OK with corresponding SISMA ranging from 30 cm to 520 cm).

For more details on the whole integrity concepts the reader is suggested to look into Hernandez et al. (2006), Oelher et al. (2004) and Paimblanc et al. (2006).

1.1.3.7 Galileo In Orbit Validation Element (GIOVE)

In preparation for the development of the Galileo system, the *European Space Agency* (ESA) launched in 2002 the *Galileo System Test Bed Version 1* (GSTB-V1). Within the GTSB-V1 project were developed (Piriz et al 2006):

- The Galileo orbit determination, integrity and time synchronization algorithms;
- An experimental ground segment consisting of a worldwide network of sensor stations;
- An experimental PTF providing the reference GST steered to TAI/UTC;
- A processing center located at the ESA headquarters in the Netherlands (ESTEC).

Within the GSTB-V2 one experimental Galileo satellite, GIOVE-A (**Fig. 1-9**), was launched on December 28 2005 from Baikonur cosmodrome.

1.1.3.7.1 GIOVE-A

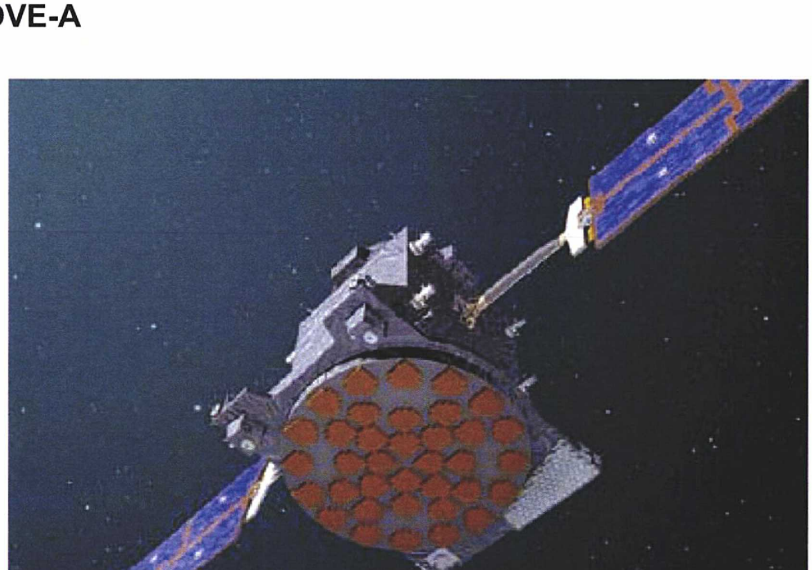

Fig. 1-9 : The GIOVE-A satellite. (Source ESA)

GIOVE-A is currently placed into MEO with a semi major axis of 29600 km, an inclination of 56° and an eccentricity of 0.002. The main objective of GIOVE-A satellite is : to secure the use of the frequencies allocated to the Galileo system; to verify the most critical technologies of the operational Galileo system, including the on-board atomic clocks and the navigation signals generators; to characterize the novel features of the Galileo signal design, including the verification of the user receivers and their resistance to multipath. The first navigation signals where broadcasted on January 12 2006.

From May 17 2006 till today GIOVE-A has been transmitting the signals illustrated in **Table 1-3**:

Frequency Band	Frequency (MHz)	Pilot/ Data	Pseudo Range	Carrier phase
L1	**1575.420**	Data	C1A	L1A
		Data	C1B	L1B
		Pilot	**C1C**	**L1C**
E5a	1176.450	Data	C5I	L5I
		Pilot	C5Q	L5Q
E5b	**1207.140**	Pilot	**C7Q**	**L7Q**
E5a+b (AltBOC)	1191.795	Pilot	C8Q	L8Q

Table 1-3 : The GIOVE-A signal mode, (source GMV)

Sites	Code	Autority	Country
Kiruna	GKIR	ESOC	Sweden
New Norcia	GNNO	ESOC	Australia
Kourou	GKOU	ESOC	French Guyana
Mizusawa	GMIZ	GFZ	Japan
Dunedin	GOUS	GFZ	New Zeland
La Plata	GLPG	GFZ	Argentina
Papeete	GTHT	ESOC	French Polynesia
Wuhan	GWUH	GFZ	China
Malindi	GMAL	ESOC	Kenya
ESTEC (Noordwijk)	GNOR	ESA/GAIN	The Netherlands
Torino	GIEN	IEN	Italy
USNO	GUSN	USNO	USA
Vesleskarvet	GVES	ESOC	Antarctica

Table 1-4 : GIOVE Mission Sensor Stations List (Crisci et al. 2006, Piriz et al. 2006)

The main characteristics of the GIOVE-A are (ESA bulletin 127):

- Mass: 614 kg;
- Size: 1.904 x 1.394 x 1.670 m (stowed envelope);
- Solar array: 2 wings of 2 panels each (0.98 x 1.74 m);
- 3-axis stabilized: nadir-pointing + yaw steering;

- Power: 633 W used / 744 W avail;
- 3 Payload chains (A,B,C);
- 2 Rb Clocks (FM4 & FM5);
- Laser Retro Reflector array of 76 corner cubes with a diameter of 27 mm each;
- Lifetime until March 2008.

The current 13 GSS used for the GIOVE-A Mission segment (GIOVE-M) experimentations are listed in **Table 1-4**. Immediately after the deployment of the ground stations and as soon as they were fully operational, several experimentations were performed in order to:

- Confirm the feasibility of Galileo signal tracking in real environment with real SIS for different receiver environments and user types ;
- Confirm signal design performance assumptions in terms of: C/N0, tracking noise, static and dynamic multipath;
- Characterise the on-board clock performances.

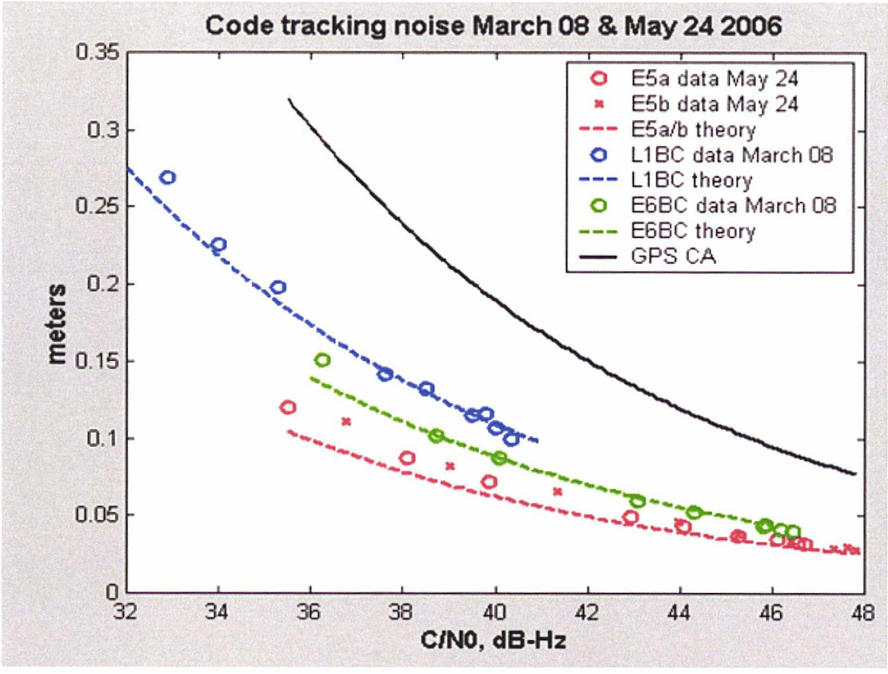

Fig. 1-10 : C/No ratio for GIOVE-A code observables compared to GPS's C/A code (Navaro-Reyes 2007).

The dimensionless signal to noise ratio or carrier-to-noise power density ratio (C/No) has been used by a number of authors as a quality indicator of GPS observables. For instance Comp and Axelrad (1998) investigated the use of SNR observable in an attempt to reduce the effect of carrier phase mutlipath. Some of the first experimentation results in matters of C/No ration were presented during the EGU 2007 general assembly and can be seen in **Fig. 1-10**. Galileo signals present lower tracking noise than GPS and the observed values are in absolute agreement with the theoretical ones.

The static analysis at the GESS sites (in **Fig. 1-11**) shows that mutlipath remains at relatively low levels for a cut-off angle of 10°.

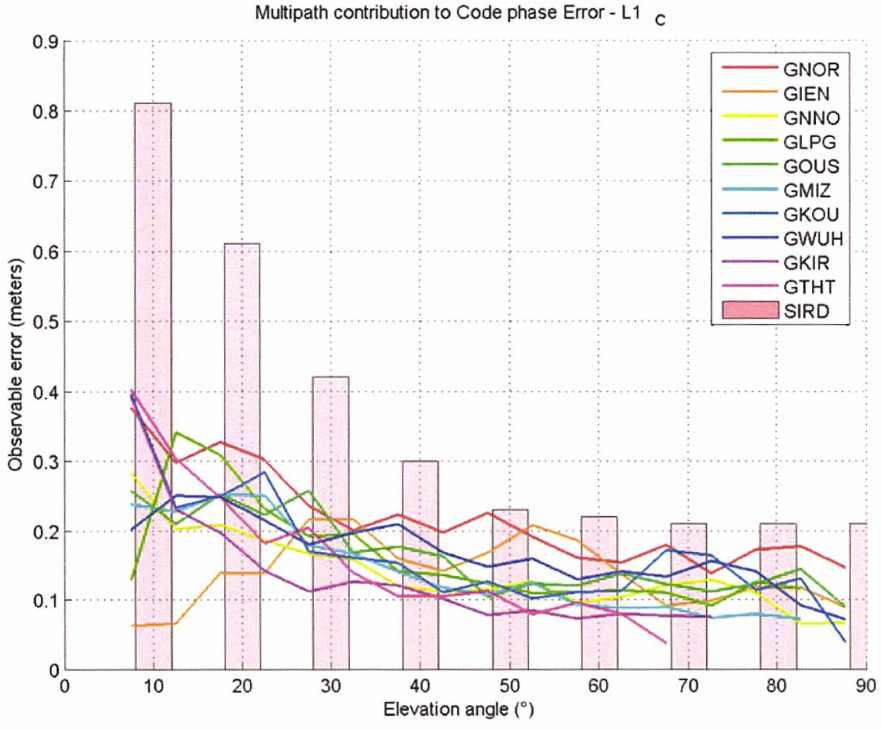

Fig. 1-11 : Code multipath estimation on static environement in GIOVE's infrastracture. SIRD is the required performance for Galileo as it is described in the SIS-ICD (Navaro-Reyes 2007)

The clock's characterisation took place from October 28 2006 to March 21 2007. As previously noted, GIOVE-A has on-board two *Rubidium Atomic Frequency Standards* (RAFS) clocks. For the evaluation of their performances an *Active Hydrogen Maser* (AHM) connected to the GIEN station, in Torino, (**Table 1-4**) was used as the reference clock for the whole experimentation. The AHM was continuously monitored versus the INRiM's (*Istituto Nazionale di Ricerca Metrologica*) ensemble of atomic clocks and compared to

external time reference scales such as the UTC realised by the BIPM in France. During the analysis period the GIOVE-A was configured to transmit the L1 and E5 signals (**Fig. 1-5**) using the nominal payload chain, driven by the RAFS *Flight Model* 4 (FM4) and *Flight Model 5* (FM5) – the two on-board clocks. The C1C-C7Q and L1C-L7Q (**Table 1-3**) ionosphere-free code and phase combinations were selected for clock characterisation, and were used together with the P1-P2 and L1-L2 ionosphere-free code and phase combinations from the GPS constellation.

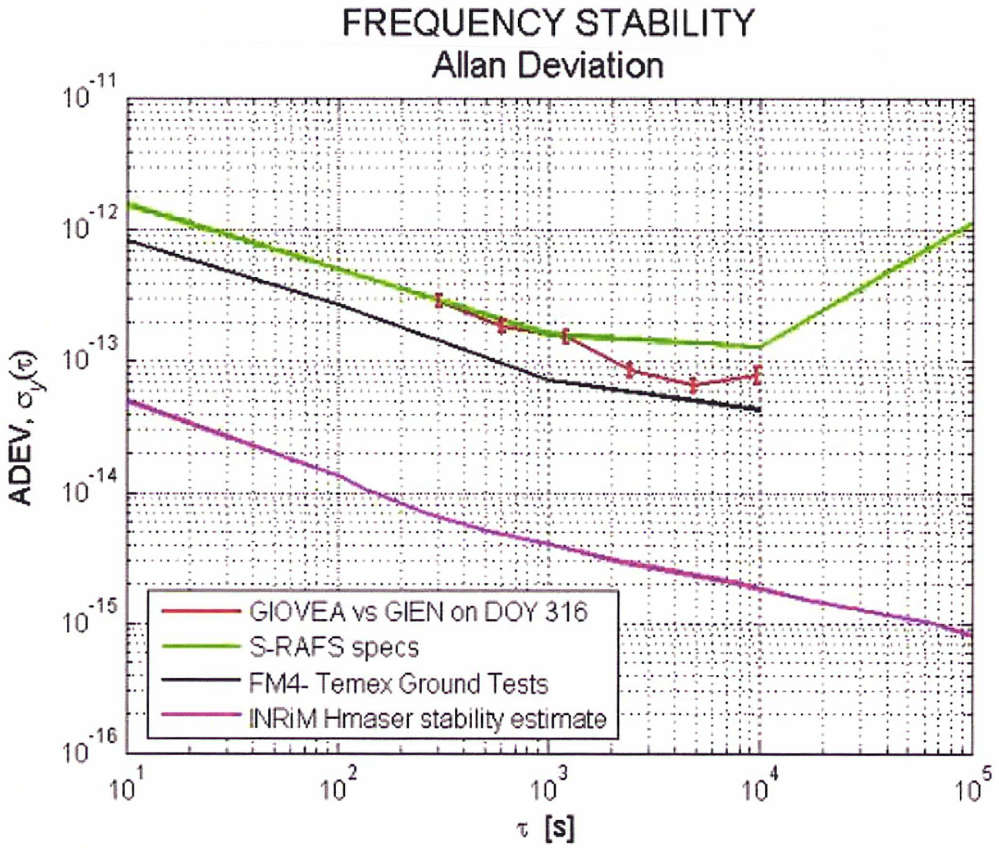

Fig. 1-12 : Frequency stability of one of the RAFS clock of GIOVE-A (Rochat et al. 2007). Notice the very good comparison between ground tests, specifications and the INRiM's Hmaser stability

The characterization of the on-board clock was also supported by the use of SLR, a high precision technique for precise orbit determination that is independent of the navigation signal generation. The SLR data where provided by the ILRS network. The technique used for clock characterization is called *Orbit Determination & Time Synchronization* (ODTS). The ODTS solved for orbits, clocks, tropospheric delay, *Inter-System Bias* (ISB), which is the differential delay between the GPS and Galileo signal paths within the station. The ISB is the equivalent of GGTO in § **1.1.3.5.1**. The estimated phase-offsets, with respect to the reference AHM, are not the pure clock as tested on the ground but rather an "apparent"

clock as seen through the complete on-board signal generation, the space propagation and the receiver network. The Allan deviations expressing the frequency stability of the atomic clocks which are derived from the ODTS technique are illustrated in **Fig. 1-12**.

Apart from the excellent performances of the two RAFS clocks, many frequency jumps occurred during the testing period especially after a payload switch-off. According to Rochat et al. (2007) these frequency jumps of the apparent clock are not unusual for young clocks. It is a common effect also observed in GPS clocks.

1.1.3.7.2 GIOVE Follow-on

The ESA's follow-on plans for GIOVE-A include a GIOVE-B and a GIOVE-A2 satellite vehicles. GIOVE-B is bound to fly by the end of 2007. GIOVE-A2 whose fate will depend from the performances of both GIOVE-A and B will probably be launched inside 2008.

On-board the GIOVE-B s/c one AHM clock will be placed together with a RAFS clock. It will be the first time that an AHM clock is tested in cavity.

1.1.4 GLONASS

The GLObal NAvigation Satellite System (GLONASS) is the dual-use Russian navigation satellite system. Its nominal constellation is composed of 24 satellites in three orbital planes with ascending nodes of 120 degrees apart. 8 satellites are equally spaced in each plane. The satellites operate in circular 25440-km orbits at an inclination 64.8° and an orbital period of 11h and 15min. The orbital planes have 15°-argument of latitude displacement relative to each other (GLONASS-ICD).

1.1.4.1 The development phase

The first satellite of the Russian navigation system GLONASS was launched in October 12 1982 and the system was introduced into operation in 1993, being deployed to the complete constellation of 24 satellites in 1995. At that epoch the system was ensuring a signal of standard accuracy for civil users and a high-accuracy for military users. During the 90's Russia faced new economical conditions and the financing of the Russian space industry was significantly reduced leading to the orbital GLONASS constellation reduction and decrease of its effectiveness.

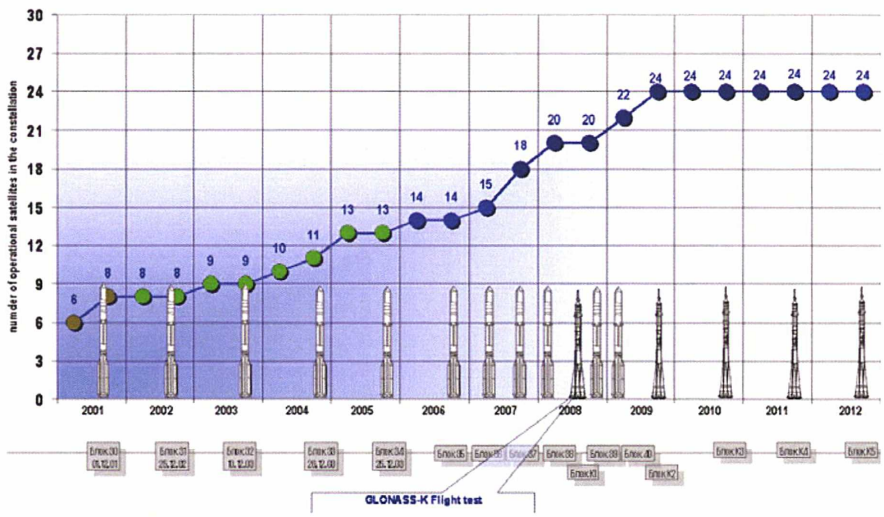

Fig. 1-13 : The GLONASS development program update. (Source Russian Federal Space Agency)

On August 20 2001 the government of the Russian Federation ratified the policy directives setting out the intent to conclusively preserve and develop this navigation system (**Fig. 1-13**). This program is expected to be completed by the end of 2011. Today the

GLONASS orbital constellation consists of 16 satellites, of which 9 satellites are GLONASS series and 7 satellites are GLONASS-M series. From these only 9 are currently operational, 3 in implementation stage and 4 at shutdown stage.

1.1.4.2 The modernization Plan

On December 25 2006 from Baikonour launch site, three modernized satellites, GLONASS-M (**Fig. 1-14**) were placed into orbit by a single launch vehicle. The 10 year modernisation plan covers the development of GLONASS-M satellites at a first stage and the proposed GLONASS-K satellites at the second stage.

Fig. 1-14 : A GLONASS-M spacecraft

The GLONASS system is being modernised based on the following main characteristics:

- Qualitative improvement of radio navigation signals. Introduction of the third frequency;
- Improvement in the stability and reliability of timing signals;
- Implementation of inter satellite links.

In the next generation GLONASS-K satellites a third civil signal at the L3 band (1194.45 to 1208.97 MHz) as well as integrity information will be added.

In matters of signal interoperability with GPS and Galileo things become more complicated since GLONASS uses FDMA and not CDMA as the previous two GNSS (see **§ 1.1.1**). Some statements made by Russians officials are suggesting that maybe the CDMA protocol will be applied in the new GLONASS-K satellites at the third civil signal.

1.1.4.3 GLONASS signals

GLONASS uses FDMA technique in both L1 and L2 sub-bands. This means that each satellite transmits navigation signal on its own carrier frequency in the L1 and L2 bands. Two GLONASS satellites may transmit navigation signals on the same carrier frequency if they are located in antipodal slots of a single orbital plane (GLONASS SIS-ICD). The nominal values for L1 and L2 carrier frequencies are defined by:

$$f_{K1} = f_{01} + K\Delta f_1$$
$$f_{K2} = f_{02} + K\Delta f_2$$

Eq. 1-1

Where: K is the frequency channel of the signals transmitted by GLONASS satellites in the L1 and L2. ; $f_{01} = 1062$ MHz; $\Delta f_1 = 562.5$ kHz; $f_{02} = 1246$ MHz; $\Delta f_2 = 437.5$ kHz

The nominal values for carrier frequencies in L1 and L2 are given in **Table 1-5**. The channel number K for any particular satellite is provided in almanac (for more information see the GLONASS ICD available at www.glonass-ianc.rsa.ru/i/glonass/ICD02_e.pdf). Before 2005 all GLONASS satellites are using the frequency channels (K) 0 through 12 and after 2005 -7 through +6.

No. of channel (K)	Nominal value of freq. in L1 sub-band, MHz	Nominal value of freq. in L2 sub-band, MHz
13	1609.3125	1251.6875
12	1608.75	1251.25
11	1608.1875	1251.8125
10	1607.625	1250.375
09	1607.0625	1249.9375
08	1606.5	1249.5
07	1605.9375	1249.0625
06	1605.375	1248.625
05	1604.8125	1248.1875
04	1604.25	1247.75
03	1603.6875	1247.3125
02	1603.125	1246.875
01	1602.5625	1246.4375
00	1602.0	1246.0
-01	1601.4375	1245.5625
-02	1600.8750	1245.1250
-03	1600.3125	1244.6875
-04	1599.7500	1244.2500
-05	1599.1875	1243.8125
-06	1598.6250	1243.3750
-07	1598.0625	1242.9375

Table 1-5 : GLONASS carrier frequencies in L1 and L2 sub-bands for each channel K. (Source GLONASS ICD)

1.1.4.4 GLONASS System Time

GPS and Galileo, GLONASS are designed to operate on the basis of the principle of one way *Time Of Arrival* (TOA) ranging. Each satellite emits its ranging signals together with a navigation message that tells the user's receiver from which satellite, from which orbital position, and what time it was broadcast. By comparing the time of a signal's arrival with the time of its transmission, a pseudo-range can be calculated.

This method assumes that all satellite clocks are synchronized with each other and with a common time scale.

GLONASS time is generated on the basis of a *Central Synchroniser* (CS) time. Satellite atomic clocks have a daily stability which is not worse than $5x10^{-13}$ sec for the GLONASS-M satellites. The CS is a set of hydrogen clocks with a daily stability of 10^{-14} sec.

The time scales of the GLONASS satellites are periodically compared with the CS time scale and are steered to UTC. Corrections to each on-board time scale relative to GLONASS time and UTC are computed by the control segment and uploaded to the users through the broadcasted ephemeris. The GLONASS time scale is periodically corrected for the integer number of leap seconds simultaneously with UTC corrections (see **§ 1.1.3.5**). This happens by changing enumeration of second pulses of on-board clocks of all GLONASS satellites.

Between GLONASS time scale and UTC there is a constant 3 hours difference.

1.1.4.5 GLONASS Coordinate system

The GLONASS broadcast ephemeris describes a position of transmitting antenna phase center of a given SV in the PZ-90 Earth-Centered Earth-Fixed reference frame. The PZ-90 system is a global system developed by Russia, similar to WGS 84 of GPS. It was realized by positioning 26 ground stations established from observations of the Geo-IK geodetic satellite (http://www.fas.org/spp/guide/russia/nav/geo.htm), including : photographing it against a star background; Doppler measurements; laser ranging; and satellite altimetry (Boucher and Altamimi 2001). It also included electronic and laser measurement of GLONASS and Etalon satellites.

The first substantial efforts to create ties in between the reference frames of GPS and GLONASS have been realized through the *International GLONASS Experiment* (IGEX-98)

(Willis 1998). This effort continued by the *International GLONASS Service – Pilot Project* (IGLOS – PP), which is a pilot project of IGS, in order to track and analyze data from the Russian GLONASS satellite constellation. The project operated for a period of four years from 2000-2003 (Reigber 2000). The goals where to establish and maintain a global GLONASS tracking network collocated with dual-frequency combined GPS/GLONASS receivers, produce service (orbits, satellite clock estimates, station coordinates, earth orientation parameters), monitor and assess GLONASS system performances, fully integrate GLONASS into IGS products (Slater 2000). Since June 8 2003 (GPS Week 1222), the CODE Analysis Center at the University of Bern has been computing rapid and final orbit products for the GLONASS satellites. CODE generates these GLONASS orbits at the same time as the GPS rapid and final orbits (Slater 2003).

The combination for the GLONASS final products is performed since GPS Week 1300 at the IGS Analysis Coordinator (Gendt 2005). The combined GPS/GLONASS IGLOS network is illustrated in **Fig. 1-15**.

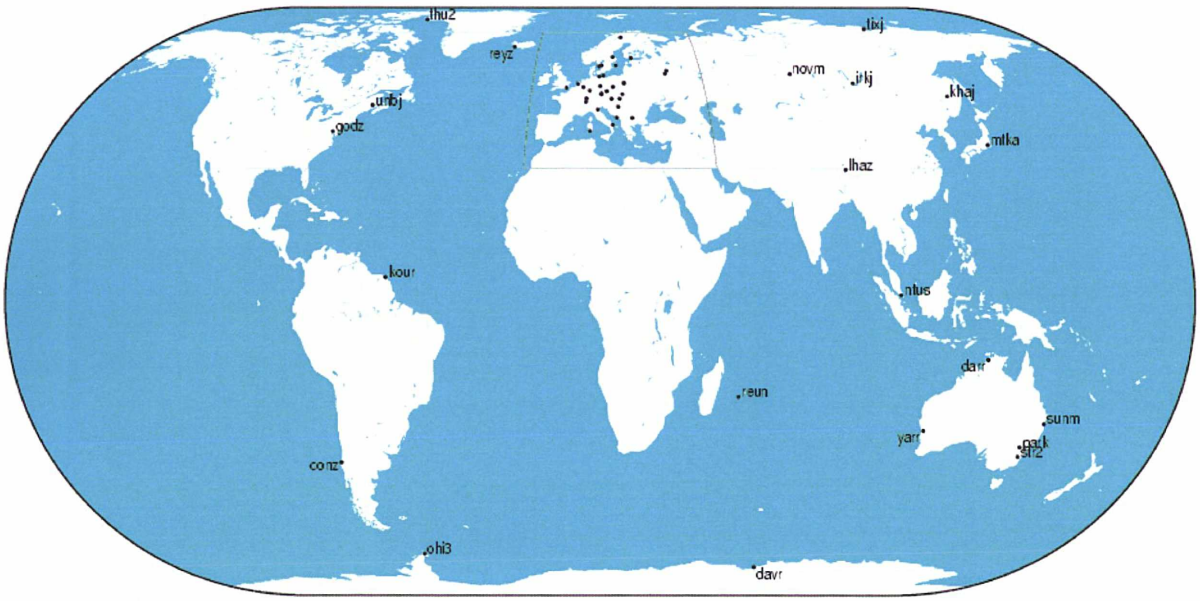

Fig. 1-15 : The IGLOS GPS/GLONASS network on Sept. 04 2007 (Courtesy of IGS).

1.1.5 Compass and Beidou

Compass is the GNSS developed by China. Like GPS, Galileo and GLONASS, the system will provide two navigation services: an open service for commercial users and an "authorised" positioning service. This system has actually started its IOC phase with the launch of the first Compass MEO on April 13 of 2007.

Beidou (North Dipper, referring to the seven stars in the constellation Ursa Major) is the local satellite navigation and positioning system operational since May 2003. It includes three satellites in geostationary earth orbits (GEO).

The whole system will consist of thirty MEO satellites in six orbital planes and five GEO Compass-Beidou satellites. The completion of the system is envisaged for 2010 with a FOC by the same year according to *China's Aerospace Science and Technology Corporation* (CASTC).

The main orbital characteristics for Compass satellites are: a semi major axis of 27800 km, an inclination of 55° and a circular orbit.

A preliminary measurement campaign made by Grelier et al. (2007) using the CNES tracking and recording system, has revealed Compass' signals spectrum in E2/L1 (Galileo/GPS), E5 (Galileo), and E5b (Galileo) bands. **Fig. 1-16** illustrates the spectrum of the future Compass system.

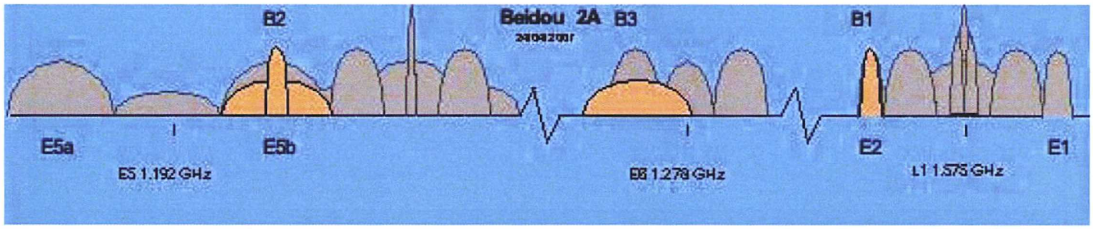

Fig. 1-16 : The Compass/Beidou frequency plan, which overlay GPS/Galileo signals (Grelier et al. 2007).

The total broadcast signals of the Compass-Beidou system will be in four frequency bands according to the International Telecommunications Union (ITU): 1561 MHz (E2), 1589 MHz (E1), 1268 MHz (E6), 1207 MHz (E5b).

1.1.6 Augmented GNSS

In addition to the global GNSS systems other regional augmentation systems of precision are on the way. These systems are called *Space-Based Augmentation Systems* (SBAS) and are used to improve integrity, reliability, accuracy and continuity of GNSS positioning and navigation. The main characteristic of these systems is that they are designated to provide a GNSS user with differential corrections for strengthening the precision in an absolute positioning mode. Apart from SBAS, also terrestrial nationwide differential correction systems exist, which usually consist of dense GNSS networks with continuous service capability.

Some of the main SBAS already in operational capability or under development are:

- The *Wide Area Augmentation System* (WAAS) constructed by the US. It increases the real-time pseudo-range accuracy from typical 10-12 m with GPS alone to 1-2 m;
- The EGNOS system is the equivalent European SBAS system. It is designed to broadcast GPS, Galileo and GLONASS corrections (Traveset-Ventura et al. 2005). EGNOS provides additional pseudorange measurements from the geostationary satellites. It consists of three geostationary satellites;
- The Beidou system which is the equivalent SBAS of china (§ 1.1.5);
- The *Quasi-Zenith Satellite System* (QZSS) is Japan's SBAS which is a constellation of three satellites inclined by 45°, in elliptic orbits, with different orbital planes in order to pass over the same ground track. The first satellite launch is planned for the year 2009 (Kogure et al. 2006);
- The Indian *GPS and GEO Augmented Navigation* (GAGAN) system is an independent seven satellite constellation that will seek to maintain compatibility with the other GNSS and augmentation systems of the region (QZSS, Beidou). Of the seven satellites three will be geostationary and the other four geosynchronous. The first payload in expected for 2007.

1.2 Summary

In this chapter we went through the most important characteristics of present and future GNSS positioning systems.

At the advent of the 21st century the total number of GNSS satellites is augmenting significantly. Up-to-day only one GNSS system is fully operational (GPS), one more is under modernisation (GLONASS) and another two are in their first implementation stages (Galileo and Compass). Together with these global positioning systems other regional complementary segments have been developed or are under development like: EGNOS in Europe; WAAS in the US; Beidou in China; QZSS in Japan; GAGAN in India. Currently the number of functional GNSS satellite vehicles raises up to 41 plus ~9 regional. In the near future, with the completion of Galileo - GLONASS – Compass this number will include more than a hundred satellite vehicles. As such, the future for ultra-high precision positioning in geosciences (Geodesy, Oceanography, Geophysics, Volcanology etc.) and in societal applications (Navigation in urban areas, fleet management, security of life, agriculture, automation etc.) becomes very promising.

For example, in mutli-GNSS combinations of the future triple-frequency geometry-free/ionosphere-free linear combinations of ranging measurements from the same satellite shall become available. These linear combinations will contain superposition of multipath and tracking signals in three or even more frequencies so information on phase multipath shall become available through observations in an absolute mode (single-satellite single-station). Multiple frequencies combinations can be translated to multi-carrier phase ambiguities which can be used as constraints to ambiguity resolutions schemes. Fast ambiguity fixing will be possible over longer distances using signals and a rather elevated number of satellites. For instance, this will be very beneficial to GNSS kinematic applications in geosciences, as the determination of coordinates, under rough conditions, of floating tracers in the open ocean, for the validation and comparison of sea-level parameters.

Nonetheless, more frequencies and systems do not always mean "easier life". On the contrary, the amount of work, for those concerned, combined with the complexity of the situation will grow tremendously. For example: conventional differencing techniques may not be possible due to different signals tracked by different receivers and channels or each signal component will have its individual bias induced by the satellite hardware and receiver hardware (Wübenna 2007).

	GALILEO	GPS	GLONASS	COMPASS
Constellation	MEO 3 planes, 27+3 nominal, (28/12/2005) 1 (GIOVE-A)	MEO 6 planes, 21+3 nominal, (17/11/2006) 16 II/IIA, 12 IIR, 3 IIR-M	MEO 3 planes, 21+3 nominal, (25/12/2006) 9 GLONASS +7 M-series	MEO 27 nominal, (13/04/2007) 1 Compass 1st version
Signal Access	CDMA	CDMA	FDMA (with possibility for CDMA in the K-series)	CDMA
Frequencies (MHz)	E5a (1176.45) E5b (1207.14) E5 (1192) E6 (1278.75) E2-L1-E1 (1575.42)	L5 (1176.45) L2 (1227.6) L1 (1575.42)	(after 2005) At each SV L1 (1609.375-1602.0-1598.062), L2 (1248.187-1246.0-1242.937) With GLONASS-K L3 (1194.45-1201.5-1208.97)	E1 (1589.742) E2 (1561.10) E6 (1268.52) E5b (1207.14)
Orbit semi-major axis (km)	29601.297	26559.7	25440	27840
Inclination	56°	55°	64.8°	55°
Services	OS, SoL, CS, PRS, SAR, integrity	SPS,PPS,(OS in Block III)	OS, military service	OS, military service
Intergrity Transmision	Yes	Yes in Block III	(integrity in the K-series)	?
Satellite Laser Ranging	GIOVE-A, Yes to all	GPS 35, 36 (future?)	all	?
Coordinate system	GTRF	WGS84	PZ-90	?
Time scale	GST (TAI)	GPS time (UTC)	GLONASS time (UTC)	?

Table 1-6 : The tomorrow's and today's GNSS characteristics

Finally, interoperability and compatibility will be the two driving mechanisms by which we will achieve a Unified Global Satellite Navigation System of Systems. The independence of each of the aforementioned systems provides greater reliability and integrity for the users and leads to a certain competition among the systems.

Having all these in mind the most important parameters of the existing GNSS systems are summarised in **Table 1-6**.

2 Geodetic components of GNSS

GNSS have been serving the geodetic community since the early beginnings of the GPS system, during the 80's. Apart from a technological achievement, the GNSS is also a scientific achievement for Geodesy.

GNSS can provide geodesists with accurate and precise positions by a measurement of the time-travel of an electromagnetic wave between a satellite in space and a GNSS receiver stationed on the surface of the Earth's crust. In order to achieve this goal the geodetic components of GNSS have to be taken into consideration such as:

- The global Terrestrial Reference System (TRF) to which the geodetic points will be referenced together with the derived products from GNSS such as orbits and clocks, EOPs, station positions and velocities ;
- The geodetic GNSS network of stations ;
- The observational model errors degrading the precision of GNSS observations ;
- The prediction of the physical processes that provoke displacements and deformations of the geodetic network of stations.

All these elements are being combined together, in order to accurately and precisely estimate, in a least squares sense, the coordinates of geodetic stations.

For instance, when two sets of coordinates of the same network corresponding to two different epochs are compared for the derivation of deformational parameters (e.g. ocean tide loading constituents) the results depend on the terrestrial reference frames used at both epochs.

In the next parts of this chapter we will see step-by-step the main parts that enter inside the duty tasks of a GNSS analyst and the scientific tasks of the present report.

A synopsis of the functional models applied and the systematic errors acting on the GNSS observables is given. Troposphere and ionosphere delays are some of the most important factors of distortion in the accuracy and precision of estimated coordinates by GNSS; the unknown integer number of cycles of the carrier phases is an important source of biases; receiver clock errors such as clock jumps and derivations from the GPS time and cycle slips during a measurement period can introduce important artifacts to the final positions estimates; variations of the center of phase of the GNSS antennas aboard the satellites and the receivers on the ground can significantly influence the scale of the system; rotations of the antennas can introduce biases; multi-path effects add noise to the final series of stations etc.

All these geodetic components of GNSS are taken into account simultaneously for the scientific investigations of this Thesis which are:

- The determination of accurate and precise deformation parameters of regional and local GNSS geodetic networks provoked by *Ocean Tide Loading* (OTL) displacements and the validation of predicted constituents ;
- The combined use of marine and terrestrial GNSS networks in order to observe water height variations of the Antarctic Circumpolar Current through the combined use of floating GNSS tracers (Buoys), tide gauge and altimetry.

2.1 Global Terrestrial Reference Frames

The physical establishment of a global *Terrestrial Reference System* (TRS) is accomplished through a global geodetic network based on the analysis of various geodetic techniques (Dermanis 2001a). Its aim is to provide unified means for describing position by means of coordinates of discrete points on the Earth's surface. Alternatively, the TRS will be the mathematical object satisfying an ideal definition in which point positions will be expressed and a *Terrestrial Reference Frame* (TRF) will become its materialization (Altamimi et al. 2002).

On the other hand there is a need in geophysics for an Earth reference frame, i.e. a frame that refers to the behavior of the deforming earth as a whole involving all its mass points and not just a set of discrete points confined on its surface. Such frames are indispensable in theories of earth rotation (Munk and MacDonald 1960) where the conversion schemes of a TRF to a geophysically meaningful Earth reference frame, such as the Tisserand axes frame, require having a straightforward comparison of the observed rotation of the terrestrial frame with respect to an inertial celestial frame. The geodetically produced TRF is generally different from the frame of Tisserand axes of the Earth's rotation theory where the relative angular momentum of its axes vanishes (Dermanis 2001a).

The optimal choice of the reference frame requires the introduction of an optimality criterion such that the apparent motion of the network points, as seen with respect to the reference system, is minimized. This condition introduces the origin and axes in a purely mathematical way by minimizing the apparent motion of the ITRF network points with respect to the reference system (Dermanis 2006):

- The origin is constant and defined by the barycenter of the N network points $\mathbf{x}_i(t)$ (treated as unit mass points), t is the time (**Eq. 2-1**). In the case of TRS the origin is defined by the center of mass of the whole Earth including oceans and the atmosphere (Altamimi et al. 2002).

$$\frac{1}{N}\sum_{i=1}^{N}\mathbf{x}_i(t) = \mathbf{m} = \text{constant}, \qquad \forall t \qquad \textbf{Eq. 2-1}$$

- The axes give the orientation of the system where its evolution in time should be ensured by the Tisserand axes principal: all relative angular momentum h (**Eq. 2-2**)

with regard to the horizontal tectonic motions over the whole Earth should vanish (No-Net-Rotation).

$$\sum_{i=1}^{N}[\mathbf{x}_i(t)\times]\frac{d\mathbf{x}_i}{dt}(t)=\mathbf{0}, \qquad \forall t \qquad \textbf{Eq. 2-2}$$

The conversion of the geodetic TRF to a Tisserand frame strongly depends on the adopted hypotheses about Earth deformation.

Some of the relative mass motions on the surface of the Earth that contribute to the displacement of points of the geodetic networks are: plate tectonics, seismic events, atmospheric and oceanic tidal and non tidal loading, hydrological loading etc.

2.1.1 The International Terrestrial Reference Frame, ITRF

The history of the ITRF goes back to 1984. The first realisation of ITRS was the ITRF88 and since then nine versions were established and published: ITRF89, ITRF91, ITRF92, ITRF93, ITRF94, ITRF96, ITRF97, ITRF2000 and the most recent one ITRF2005 (Altamimi et al. 2007). For more details regarding the history and description of ITRF the reader may refer to the list of ITRF papers given in the references of this Thesis (Boucher et al. 1996, Sillard et al. 1998, Boucher et al. 1998, Boucher et al. 1999, Altamimi et al. 2002).

According to IERS the basic idea of ITRF is to combine station positions computed by various analyses centers which process observations of space geodesy techniques, such as VLBI, SLR and LLR, GPS and DORIS (**Fig. 2-1**). Each of these techniques and each analysis center materialises a different TRF.

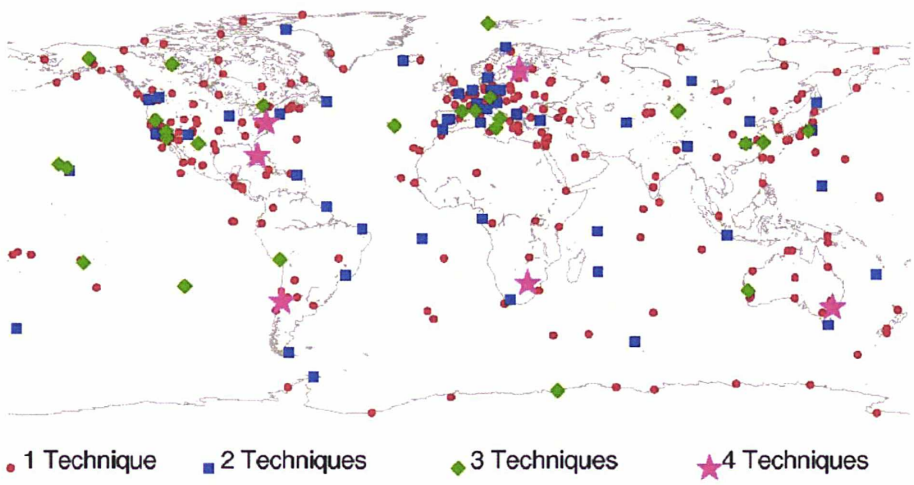

Fig. 2-1 : Co-location sites embedded in the implementation of ITRF (Altamimi et al. 2007)

The access of a simple user to the ITRF is accomplished through the use of the coordinates and velocities of the stations of each space geodesy technique.

The transition between two different reference frames consists of the transformation of the Cartesian coordinates of TRF1, X_1 to TRF2, X_2 characterized by a 7 parameter Euclidian similarity transformation:

$$X_2 = X_1 + T + D \cdot X_1 + R \cdot X_1 \qquad \textbf{Eq. 2-3}$$

Where: T is the three dimensional vector of the origin translation T_1, T_2, T_3; R is the orthogonal matrix of rotation that contains the set of the three Euler angles R_1, R_2, R_3; D = scale - 1. The number of transformation parameters becomes 14 when we consider as well their evolution in time.

2.1.2 The TRF network combination model

As previously stated, the final ITRF frame will be the product of global combinations of the time-series of stations from all the space geodesy techniques. The combination model consists of transforming each individual TRF of each technique to a given TRF. This is the same procedure in the case where a classical type of GNSS network is set up and the network's coordinates will be transformed to the desired TRF. These coordinates at some reference epoch are used as unknown parameters and their variation with time gives rise to displacements which are functions of time.

The combination model is based on **Eq. 2-3** and a more expanded form for an individual solution *s*, and each point *i* is:

$$\begin{cases} X_s^i = X_c^i + (t_s^i - t_0)\dot{X}_c^i + T_k + D_k X_c^i + R_k X_c^i \\ \qquad +(t_s^i - t_k)\left[\dot{T}_k + \dot{D}_k X_c^i + \dot{R}_k X_c^i\right] \\ \dot{X}_s^i = \dot{X}_c^i + \dot{T}_k + \dot{D}_k X_c^i + R_k X_c^i \end{cases} \qquad \textbf{Eq. 2-4}$$

Where: X_s^i is the position of each individual solution (e.g. a weekly GPS solution) at epoch t_s^i ; $\dot{X}_s^i$ the velocity expressed in a given TRF k; D_k is the scale factor; T_k the translation vector ; R_k the rotation matrix.

The combination (for the TRF) consists in: estimating positions X_c^i at a given epoch t_0 ; velocities $\dot{X}_c^i$ expressed in the combined frame c; transformation parameters T_k, D_k, R_k at an epoch t_k and their rates $\dot{T}_k, \dot{D}_k, \dot{R}_k$ from the combined TRF to each individual frame k.

In addition to the above equation, EOPs can be added in the combination process such as the pole coordinates x_s^p, y_s^p, the universal time UT_s as well as their daily time derivatives $\dot{x}_s^p, \dot{y}_s^p$ and LOD_s provided by the IERS (Gambis 2004, Altamimi et al. 2005):

$$\begin{cases} x_s^p = x_c^p + R_{2_k} \\ y_s^p = y_c^p + R_{1_k} \\ UT_s = UT_c - \dfrac{1}{f} R_{3_k} \\ \dot{x}_s^p = \dot{x}_c^p + \dot{R}_{2_k} \\ \dot{y}_s^p = \dot{y}_c^p + \dot{R}_{1_k} \\ LOD_s = LOD_c + \dfrac{\Lambda_0}{f} \dot{R}_{3_k} \end{cases} \qquad \textbf{Eq. 2-5}$$

where $f = 1.002737909350795$ is the conversion factor from UT into sidereal time. Considering $LOD = -\Lambda_0 \dfrac{dUT}{dt}$, Λ_0 is homogeneous to time difference, so that $\Lambda_0 = 1$ day in time unit. The link between TRF and EOP is ensured through the 3 Euler rotation angles of R_1, R_2, R_3 plus their time derivatives.

2.1.2.1 The Datum problem or Zero order Design

According to Dermanis (1985) , coordinates of the points of a geodetic network define the position of the network with respect to the reference frame, or the position of a reference frame with respect to the network.

The normal equation system of weekly solutions, which is referring to **Eq. 2-3**, has a rank deficiency of 7 corresponding to the number of transformation parameters needed to define the reference frame while the normal equation of the global combination process into a long-term solution of **Eq. 2-4** has a deficiency rank of 14.

In the case of coordinate's transformations, the number of degrees of freedom leaves the observations invariant (Dermanis 1985). The datum defect or Zero order design problem (Dermanis 1985) due to the rank deficiency can be overcome by means of a number of constraints on the parameters (coordinates or transformation parameters). Such constraints that define the reference frame without distorting the shape and size of the network are called minimal constraints. When added to the normal equations they reduce the number of independent parameters and allow for one unique solution.

The simplest way, of defining the reference frame or aligning a solution to the TRF in question, is by fixing the coordinates (at least 6, three for rotation and three for translation of the network) of a set of stations to their TRF values or by applying the minimal constraints to the parameters of the transformation in **Eq. 2-3** and **2-4**. For more details on minimal constraints the reader is suggested to look in Dermanis (1985), Sillard and Boucher (2001), Altamimi et al. (2007).

Nevertheless, it is known that geodetic observations are not, in general, insensitive to all degrees of freedom of a similarity transformation. For example, a technique such as VLBI is sensitive to orientation and not to the origin of the coordinate system. GPS is sensitive, to a certain degree, to geocentre but not to orientation. The above properties are of course dependent on the distribution of the network, and a continental network has, in any case, a low sensitivity to geocentre especially when relative positioning is performed. So in the case of a GPS continental network which is viewed as a plan from the satellite height the geometrical problem is equivalent to defining a 2-D reference frame associated to a plan while we have to define a 3-D reference frame. Therefore, $7 - 4 = 3$ degrees of freedom have to be defined.

2.1.2.2 Geocenter variations

Up to now the current time evolution of the ITRF is defined as linear to account mainly for tectonic plate motion while no deformation model or geocentre variations are taken into consideration (Altamimi et al. 2005, Dermanis 2006).

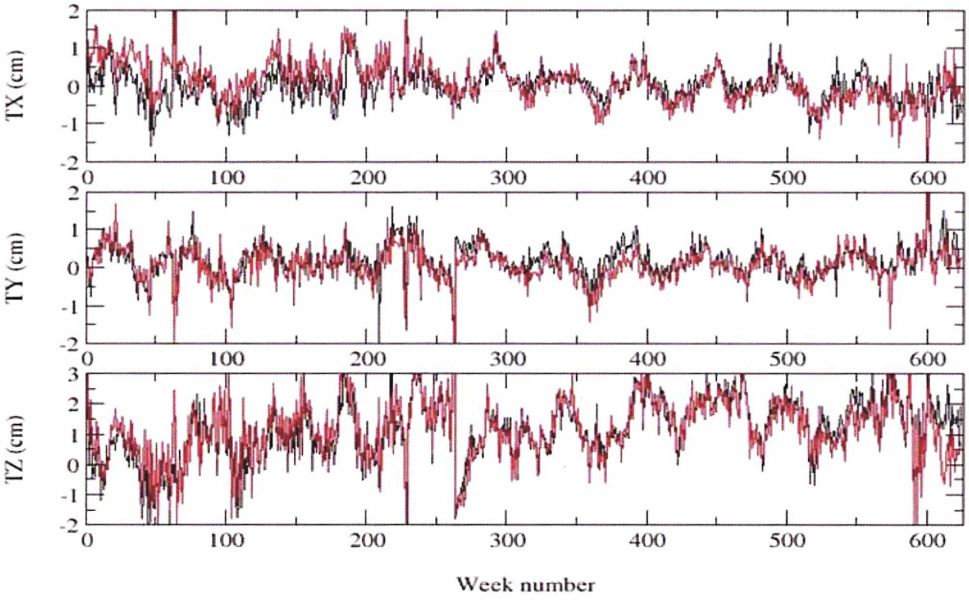

Fig. 2-2 : 12 years of weekly geocenter time-series wrt ITRF2000 from SLR (Coulot et al. 2005)

The geocentre variations are estimated either by dynamic or geometric methods. The dynamic method is based on the estimation of the degree one terms of the gravitational field while the geometric method is based on the estimation of the three translation parameters (in **Eq. 2-3**) with respect to an assumed geocentric ITRF (**Fig. 2-2**). The geocentre motion undergoes annual, semi-annual, diurnal and semi-diurnal variations due to mass distributions (atmosphere and oceans) of the solid Earth (including the interior) as seen in **Fig. 2-2** (Watkins and Eanes 1997, Dong et al. 1997, Bouillé at al. 2000, Moore and Wang 2003, Dong et al. 2003, Blewitt 2003, Coulot et al. 2005, Lavallée D. et al. 2006).

2.1.3 The Combination Research Center (CRC) project

Up-to-date two types of TRS realisations exist inside the IERS. The one is official and the other is a pilot project.

The first is formed by using the final reference frame products (station time-series, positions and velocities) of each Technique Centre (TC) and by stacking them into a global combination process. This is the today's procedure in creating the ITRF. For that purpose the IERS relies on each TC themselves organized in International Services (IGS, *International VLBI Service*; IVS, ILRS, and *International Doris Service*; IDS) whose first role is to promote the appropriate use of the geodetic technique. These services gather EOPs and reference frames inputs from the different analysis Centres and generate combined products or normal equation files in a commonly adopted format (*Software Independent Exchange*, SINEX). Usually these products are achieved independently per technique by each TC without having the necessary consistency (for instance due to different a-priori models and software). Then these products are gathered by IERS in order to be combined in the global combination process that will form the final ITRF.

The second approach enables the pilot project named *Combination Research Centers* (CRC), which is under development by the IERS (Biancale et al. 2007). The leader of this project in France is the GRGS.The IERS CRC have the task to study a homogeneous way for insuring consistency in the creation of an ITRF. This is succeeded by:

- combining all techniques first at the level of each Analysis Centers;
- using if possible a unique software, or at least the same a priori models for analyzing different techniques;
- generating simultaneously EOPs and TRF;
- evaluating the gain of the method.

The role of the CRC is to become, in a certain meaning, an analysis centers for all techniques and products (Biancale et al. 2007). In **Fig. 2-3** we can see the basic difference of the first versus the second way of creating an ITRF.

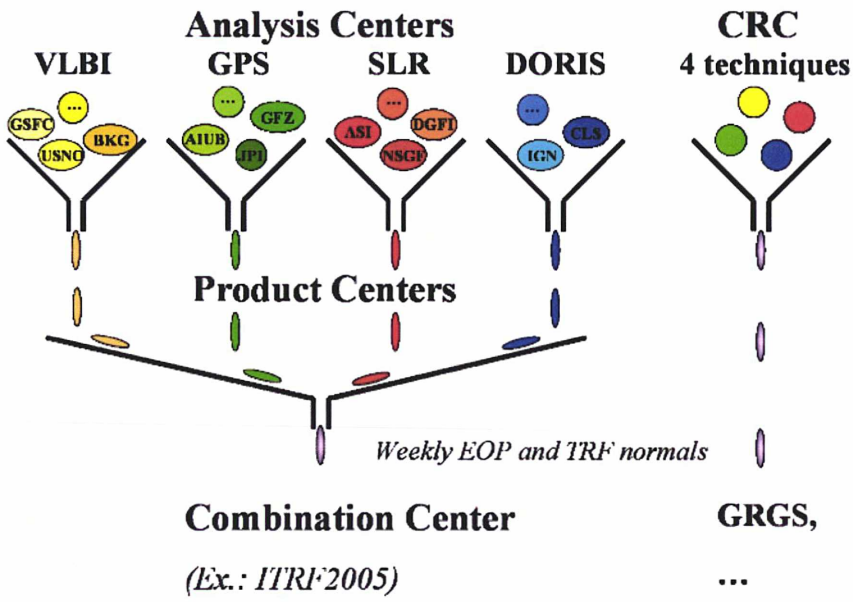

Fig. 2-3 : The two ways of creating an ITRF

The CRC approach has the advantage that any inconsistencies created in the today's ITRF process by the use of different ad-hoc models and software by each analysis center, for each space geodesy technique, will be extremely minimised.

2.1.4 GRGS as CRC/IERS (Combination Research Centre)

The GRGS has been a pioneer in studying the combination of geodetic techniques at the observation level (that means merging full normal equations with all parameters from the different space techniques) since the year 2000. It participates to the IERS Combination Pilot Project (http://www.iers.org) since the beginning of 2004 and is organizing itself through different national geodetic entities of France such as:

- OCA (Grasse) provides the SLR combinations;
- CNES (Toulouse), processes the *Laser Lunar Ranging* (LLR) combinations with contribution from the Paris Observatory;
- CNES/*Collecte Localisation Satellites* (CLS) (Toulouse), creates the GPS and DORIS combinations ;
- Bordeaux Observatory provides the VLBI combinations ;
- and Paris Observatory performs combinations with contribution from IGN (Marne-la-Vallée)

The structure of the GRGS CRC current tasks is illustrated in **Fig. 2-4**.

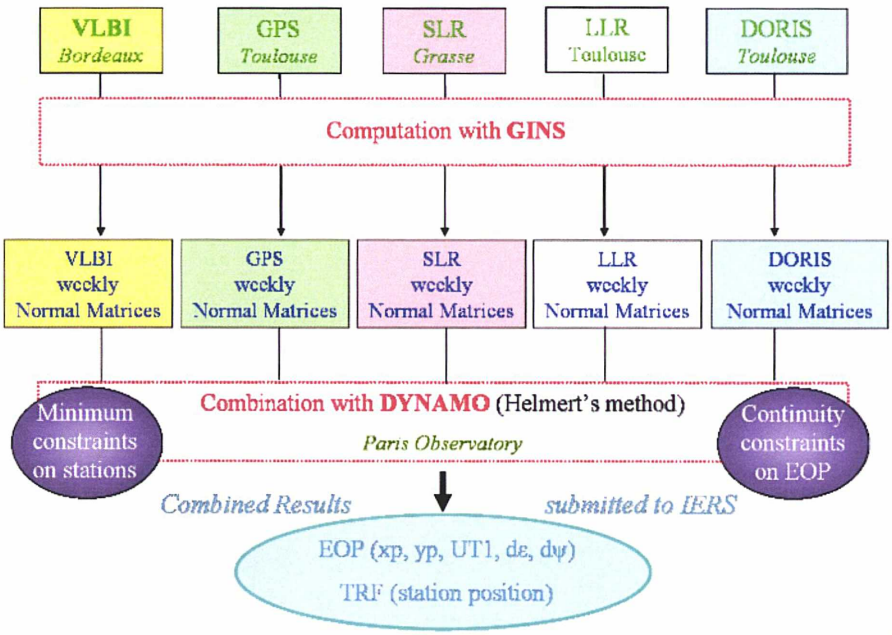

Fig. 2-4 : The GRGS CRC structure scheme (Biancale et al. 2007)

GRGS delivers routinely weekly SINEX files (inter-technique products) to IERS since 2005 in parallel with the intra-technique products from IGS, ILRS, IVS, and IDS.

The big advantage of the GRGS CRC approach is that it uses a unique geodetic software GINS (*Géodésie par Intégrations Numériques Simultanées*) for all the space geodesy techniques illustrated in **Fig. 2-4** developed and maintained by the CNES GRGS team. This software is being used for: orbit computations around any planetary body (Earth, Sun, other planets or small bodies); for gravity field modeling of the Earth (EIGENGL04s) and planets; other dynamical parameters such as solid or oceanic tides; EOPs determinations; observations of the deformations of local or global geodetic networks etc. It has the unique capability, compared to other well established geodetic software, to process all types of geodetic measurement homogeneously with the same ad-hoc models for SLR, LLR, DORIS, GNSS, VLBI, DSN, Altimetry (direct and crossover). The final ITRF by the GRGS CRC pilot project is extremely consistent due to its homogeneous approach (Biancale et al. 2007).

2.2 Geodetic GNSS network of stations

Like any other geodetic technique, GNSS, needs to have a reference network of stations for its definition and alignment to a given ITRF. Several categories of GNSS networks exist. In function with the type of use these networks are categorised in:

- *Global GNSS networks*. They are expanded over the whole globe and are mostly used for: reference frame definitions; orbit and clocks, station positions and velocities, EOP parameters products; global deformation studies; global models validations like troposphere, ionosphere etc. A type of this network is the IGS global GNSS network (in **Fig. 2-8**). Their baselines can vary in between 100 km and some thousand km.
- *Regional GNSS networks*. They are expanded over a continent (Europe, Asia, North or South America, Antarctic etc.) and are mostly used for: deformation studies like tectonic plate motion determination; serving as ties to the global network and reference frame; studies of the troposphere and ionosphere etc. Some examples of these networks are: the *European Permanent Network* (EPN) which defines the *European Reference Frame* (EUREF) (http://www.epncb.oma.be) (in **Fig. 2-5**); the US *Continuous Operating Reference Stations* (CORS) network (in **Fig. 2-6**) ; the *Australian Regional GPS Network* (ARGN); the *Asian Pacific Regional Geodetic Project* (APRGP) network etc.

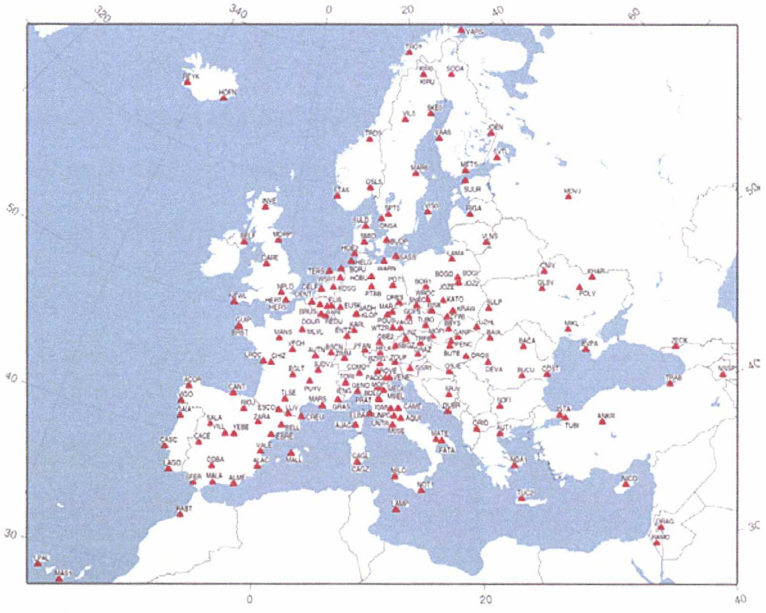

Fig. 2-5 : The EPN/EUREF GPS permanent network

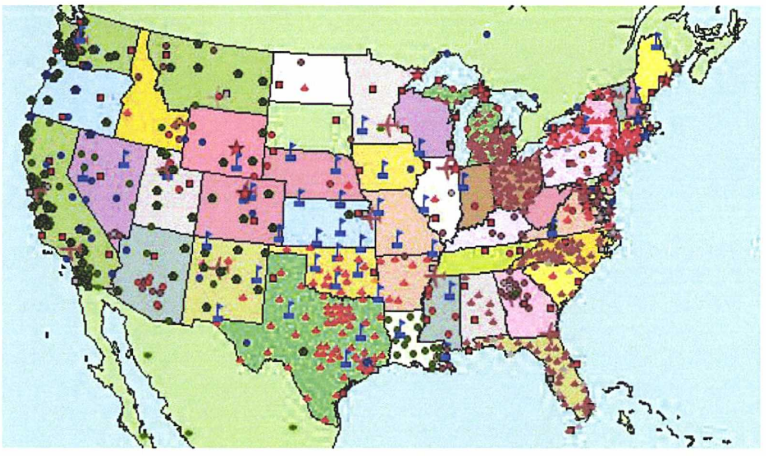

Fig. 2-6 : CORS national stations (source National Geodetic Survey, NGS)

- *National and local GNSS networks*. They are mostly expanded inside the frontiers of a national entity. Their use is concentrated to the needs for : professional uses in topography and cartography, study of the water content in the atmosphere, tomography of the ionosphere, local deformations due to ocean loading or tectonic activities, determination of fault slips, natural hazards risk etc. Examples of these types of networks can be found in many countries like: the French Permanent GPS network (*Reseau GPS Permanent*, RGP (in **Fig. 2-7**) of the *Institute Géographique National* (IGN), the REGAL GPS permanent network a collaboration of Alpine

observatories in order to study the deformations the Alps (in **Fig. 2-7**), the Japanese GEONET, the Swedish SWEPOS, the Swiss AGNES, the German ASCOS and SAPOS, the Austrian APOS, the Hellenic HEPOS etc.

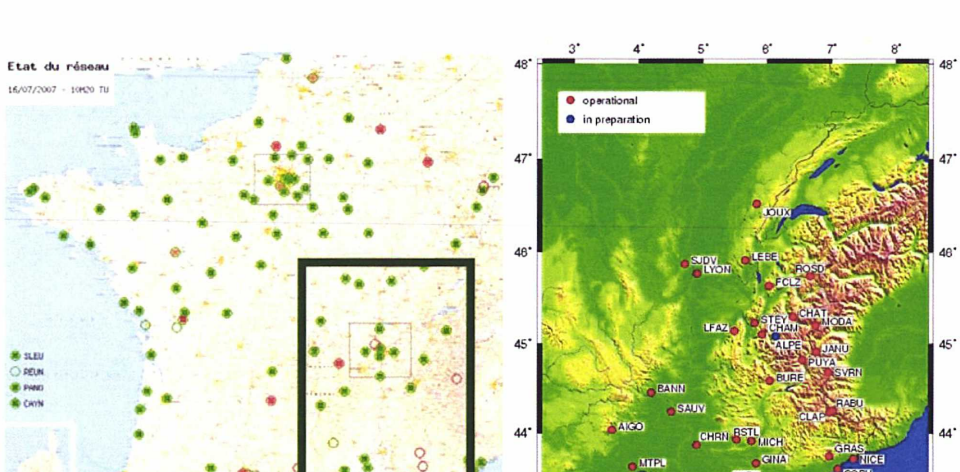

Fig. 2-7 : The *Réseau GPS Permanent* (RGP) of the French *Institute Géographique National* (IGN) (left) and the REGAL permanent GPS network for the tectonic surveillance of the Alpes (right).

- *Dedicated campaign GPS networks*: are all types of local GPS networks which are not permanent. Usually, the data-set of these networks expands from a few days to a few weeks and are used in studies like: the positioning of floating tracers for the calibration of tide gauges or altimetry; the validation of ocean tide models around a specific geographical area; the study of plate tectonics by dedicated campaigns forming a long GPS time-series etc.

2.2.1 The mission of the International GNSS service (IGS)

The official start of the IGS (formerly International GPS Service) took place on the 1st of January 1994. Usually the International Association of Geodesy (IAG) General Meeting in August 1989 in Edinburgh, UK, is considered as the starting point for the IGS.

The current infrastructure of IGS consists of: a global network of permanent GNSS tracking stations (see **Fig. 2-8**), regional data centres, global data centres, *Analysis Centres*

(ACs), *Associate Analysis Centres* (AACs), *Analysis Center Coordinator* (ACC), *Central Bureau* (CB), *Governing Board* (GB) and working groups.

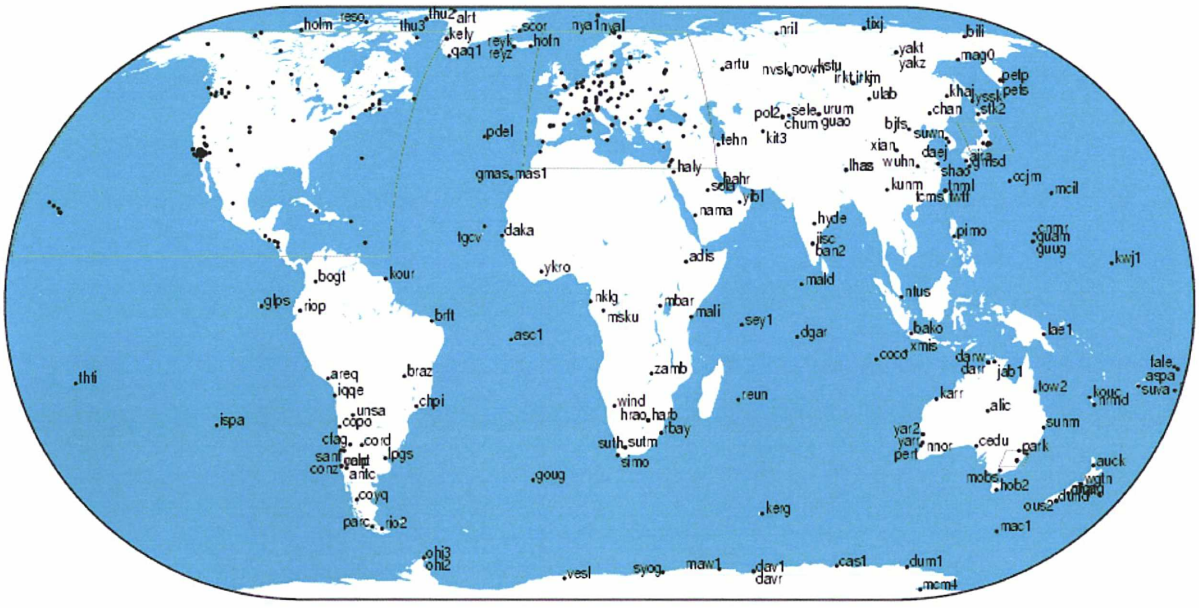

Fig. 2-8 : The IGS tracking stations network at Sept. 4 2007 (Courtesy of IGS)

The primary objective of the IGS is to provide the reference system for a wide variety of scientific and practical applications involving GNSS. To fulfil its role the IGS produces a number of "fundamental" products used in the current Thesis which are:

- Data from a global network of over 380 permanent, geodetic GNSS stations operated by more than 100 worldwide agencies (Dow and Neilan 2006);
- Reference frame products like station time-series, positions and velocities ;
- GPS and GLONASS satellite orbits and clocks and receiver clocks ;
- EOPs;
- Station specific *Tropospheric Zenith Delay* (TZD) parameters ;
- Global ionosphere maps.

The most principal ACs that participate in the production of the IGS reference products are:

- The *Center for Orbit Determination in Europe*, AIUB, Switzerland (CODE)
- The European Space Operations Center, ESA, Germany (ESA)
- The *GeoForschungsZentrum*, Germany (GFZ)
- The *Jet Propulsion Laboratory*, USA (JPL)

- The *National Oceanic and Atmospheric Administration / National Geodetic Survey*, USA (NOAA/NGS)
- The *Natural Resources Canada*, Canada (NRC)
- The *Scripps Institution of Oceanography*, USA (SIO)
- The *U.S. Naval Observatory*, USA (USNO)
- The *Massachusetts Institute of Technology*, USA (MIT)

According to the IGS's strategic plan (Blewitt et al. 2006) its mission statement currently reads as follows: "The International GPS Service is committed to providing the highest quality data and products as the standard for global navigation systems (GNSS) in support of earth sciences research, multi-disciplinary applications, and education. These activities aim to advance scientific understanding of the Earth system components and their interactions, as well as to facilitate other operational applications benefiting society."

2.2.2 GRGS as an analysis center of the IGS

Since the 10th of July 2007 GRGS has entered an evaluation test period in order to become a future IGS AC. GRGS has been producing its own GNSS and reference frame products since 2005: orbits and clocks for GPS satellites, stations positions and velocities. The GNSS products are based on a global sub-network of ~70 GPS IGS stations. For a homogeneous and high quality processing, GINS GNSS software is being used. The today's overall quality of GRGS GPS orbits in terms of agreement when compared to the final IGS sp3 products, is being evaluated and could be better than 5 cm (3D-RMS).

2.3 The GNSS Observations: models and errors

The most important aspects of the observation equations for GPS are reviewed. For more information the reader is referred to, e.g. Xu (2003), Springer (2000), Brockmann (1997), Rothacher (1992). In the mathematical models of this section the following notation is used:

r ..... index of a particular receiver;

s ..... index of a particular satellite;

t ..... signal reception time (GPS time);

τ ..... Signal travelling time between satellite and receiver;

δ_r ..... error of the receiver clock at time t with respect to GPS time;

δ_s ..... error of the satellite clock at time t- τ with respect to GPS time;

t_r ..... reading of the receiver clock at signal reception time; $t_r=t+\delta_r(t)$;

t^s ..... reading of the satellite clock at signal emission time; $t^s=t+\delta^s(t)$;

$\mathrm{x}^s(t-\tau)$ ..... position of satellite s at signal emission time t- τ ;

$\mathrm{x}_r(t)$ ..... position of receiver r at signal reception time t ;

$\rho_r^s(t-\tau,t)$ ..... geometrical distance between satellite s (at the signal emission time t- τ) and receiver r (at signal reception time t) which will contain all errors related to the satellite POD and station displacements

2.3.1 The Code and Phase Observation Equation

Using the known codes p_1 and p_2 and the two phases L_1 and L_2 of GPS the observation equations can be written as follows:

$$
\begin{aligned}
p_{1r}^s(t) &= \rho_r^s(t-\tau,t)+c\delta_r(t)-c\delta^s(t-\tau)+I_r^s(t-\tau,t)+T_r^s(t-\tau,t)+\\
&\quad d_r(t)+d^s(t-\tau)+m_r^s(t-\tau,t)+v_{1r}^s(t)\\
p_{2r}^s(t) &= \rho_r^s(t-\tau,t)+c\delta_r(t)-c\delta^s(t-\tau)+aI_r^s(t-\tau,t)+T_r^s(t-\tau,t)+\\
&\quad d_r(t)+d^s(t-\tau)+m_r^s(t-\tau,t)+v_{2r}^s(t)
\end{aligned}
\qquad \textbf{Eq. 2-6}
$$

$$L_{1r}^{s}(t) = \rho_r^s(t-\tau,t) + c\delta_r(t) - c\delta^s(t-\tau) - I_r^s(t-\tau,t) + T_r^s(t-\tau,t) + d_r(t) + d^s(t-\tau) + m_r^s(t-\tau,t) - \lambda_1 N_{1r}^s(t-\tau,t) + v_{1r}^s(t)$$

$$L_{2r}^{s}(t) = \rho_r^s(t-\tau,t) + c\delta_r(t) - c\delta^s(t-\tau) - aI_r^s(t-\tau,t) + T_r^s(t-\tau,t) + d_r(t) + d^s(t-\tau) + m_r^s(t-\tau,t) - \lambda_2 N_{2r}^s(t-\tau,t) + v_{2r}^s(t) \qquad \textbf{Eq. 2-7}$$

Where:

c is the light speed; $c\delta_r(t)$ and $c\delta^s(t-\tau)$ are the receiver's and satellites' clock errors (in meters) respectively ; $I_r^s(t-\tau,t)$ is the signal delay and respectively the phase advance due to the free electrons in the Earth's atmosphere and as a dispersive medium the refractive index of the GPS signals is frequency dependent with $\alpha = \frac{f_1^2}{f_2^2} \approx \left(\frac{154 f_0}{120 f_0}\right)^2 = 1.647$; $T_r^s(t-\tau,t)$ is the tropospheric refraction and the effect is the same for both code and phase (does not depend on the frequency) ; $d_r(t)$ and $d^s(t-\tau)$ are instrumental internal time delays in the receiver and the satellite; $m_r^s(t-\tau,t)$ is the multipath effect; $v_{1,2r}^s(t)$ are random errors in the code and phase ; $N_{1,2r}^s(t-\tau,t)$ is the unknown integer number of cycles or else called the integer phase ambiguity.

2.3.2 Linear combinations of phases and codes

In order to eliminate some of the effects in **Eq. 2-6** and **2-7** we may form differences or combinations of the original observations equations.

2.3.2.1 Single (SD) and Double differences (DD)

The *Single Differences* (SD) is the linear combination that eliminates: the satellites clock error if the combination is between two stations r_A, r_B and one satellite *s*; the receiver's clock error if the combination is between two satellite and one stations; the carrier phase ambiguity if the combination is at two different epochs between a satellite and one station.

$$L^{s}_{r_A r_B}(t) \equiv L^{s}_{r_B}(t) - L^{s}_{r_A}(t) \qquad \textbf{Eq. 2-8}$$

The *Double Differences* (DD) is a linear combination of simultaneous measurements or the linear combination of two single difference measurements at the same epoch (**Fig. 2-9**).

$$L^{s_i s_k}_{r_A r_B} = L^{s_k}_{r_A r_B} - L^{s_i}_{r_A r_B} \qquad \textbf{Eq. 2-9}$$

In this linear DD observation both the satellite and receiver clocks effects are eliminated or extremely minimised.

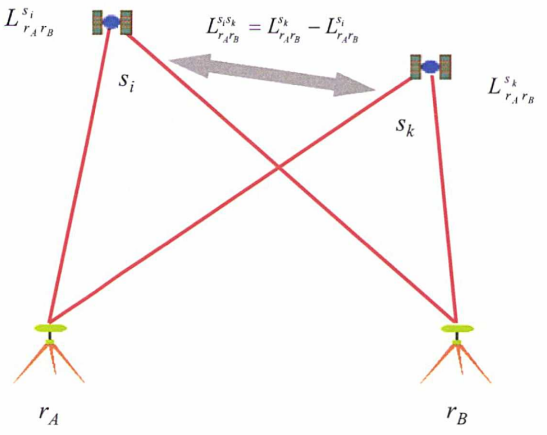

Fig. 2-9 : The Double Differences of Single Differences

The synthetic observations such as the SD and DD are correlated and their variance-covariance matrix and weight matrix will not be diagonals. According, to the error propagation law if b are the linearized model of observations with $C_b = \sigma^2 I$ their variance-covariance matrix, the synthetic observations b' will have $C_{b'} = DC_bD^T$ as a variance-covariance matrix.

For the case of two SD we will have:

$$\mathrm{b}_{1_{SD}} = \begin{bmatrix} L^{s_A}_{r_A r_B} \\ L^{s_B}_{r_A r_B} \end{bmatrix} = \begin{bmatrix} -1 & 1 & 0 & 0 \\ 0 & 0 & -1 & 1 \end{bmatrix} \begin{bmatrix} L^{s_A}_{r_A}(t) \\ L^{s_A}_{r_B}(t) \\ L^{s_B}_{r_A}(t) \\ L^{s_B}_{r_B}(t) \end{bmatrix} = \mathrm{D}_{1_{SD}} \mathrm{b}_0 \qquad \textbf{Eq. 2-10}$$

$$\mathrm{C}_{\mathrm{b}_{1_{SD}}} = \mathrm{D}_{1_{SD}} \mathrm{C}_{\mathrm{b}_0} \mathrm{D}^T_{1_{SD}} = 2\sigma^2 \mathrm{I}_2$$

And for the case of two DD of the same epoch with one satellite in common it will be:

$$\mathrm{b}_{2_{DD}} = \begin{bmatrix} L^{s_A s_B}_{r_A r_B} \\ L^{s_A s_C}_{r_A r_B} \end{bmatrix} = \begin{bmatrix} -1 & 1 & 0 \\ -1 & 0 & 1 \end{bmatrix} \begin{bmatrix} L^{s_A}_{r_A r_B} \\ L^{s_B}_{r_A r_B} \\ L^{s_C}_{r_A r_B} \end{bmatrix} = \mathrm{D}_{2_{DD}} \mathrm{b}_{1_{SD}} \qquad \textbf{Eq. 2-11}$$

$$\mathrm{C}_{\mathrm{b}_{2_{DD}}} = \mathrm{D}_{2_{DD}} \mathrm{C}_{\mathrm{b}_{1_{SD}}} \mathrm{D}^T_{2_{DD}} = 2\sigma^2 \begin{bmatrix} 2 & 1 \\ 1 & 2 \end{bmatrix}$$

2.3.2.2 The ionosphere-free combination (L_3)

From **Eq. 2-6** and **2-7** ionosphere-free (iono-free) combinations can be formed

$$\begin{aligned} L_3 &= \frac{\lambda_2^2}{\lambda_2^2 - \lambda_1^2} L_1 - \frac{\lambda_1^2}{\lambda_2^2 - \lambda_1^2} L_2 = \frac{f_1^2}{f_1^2 - f_2^2} L_1 - \frac{f_2^2}{f_1^2 - f_2^2} L_2 = \\ &= \frac{77^2}{17 \cdot 137} L_1 - \frac{60^2}{17 \cdot 137} L_2 \\ &= 2.5457\, L_1 - 1.5457\, L_2 \end{aligned} \qquad \textbf{Eq. 2-12}$$

The wavelength of this combination is $\lambda_3 = 6.3$ mm. The same relations are valid for the ionosphere-free ambiguity N_3. The ionospheric path delay is practically eliminated. It is the main combination used in the un-differenced and DD level.

2.3.2.3 The wide-lane combination (L_{WL})

The wide-lane combination has the advantage to create a synthesized observable with a very big wavelength of $\lambda_{WL} = 86.19$ cm which favourizes small errors $\frac{\sigma_{L_{WL}}}{\lambda_{WL}}$ in the estimation of

the integer ambiguity cycles N_{WL} from this combination. It is often used for ambiguity resolution on the DD level.

$$L_{WL} = \frac{1}{\lambda_2 - \lambda_1}(\lambda_2 L_1 - \lambda_1 L_2) = \frac{1}{17}(77L_1 - 60L_2) \qquad \textbf{Eq. 2-13}$$
$$N_{WL} = N_1 - N_2$$

2.3.2.4 The narrow-lane combination (L_{NL})

The narrow-lane combination is:

$$L_{NL} = \frac{1}{\lambda_1 + \lambda_2}(\lambda_2 L_1 + \lambda_1 L_2) = \frac{1}{137}(77L_1 + 60L_2) \qquad \textbf{Eq. 2-14}$$

The wavelength ($\lambda_{NL} = \frac{c}{(f_1 + f_2)} = \frac{\lambda_1 \lambda_2}{\lambda_1 + \lambda_2} = 10.71\,\text{cm}$) of this combination is useful when we want to estimate the ambiguities of the DD iono-free combination.

2.3.2.5 The ionospheric geometry-free combination (L_{ion})

This combination is independent of receiver or satellite clocks and geometry (orbits, station coordinates). It only contains the ionosphere delay and the initial phase ambiguities. It is very well suited for the estimation of ionospheric models and for cleaning un-differenced data (Springer 2000). It is used in geophysical studies for the detection of disturbances in the ionosphere. Furthermore, it can be very useful for the detection of cycle slips in high state dynamics situations; for instance when we want to determine the positions of a moving vessel and a floating tracer in the open ocean.

$$L_{ion} = L_{NL} - L_{WL} = -\frac{2\lambda_1 \lambda_2}{\lambda_2^2 - \lambda_1^2}(L_1 - L_2) = -\frac{2 \cdot 60 \cdot 77}{17 \cdot 137}(L_1 - L_2) \qquad \textbf{Eq. 2-15}$$

2.3.2.6 Combinations for Ambiguity determination

The iono-free ambiguity from **Eq. 2-12** can be written as:

$$\begin{aligned} N_3 &= \frac{f_1^2}{f_1^2 - f_2^2}\lambda_1 N_1 - \frac{f_2^2}{f_1^2 - f_2^2}\lambda_2 N_2 \\ &= \frac{c}{f_1^2 - f_2^2}\left(f_1 N_1 - f_2 N_2\right) \\ &= \frac{c f_2}{f_1^2 - f_2^2} N_{WL} + \frac{c}{\left(f_1 + f_2\right)} N_1 \end{aligned} \qquad \textbf{Eq. 2-16}$$

Then by using the *Melbourne-Wübbena* (Melbourne 1985) combination:

$$L_{MW} = -\frac{1}{\lambda_1 + \lambda_2}(\lambda_2 p_1 + \lambda_1 p_2) + \frac{1}{\lambda_2 - \lambda_1}(\lambda_2 L_1 - \lambda_1 L_2) \equiv L_{WL} - P_{NL} \qquad \textbf{Eq. 2-17}$$

We can estimate a-priori values for the wide-lane ambiguity. From **Eq. 2-13** we get:

$$\begin{aligned} L_{MW} &= -\lambda_{MW}(N_1 - N_2) \\ &= -\lambda_{MW} N_{WL} \end{aligned} \qquad \textbf{Eq. 2-18}$$

Where $\lambda_{MW} = \frac{\lambda_1 \lambda_2}{\lambda_2 - \lambda_1} = 86.19 = \lambda_{WL}$

By introducing this correction for the ambiguities of the wide-lane combination in **Eq. 2-16,** an initial estimate for the N_1 ambiguity can be obtained.

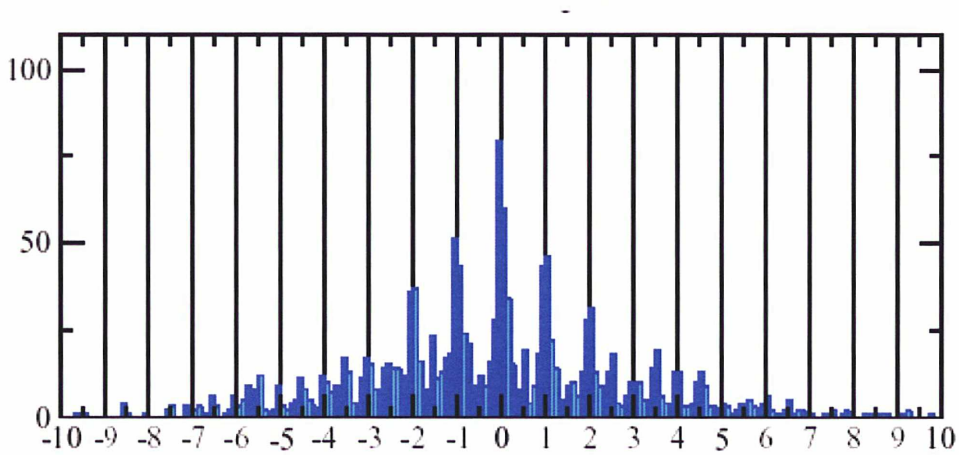

Fig. 2-10 : Distribution of the wide-lane ambiguities N_{WL} (in cycles) (source Noveltis)

Next, the best combination of wide-lane and N_1 ambiguities that gives the estimation of the ionosphere-free N_3 ambiguity the closet to an integer value is investigated. Once the

space of the difference of the fixed iono-free ambiguity minus the real one has been checked for an upper bound (divided by the narrow lane wavelength) and the relative standard deviation of two successive combinations is more than 50% then the iono-free ambiguity will be fixed. An example of N_{WL} ambiguities distribution around their integer values in terms of a cycle can be seen in **Fig. 2-10**.

This is the main philosophy of the *Quasi Ionosphere Free* (QIF) ambiguity fixing strategy which it has been implemented in Bernese (Hugentobler et al. 2001) and in GINS software. For more details on this type of ambiguity fixing, by the use of the linear combinations, look in Hugentobler et al. (2001), Blewitt (1989) and Dong and Bock (1989).

2.3.2.7 New GNSS signals, new combinations

As previously mentioned in **Chapter 1**, with the arrival of Galileo, the three frequencies in GPS and GLONASS and the four in Compass a whole new horizon for new linear combinations between GNSS frequencies has opened.

For instance, the use of triples frequencies will allow for *Three Carrier Ambiguity Resolutions* (TCAR) to be achieved with only observations in the line-of-sight (un-differenced) instead of double differences. In parallel there will be benefits for multipath detection. Till now no single-station multipath from dual phase observables exists. The only known way to extract multipath information is through residuals of short baseline processing (Estey and Meertens 1999). This method requires two stations and has the major drawback that residuals are not referred to individual satellites and multipath errors might get mixed if the stations are too close together. The triple-frequency phase combinations provide a valuable indication of phase multipath from single-station data, which is not available in today's two-frequency GNSS. The limitation of this indicator is that multipath for individual frequencies cannot be extracted as is the case for variations in the code observables (Simsky 2006).

According to Wübenna (2007) all the aforementioned linear combinations will be based in the following model:

$$L_{n,m,k} = \lambda_{comb}\left(\frac{n_1}{\lambda_1}L_1 + \frac{n_2}{\lambda_2}L_2 + \frac{n_3}{\lambda_3}L_3 \ldots.\right) \qquad \textbf{Eq. 2-19}$$

Where: n,m,k are integer coefficients. The apparent frequency f_{comb} and wavelength λ_{comb} will also be a function of these coefficients.

$$f_{comb} = n_1 \cdot f_1 + n_2 \cdot f_2 + n_3 \cdot f_3 + ...$$
$$\lambda_{comb} = \frac{1}{\frac{n_1}{\lambda_1} + \frac{n_2}{\lambda_2} + \frac{n_3}{\lambda_3} + ...} \qquad \textbf{Eq. 2-20}$$

So if we consider all the signals from the four GNSS described in **Table 1-6** we can form several combinations for wide lanes and narrow lanes, or with big wavelengths or even more combinations with low ionospheric influence such as:

Table 2-1 : The GPS three frequency combinations. The M-Iono is the ionosphere amplification factor relative to L_1 and sigma-L_{comb} is the final noise of the synthetic phase

n1	n2	n3	λ_{comb} (m)	M-Iono (cycles)	M-Iono	sigma-L_{comb} (m)
1	0	0	0,1903	1	1	0,0019
0	1	0	0,2442	1,2833	1,6469	0,0024
0	0	1	0,2548	1,3391	1,7933	0,0025
Wide Lanes						
1	-1	0	0,8619	-0,2833	-1,2833	0,0122
0	1	-1	5,8610	-0,0558	-1,7186	0,0829
1	0	-1	0,7514	-0,3391	-1,3391	0,0106
Narrow Lanes						
1	1	0	0,1070	2,2833	1,2833	0,0015
0	1	1	0,1247	2,6225	1,7186	0,0018
1	0	1	0,1089	2,3391	1,3391	0,0015
Low Ionosphere						
4	0	-3	0,1081	-0,0174	-0,0099	0,0054
4	-1	-2	0,1102	0,0384	0,0222	0,0050
Big Wavelength						
1	-2	1	1,0105	-0,2275	-1,2083	0,0248
1	-3	1	-0,3220	-1,5109	2,5569	-0,0107
1	-4	3	1,5424	-0,1159	-0,9397	0,0786
1	-5	4	2,0932	-0,0601	-0,6616	0,1357

Table 2-2 : The GLONASS three frequency combinations. The M-Iono is the ionosphere amplification factor relative to L_1 and sigma-L_{comb} is the final noise of the synthetic phase

n1	n2	n3	λ_{comb} (m)	M-Iono (cycles)	M-Iono	sigma-L_{comb} (m)
1	0	0	0,1863	1	1	0,0019
0	1	0	0,2402	1,2893	1,6623	0,0024
0	0	1	0,2502	1,343	1,8036	0,0025
Wide Lanes						
1	-1	0	0,8302	-0,2893	-1,2893	0,0117
0	1	-1	6,0098	-0,0537	-1,7315	0,0850
1	0	-1	0,7295	-0,343	-1,3430	0,0103
Narrow Lanes						
1	1	0	0,1049	2,2893	1,2893	0,0015
0	1	1	0,1225	2,6323	1,7315	0,0017
1	0	1	0,1068	2,3430	1,3430	0,0015

Table 2-3 : The Compass four frequency combinations. The M-Iono is the ionosphere amplification factor relative to L_1 and sigma-L_{comb} is the final noise of the synthetic phase

n1	n2	n3	n4	λ_{comb} (m)	M-Iono (cycles)	M-Iono	sigma-L_{comb} (m)
1	0	0	0	0,1886	1	1	0,0019
0	1	0	0	0,1920	1,0183	1,0370	0,0019
0	0	1	0	0,2363	1,2532	1,5706	0,0024
0	0	0	1	0,2483	1,3169	1,7344	0,0025
Wide Lanes							
1	-1	0	0	10,4676	-0,0183	-1,0183	0,1480
0	1	-1	0	1,0247	-0,2349	-1,2762	0,0145
1	0	-1	0	0,9333	-0,2532	-1,2532	0,0132
1	0	0	-1	0,7836	-0,3169	-1,3169	0,0111
0	1	0	-1	0,8470	-0,2986	-1,3411	0,0120
0	1	0	0	0,1920	1,0183	1,0370	0,0019
0	0	1	-1	4,8842	-0,0637	-1,6504	0,0691
Narrow Lanes							
1	1	0	0	0,0951	2,0183	1,0183	0,0013
0	1	1	0	0,1059	2,2716	1,2762	0,0015
1	0	1	0	0,1049	2,2532	1,2532	0,0015
1	0	0	1	0,1072	2,3169	1,3169	0,0015
0	1	0	1	0,1083	2,3353	1,3411	0,0015
0	1	0	0	0,1920	1,0183	1,0370	0,0019
0	0	1	1	0,1211	2,5702	1,6504	0,0017

Table 2-4 : The Galileo five frequency combinations. The M-Iono is the ionosphere amplification factor relative to L_1 and sigma-L_{comb} is the final noise of the synthetic phase

n1	n2	n3	n4	n5	λ_{comb} (m)	M-Iono (cycles)	M-Iono	sigma-L_{comb} (m)
1	0	0	0	0	0,1903	1	1	0,0019
0	1	0	0	0	0,2344	1,232	1,5178	0,0023
0	0	1	0	0	0,2483	1,3051	1,7032	0,0025
0	0	0	1	0	0,2515	1,3217	1,7468	0,0025
0	0	0	0	1	0,2548	1,3391	1,7933	0,0025
Wide Lanes								
1	-1	0	0	0	1,0105	-0,2320	-1,2320	0,0143
0	1	-1	0	0	4,1865	-0,0731	-1,6079	0,0592
1	0	-1	0	0	0,8140	-0,3051	-1,3051	0,0115
1	0	0	-1	0	0,7819	-0,3217	-1,3217	0,0111
1	0	0	0	-1	0,7514	-0,3391	-1,3391	0,0106
0	1	0	-1	0	3,4558	-0,0897	-1,6283	0,0489
0	1	0	0	-1	2,9305	-0,1071	-1,6498	0,0414
0	0	1	-1	0	19,8014	-0,0166	-1,7249	0,2800
0	0	1	0	-1	9,7684	-0,0340	-1,7477	0,1381
0	0	0	1	-1	19,2793	-0,0175	-1,7699	0,2726
Narrow Lanes								
1	1	0	0	0	0,1050	2,2320	1,2320	0,0015
0	1	1	0	0	0,1206	2,5371	1,6079	0,0017
1	0	1	0	0	0,1077	2,3051	1,3051	0,0015
1	0	0	1	0	0,1083	2,3217	1,3217	0,0015
1	0	0	0	1	0,1089	2,3391	1,3391	0,0015
0	1	0	1	0	0,1213	2,5537	1,6283	0,0017
0	1	0	0	1	0,1221	2,5711	1,6498	0,0017
0	0	1	1	0	0,1250	2,6267	1,7249	0,0018
0	0	1	0	1	0,1258	2,6442	1,7477	0,0018
0	0	0	1	1	0,1266	2,6608	1,7699	0,0018
Low Ionosphere								
5	-3	1	-4	2	0,1058	0,0007	0,0004	0,0078
4	0	1	-3	-1	0,1088	0,0010	0,0006	0,0057
4	0	0	-1	-2	0,1087	0,0001	0,0000	0,0050
3	3	0	0	-5	0,1119	0,0003	0,0002	0,0073
Big Wavelength								
1	-3	1	-3	4	3,9389	0,0006	0,0129	0,2363
0	2	-5	-2	5	14,9522	-0,0091	-0,7145	1,1387
0	1	-1	-4	4	31,8589	-0,0032	-0,5370	1,8577
0	1	-2	-1	2	11,8168	-0,0216	-1,3394	0,3737

2.3.3 GNSS orbit errors

The effect of an orbit error $d\rho$ on an estimated baseline component is given by the following "rule of thumb" (Springer 2000):

$$dx \approx d\rho \frac{b}{\rho} \qquad \textbf{Eq. 2-21}$$

Where b and dx are baseline length and baseline component error and $d\rho$, ρ are orbit error and satellite distance respectively.

The accelerations that perturb the orbit of a GPS satellite and add errors in its final positions are:

- Earth's oblateness (C_{20}) ;
- Non-sphericity of the Earth gravity potential ;
- The Moon-Sun and Planets gravitational acceleration ;
- The solar radiation pressure;
- The Earth's solid and ocean tides ;
- Relativistic effects ;
- The Earth's albedo ;
- The satellite's thermal re-emission ;

The evaluation of the precision in GNSS POD can de accomplished through comparisons to an external reference. For instance, the estimated GPS orbits can be evaluated by a simple comparison to the more precise IGS sp3 orbits (see §2.2.1). An example of such comparison is the GRGS evolution of the GPS POD in 2 years from ~20 cm to ~10 cm 3D-RMS with respect to the IGS final orbits, applying all the necessary perturbation corrections previously mentioned (can be seen in **Fig. 2-11**).

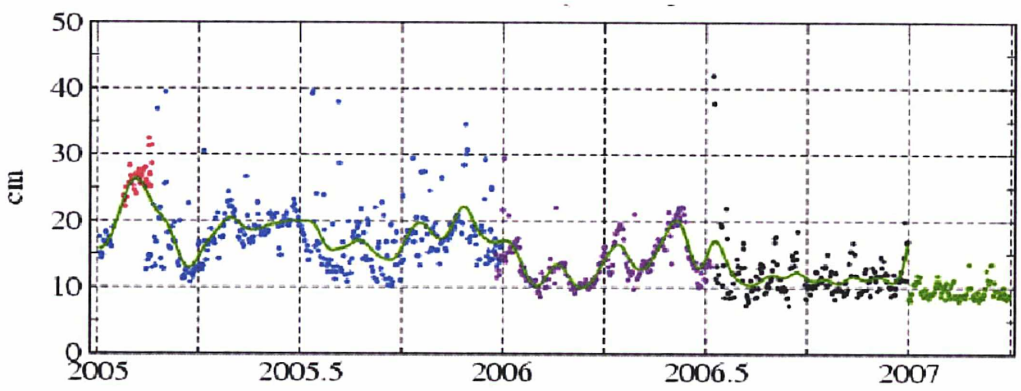

Fig. 2-11 : GPS orbit overlaps from GRGS vs IGS comparison

The perturbation forces are mainly separated in two big categories: the gravitational and non-gravitational ones. Today the influences of these forces on the GNSS satellites are very well modelled. Nonetheless, the most important non-gravitational force that of the *Solar Radiation Pressure* (SRP), is still under investigation. A study of inter-model comparison as well as the impact on the POD of the GNSS satellites will be presented in § **3.2.2.1**.

2.3.4 Observational model errors of GNSS

Since May, 2, 2000 the *Selective Availability* (SA), a mean of degradation of the GPS signals' precision, has been shut off under the U.S. DoD's policy. When SA was active three types of data were degraded: the broadcast orbital information, the broadcast value of the satellite clock offset and the satellite oscillator frequency. The most important one was the dithering of the frequency of the satellite oscillator which was directly affecting the phase observables used in geodesy (Feigl et al. 1991).

Double and single differences or linear combinations on the same frequency have the advantage to eliminate a certain number of "nuisance parameters" that would reduce the precision of the GNSS observations but not all. On the other side in Precise Point Positioning applications (Cao and Chen 2004, Cheng et al. 2002, Héroux and Kouba 2001, Kouba and Héroux 2000, Zumberge et al. 1997), the presence of precise satellite clocks offset values and the estimation of station clocks are unavoidable. Consequently, the exact knowledge of hardware or environmental related error models becomes mandatory.

These errors appear in the pre-processing stage and can be detected through raw-data snooping procedures or during the estimation phase of the final coordinate GPS time-series

and can be compensated with the introduction of proper ad-hoc error functions in the observational model.

For instance, cycle slips and clock jumps are one of the most significant sources of systematic errors in the GPS observations and proper corrections must be applied at the pre-processing level. Examples of such corrections applied in real data sets are presented in the following sections. Additionally, satellite orbit errors, propagation effects, clock errors, relativistic effects, antenna phase center variations, antenna rotations (phase wind-up) and multipath, all provoke systematic and random effects on the phase and code pseudo-ranges during the main processing scheme of a GNSS coordinate time-series solution. A description on some of these effects and notably troposphere, ionosphere and antenna phase center variations is given in the following.

2.3.4.1 Clock Jumps

Clock jumps are provoked from poor performance receiver oscillators which deviate from the GPS time scale (or UTC). For instance a clock jump of 1ms will provoke a discontinuity of ~300km on the code observables and an integer number of cycles in the phase observables: 1575420 for L1 and 1227600 for L2. The clock will reset in order to be kept within 1 ms of the nominal sampling time. Both the recorded time and the pseudo-range and phase measurements will show a discontinuity corresponding to 1 ms. Theses discontinuities should be removed by applying corrections. One way is as follows: from **Eq. 2-6** the pseudo-range from the known codes is:

$$p_r^s = c\left(\left(t+\delta_r\right)-\left(t-\tau+\delta^s\right)\right) \qquad \textbf{Eq. 2-22}$$

The jumps are recorded in δ_r. The corrections to the observables will be $c\cdot\delta_r$ for the code and $f\cdot\delta_r$ for the phase. Where $c = 2.99792458e+08$ m/sec is the velocity of light, and f the frequency in L_1 or L_2.

Let us examine 5 separate cases where the impact of these clock jumps on the observables of the phases and codes is quantified:

- 1st Case: The GPS station BRST (Brest, France).

The receiver of this station is a Trimble 4000SSI and the time record inside the RINEX file for day-of-year 197 2004 shows that the receiver's clock effectuates 1 ms resets every 1 h (**Fig. 2-12**).

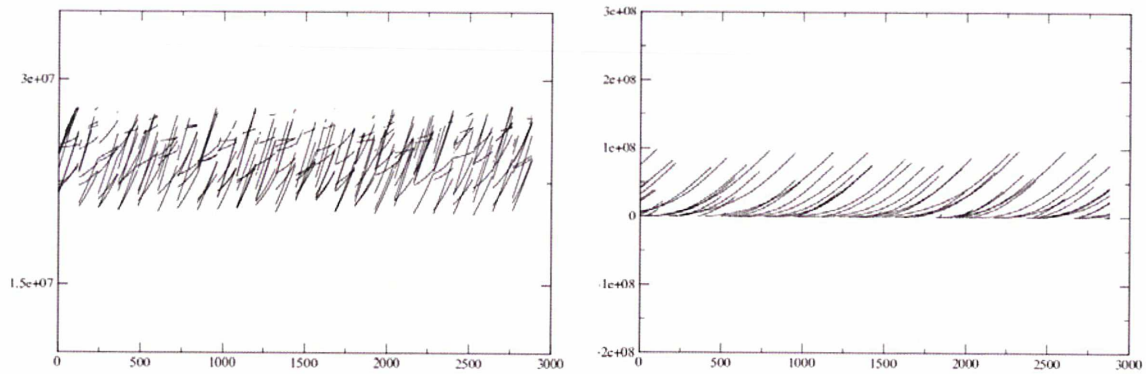

Fig. 2-12 : BRST: (left) C1 pseudo-range; clock jumps are visible every hour. (Right) L1 observable; the clock's resets provoke interruptions in the satellites passages every hour. Y-axis units are in meters for C1 and cycles for L1. X-axis units are epochs for 30s acquisition time of doy 197

- 2nd Case: The GPS station ZIMM (Zimmerwald, Switzerland).

The station's receiver is a Trimble 4700. The time record in the RINEX file does not present any discontinuities. Nonetheless, by observing carefully the observables for the code and phase in **Fig. 2-13,** we immediately see several jumps on C1 and none for L1.

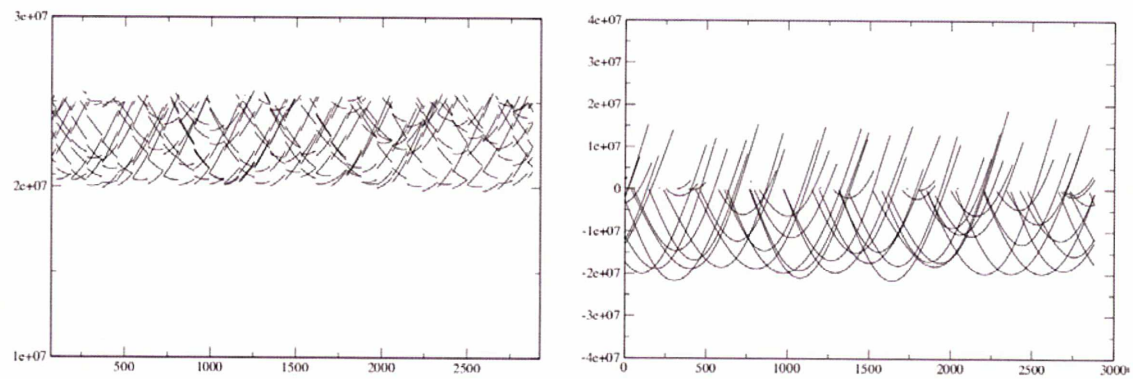

Fig. 2-13 : ZIMM: (left) C1 pseudo-range; clock jumps are visible every hour. (Right) L1 observable; the clock's resets do not seem to have an effect on the phase observable. Y-axis units are in meters for C1 and cycles for L1. X-axis units are epochs for 30s acquisition time of doy 197

It seems that the record time of the RINEX file has been corrected except for the C1 observables. In order to further apply the standard correction (multiplied by the jump) on each observable we will have to artificially add the jumps in the phases or in the ambiguities. Though, the first choice is preferable. If in any case these corrections have been applied already, then in the resulting ambiguities we will notice large standard deviations.

- 3rd Case: The GPS Station PALM (Palmer, Antarctica)

An Ashtech Z-XII3 receiver is used for this station. It records data every second. It is being used as a reference station for the altimetric cross-validation experiment south of the Drake Passage (see **Chapter 5**). No discontinuities are observed inside the RINEX file neither during the screening of the phase and code observables as illustrated in **Fig. 2-14**. The clock of this receiver behaves normally.

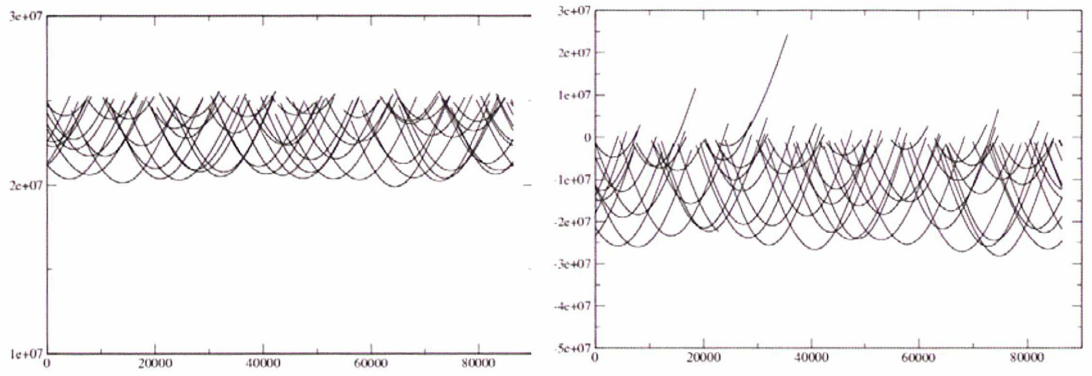

Fig. 2-14 : PALM: (left) P1 pseudo-range; no clock jumps exist. (Right) L1 observable; Y-axis units are in meters for P1 and cycles for L1. X-axis units are epochs for 1s acquisition time of doy 017 2006.

- 4th Case: The GPS Buoys BOHI (Antarctica) and BS07 (Drake campaign)

The receiver is a Trimble 1249 for BOHI and a Trimble 5700 for BS07. During the Drake campaign we recorded data from a GPS buoy deployed near the peninsula of O'Higgins (BOHI) and we used the estimated sea surface height (SSH) observations in order to compare them to a bottom pressure tide gauge and altimetry from Jason-1 on doy 028, 2006. The BS07' sea state estimates have served as a reference surface definition for the ship's floating line determination during the doy 017, 2006. From the BOHI session we recorded a total of ~4 hours from 06 1 28 13 23 32.0000000 to 06 1 28 17 23 10.9950000. From the epoch 06 1 28 13 56 39.9990000 till the end of the session, the receiver's clock has deviated continuously by about 4 ms from the GPS time (UTC) without any clock adjustments. This

has an immediate trend-like effect on the code and phase observables as it can be seen in **Fig. 2-15.**

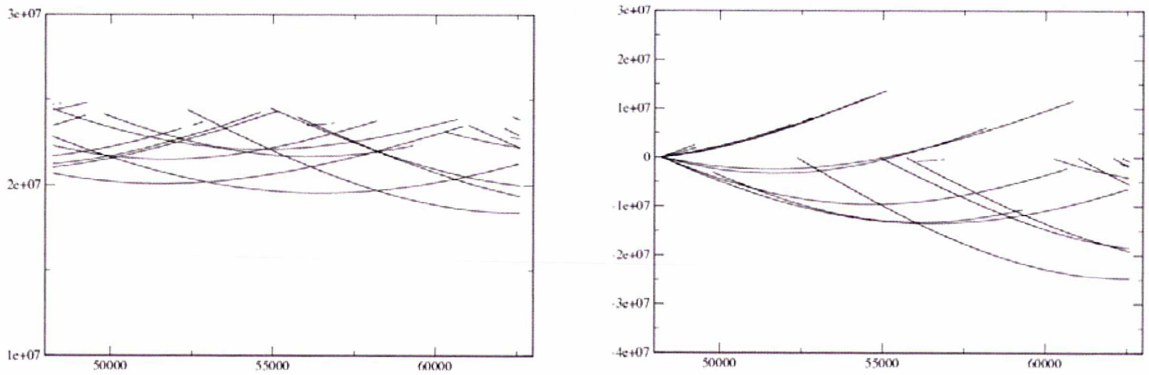

Fig. 2-15 : BOHI: (left) C1 pseudo-range; no clock jumps exist but for a trend. (Right) L1 observable the same trend exists here; Y-axis units are in meters for C1 and cycles for L1. X-axis units are epochs for 1s acquisition time from epochs 06 1 28 13 23 32.0000000 to 06 1 28 17 23 10.9950000.

The BS07 session took place in a higher dynamic state environment. We recorded data in the open ocean from 06 1 17 16 56 53.0000000 to 06 1 17 18 4 15.0000000. No ms clock jumps were observed in the record time of the RINEX file but eventually two well referenced jumps exist in the code and in the phase observables as can be seen in **Fig. 2-16**.

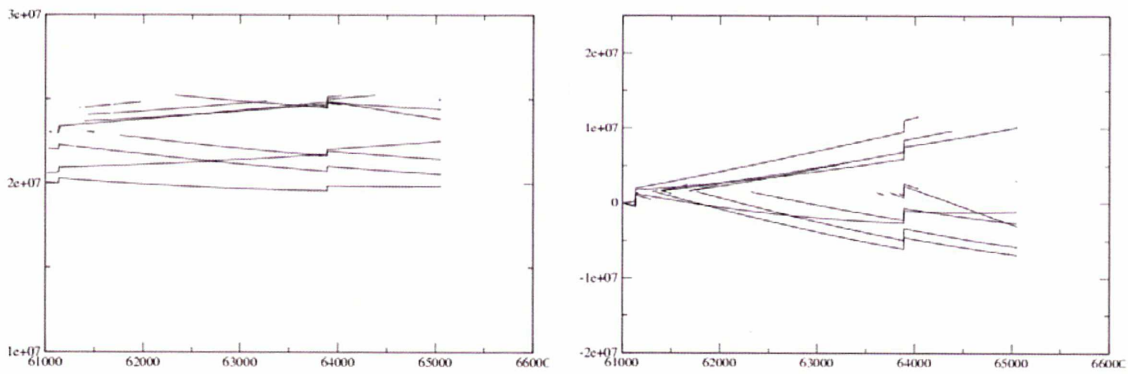

Fig. 2-16 : BS07: (left) C1 pseudo-range; two distinctive clock jumps exist. (Right) L1 observable the same two jumps exists here; Y-axis units are in meters for C1 and cycles for L1. X-axis units are epochs for 1s acquisition time from epochs 06 1 17 16 56 53.0000000 to 06 1 17 18 4 15.0000000.

2.3.4.2 Cycle slips

Cycle slips are integer discontinuities in the carrier phase data caused by receivers loosing lock on GPS signals. A prerequisite to high precision GPS-based geodesy is the reliable detection and where possible, correction of cycle slips (Blewitt 1990).

For detection and reparation of cycle slips several algorithms exist (Kleusberg et al. 1993, Lichtenegger and Hofmann-Wellenhof 1990, Bastos and Landau 1988, Han 1997, Collin and Warnant 1995).

One of the most frequently used is that of the higher order time differences of the raw data time-series. The scheme consists of forming the differences of the multiples of a certain polynomial order n as $\Delta^{n+1}L_k = \Delta^n L_k - \Delta^n L_{k-1}$. The main disadvantages of this method are that data-set-specific tolerance values have to be set (time differences that are greater than the tolerances indicate the presence of a cycle slip). As GNSS data at the observation level contain noise, the efficient detection of a cycle slip will be a function of it. For instance, synthesised data of linear combinations can be used for the formation of theses finite differences. As such any eventual perturbations due to nuisance parameters (e.g. ionosphere) will be eliminated and cycle slips can be detected above the noise level of the data time-series. But this is not always the case for all combinations and all types of data as we will see in the following examples. This method is currently implemented in the GINS GNSS software.

As an example, in **Fig. 2-17** I present the 4th order time differences of each data-set of the previously mentioned GPS stations (BRST, ZIMM, PALM, BOHI, BS07) by forming at every case the synthetic observations from:

- the Melbourne-Wübenna (**Eq. 2-17**) combination;
- the ionosphere-free combination (**Eq. 2-12**);
- the ionospheric geometry-free combination (**Eq. 2-15**);

The time differences of the L_{MW} combination present a rather high noise level (left column of **Fig. 2-17**). Firstly, at the stations that are in motion (MW combination is independent from geometry) like BOHI (**Fig. 2-17a**) and BS07 (**Fig. 2-17b**), the noise is ~10 m. This reflects the fact that both receivers make use of the less precise C1 code. The same is the case for the stable stations like BRST (**Fig. 2-17d**) and ZIMM (**Fig. 2-17e**).

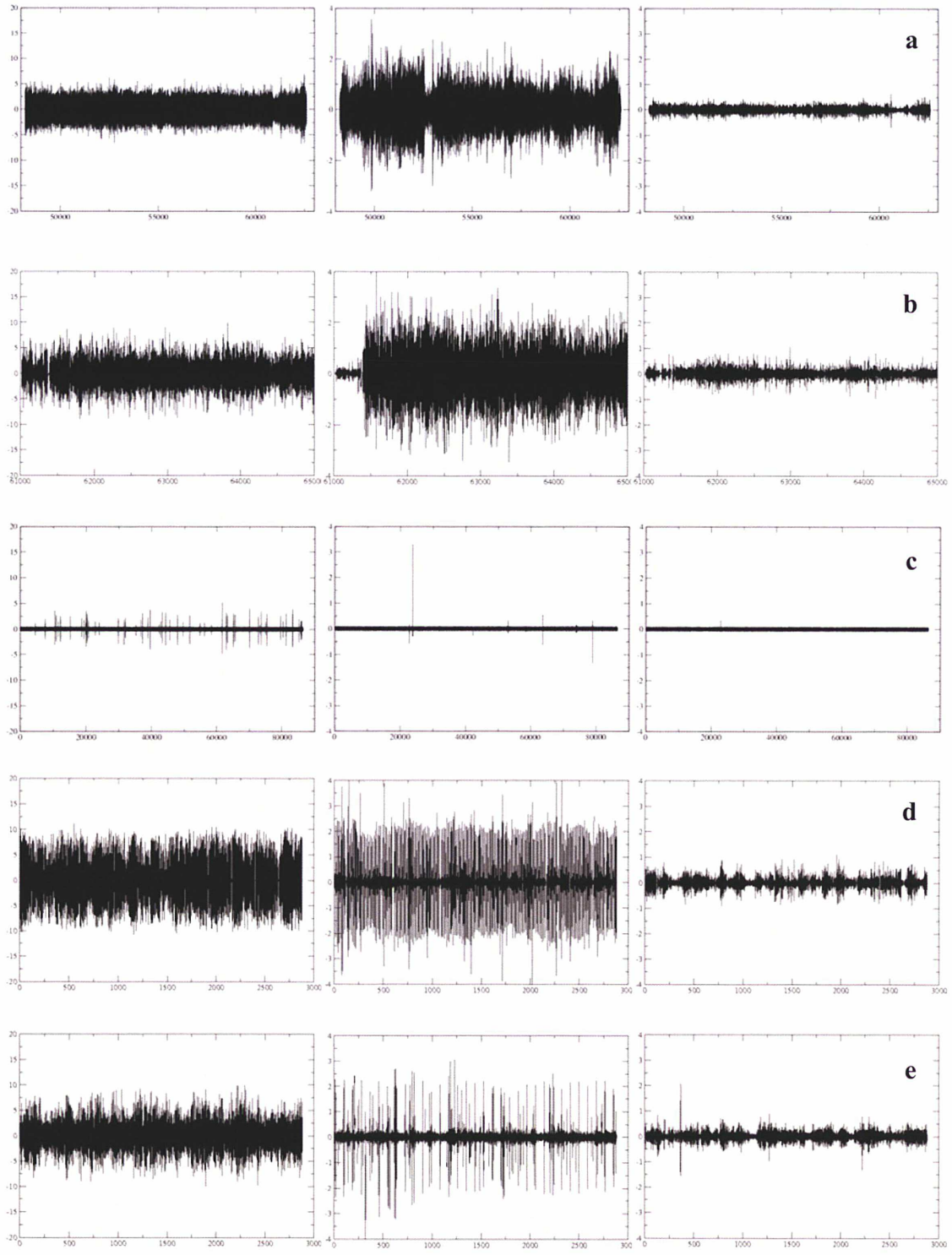

Fig. 2-17 : (a) BOHI, (b) BS07, (c) PALM, (d) BRST, (e) ZIMM, (Left column) Melbourne-Wübenna : L_{WM}, (Center column) Iono-free : L_3, (Right column) Geometry free L_{ion}. Y-units are in meters and X-axis units are in epochs of 30s or 1s.

The noise is smaller at PALM because it has the only receiver among these stations that is using the more precise P1 code. Immediately we understand that for the stations that make

use of the C1 code the noise RMS errors are even larger than one wide-lane cycle thus making the detection of a cycle slip not possible below the amount of noise in the raw time-series of the Melbourne-Wübenna combination. On the contrary, in the case for PALM, the noise level reaches ~20 cm well below 0.5 wide-lane cycles (Springer 2000), and cycles slips or outliers become detectable as can be seen in **Fig. 2-17c.**

In the Ionosphere-free combination (middle column of **Fig. 2-17**) we observe three different situations. Firstly, at the two buoys, BOHI and BS07, the noise level remains high enough around 4m because these stations are in constant motion and the ionosphere-free combination can not eliminate the geometry. Secondly, at PALM the noise level is around ~6 cm which reflects the high quality of this station and its clock. Thirdly, the time differences for ZIMM and mostly for BRST represent several sudden peaks related to the clock's resets for both cases (see further up in the cycle slips examples). Though it worth noting that in the record time inside the RINEX file of ZIMM we do not see any of these jumps appear, as previously noted during the cycle slips examples. That means that there is a discontinuity in the phase observables not visible in the screening graph of **Fig. 2-13**.

In the geometry-free combination (right column) the noise level reduces significantly for all cases. It must be noticed that this combination leaves the influences of the ionosphere. Remarkable reduction of the noise is observed for the moving buoys BOHI and BS07 (~50 cm). With this combination, apart from the geometry, we eliminate as well the receivers' clocks errors. The advantage is more obvious in the case of stations with clock jumps, such as BRST and ZIMM, where the peaks disappear as seen from **Fig 2-17d** and **Fig 2-17e.** In these two stations the noise level drops down to ~50 cm. Even for PALM there is a factor two reduction of the noise when compared to the ionosphere-free combination.

In conclusion, one of the most important issues in the pre-processing level of raw GNSS data is the detection and reparation of cycle slips. The quality of the clocks with visible or apparent frequent jumps, from each receiver, and the kind of linear synthesized combinations used together with the dynamic state of the GNSS station (moving or stable) are also critical factors that need to be taken into account so as to efficiently detect all possible cycle slips and eliminate outliers.

2.3.4.3 Troposphere

The correction of the delay of radio waves by the neural atmosphere (the non-ionized) is most often defined in terms of the contribution of the hydrostatic and wet components of the troposphere (Niell 1996).

The zenith delay is determined by the integration of refractivity vertical. The atmosphere is very close to hydrostatic equilibrium meaning that surface pressure is given by the vertical integration of density. Since the first term in refractivity depends only on density, its vertical integration will depend only on surface pressure. This integral is called the "*Zenith Hydrostatic Delay* (ZHD)" or as often mentionned "dry delay" (Herring 2005).

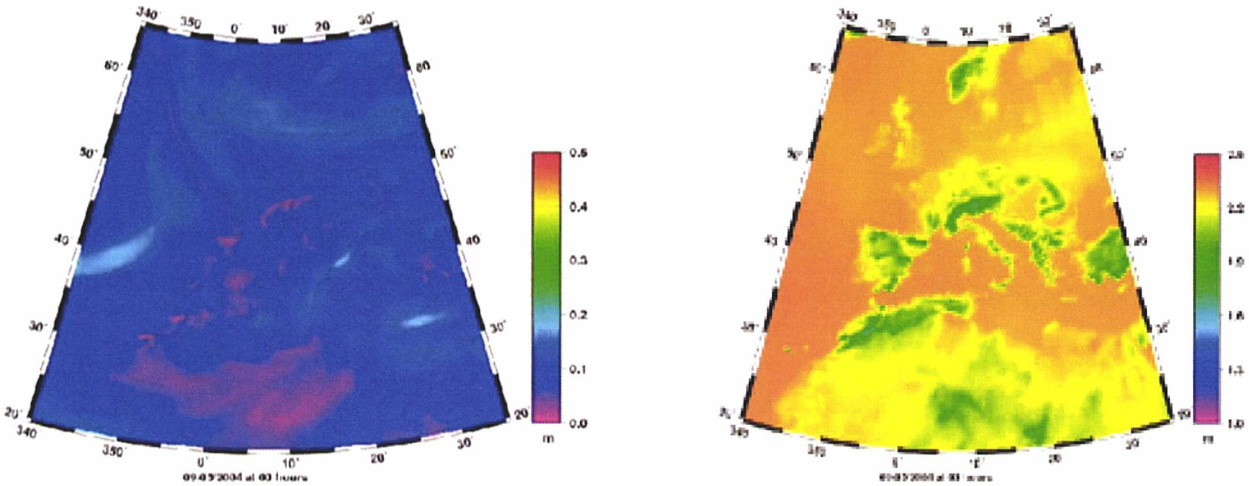

Fig. 2-18 : (left) A-priori wet and (right) dry corrections from the ECMWF model. Scale bars are in meters

The water vapor delay (second term in refractivity) is not so easily integrated because of distribution of water vapor with height. Surface measurements of water vapor pressure (deduced from relative humidity) are not very effective because it can be dry at surface and moist above and visa versa (Herring 2005). The effective method is to sense the whole column of water vapor. This can be done either by terrestrial ground measurements with *Water Vapor Radiometers* (WVR) or by laser profiling, LIDAR. Both methods are very expensive. Another approach in a more global and cheaper way is to use global numerical weather prediction models of the *European Center for Medium-Range Weather Forecasts* (ECMWF) and the *National Center for Environmental Prediction* (NCEP). They provide

values every 6 hours. These models have the disadvantages that they contain large uncertainties in the Arctic regions and that local troposphere variability is not easily detected.

An example of these models of dry and wet corrections over Europe, at midnight on the 5th of May 2004, from the ECMWF model is illustrated in **Fig. 2-18**.

In order to relate tropospheric delay (azimuth-independent part of the neural atmosphere) at lower zenith angles (*Zenith Tropospheric Delays*, ZTD, or path delays, ZPD), special mapping functions are used (Marini 1972, Davis et al. 1985, Niell 1996, Niell 2000, Guo and Langley 2003, Boehm and Schuh 2004, Schuh and Boehm 2004). Their basic form was introduced by Marini (1972) and matches the behaviour of the atmosphere at near-zenith and low elevation angles by a continued fraction of the form :

$$m(\varepsilon) = \cfrac{1}{\sin(\varepsilon) + \cfrac{a}{\sin(\varepsilon) + \cfrac{b}{\sin(\varepsilon) + \cfrac{c}{\sin(\varepsilon) + \cdots}}}} \qquad \textbf{Eq. 2-23}$$

Where: ε is the given elevation angle; m the mapping function; and a, b, c are estimated coefficients.

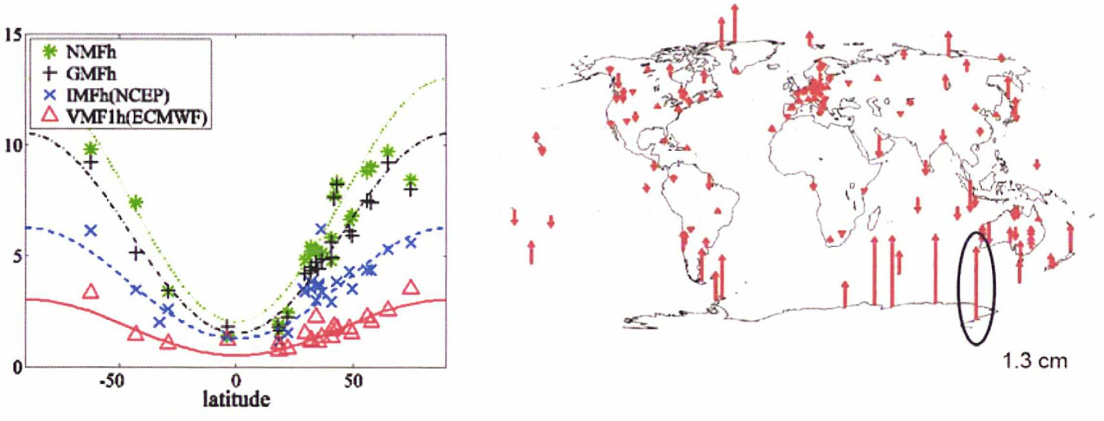

Fig. 2-19 : (left) Height equivalent (y-axis in mm) scatter for 5° minimum elevation from Niell (2005) and (right) station height differences between VMF and NMF GPS solutions (Boehm et al. 2006); NMF : Niell mapping function (Niell 1996), GMF : Global Mapping Function (Boehm et al. 2006b), IMF : Isobaric Mapping Function (Niell 2000), VMF : Vienna Mapping Function (Boehm and Schuh 2004).

The azimuth-dependent part of the neural atmosphere (Davis et al. 1993, Bar-Sever et al. 1998) is described by the north and east gradients. Both are used to determine the gradient at the azimuth of the observation, which is then mapped with the gradient mapping function to the elevation of the observation (Boehm and Schuh 2007).

The choice of the mapping functions affect mostly:

- the time-series of station positions. According to Neill (2005) , Vey et al. (2006), and Tesmer et al. (2007) the mean station height differences present the largest offsets in high latitudes (**Fig. 2-19**). Tesmer et al. (2007) have shown that discrepancies between time-series of station heights computed with different mapping functions reveal annual periodic signals with amplitudes up to 5 mm.
- the ZTD parameters. The cut-off elevation angle sensitivity from Vey et al. (2006) has showed ZTD differences larger than 3 mm for an elevation mask reduction from 15° to 3°.
- the scale, origin and geometry of the Terrestrial Reference Frame. Scale differences between TRF realizations reflect the corresponding "mean height differences" between TRFs. Origin differences reflect the corresponding geocentre translation differences. According to Vey et al. (2006) and Tesmer et al. (2007) the effect of mapping functions on the scale in one year can reach 0.2 ppb (parts-per-billion 10^{-9}) corresponding to 1.3 mm in the height on the Earth's surface, and to 3 mm in the origin.

2.3.4.4 Ionosphere

The ionosphere refraction is the signal delay respectively phase advance due to the free electrons in the Earth's atmosphere. As a dispersive medium for microwave signals, the amount of the refraction index will be dependent on the signal's frequency and on the total electron content (TEC) in the atmosphere. The TEC can vary significantly during the diurnal rotation and annual revolution of the Earth around the sun and during the solar cycle activity (every ~11 years).

In precise positioning applications we usually form the synthetic ionosphere-free L_3 combination of L1 and L2 phase observables. This combination is sufficient enough to eliminate the first order zenith ionospheric group delay (phase advance), which according to

Bassiri and Hajj (1993) , Fritsche et al. (2005), ranges between ~1 m to16 m for L1 and ~2 m to 27 m for L2. The second and third order ionospheric delays are not eliminated within the L_3 combination. Bassiri and Hajj (1993) have estimated the effect of the ionospheric group delay of the second and third order to be 1.6 cm and 3.3 cm and to .86 mm and 2.4 mm for L1 and L2 respectively. Fritsche et al. (2005) have demonstrated that the GPS stations residuals after a 7 parameter transformation with respect to ITRF2000 indicate a southward shift of 1 mm to 4 mm in horizontal and a latitude-dependent change in station height of ~5 mm at the maximum, only when the 1st order ionospheric term is considered. Heflin et al. (2002) obtained a shift in the origin of x ~ + 5.0 mm, y ~ - 1.9 mm, z ~ + 3.7 mm for a GPS-derived global reference frame relative to ITRF2000.

If a millimetre level accuracy is to be accomplished in a global GPS network positioning approach, at least the second order effect has to be taken into account. This is not the case for a regional or local network using the DD approach were the remaining ionospheric effects will be differentiated inside the DD algorithm.

2.3.4.5 The tracking/satellite Antenna Phase Center offsets

The antenna phase center offset is the 3D position vector of each carrier phase center inside the physical body of the GPS antenna with respect to an external *Antenna Reference Point* (ARP).

The phase response of GPS tracking antennas does not correspond to an ideal point source. The signal wave-fronts of constant phase do not form perfectly hemispherical shells. Instead, the phase center can vary depending on viewing direction. If these antenna effects are not being accounted for, several cm (IGSMAIL 5189) can occur in estimates of the antenna position and thus in the station's coordinates.

The antenna *Phase Center Variations* (PCVs) and their influences on positions of stations and the scale relative to an TRF of a GNSS network have been till recently a major issue of discussions inside the geodetic community (Wu et al. 1993, Menge et al. 1998, Mader 1999, Springer 2000, Rothacher and Mader 2003, Zhu et al. 2003, Schmid and Rothacher 2003, Ge et al. 2005, Schmid et al. 2005a, Rothacher and Schmid 2006, Bar-Sever et al. 2006, Schmid et al. 2006, Wübenna et al. 2006, Gendt et al. 2007, Herring 2007, Altamimi et al. 2007).

According to IGSMAIL 5189 in the IGS ACs Workshop held at Silver Spring in 1996 it was decided that relative antenna phase center offset corrections would be applied by June, 30, 1996 for the first time. These corrections were determined realtive to a reference Dorne/Margolin choke ring antenna type T (AOAD/M_T) from a short-baseline field measurements procedure (Mader 1999). With respect to this "relatively determined" phase center offsets the station-specific antenna PCVs were measured as a function of the elevation angle of the GPS satellites. A similar procedure was used to calibrate the GPS satellite's transmitting antennas for each block by Mader (2000) but was never used operationally (U. Hugentobler personal communication) .

Nevertheless, several problems occurred from the use of these "relative" values which were mostly related to discrepancies and correlations, such as in between: tracking antenna offsets and PCVs; satellite antenna offsets ; estimated station heights and estimated troposphere parameters; scale differences of the IGS TRF and ITRF. Another issue was the fact that these relative phase center corrections were only valid for small range baselines. Springer (2000) has demonstrated all these difficulties. The solution was to use an external calibration procedure for the tracking antennas known as "absolute" phase center corrections. In this way Schmid et Rothacher (2003) have found that transmitting antenna phase center corrections (offsets and PCVs) were possible to be determined by using absolute tracking antenna models (Menge et al. 1998). Ge et al (2005) have demonstrated that estimated satellite-specific offsets by using the relative tracking antenna models, for satellites belonging to the same block, are not homogeneous. Both the estimated offsets and the network scales of the re-adjusted solutions proved that the IGS offsets lead to a scale bias of about 1 ppb over 7 years.

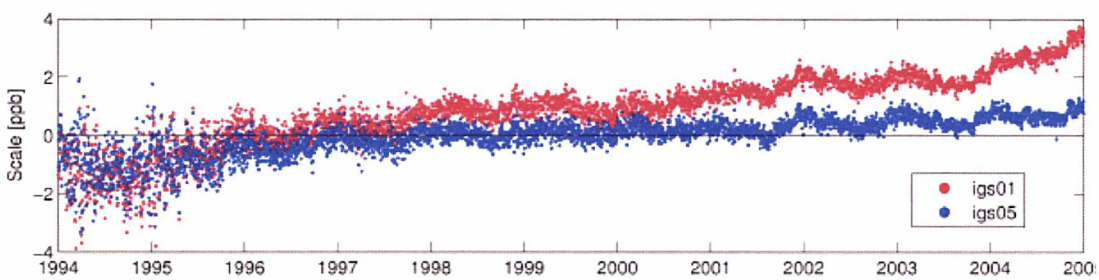

Fig. 2-20 : Scale rate caused by inconsistent satellite antenna offsets (Gendt et al. 2007)

The switch to the "absolute" antenna corrections models (for offsets and PCVs) and those inferred by them (for the satellites' antennas) took place on November, 6, 2006 (IGSMAIL 5438).

The new IGS reference frame IGS05 realisation was established on October, 9, 2006 together with the long expected ITRF2005 (Altamimi et al. 2007) on October, 5, 2006. Soon after the application of the new antenna models, Gendt et al (2007) have demonstrated the impact on the IGS' scale consistency when compared to the ITRF2000 and ITRF2005. The resulting scale improvements in discrepancy before and after the switch were 0.35 to 0.15 ppb for IGS00 TRF and 0.24 to 0.04 ppb for IGS05 (**Fig. 2-20**). Herring et al. (2007) has arrived to the same conclusion for the scale with an additional remark on the dependence of the GPS frame translation origin on the Z-direction from the SRP parameters.

The reduction of the scale inconsistency with respect to the ITRF had an immediate impact on the stations' height position time-series and consequently on the correlated TZD parameters. Schmid et al. (2005a) have shown that the troposphere bias between GPS and VLBI drops down to -0.8 mm for satellite-specific absolute antenna models wrt to a 5.3 mm for relative models.

2.4 Modeled stations displacements

In this paragraph some of the basic displacement model corrections applied on the GNSS stations will be presented. These corrections are included in the IERS 2003 updated conventions of June 20 2007 (IGSMAIL 5614) and they mostly concern:

- Ocean Tide Loading displacements (one of the most important);
- Non-tidal ocean loading displacements;
- Center of mass corrections due to ocean tide mass ;
- Effect of the solid Earth tides (the most important) ;
- Displacements due to rotational deformation caused by the polar motion ;
- Displacements due to ocean pole tide loading (caused by the centrifugal effect of polar motion on the oceans) ;
- Displacements due to atmospheric loading ;
- Displacements due to hydrological loading ;

The fortnight, diurnal and semi-diurnal time domain is the main characteristic of most of the aforementioned station displacements. The ocean tide loading that this Thesis is investigating on is thoroughly investigated in **Chapter 4**. The low-frequency displacements (annual, semi-annual, decadal) are mainly those related to tectonic activities like plate motion, post-seismic deformations, land subsidence etc. In the following, only the displacements due to hydrological loading, atmospheric loading, and effects of the solid Earth, center of mass corrections and non-tidal loading will be discussed.

2.4.1 Non-tidal loading displacements

The non-tidal loading deformations are caused by non-tidal variations of the sea level mainly due to atmospheric pressure forcing and wind effects.

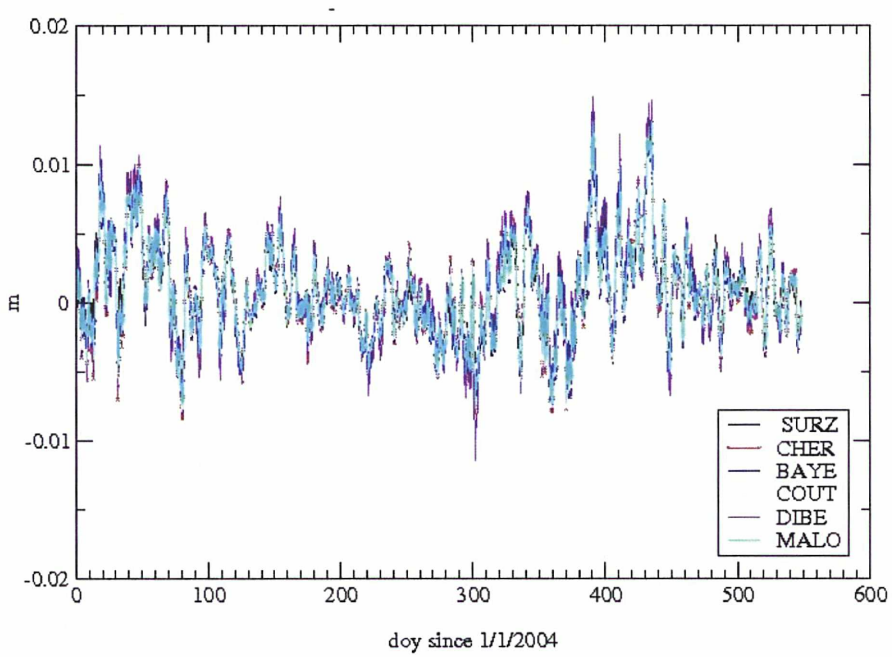

Fig. 2-21 : Non-tidal loading displacements from MOG2D model at GPS stations between 47°-50°N on the shelf of Brittany. (J. Marty personal communication)

Till recently, only the static response of the ocean to atmospheric forcing has been taken into account. This classical assumption formulates the *Inverse Barometric* (IB) correction. The validity of this IB assumption depends on the time scales considered: the

ocean response to atmospheric pressure generally differs from the IB at periods shorter than 3 days and at high latitudes (Carrère and Lyard 2003).

A new hydrodynamic finite element model MOG2D-G (2D Gravity Waves model) has been created by Carrère and Lyard (2003). This model takes into account the high frequency (HF) atmospheric forced variability of the global ocean. MOG2D is barotropic, non linear and time stepping (Lynch and Gray 1979).

In **Fig. 2-21** the displacements due to non-tidal ocean loading for a set of GPS stations, dispersed on the geographical coastal area of Brittany, France, between 47° - 50° North-Latitude were calculated. The maximal loading has several mm to 2 cm variability with periods from ~10 days to ~30 days. In the present example the loading effect is identical to all stations. So its impact on the final position time-series will depend on the strategy of the positioning scheme. If the GPS network is a regional one and the processing is done by forming DD baselines (relative positioning) then these displacements will be eliminated by the differentiation process of the DD algorithm. Though, if the network is expanded to a bigger area, like a global network or the positioning mode is absolute such as PPP then the non-tidal loading displacements should be taken into account. The last conclusion agrees with the recommended revision on chapter 7 of the IERS conventions in handling non-tidal displacements in data reductions (www.bipm.org/utils/en/events/iers/Conv_PP1.txt).

2.4.2 Center of the mass corrections due to ocean tides

According to **§ 2.1.2.2** the position of the center of mass of the system of solid Earth, fluid and atmosphere undergoes periodically motions due to the external forces acting upon it, such as ocean tides. The geodetic stations which are fixed on the solid Earth will be subject to the counter-motion of the center of mass which takes place in order to counterbalance the displacement of masses.

Space geodesy techniques such as Satellite Laser Ranging (SLR) (Watkins and Eanes 1997), and the Global Positioning System (GPS) are fixed in space and are in principle able to detect this centre of mass motion of the solid Earth (Scherneck et al. 1999).

On the other hand, the predicted loading effects are insensitive to this counter-balance motion of the Earth's geocentre. While using GPS for validating ocean tide models,

the stations of the network will already contain this geocentre motion. As such the two frames defined by the ocean tide models and the GPS are inconsistent. A correction must be applied to the predicted displacements.

For instance, when a regional network is being used, every translational motion of the geocentre will map into the stations' time-series if the GPS satellite orbits are held fixed in the processing scheme. When these time-series are used for detecting high-frequency displacements due to ocean loading, they already contain the geocentre motion. In order to be comparable with the ocean tide model predictions, the latter have to account for the geocentre motion, as Scherneck at http://www.oso.chalmers.se/%7Eloading/cmc.html demonstrates. This will be the case were a global GNSS network is used and translational parameters (un-correlated) are not estimated, or in the case of a regional network the positioning scheme is based upon un-differenced observables. For a regional network with DD baselines this geocenter motion will be eliminated, if not at least extremely minimised inside the differentiation process of the baseline formation thus bringing the two frames into consistency.

2.4.3 Effects of the solid Earth tides

It is well known that the position of a point on the Earth's surface varies over a range of temporal scales due to the elastic response of the crust to the external tide generating potential (sun, moon and planets) (Melchoir 1983). The resulting response is called the solid Earth tide and can account for displacements up to 0.4 m. The most predominant signals are located in the semi-diurnal and diurnal bands. As previously shown by Watson et al. (2006), mis-modelling of the solid Earth tides can propagate into coordinates and troposphere parameters of the level of annual amplitudes of ~1.6 mm in the vertical component and ~2 mm of diurnal signals in ZTD parameters.

2.4.4 Displacements due to atmospheric loading

Temporal and geographic pressure variations in the atmosphere provoke vertical surface mass loading displacements of the Earth's crust. According to vanDam and Herring (1994) these loading displacements due to changes in the atmospheric pressure can account for up to 24 % of the total variance in the GPS height time-series estimates. The detected loading amplitudes are larger at higher latitudes where pressure variations are more important.

The principal method for calculating the displacements of geodetic points due to atmospheric loading mainly falls into two categories.

The first is based on the use of the gravitational potential of a simple layer, which is induced by the atmospheric masses and it can be derived from the atmospheric surface pressure and its variations (Biancale and Bode 2002). This method makes extended use of the development of the potential in spherical harmonics and the hypothesis of an elastic Earth where the displacement is proportional to the excitation. The loading on the surface is calculated from the pressure grids of global numerical models such as ECMWF. These models take into account both the constant part of the atmosphere and its high-frequency variations mainly due to the diurnal and semi-diurnals solar (S_1 and S_2) tides (Biancale and Bode 2002).

The second one consists from computing the atmospheric loading displacements by convolving Farrell's elastic Green's functions (Farrell 1972) with global pressure data. Green's functions describe the response of the Earth to a point load on its surface. While they are determined by the angular distance between the load element and the station point, they are assigned to each grid element and are then multiplied by the atmospheric load in that element (vanDam and Herring 1994). The results are summed over all grid units to provide the radial and horizontal displacements at the station point.

In **Fig. 2-22** a comparison of the displacements due to ocean loading, atmospheric loading, pole tides and solid Earth tides over two GPS stations is given. GRAZ (Austria) station is situated in the Northern hemisphere and KOUR (French Guyana) station very close to the equator.

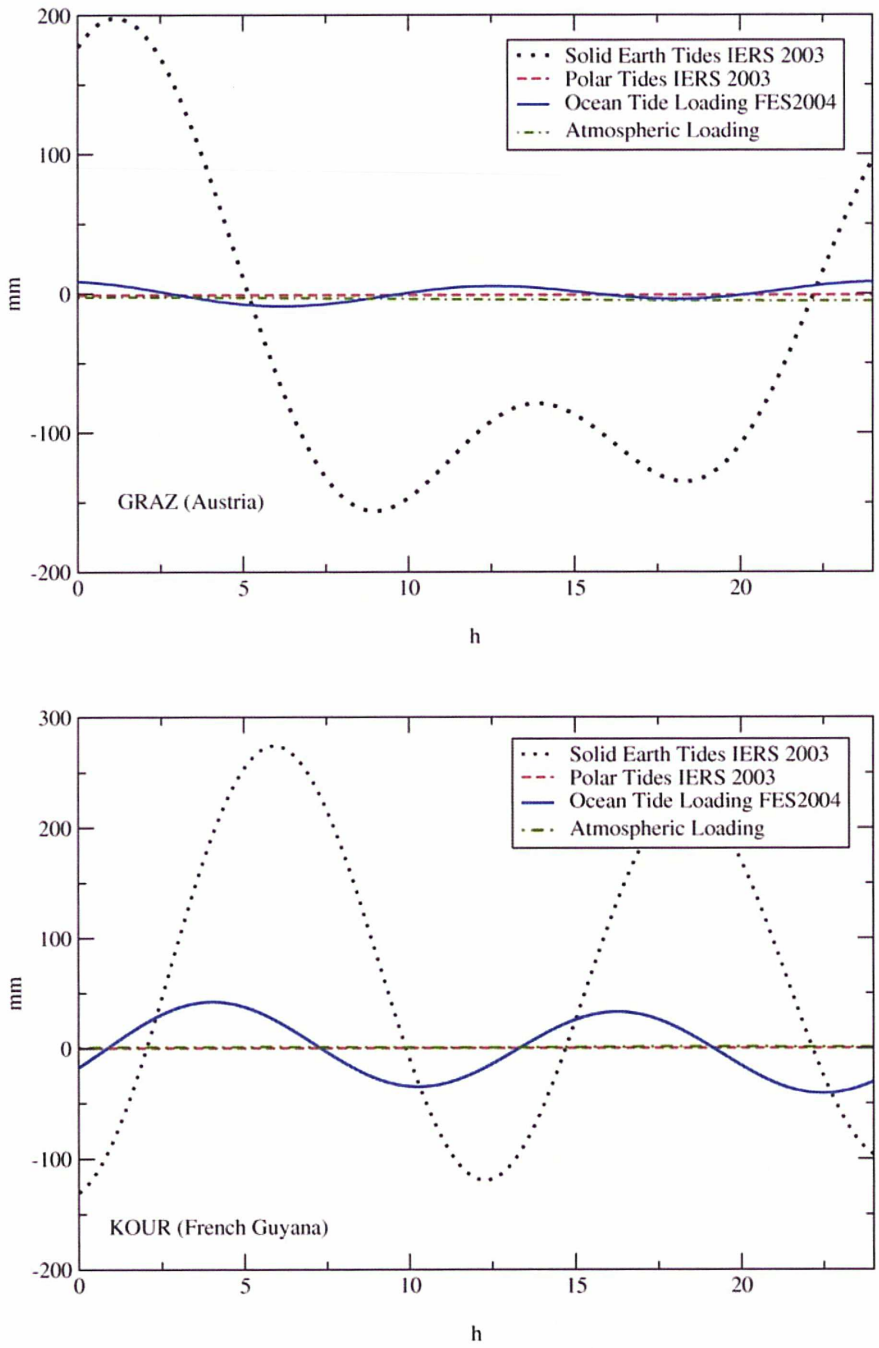

Fig. 2-22 : Ocean loading, atmospheric loading (ECMWF), Polar tides and solid Earth tides displacements in mm over GRAZ (47.061°N and 15.4934°E, Austria) and KOUR (5.2521°N and 307.1940°E, French Guyana) GPS stations over doy 03 2006.

2.4.5 Displacements due to hydrological loading

Among the previous load displacements of individual GNSS sites, are as well those due to variations in the distribution of water, snow, ice on land. Of these, the effects of large-scale terrestrial water storage are the less understood. Their timescales, mostly seasonal, are associated with climate-driven transport of water on the surface of the Earth.

The redistribution of water on the surface of the Earth will act as a change in load, or weight, on the crust of the Earth. To extend further more, theses mass variations associated with the hydrological cycle will provoke variations in the geoid height sensed by space geodesy gravimetric techniques such as GRACE (Ramillien et al. 2005, Lemoine et al. 2007). The temporal variations in the geoid can be transformed into equivalent water height variations.

The associated normalised spherical harmonics of the Earth's gravity potential (Stokes coefficients), their annual, semi-annual and seasonal variability together with the proper set of Love numbers calculated from the corresponding Earth model will give the final radial displacements.

Nevertheless, GRACE gravity field does not contain the degree one geocentre deformational component as GPS does. A correction must be applied to the displacements issued from GRACE, according to Blewitt (2003).

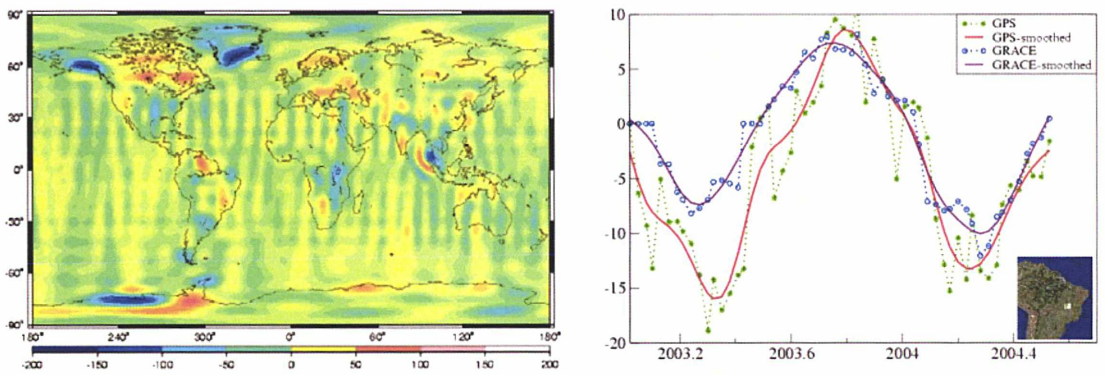

Fig. 2-23 : (Left) Equivalent water height (mm/10-day) trend over 2002-2006 from the GRACE 10-day GRGS gravity field and (right) hydrological loading displacements from GRACE and GPS in BRAZ (station) situated at the Amazonian basin (the satellite image is from google map)

In **Fig. 2-23** an example of comparison is given for the trend of the equivalent water height (mm/10-days) on the globe (Biancale et al. 2006) and the loading displacements issued from GRACE and GPS data in the Amazonian Basin. From the right figure we can see how well

the two hydrological loading signals compare (Fazilova et al. 2006). It is worth mentioning that the GRACE's loading time-series have not been corrected for the geocentre motion and some mm error should be considered.

2.5 Summary

The purpose of this chapter is to introduce an updated description of the most recent issues in GNSS observations and which have occupied my research during the last period.

The geodetic components of what make the GNSS a valuable tool for geodesists were overseen. From the modern implementation of a TRF to the high and low frequency displacements of the discrete geodetic points on the surface of the Earth's crust, everything is connected.

An updated budget of the systematic effects on the GNSS observables and the ways to deal with them were examined. Examples with real data from different GPS receivers have demonstrated the advantages and disadvantages of current algorithms at the pre-processing level. Receiver clock drifts and cycle slips present a serious aspect for precision and accuracy in kinematic and static positioning by GNSS. Higher order ionospheric delay terms not eliminated by classical linear combinations of the carrier phases can introduce important systematic effects especially when sub-mm level accuracy is required during absolute (PPP) or relative positioning of huge global networks. The effect of the troposphere on the GNSS observables depends on the mapping function used. From previous studies it has been demonstrated that different mapping functions will introduce different levels of discrepancies in the coordinate time-series. The exact position of the antenna's phase center with respect to an external reference point (ARP) will depend on the antenna's calibration method used. Additionally the phase center not being a constant point will vary depending on the viewing direction of the observations. Furthermore, it has been demonstrated that non-tidal oceanic loading and hydrological loading can provoke significant displacements of geodetic stations upon the Earth's crust, with low and high-frequency spectrum, and which if not modelled can provoke misinterpreted signals in the final GNSS time-series.

The complete and updated budget from this chapter on the effects acting on the geodetic parameters of the GNSS constituents (stations, TRF, observations) is summarised in the following **Table 2-5** .

	Parameters affected	Order of Magnitude
Systematic Effects		
Cycle slips	- on position (3D)	20 m to 20 cm
Clock jumps	- on position (3D)	1 ms = ~300 km
Antenna Phase Center offsets and variations	- on position (3D)	0.2 mm to several cm
	- on the TRF scale	0.02 - 0.25 ppb
	- on TZD	0.8 mm - 5.3 mm
Signal delays		
Troposhere	- on the TRF scale (mapping function)	0.2 ppb
	- on the height time-series (mapping function)	1.3 mm
	- on the height time-series	wet vapor delay 0.0 to 20 cm
	- on the height time-series	zenith hydrostatic delay 1 m to 2.5 m
Ionosphere (frequency dependent) -zenith phase advance-	- on L1	1 st order term .1 m to 16 m
	- on L1	2 nd order term ~2 cm
	- on L1	3 rd order term ~1 mm
	- on L2	1 st order term .2 m to 27 m
	- on L2	2 nd order term 3.3 cm
	- on L2	3 rd order term ~3 mm
Stations' displacements		
Non-tidal loading	- on the height time-series	High-frequency several mm
	- on the height time-series	Low-frequency ~2 cm
Center of the Earth' Mass Correction	- on the TRF origin	several cm
	- on position (3D) depending on the processing scheme	0 - 2 cm
Solid Earth Tides	- on position (3D)	40 cm
	- un-modelled effect on the height time-series	Low-frequency ~2 mm
	- on TZD	2 mm
Atmospheric loading	- on the height time-series	several mm
Pole Tides	- on position (3D)	several mm
Ocean loading	- on position (3D)	High-frequency 0 to 15 cm
	- un-modelled effect on the position (3D)	Low-frequency several mm
Hydrological Loading	- on the height time-series	Low-frequency ~3 cm

Table 2-5 : Observational model budget and the effects on GNSS parameters

3 GINS – GNSS software: updates and validations

The GRGS Space Geodesy department of the CNES in France has been created in 1971. Since that epoch the GRGS is developing the scientific software for space geodesy namely GINS.

At the beginning of this Thesis, GINS was designed for standard GNSS operation:

- Processing of global GNSS networks ;
- daily and weekly mean-solutions in a weighted least square sense;
- Position time-series in a X,Y,Z geocentric coordinate system ;
- Float ambiguity solutions ;

During the past 3 years of this PhD study and in order to be able to accomplish my research on the regional and local terrestrial and maritime GNSS networks, the following improvements in the software code have been added:

- Introduction of a unified local geodetic system in the position time-series ;
- Ambiguity resolution by applying the QIF method (see **§ 2.3.2.6**) the same as applied in the Bernese software (Hugentobler et al. 2001) ;
- Possibility to have position time-series in higher frequencies (hours, minutes, seconds) than of a 1-day or 1-week solutions ;
- Implementation of new processing strategies for local geodetic networks ;
- Modifications of scripts and table dimensions inside the GINS' code ;
- Implementation of new SRP models for POD of the GNSS satellites including GIOVE-A, the first satellite of the future Galileo European global positioning system.

3.1 Processing GNSS data inside GINS

The up-to-date GNSS data processing with GINS software is implemented in the following steps:

- The formation of a coordinate file containing GNSS stations from a local, regional or dedicated campaign network ;
- The concentration of all necessary data files (RINEX, SINEX, satellite ephemerides, clocks) in a pre-defined directory ;
- The data-editing : clock jump corrections, cycle slips corrections ;
- The formation of synthetic observables: un-differenced or double-differenced data of the iono-free combinations ;
- The processing scheme implementation by the *GINS' Directory-File* (GDF) ;
- The output screening of the processing in the GINS' Listing-File (GLF);
- For stacking and manipulation of normal equations, use of the DYNAMO software package in order to apply minimal constraints for the datum realisations, reduce or eliminate un-necessary parameters ;

The flow of GINS' GNSS data processing is described in the following **Fig. 3-1**

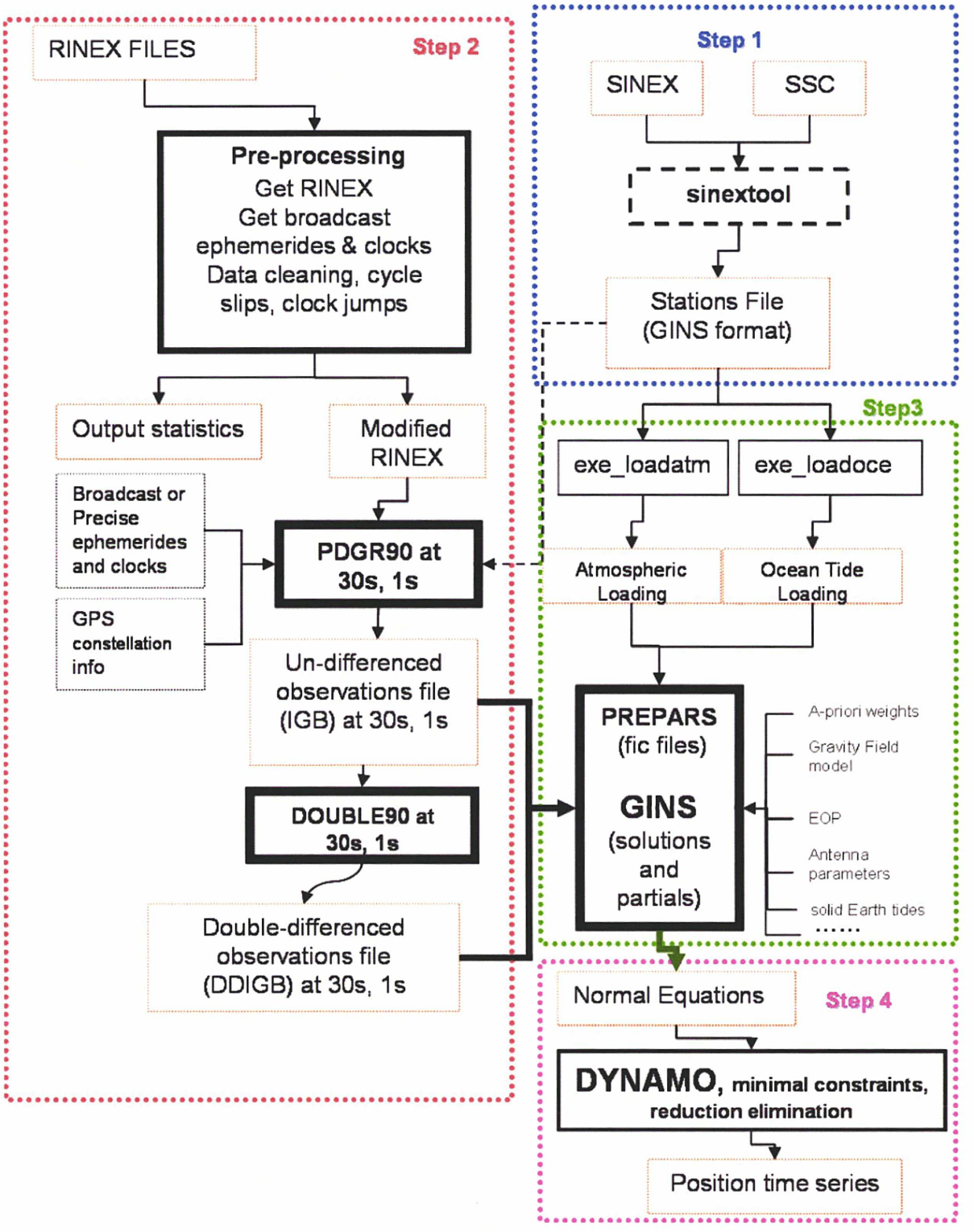

Fig. 3-1 : The GINS processing flow for high-frequency GNSS positioning

3.1.1 Step 1: The station file

An external utility is used to get the stations file in a format compatible to GINS. Some of the information about the stations should be concentrated in a SINEX format file which will serve as input for this utility. The information must contain:

- The name and DOMES number of the station's marker (ITRF format) ;
- The type of the station (SLR, DORIS, GPS, VLBI, …) ;
- The marker's position in XYZ coordinates ;
- The eccentricity vector between the marker and the antenna phase center ;
- The type of the antenna (IGS conventions) for GPS stations ;
- The reference datum of the coordinates and the linear velocities.

The final outcome will be a station file adapted to GINS' format.

3.1.2 Step 2: The pre-processing phase

The pre-processing phase consists of multiple operations. The broadcast GNSS ephemeris and clocks are downloaded. The *PDG_DECAL* module takes care of the millisecond clock jumps (see **§ 2.3.4.1**) in the RINEX record time. Next the cycle slip detection is performed with the aid of the time differences as described in § **2.3.4.2**. Approximative values of the wide-lane ambiguities are estimated in order to serve as input for the iono-free observable. Additionally, it is possible to specify individual thresholds for the code and phase observations, above which a cycle slip will be defined.

Modified and edited RINEX files will serve as input to *PDGR90*. Inside these new RINEX files the estimated N1 and Nw ambiguities are listed along with the other observables for phase and code flagged by the number of corresponding cycle slips.

The *PDGR90* forms the un-differenced observation file. The program takes care of incomplete or absent observables and links the observations to the stations file, the broadcast clocks and ephemeris, and the GPS constellation information. The un-differenced output file contains the ionosphere-free combination (see **§ 2.3.2.2**) for each station and for each

satellite. Several passes could be eliminated depending from the number of cycle slips detected and the elevation of the satellites, so care must be taken for special cases. This file can be used directly in GINS for the absolute-positioning mode.

Double90 is responsible for the formation of the DD from the un-differenced observation file given out by *PDGR90*. This module uses the stations file to calculate the baseline lengths between the different stations present in the un-differenced observation file. Independent baselines are formed with priority to those that have the biggest number of common satellite observations between stations. The output DD file is used in GINS for the relative positioning mode.

3.1.3 Step 3: The strategy implementation and adjustment

The *exe_loadatm* and *exe_loadoce* scripts take as input the stations file and give as output the 3D atmospheric and ocean tide loading displacement coefficients in amplitudes and Greenwich phase-lags for each station.

Next the GDF must be tuned with the proper key functions that will determine the strategy followed and executed by GINS.

The module *PREPARS* accounts for any ad-hoc models and observations such as station displacements, EOPs, gravity field, etc., by concatenating the corresponding files. Calculations are not performed in this module; it prepares the complete data set for subsequent processing in GINS.

GINS processes the DD or un-differenced observations and calculates the partial derivatives of the required geodetic parameters (station positions, EOPs, orbital parameters, troposphere parameters, ambiguities, etc.). In a weighted least squares sense, several iterations are performed, during which the geodetic parameters are adjusted and certain observations are eliminated based on the elimination residual criteria specified inside the GDF. It is possible to either fix or not fix the estimated ambiguities. The iterations will proceed till convergence of the final residuals. As an output we get the final estimates or normal equations that can serve as input for *DYNAMO*.

An example of the models used in GINS is listed in **Table 3-1**:

Dynamic Models	Gravity Field EIGEN-GL04S
	IGS sp3 fixed orbits
	EOPC04
	J2000 inertial frame
Observational models	Troposphere: ECMWF
	Loading (Ocean/FES2004 and Atmosphere/ECMWF)
	Solid Earth tides: IERS03
	Relative or Absolute Antenna models PCVs

Table 3-1 : Ad-hoc dynamic and environment models for GNSS positioning with GINS

3.1.4 Step 4: Stacking of normal equations – final coordinate time-series estimation

DYNAMO is used for inverting and stacking the normal equations provided by GINS. It is possible to eliminate and reduce un-necessary parameters, specify continuity and minimal constraints to the individual geodetic parameters for the datum definition (see **§ 2.1.2**).

The estimated geodetic parameters (station coordinates time-series and post-fit residuals, troposphere zenith delays, ambiguities, orbital parameters, EOPs) with the associated un-certainties are the final outputs.

3.2 Validations

After the implementation of the aforementioned modifications a certain series of validations test were performed before proceeding to the final studies.

The validation tests are mostly separated into two large categories, those in terms of position time-series and POD.

For the first case, I used the 102-day observations of the G2 GPS dedicated campaign serving to study the OTL in Brittany (see **§ 4.2.2.2**) and I compared the estimated coordinate time-series and local OTL constituents to those from the solutions of other software and notably : GAMIT 10.21 (King and Bock 2005), GIPSY/OASIS II (Zumberge et al. 1997) and Bernese 5.0 (Dach et al. 2007).

In the second case, inter-comparisons between the final GINS' GPS orbits, estimated with different SRP models, to the IGS sp3 precise orbits were performed. Additionally, SLR observations and comparisons of the range residuals of the distance between the satellite and the observation site obtained from both GINS and IGS sp3 orbits were also used. Furthermore, the network effect to the reference system of the GPS SLR orbits was quantified as well as the determination of the perturbation periods and orbital elements of the first Galileo satellite GIOVE-A.

3.2.1 Intra-software position time-series comparisons

In the first part of the validations I collaborated with research teams from the *Laboratoire de Géodésie et Géomatique* (L2G) of the *Ecole Supérieur des Géomètres et Topographes* (ESGT), the *Laboratoire de Recherche en Géodésie* (LAREG) of *Institute Geographique National* (IGN), the *Institute de Physique du Globe de Strasbourg* (IPGS).

The aforementioned GPS data processing solutions of existing software were used. The aim was to validate the modifications in GINS GNSS software in matters of high-frequency positioning of a local or regional GNSS network.

3.2.1.1 Data sets and strategies

Four independent software position time-series solutions of 102 days from 9 GPS campaign stations were compared. The strategies followed at each of the four solutions are summarised in **Table 3-2**:

	Bernese 5.0	GAMIT 10.21/ GLOBK	GINS/DYNAMO 7.1	GIPSY/OASIS II
Parameter estimation	Least Squares	Least Squares	Least Squares	Precise Point Positioning "Kalman Filter"
Ambiguity	Fixed (on 24 h)	Fixed (on 2 h)	Fixed (on 24 h)	float
Session	DD 2 h	DD 2 h	DD 24 h	Un-differenced 24 h
Station estimation	Network resolution every hour	Network resolution every hour	Network resolution every hour	Stochastic (random walk) every hour
EOPs	IERS standards	IERS standards	IERS standards	IERS standards
POD	IGS orbits (fixed)	IGS orbits (fixed)	IGS orbits (fixed)	JPL orbits (fixed)
ZTD	1 ZTD (30 min) No gradient Niell hydrostatic MF	5 ZTD / 2 hrs No gradient Niell hydrostatic MF	1 ZTD (1 h) No gradient Marini type MF	1 wet zenithal (random walk 5 min) 1 gradient (random walk 15 min) Lanyi-C hydrostatic MF
Solid Earth tides corrections	IERS2003 standards	IERS2003 standards	IERS2003 standards	Williams and Melchior
Polar tide correction	IERS2003 standards	IERS2003 standards	IERS2003 standards	Yoder
Atmospheric loading correction	No	No	ECMWF (6 h)	No
Cut-off angle	10°	10°	10°	15°
Datum Definition				
Permanent stations used	16 IGS Stations	16 IGS Stations	14 IGS Stations + Orbit reference frame	Orbit reference frame
A priori coordinates	ITRF2000 corrected with FES2004 predicted OTL	ITRF2000 corrected with FES2004 predicted OTL	ITRF2000 corrected with FES2004 predicted OTL	
Constraints	**0,1 mm constr. to 7 IGS sites**	**loose constraints + stabilization to 10 IGS sites**	**1 mm constr. to 15 IGS Continuity constr. (3 cm/h) to campaign and RGP stations**	

Table 3-2 : Summary of the 4 software strategies applied

3.2.1.2 Comparison results

The inter-comparison is based on the analysis of each estimated coordinate time-series component. The station time-series compared are: Brest (BRST), Cherbourg (CHER), Coutances (COUT), Le Diben (DIBE), Le Mans (MANS), Rennes (RENN), Paimpol (PAIM), Saint Ygeaux (YGEA), and Trévignon (TREV). The geographical location of these stations can be seen in **Fig. 4-2** of **Chapter 4**.

The validation analysis is divided into four different steps:

1. High-frequency position time-series between the four solutions for one station on a short period (**Fig. 3-2**).

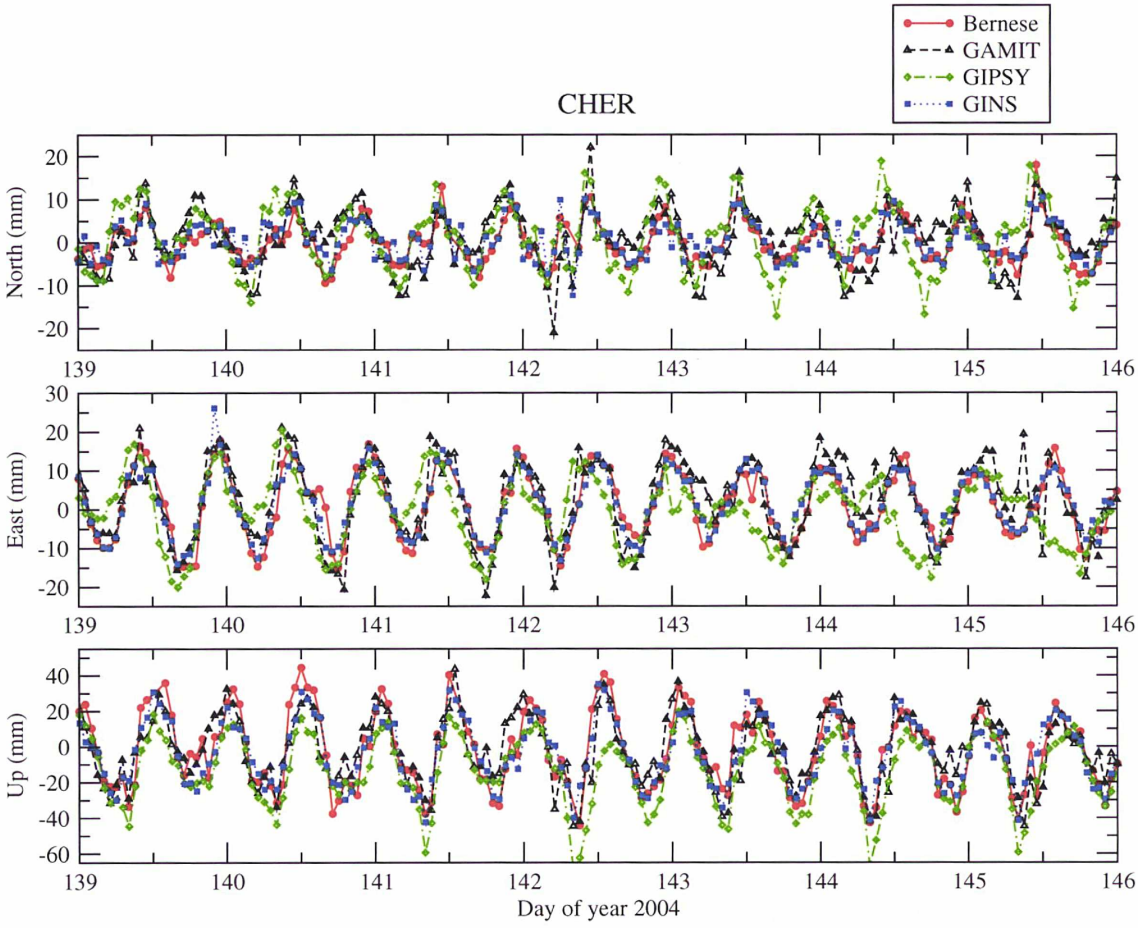

Fig. 3-2 : Extract of 7 days of the 3D position time-series (in mm) for a representative campaign station (CHER) from the four solutions: red circle for Bernese, black triangle for GAMIT, green diamond for GIPSY, and blue square for GINS

The site CHER was selected as representative of the results from all stations. A periodic signal is present in all vertical and horizontal components. The four solutions seem to be globally consistent in terms of periodicity and peak-to-peak displacements.

2. Differences in terms of *Root Mean Square* (RMS) scatters, in 3D (**Fig. 3-3**).

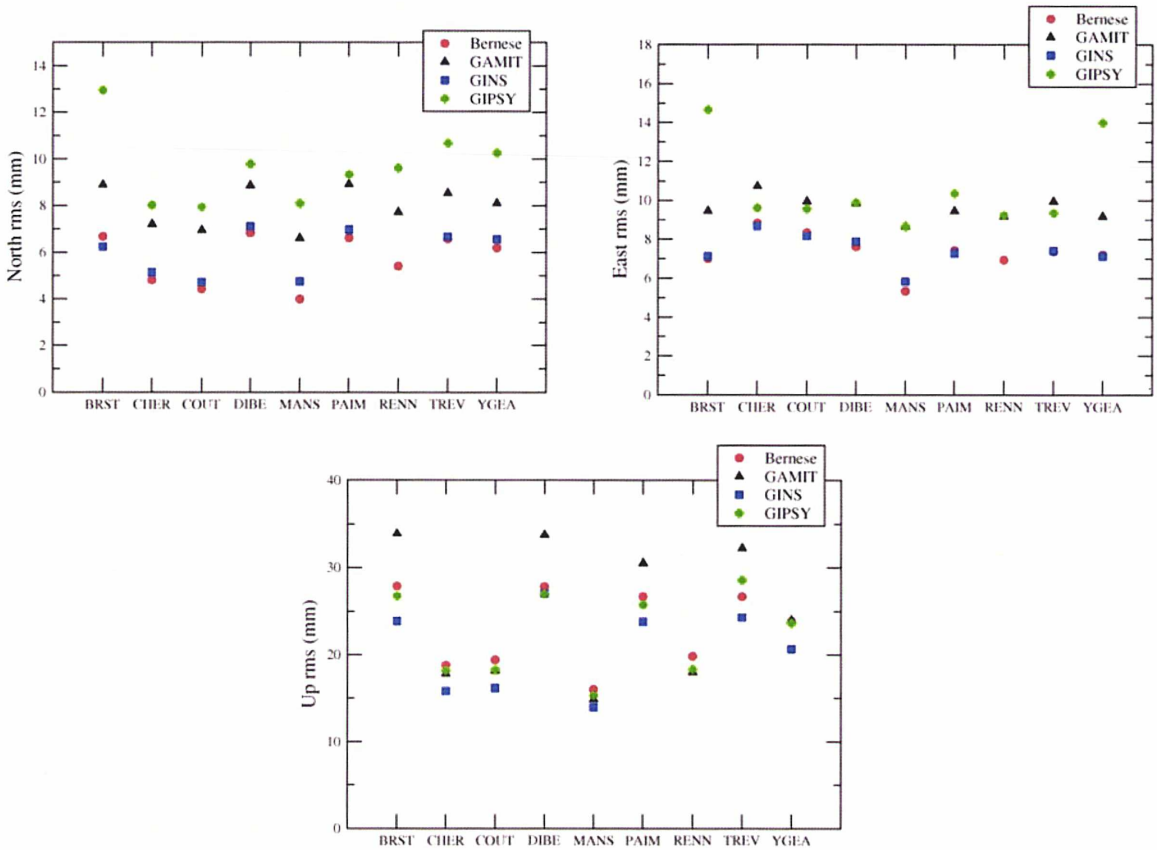

Fig. 3-3 : 3D RMS scatters (in mm) for each station time-series solution in North, East and Vertical directions

Fig. 3-3 shows the RMS scatters obtained from each station of each solution in all three components.

These inter-comparisons are performed after removing the mean and the linear trend from each coordinate time-series. Largest outliers are removed and lacks of data are identified for each solution. Analyzing the RMS scatter of the time-series, allows us to examine if the amplitude of the signal obtained by the different solutions is similar for each station. For the north component, we can notice that two groups are formed: Bernese and GINS solutions are in good agreement and show smaller scatter than the 2 other solutions. GIPSY solution exhibits the strongest signal for this component. For the

east component, the two groups are less separated and Bernese and GINS solutions still have the best agreement. The four solutions have the highest discrepancies at MANS. For the vertical component, we can notice that GAMIT solution disagrees with the other solutions for four stations (BRST, DIBE, PAIM, and TREV) showing a much stronger scatter. In total GAMIT solution seems to always exhibit the largest scatter for whatever component considered.

3. Linear regression correlation coefficients of each 3D time-series solution from the 9 stations are calculated. The results are illustrated in **Table 3-3**. The mean values are computed by excluding two stations, MANS and RENN, which exhibit large discrepancies in the RMS scatter tests.

	Bern/ Gins	Bern/ Gamit	Bern/ Gipsy	Gins/ Gamit	Gins/ Gipsy	Gamit/ Gipsy	Mean
BRST	0.811	0.897	0.674	0.857	0.680	0.787	**0.784**
CHER	0.777	0.794	0.703	0.729	0.666	0.679	**0.724**
COUT	0.801	0.810	0.685	0.759	0.664	0.671	**0.732**
DIBE	0.854	0.892	0.796	0.860	0.796	0.866	**0.844**
MANS	0.609	0.661	0.446	0.464	0.340	0.461	**0.497**
PAIM	0.862	0.895	0.762	0.857	0.771	0.802	**0.825**
RENN	-	0.752	0.544	-	-	0.551	**0.616**
TREV	0.815	0.860	0.738	0.817	0.744	0.764	**0.789**
YGEA	0.796	0.850	0.617	0.767	0.526	0.683	**0.706**
Mean up	**0.817**	**0.857**	**0.711**	**0.807**	**0.692**	**0.750**	**0.772**
Mean north	**0.798**	**0.768**	**0.628**	**0.722**	**0.625**	**0.543**	**0.681**
Mean east	**0.803**	**0.727**	**0.491**	**0.693**	**0.489**	**0.570**	**0.629**

Table 3-3 : 3D Correlation coefficients between two solutions for different GPS stations. The 3D mean correlation coefficients over all stations are indicated in the last column.

For the vertical component, the mean correlation coefficient is 77 % if all solutions are merged. GINS' solution seems to be very well correlated to the others in vertical as well as in horizontal. The correlation coefficient in the vertical exhibits the 80 % level compared to GAMIT's and Bernese's solutions and 69 % level compared to GIPSY's solution.

In the north component, the correlation with GAMIT's and Bernese's solutions amounts to 72 % and 80 % respectively, contrary to about 62 % with GIPSY's solution.

Finally, for the east component, the correlation coefficient is 80 % and 69 % with Bernese's and GAMIT's solutions respectively. The worst correlation coefficient in East comes from the comparison to GIPSY's solution which results about 49 %.

The three solutions of Bernese, GAMIT and GINS present a mean 3D correlation coefficient of about 82 % and 52 % when GIPSY's solution is included.

To conclude, GINS' solutions are validated with respect to the regression analysis performed.

4. Comparisons of the in-phase and out-of-phase 3D displacement coefficients in the semi-diurnal band (**Fig. 3-4**) at the 9 GPS campaign stations are realised.

   Concerning the phase on the horizontal components, a good agreement is observed (differences lower than 40°) for GAMIT, GINS, and GIPSY solutions, except in BRST station which presents the highest discrepancies (~100°) for the east component. Bernese's solution generally represents an important phase shift which can reach at complete phase opposition for some stations (MANS, PAIM, and YGEA). The four solutions are in a very good agreement at CHER, COUT, and RENN stations. For the vertical component, the phase discrepancies are lower than 15-20° between the 3 solutions of GAMIT, GINS and GIPSY.

   The phase shift of Bernese's solutions at certain stations could be related to a "bug" in the solid earth tides displacement corrections present in versions 4.2 and 5 (Hugentobler, personal communication).

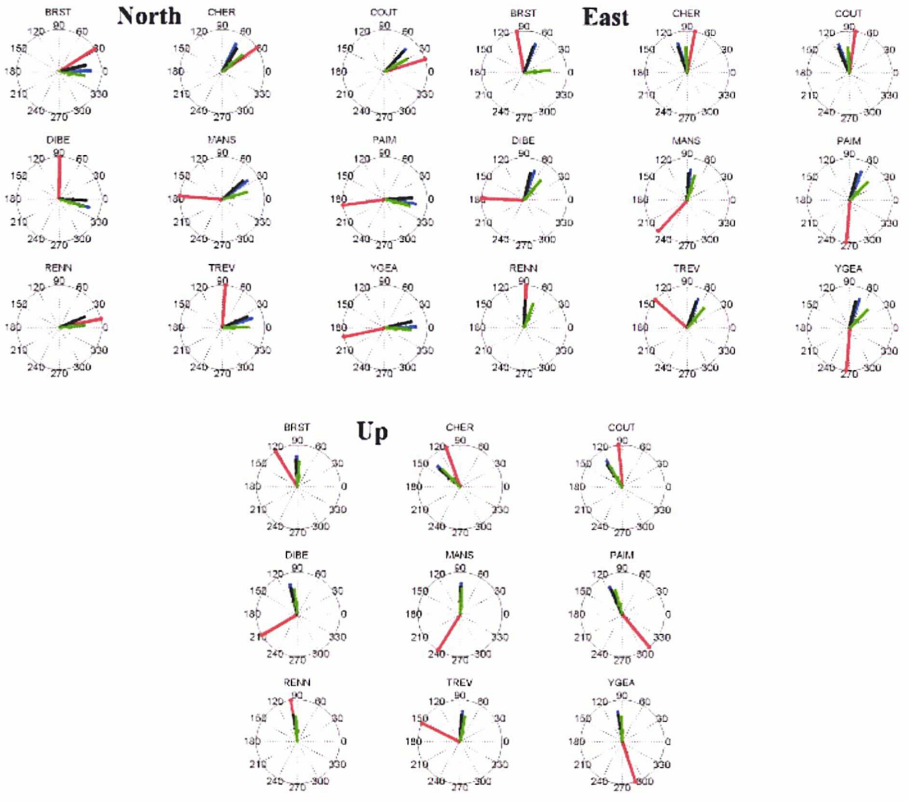

Fig. 3-4 : Phasor plots of the intra-software solutions in North, East and Vertical. (red) Bernese, (Green) GIPSY, (Blue) GINS, (Black) GAMIT

In the amplitudes all strategies have disagreements which are constrained to the level of discrepancies between models and initial corrections applied to each solution. Consequently, the comparisons are valid up to the level of discrepancies between the ad-hoc models.

In conclusion GINS' GPS position time-series results were compared to those of three well established, globally known, scientific software packages and the level of agreement between the aforementioned tests validates the current modifications.

The support from: J. Nicolas, L. Morel, S. Durand (L2G of ESGT), M. Vergnolle and M.-N. Bouïn (LAREG/IGN) and F. Masson (IPGS) who provided GPS data and solutions from Bernese, GIPSY-OASIS, and GAMIT/GLOBK, is greatly acknowledged.

3.2.2 POD validations

The POD validations are separated in two parts. The first is concentrated in the implementation of the SRP models for the GPS satellites and the impact on the accuracy comparing to the final IGS sp3 orbits. The second one is focusing on the SLR POD evaluation of the GIOVE-A first Galileo satellite and the SLR network effect on the reference system of the GPS 35-36 satellites.

The statistical interpretations were performed by using internal and external RMS misfit overlaps of 2-day arcs according to **Eq. 3-1.** An orbit overlap is defined by the comparison of the satellite's position between the common (here 1-day) time-span of two successive orbits:

$$rms_{misfit} = \sqrt{\frac{\left(\mathrm{x}^{arc1} - \mathrm{x}^{arc2}\right)^2}{n}}$$

$$rms_{3D} = \sqrt{rms^2_{Radial} + rms^2_{Along} + rms^2_{Cross}} \qquad \textbf{Eq. 3-1}$$

Where x^{arc1} and x^{arc2} are the 3D geocentric coordinates of the GNSS satellite from the 1st and 2nd arc respectively and n is the total number of common points in the overlapping arc.

3.2.2.1 Improving Solar Radiation Pressure (SRP)

As previously mentioned in paragraph § **2.3.3** SRP is the most important non-gravitational perturbation on the position state of the GNSS satellites and not only. Its possible impact on the Z-shift of the geocentre of the GPS frame compared to ITRF has been evocated by Herring (2007). Urschl et al. (2007) showed that when modelling SRP a signal in the geocentre time-series in the Z-translation at ~351 days appears. This period corresponds to the draconic year (= the "GPS year": the interval required for the constellation to repeat its inertial orientation with respect to the sun) of 352.43 days. Ray et al. (2006) and Ostini et al. (2007) demonstrated the existence of this signal in the residuals of GPS stations coordinates time-series. They pointed out that this period cannot be interpreted in the geophysical sense.

About one percent of the acceleration due to SRP is acting in a direction other than that of the incident solar light (Hugentobler et al. 2003). Direct SRP can be pictured as the net momentum imparted to the SV by photons striking and recoiling from its opaque surfaces. Indirect SRP (predictable and anomalous) is caused for example by:

- the effects of the Earth's albedo radiation pressure;
- the satellite's heat flow re-radiated from the body's surface. This force is directed along the positive radial direction when the heating source is the Earth and to all directions for the heating coming from the sun. Part of this force could explain the Y-bias correction (Duha et al. 2006);
- the result of out-gassing from the apogee engine, the solar panels, the multilayered insulation that wraps the satellite body (Fliegel et al. 1992, Fliegel and Gallini 1996, Slabinski 2004) ;
- the along-track acceleration produced by a force in the body fixed +Y or –Y direction that is along the nominal axis of the solar-panel center beams. Misalignments of these beams or of the solar-sensors could provoke a force for which a Y-bias must be accounted for. During and after an eclipse, misalignments are more severe. The misalignment angle is sometimes called yaw-bias (Bar-Sever 1996, Bar-Sever et al. 1996, Hugentobler et al. 2003).

In general an exact representation of the spacecraft's attitude is needed when we model SRP (**Fig. 3-5**). As such the following referentials are used:

- R (radial), T (tangential), N(normal) to the orbital plane ;
- Z (points towards the Earth center), Y (points along the nominal axis of the solar panels), X (completes the system);
- D (points towards the incident solar light), Y (points along the nominal axis of the solar panels), X (completes the system).

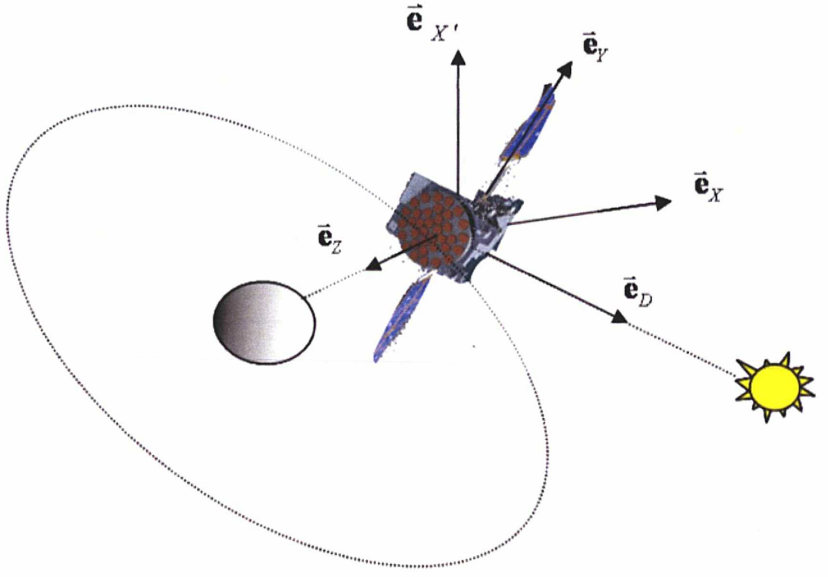

Fig. 3-5 : The GNSS attittude models XYZ and XYD

The SRP models implemented in GINS and used for the current POD validation tests are:

- The *Box-and-Wing* (B-W) (Dobler 2006) a purely analytical model of CNES/GRGS which represents the direct SRP forces by the use of the specularity and reflectivity coefficients of the GPS satellites body surfaces. Updates for the Block-IIR satellites were added along with the coefficients for the Earth's albedo inside GINS software. The total B-W SRP is calculated from :

$$\vec{F}_{SRPtotal} = -C\left(\frac{d_\Theta}{d}\right)\sum_i \frac{S}{m}\left|\cos\theta\right|\cdot\left(\begin{array}{l}\left(1-K_dK_s\right)\vec{\beta}_\angle + \\ +\left(\begin{array}{l}\frac{2}{3}\left(K_d\left(1-K_s\right)+K_a\varepsilon\right) \\ +2K_dK_s\cos\theta\end{array}\right)\vec{\beta}_\perp\end{array}\right) \qquad \textbf{Eq. 3-2}$$

Where:

- C is a solar constant = 4.5 10^{-6} N/m^2 at 1 AU ;
- $\frac{d_\Theta}{d}$ is the ratio of the true to observed distance ;

- $\frac{S}{m}$ is the ratio of the area of a flat surface S to the total mass of the body m ;
- $\bar{\beta}_{\perp}$ is the "normal" unity vector perpendicular to the surface ;
- $\bar{\beta}_{\angle}$ is the unity vector in the direction satellite-sun ;
- K_s is the specularity coefficient ;
- K_d is the reflectivity coefficient ;
- K_a is the absorption coefficient ;
- ε is the infra-red re-emission ;
- θ is the angle between the incoming solar ray and the normal to the surface .

- The Rockwell analytical models T20 and T30 with empirical augmentation developed by Fliegel et al. (1992) and Fliegel and Gallini (1996). T30 was the most recent update for the Block-IIR inside GINS ;
- The *University College of London* (UCL) analytical model (used only for Block-IIR) which simulates the incident photon flux using a pixel array (Ziebart et al. 2005). It was recently implemented in GINS as well;
- The empirical updated version of the "GPS Solar Pressure Model 1997" (GSPM.97) for Block-IIA and IIR SRP model by Bar-Sever and Kuang (2003).

3.2.2.1.1 3D RMS misfits

The comparisons at this stage are performed only externally with respect to the IGS sp3 final orbits. The parameterisation of the strategy follows the one in Melachroinos et al. (2006) by the use of a global GPS IGS network of ~70 stations in un-differenced mode as illustrated in **Fig. 3-6.** The four aforementioned SRP models are applied in each case and the total RMS misfit to the IGS orbits is extracted. Furthermore an SRP scale factor, a Y-bias and its drift are adjusted. The nominal attitude is at the DYX system.

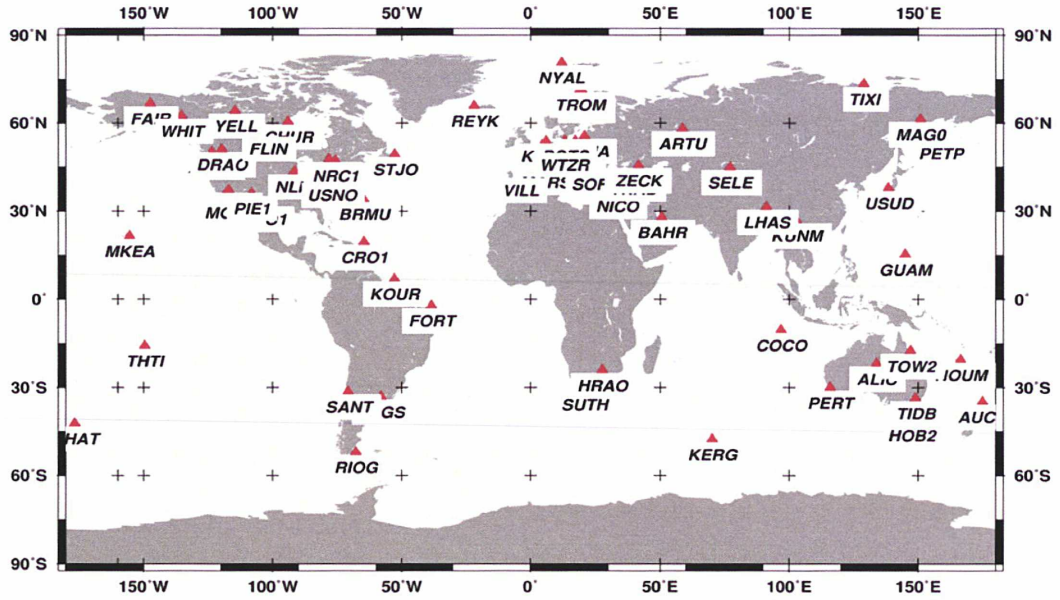

Fig. 3-6 : The network of 70 globally distributed GPS stations used for GINS GNSS POD

The comparison of the produced orbits with the four different classes of SRP models is illustrated in **Fig. 3-7**.

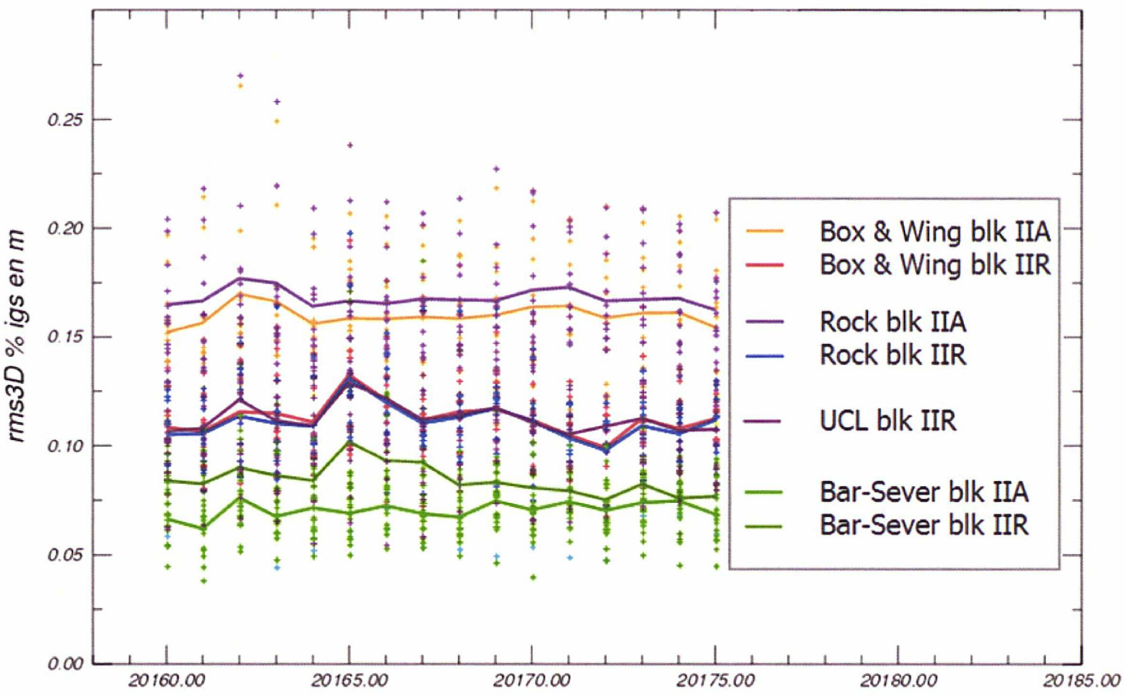

Fig. 3-7 : 3D RMS misfits to the IGS sp3 orbits for different SRP models

The curves are classified into Block-IIA and IIR satellites. The abscissa represents the time scale in Julian dates from January 1 1950 and the corresponding time length in Gregorian date is March 13 through 28 2005.

From **Fig. 3-7** we principally conclude that the POD performances, with a simple dynamic parameterisation, have better agreement when using the updated GSPM.97 model. The three SRP models for the Block-IIR s/c, T30, B-W and UCL give a difference of 2 cm with respect to the GSPM.97 model. The other two models for Block-IIA s/c, T20 and B-W give the largest differences of the order of ~7 cm with respect to the GSPM.97 parameterisation.

3.2.2.1.2 Internal vs external overlaps

In this paragraph I study the performances of each of the four SRP models by adjusting different orbit dynamic parameters in each case. The goal is to reach a significant improvement of the parameterization for the B-W model by adding more empirical forces to the final adjustments. Results from these tests are illustrated in **Fig. 3-8** trough **3-11.**

The abscissa contains the 3D-RMS misfits made with successive GPS orbits compared internally (only GINS GPS orbits) and the ordinate the 3D-RMS misfits of the external comparison between GINS GPS orbits and IGS sp3 orbits. The time period is 16 days the same as in **Fig. 3-7**. The different colour illustrations represent the four different dynamic parameterisations for all GPS Blocks.

- Yellow represents the adjustment for one SRP scale factor and Y-bias plus its drift / arc ;
- Purple represents the adjustment for one SRP scale factor plus 2 periodic coefficients (sin and cos) per revolution and an Y-bias plus a drift / arc ;
- Red represents the adjustment for one SRP scale factor, an Y-bias and 2 harmonic accelerations in the X and D system per revolution per arc ;
- Light-blue represents the adjustment for one SRP scale factor, an Y-bias and 2 harmonic accelerations in the T and N system per revolution per arc.

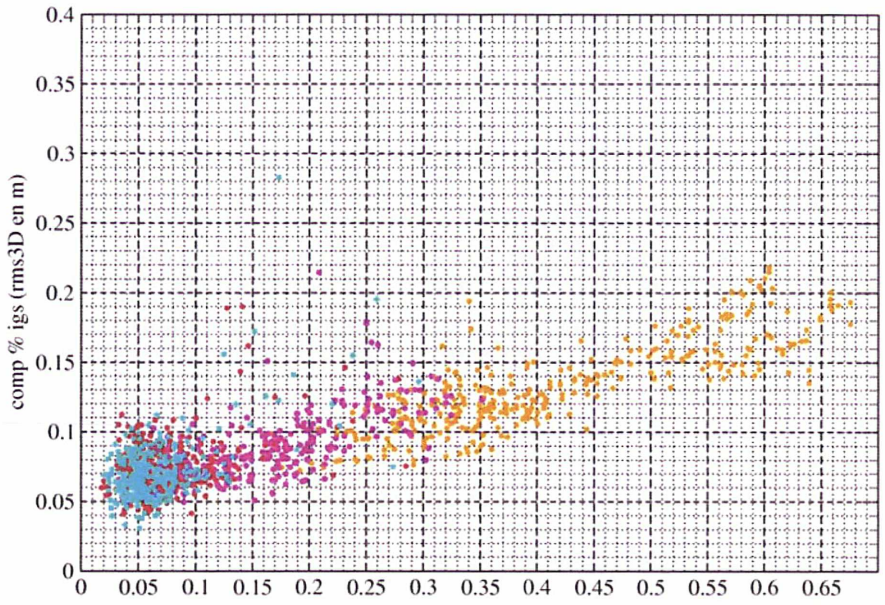

Fig. 3-8 : Internal vs external 3D-RMS misfits for GINS GPS orbits with the B-W SRP model in four different parameterisations. Units are in meters.

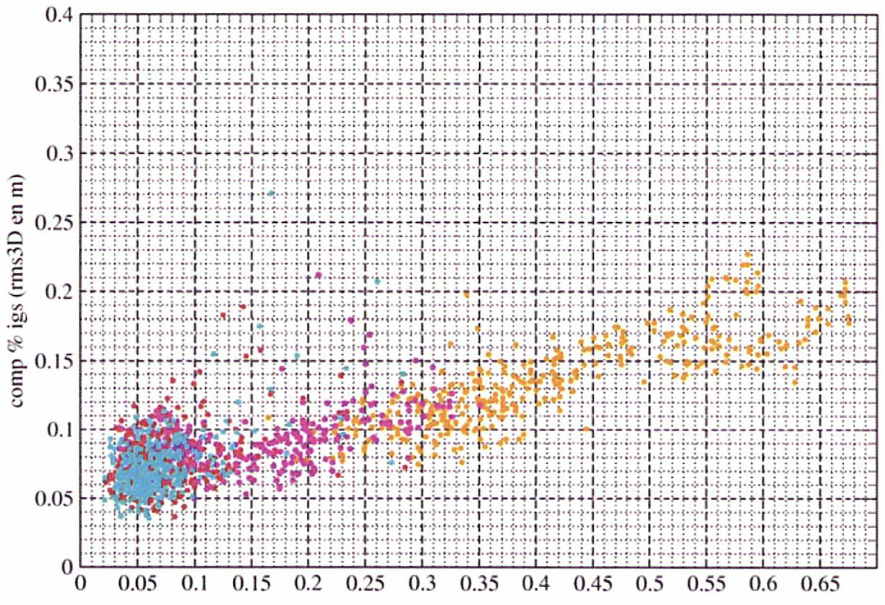

Fig. 3-9 : Internal vs external 3D-RMS misfits for GINS GPS orbits with the Rock T20 and T30 SRP models in four different parameterisations. Units are in meters.

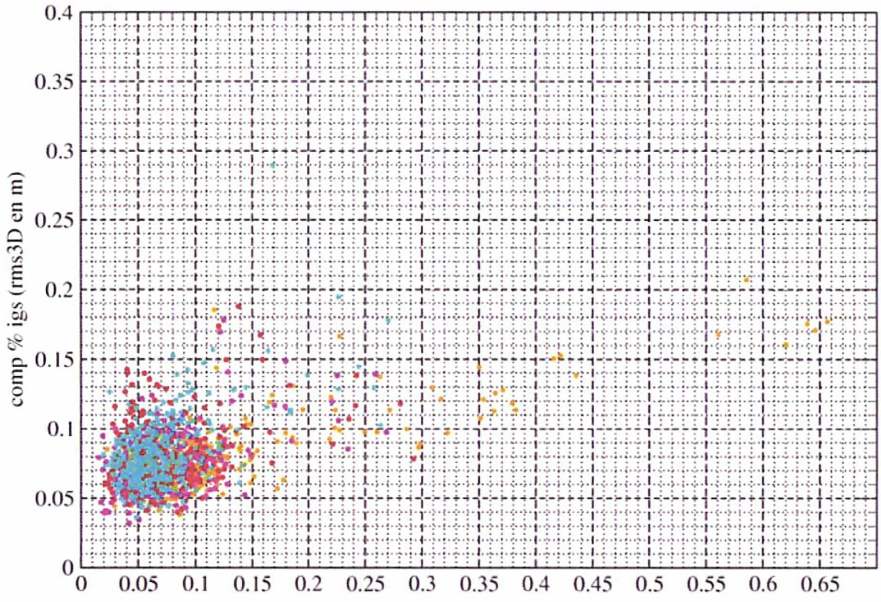

Fig. 3-10 : Internal vs external 3D-RMS misfits for GINS GPS orbits with the GSPM.04 SRP model in four different parameterisations. Units are in meters.

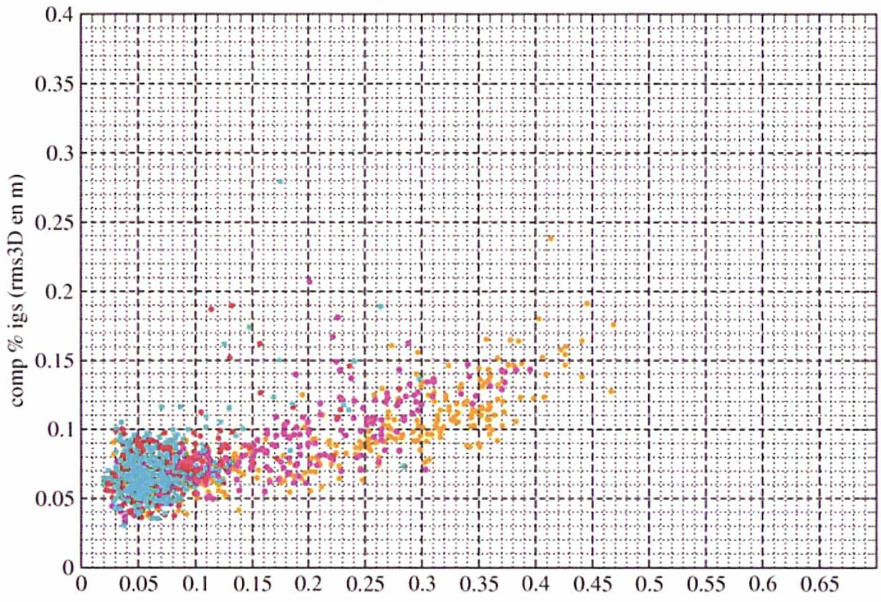

Fig. 3-11 : Internal vs external 3D-RMS misfits for GINS GPS orbits with the UCL SRP model in four different parameterisations. Units are in meters.

The internal 3D-RMS misfit in the last two strategies (colours red and light-blue) drops down from 30 cm to 5 cm in mean values compared to the first two strategies (colours yellow and purple), after the inclusion of the periodical terms either in T, N or X, D directions for all SRP models except for the GSPM.97 model. It is remarkable to notice that the largest effects in the POD using B-W, T20 and T30, and UCL models comes from the inclusion of the forces in the T, N or X, D directions and their periodical terms. The UCL solution contains the GSPM.97 model only for the Block-IIA satellites, and in this way we can evaluate the impact of the SRP model only on the Block-IIR s/c. The GSPM.97 updated model seems to perform neither worse nor better with the inclusion of the directional forces which is certainly due to the model's high performance. The performances of B-W reach those of GSPM.97 when the harmonic accelerations are taken into account.

Furthermore, it seems that we cannot distinguish easily which attitude system, in the case of the B-W SRP model, is the most appropriate for the harmonic accelerations. For this reason the scale factor which will absorb all un-modelled variations of direct SRP forcing was calculated. It is evident that the lower the correction to this scale factor the better the model will be. The tests are concentrated only on the B-W SRP model.

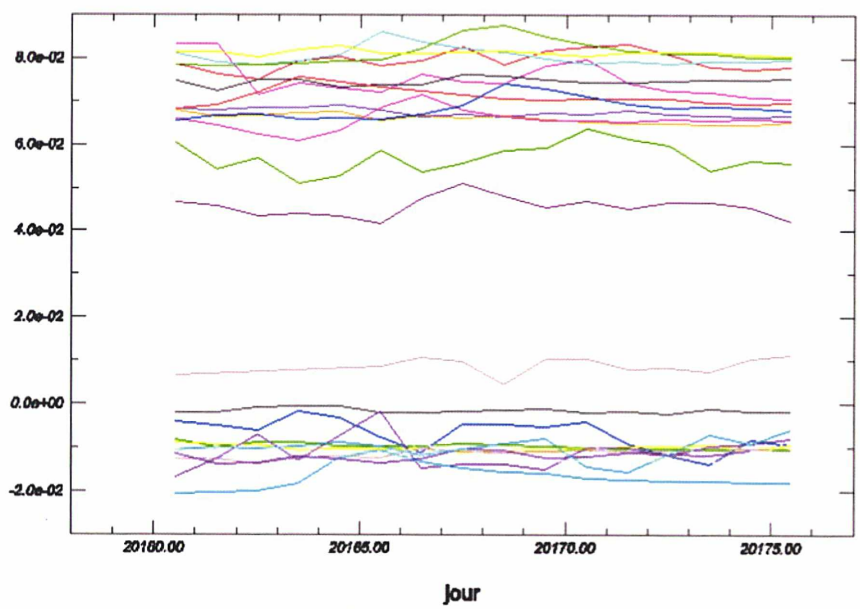

Fig. 3-12 : Post-fit residuals of the scale factor with the adjustment of forces in the X and D directions for the B-W SRP model.

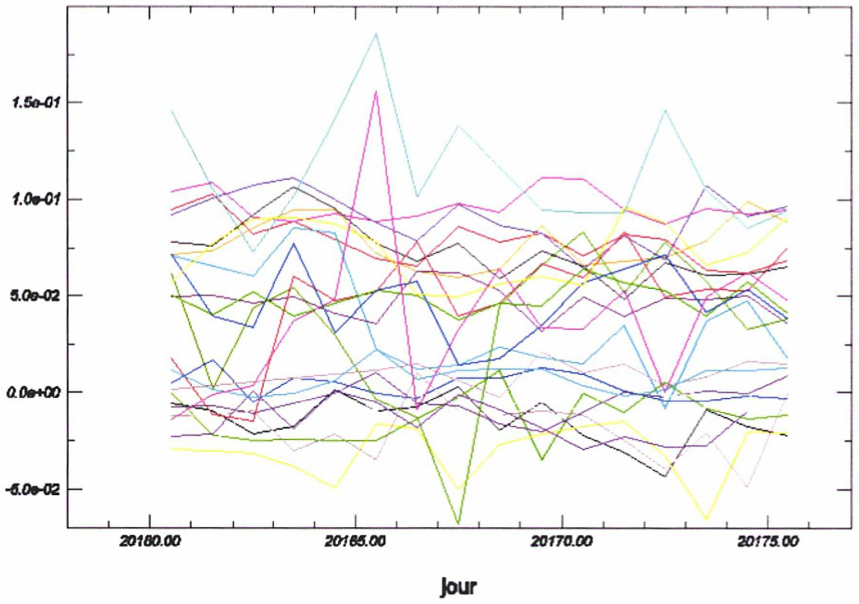

Fig. 3-13 : Post-fit residuals of the scale factor with the adjustment of forces in the T and N directions for the B-W SRP model.

Fig. 3-12 represents the post-fit residuals of the scale factor with the adjustment of harmonic accelerations in the X and D directions. **Fig. 3-13** illustrates the post-fit residuals when periodical forces in the T and N directions are estimated. By comparing the erratically changing variations of the scale factor in **Fig. 3-13** with respect to the more coherent one in **Fig. 3-12** we immediately understand that errors in the SRP of the B-W model are better absorbed when forces are included in the solar oriented XYD directions than when defined by the orbital plane RTN directions.

3.2.2.1.3 SLR residuals test

According to Urschl et al. (2006) the SLR bias residual is the difference between the SLR observed range and the computed range (GNSS orbit and ITRF SLR site coordinates). Those observed range biases for GPS 35/36 were found to be -3.1 cm and -2.8 cm respectively with respect to the IGS final orbits from Urschl et al. (2006). The resulting range residuals are primarily an indicator of the radial accuracy of the microwave orbits. Thus SLR measurement provides a completely independent mean for validating microwave orbits. This

method is applied here in order to evaluate the performances of GINS GPS orbits with respect to the IGS final orbits.

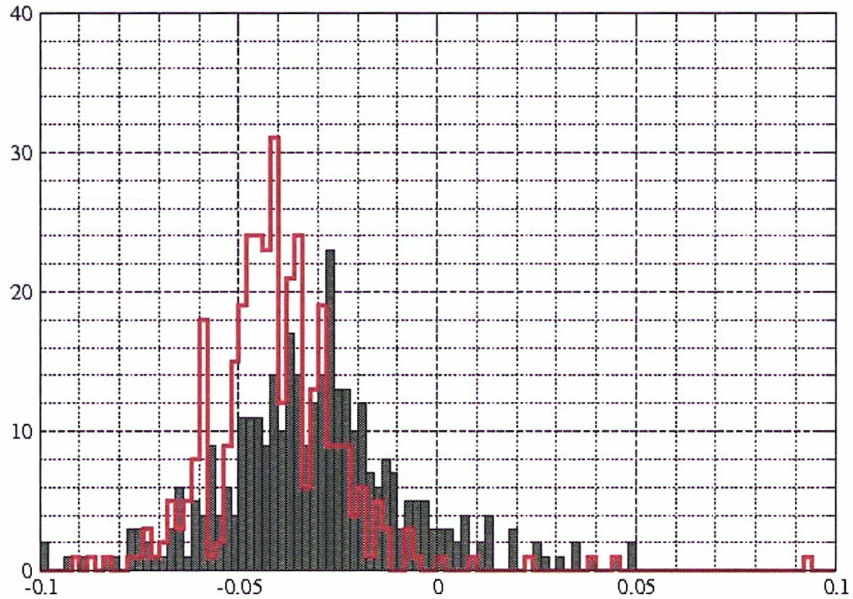

Fig. 3-14 : Mean SLR observed range biases (m) for PRN 05/06 wrt IGS (in red) and GINS (in black) microwave orbits in year 2005.

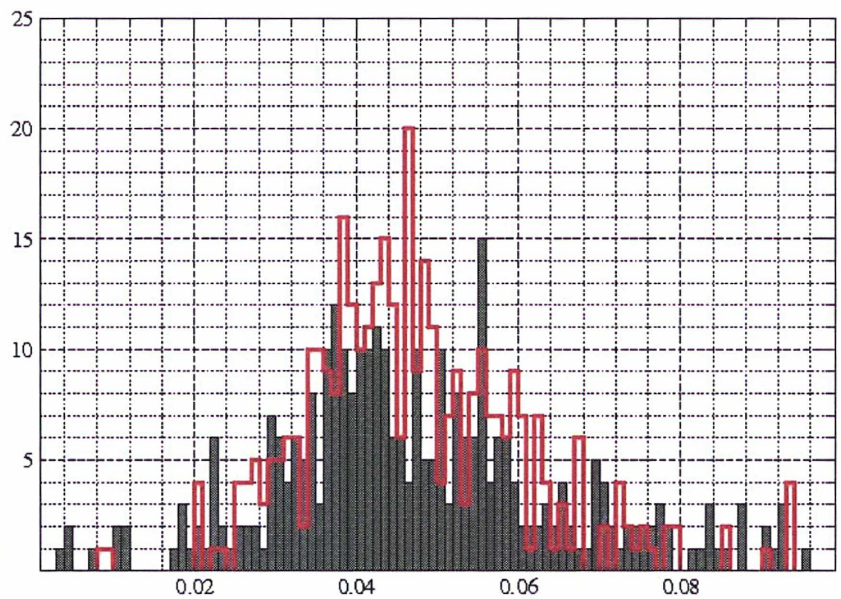

Fig. 3-15 : The mean RMS of range residuals (standard deviation) (m) per SLR stations for PRN 05/06 wrt IGS (in red) and GINS (in black) microwave orbits in year 2005.

In the same period of March 13 through 28 2005 the predefined strategy for the GPS microwave orbit estimation was applied:

- B-W SRP model ;
- One scale factor, accelerations in X and D directions plus 2 per revolution terms for every day-arc included ;
- Phase-wind-up corrections to the effect of circularly polarised radiation on the phase measurements;

The histograms in **Fig. 3-14** and **Fig. 3-15** represent SLR range biases and RMS range residuals per station (standard deviation) and show respectively that the existing quality of the GINS microwave orbits is that of the IGS ACs. By introducing the B-W model for direct SRP together with accelerations in the D and X directions, the mean range bias of GINS' microwave orbits, for both GPS 35/36 s/c, has reduced to -2.9 cm with respect to a -3.7 cm when the IGS orbits are used. The mean SLR stations' RMS residuals (standard deviation) with respect to the GINS' microwave orbits are less dispersed than those to the IGS orbits, at least for this testing period, and vary respectively around 4 cm (GINS orbits) and 4.5 cm (IGS orbits).

In conclusion, the tested comparisons of the 3D-RMS misfit overlaps and SLR range biases to the IGS final orbits show that the current SRP B-W model together with the new dynamic configuration in a solar-oriented attitude referential, results in GINS GPS orbits of quality comparable to the one from IGS ACs.

Calculations and comparisons from D. Dobler's engineering diploma dissertation, which I co-supervised, were greatly appreciated.

3.2.2.1.4 SLR network-effect on the GPS 35 and 36 reference frame

In this study we are using 10 days of SLR data, for the GPS 35 and 36 satellites, from June 6 through 16 2006. In this period most of the SLR stations where pointing to the GIOVE-A satellite and the SLR tracking data for the two GPS satellites have always been sparse. In this investigation the challenge consists in discovering the achievable orbit accuracy of GINS with sparse tracking data for the two GPS satellites and quantifying the SLR network effect on the GPS reference frame with respect to the ITRF. The analysis of the SLR orbits for both GPS satellites is based on the overlaps to the precise IGS sp3 orbits and on the

residuals in radial, normal and along-track directions. Transformation parameters between the fitted SLR arcs and the IGS sp3 orbits are adjusted.

The present methodology has been applied many times in the last 10 years and many studies, like Pavlis (1995), Appleby and Otsubo (2000), Hujsak et al. (1998) have investigated the undergoing problems of SLR sparse tracking orbit determination.

Table 3-4 and **3-5** compare the fitted orbits to the IGS sp3 orbits in terms of position differences in the radial, normal and tangential directions. The RMS is at the level of 3 cm in radial, 47 cm in cross-track and 23 cm in along-track direction for GPS 35.

GPS-35 RMS Misfits (cm)

Earth Along (Tangential)	23.81
Earth Normal	47.25
Earth Radial	3.24

Table 3-4 : GPS 35 10-day SLR arc overlap wrt. IGS sp3 final orbits.

GPS-36 RMS Misfits (cm)

Earth Along (Tangential)	9.55
Earth Normal	25.75
Earth Radial	2.03

Table 3-5 : GPS 36 10-day SLR arc overlap wrt. IGS sp3 final orbits.

For the case of GPS 36 the level of agreement is respectively 2 cm, 9 cm and 25 cm in the radial, along-track, cross-track directions.

When one station in the southern hemisphere tracks GPS 36, for the same period, the RMS misfit, compared to the one for GPS 35, drops down by a factor of 2. This reflects the effect of the SLR network distribution in the southern hemisphere.

In order to further quantify any systematic effects on the GPS orbit reference frame, a 7-parameter Helmert transformation between the SLR-only orbits and the IGS sp3 orbits is applied. **Table 3-6** and **3-7** summarize the statistics from this comparison.

Tx (mm)	-7.8 +/- 9.
Ty (mm)	-.4 +/- .9
Tz (mm)	**59.8 +/- 9.**
S (ppb)	$.620124 \times 10^{-9} +/- .375 \times 10^{-9}$
S (mm)	**16.5 +/- 10**
Rx (arcmin)	$-.33 \times 10^{-3} +/- .1 \times 10^{-3}$
Ry (arcmin)	$.01 \times 10^{-3} +/- .1 \times 10^{-3}$
Rz (arcmin)	$\mathbf{-.24 \times 10^{-2} +/- .1 \times 10^{-3}}$

Table 3-6 : Helmert transformation wrt. the IGS microwave orbits for GPS 35 JJULD 20610-20620 in mm.

Tx (mm)	2.2 +/- 5.3
Ty (mm)	. 8 +/- 5.3
Tz (mm)	**45.3 +/- 5.3**
S (ppb)	$.712820 \times 10^{-10} +/- .2 \times 10^{-9}$
S (mm)	**1.9 +/- 5.**
Rx (arcmin)	$-.30 \times 10^{-3} +/- .5 \times 10^{-4}$
Ry (arcmin)	$.04 \times 10^{-3} +/- .5 \times 10^{-4}$
Rz (arcmin)	$\mathbf{-.14 \times 10^{-2} +/- .5 \times 10^{-4}}$

Table 3-7 : Helmert transformation wrt. the IGS microwave orbits for GPS 36 JJULD 20610-20620 in mm.

Both Z-translation coefficients are significant with 60 mm (± 10 mm) and 45 mm (± 5 mm) for GPS 35 and 36 respectively. This offset may reflect the non-homogeneity of the SLR tracking stations in the global network. In addition, there is a factor of 8 difference in the scale for GPS 35 and 36 with respect to the reference frame defined by the IGS sp3 orbit. This effect is related to the poor number of southern tracking SLR tracking stations.

Finally, the overall misfit of SLR-only orbits calculated by GINS is 2 cm to 3 cm in radial direction for GPS 35 and 36 satellites. The consistency of the reference frame varies in between 4 cm to 6 cm in the z-shift and 0.1 cm to 1.6 cm in the scale for GPS 35 and 36 respectively.

3.2.2.2 GIOVE-A orbits

GIOVE-A is the first satellite of the future Galileo global navigation system. It has been developed by Surrey Satellite Technology Ltd and the ESA (*European Space Agency*). It was launched from Baikonur Cosmodrome on December 28 2005 and placed into a MEO with a semi major axis of 29600 km, an inclination of 56° and an eccentricity of 0.002 (see § **1.1.3.7**). GIOVE-A is equipped with a *Laser Retro Reflector* (LRR) array having 76 corner cubes with a diameter of 27 mm each (*ESA-EUING-TN/10206*), which provides 40 % more return energy than the GPS 35 and 36 LRR arrays (ILRS). The final constellation of Galileo will consist of 27 operational spacecrafts all equipped with such identical LRR arrays. After the launch of GIOVE-A, ESA has requested ILRS an SLR campaign support during Spring and Summer 2006 (http://www.esa.int). The purpose of these campaigns was to provide data for the characterization of the satellite's on-board clock (§ **1.1.3.7**).

The first of theses campaigns has taken place during May 22 and July 24 2006, with the participation of 13 globally distributed SLR stations (**Fig. 3-16**) and it continues up-to-day.

I present the results for the GIOVE-A SLR-only POD with GINS for the period that extends from June 5 to November 25 2006. The orbit validation is based on internal overlaps of fitted SLR orbits of 5-days having a 2-day common segment and on the comparison of the pre-fit and post-fit station residuals.

The attitude model used for GIOVE s/c is illustrated in **Fig. 3-5** and corresponds to the XYD coordinate frame.

For GIOVE-A, I implemented in GINS a new B-W SRP model including respectively 16 surface sections with approximate reflectivity and specularity coefficients. The following GIOVE-A dimensions are used in the B-W model:

- Total mass : 614 kg (source ESA);
- Main body dimension : 1.3 m * 1.8 m * 1.65 m (Height x Width x Length) (source ESA);
- Wing dimension : 0.98 m * 1.74 m * 4 (in total 4 surface sections) (source ESA);

The network of global SLR stations is illustrated in **Fig. 3-16** and the estimation strategy is described in **Table 3-8.**

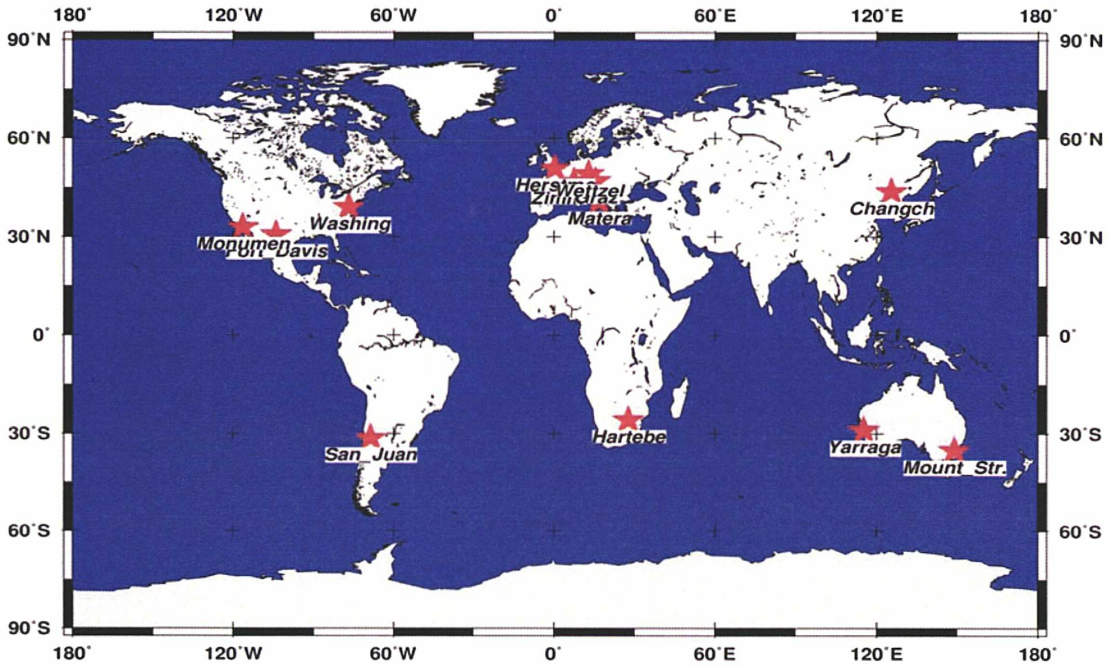

Fig. 3-16 : The GIOVE-A global SLR network

I have processed observation sets of 5-day arcs including 2 per revolution terms each 2.5-days (with a-priori constraints) in X, D directions. An additional acceleration along the s/c's Y-axis, the so-called Y-bias, is also adjusted, together with a scale factor for each arc. Initial conditions for the numerical integrator are introduced from the adjusted values of an analytical approach based on the SLR data only.

A first evaluation of the SLR orbits is performed by examining the station-specific residuals with respect to the integrated satellite positions. This part gives a first indication of the accuracy in the radial direction which varies between + 20 cm and to – 20 cm excluding outliers at peculiar dates. In **Fig. 3-17** these outliers are present for specific dates and are common to all 13 SLR stations. The dates are: June 27 to July 1 and October 16 to 21.

GINS 7.1	***GIOVE-A***
Datum definition	ITRF 2000, EOPC04
Tidal displacements	IERS03
Gravity field	EIGEN-GL04S(20x20)
Atmospheric loading Ocean loading	ECMWF FES2004
Troposphere	Marini-Murray
Solar Radiation Pressure	Box-and-wing
Albedo and infra-red	Analytical model (10°x10°)
Satellite's retro-reflector offsets	x=0.828, y=0.655, z=-0.688
Attitude model	X, Y, D
Numerical integration	Cowell 8^{th} order, step size180s
Parameter adjustment	6 orbital parameters, 1 SRP coeff., 1 Y-bias, 2 X, D per-revolution (cos, sin)

Table 3-8 : The GIOVE-A orbit estimation strategy

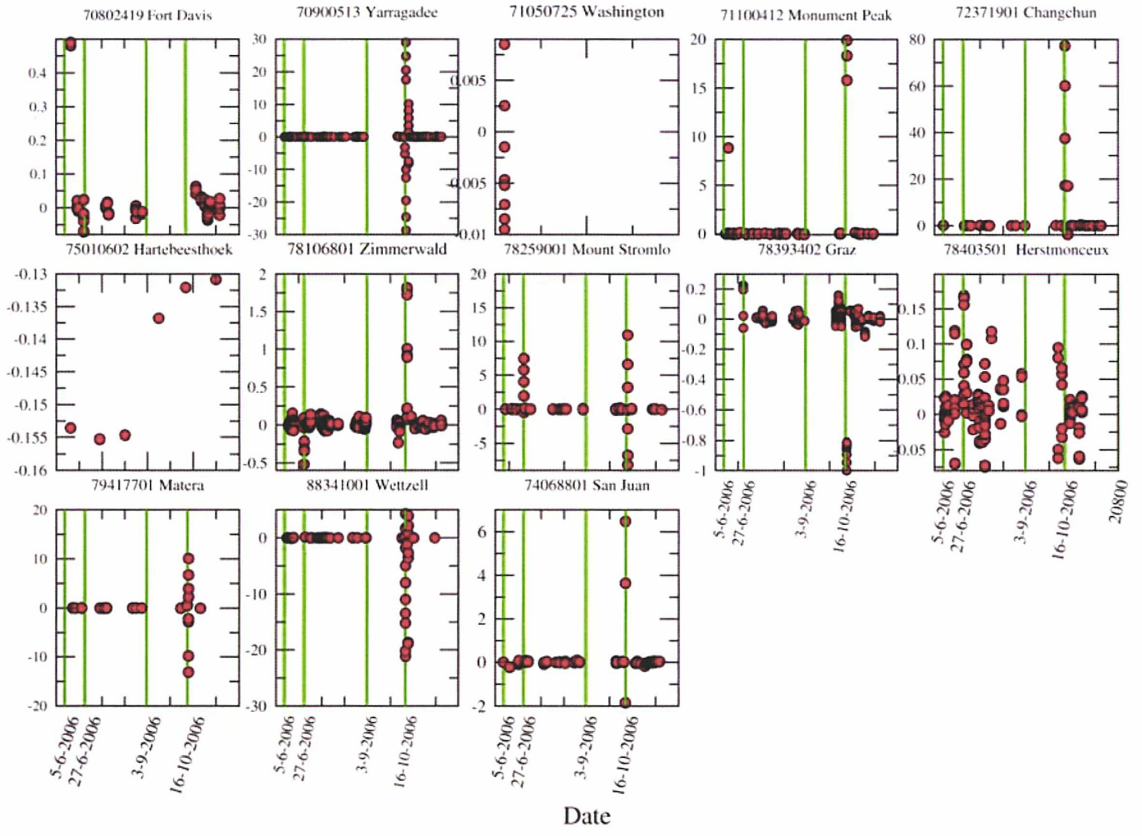

Fig. 3-17 : Station-specific SLR residuals for the periods of June 5 to November 25 2006

After fitting the orbit to the SLR data the internal RMS misfit analysis for each 5-day arc is realized in order to evaluate the level of accuracy of the fitted SLR orbits. The results of the RMS misfit residuals, the total number of normal points and the post-fit weighted residuals are presented in **Fig. 3-18.**

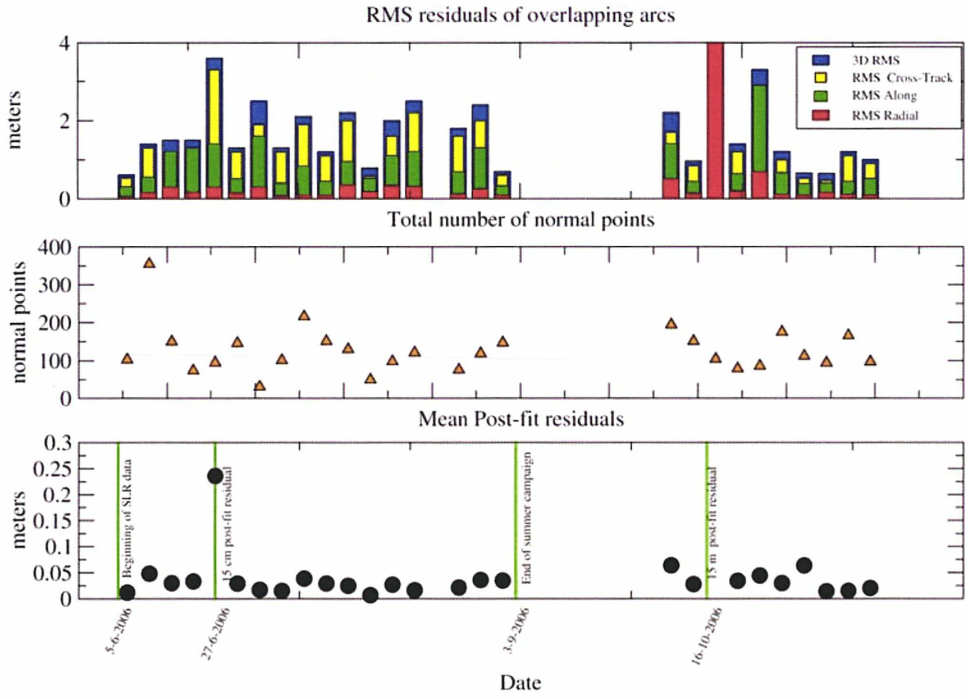

Fig. 3-18 : (a) RMS misfit residuals between successive 5-day SLR arcs overlapped over 2 central days. (b) The amount of normal point observations during the period June 5 to November 25 2006. (c) The total Post-fit residuals for the same period.

From **Fig. 3-18 (c)** we observe the mean global post-fit residuals. For June 27 to July 1 2006 and October 16 to 21, the two orbits contain the same type of outliers observed in the per-station pre-fit residual analysis, which is 23 cm and 16 m respectively, while the overall radial accuracy varies less than 5 cm in the rest of the 5-day arcs.

The RMS of the overlap misfit analysis is given in **Fig. 3-18 (a).** The misfit residuals are of the order of 3.6 m and 420 m in 3D, 30 cm and 86 m in radial, 1.4 m and 344 m in along-track and 3.3 m and 240 m in cross-track (tangential), for the same two overlapping dates respectively. Immediately, we conclude that for these two periods of time, major un-expected perturbation events or manoeuvres of the satellite, for which our dynamic model cannot account for, must have taken place. These outliers cannot have been provoked from an insufficient number of normal points since for both arcs the total number of observations is 95 and 104 normal points respectively as seen from **Fig. 3-18 (b)**.

To conclude, the capacity to estimate SLR-only orbits for GIOVE-A s/c has been implemented and evaluated in the GINS GNSS software. The generated orbits are internally accurate to the level of 5-10 cm radially as can be seen in **Fig. 3-18 (a)** and **(c)**.

Unknown maneuvers and perturbations are a critical issue for the GIOVE-A POD. These maneuvers took place somewhere during June 27 to July 1 2006 and October 16 to 21 2006 as seen from the pre-fit and post-fit mean residuals of all the SLR stations and the internal RMS overlap analysis in **Fig. 3-17** and **Fig. 3-18.** Not announced maneuvers or un-modeled perturbations can be dealt with the adjustment of stochastic pulses during the perturbation period.

I have used an analytical B-W SRP model with approximate specularity and reflectivity coefficients. A further improvement in the POD will be the adjustment of these coefficients together with the LRR arrays offsets in at least one "GPS year" time period by making use as well of the most accurate radiometric observations in L_1 and E_5 bands.

3.3 Summary

At the beginning of this chapter the basic modifications of the updated GINS GNSS software were presented. The processing scheme of GNSS data with GINS software has been described in a step-by-step process. Validation tests of the new modifications were separated into two large categories.

The GINS' high-frequency estimated GPS position time-series were cross compared to the ones issued from well-known scientific software packages. These software were : GAMIT 10.21 (King and Bock 2005), GIPSY/OASIS II (Zumberge et al. 1997) and Bernese 5.0 (Dach et al. 2007). The comparisons were made using the observational set of 9 GPS dedicated campaign stations used in order to study OTL in Brittany (see **Chapter 4**). The comparisons have demonstrated the validation of the modifications issued for the first time in the GINS software. The linear correlations of more than 80 % with respect to the other solutions and the agreement in the periodicities of the high-frequency time-series indicate the high level reliability of GINS' results.

During the second set of validations tests the ability and performance of GINS to give accurate and precise POD results for the GPS satellites against a series of recently implemented SRP models was investigated. More emphasis was given to the newly modified B-W SRP model for GPS satellites. The GINS' GPS orbit tests were based on internal and external comparisons to the IGS sp3 orbits. Successive arcs with 1-day common segment overlaps were evaluated. The statistical interpretations were based on the internal

and external RMS misfit of **Eq. 3-2.** The internal 3D-RMS misfits were found to be 5 cm with the inclusion of periodical terms in the solar oriented and orbital plane directions. The external 3D-RMS misfit compared to the IGS orbits varied between 5 cm and 10 cm. By comparing the variations of the post-fit residuals of the estimated scale factor for each case the coherence of the dynamical parameterization was demonstrated. Histograms of SLR range residuals and biases were calculated. The SLR observed ranges were computed using GINS and IGS microwave orbits for both GPS 35 and 36 satellites. The respective biases produced were: -2.9 cm and -3.7 cm when GINS and IGS orbits were used. The mean SLR station RMS range residuals with respect to the GINS' microwave orbits were found to be about 4 cm. These were less dispersed to those calculated with the IGS orbits of 4.5 cm. Finally the B-W SRP parameterization in a solar-oriented attitude referential was selected as the ideal configuration.

Furthermore, the precision of the SLR-only POD for the GPS 35 and 36 satellites and the SLR network effect on the orbit reference frame were quantified. The precision was found to be around 2 cm to 3 cm radially and the consistency of the SLR reference frame with respect to the IGS reference frame arises up to 4 cm – 6cm in the z-shift and 0.1 cm – 1.6 cm in scale for GPS 35 and 36 orbits respectively during the time (June 6 to 16 2006) of the experiment.

Finally the SLR-orbits for GIOVE-A were evaluated by internal RMS misfits comparisons together with the performance of a new B-W model specially implemented for this satellite. The radial accuracy of the SLR-only GIOVE-A orbits in a period from June 5 to November 25 2006 varies from 5 to 10 cm. The analysis of the global post-fit residuals and the RMS misfits has revealed periods of unannounced manoeuvres or un-modelled perturbations for which a special stochastic parameterization is needed. The first implementation steps for the POD of the future Galileo system were accomplished.

4 Ocean Tide Loading Displacements of GNSS networks in Brittany, France

In § **2.4** of this thesis, it is mentioned that ocean tide loading is one of the most important reasons for periodic displacements at geodetic stations after solid Earth tides. In **Fig. 2-22** of the same chapter this type of effect has been quantified compared to displacements due to atmospheric loading, solid Earth tides and pole tides. The response of the oceans, unlike for the solid Earth, is strongly dependent on local and regional conditions that affect fluid flow.

This chapter, which represents the main part of my PhD Thesis, is referring to the study of *Ocean Tide Loading* (OTL) displacements and validation of models through the use of the GNSS technology.

According to the IGS Position paper "*Identification and Mitigation of GNSS errors*" research activities should be stimulated in studying the effects of suspected error sources in the position time-series of geodetic stations. All aspects of GNSS geodesy are potentially

involved from field observations through data analysis and interpretation (Hugentobler et al. 2006).

As such, I studied the option of using GNSS as a validation tool for ocean tide models in a complex coastal area, that of Brittany, through the comparisons of observed (from GPS) versus predicted (from tide models) OTL 3D-displacements. The order of the observed 3D-displacements is most of the time superior to the magnitude of errors induced in the GNSS observations. Nevertheless, for the correct interpretation of the geophysical signal, together with the validation process, the following aspects that can affect the accuracy of the final positions of GPS stations and their estimates are simultaneously analysed:

- The datum stability ;
- The influence of OTL on the TZD parameters ;
- The aliasing effects of un-modelled OTL signals on the position time-series ;

4.1 Modelling OTL

The crustal loading at a particular location due to a given tidal harmonic is computed by integrating the tide height with a set of Green's functions which define the Earth's rheology and relaxation deformation models, carrying the integration over all ocean masses. The total loading may be obtained by summing the effect of all harmonics.

The complex OTL displacement (amplitude and phase) at every point on the solid Earth surface's, colatitude and longitude (θ, λ) are computed as:

$$\Delta u = \iint_{Ocean} G(\psi)\bar{h}(\theta', \lambda')\sin\theta' d\theta' d\lambda' \qquad \textbf{Eq. 4-1}$$

where $\bar{h}$ is the tidal height at the point of colatitude θ' and longitude λ'; $G(\psi)$ is the Green's function computed from the load Love numbers. For the vertical displacement, the Green's function depends only on the h'_n numbers:

$$G^v(\psi) = \frac{G}{g}\sum_{n=0}^{\infty} h'_n P_n(\cos\psi), \qquad \textbf{Eq. 4-2}$$

where $P_n(\cos\psi)$ are the Legendre polynomials of order n, G the gravitational constant, g gravity, ψ the angular distance between the application point of the load (θ',λ') and the observation point (θ,λ) :

$$\cos\psi = \cos\theta\cos\theta' + \sin\theta\sin\theta'\cos(\lambda-\lambda'), \qquad \textbf{Eq. 4-3}$$

Equivalently the horizontal components are derived from the horizontal displacement load Love numbers l'_n, and as there is no horizontal displacement for $n=0$:

$$G^h(\psi) = \frac{G}{g}\sum_{n=1}^{\infty} l'_n \frac{\partial P_n(\cos\psi)}{\partial\psi}, \qquad \textbf{Eq. 4-4}$$

The final loading effect will be expressed in amplitudes and Greenwich phase lags summed over the global surface tidal grid for vertical, eastward and northward directions.

4.2 Ocean tide loading (OTL) displacements from global and local grids: comparisons to GPS estimates over the shelf of Brittany, France.

Advances in space-geodetic positioning techniques in recent years have made it possible to acquire direct geodetic measurement of many of the non-tidal phenomena associated with the dynamics of the Earth's crust, including postglacial rebound, tectonic deformation, polar motion and atmospheric mass movements (Lambert et al. 1998). Apart from the non tidal part of the Earth's deformations, geodetic techniques are very efficient in monitoring deformations caused by transport of masses in the oceans which in close distance from the coasts can provoke significant loading displacements.

Validation of OTL models through observations in complex coastal areas becomes mandatory for geodetic applications of high precision such as the determination of the Earth's rheology (Baker and Bos 2003, Baker at al. 1996), the estimation of *Vertical Land Motion Rates* (VLMR) at tide gauge sites by examining the long time-series of geodetic stations for any spurious signals or even the implementation of new ocean tide models through the use of the *Loading and Self Attraction* (LSA) term.

In coastal regions OTL can cause vertical motions of several centimeters and horizontal motions over a centimeter, large enough to be measured with space geodetic

techniques such as GPS (Vey et al. 2002, Dragert et al. 2000, Khan and Tscherning 2001). Furthermore, long-period GPS height time-series in areas with strong OTL displacements can suffer from un-modelled sub-daily periodic ground displacements (Penna and Stewart 2003). Such effects of periodic displacements can be largely propagated by "data averaging", adopting a GPS processing session length equal or close to the period of the displacement considered (Penna et al 2007, Stewart et al 2005). The result is that these tidal signals will appear in the final coordinate time-series as aliased signals (see § **4.2.6)** with longer periods than the original semi-diurnal and diurnal signals. The effects in long time GPS series can reach amplitudes of several mm (Penna et al 2007). For example, periods of ~13.6 days have been found in GPS time-series when combining VLBI and GPS for the development of combined UT1/LOD and nutation time-series (J. Ray personal communication) which were attributed to tidal effects. As such accurate predictions of such displacements are needed.

The purpose of this study is to evaluate a selection of ocean tide models around the shelf of Brittany and Cotentin, in the northwestern part of France, through GPS positioning. In the past, Llubes et al. (2001) used an FG5 absolute gravimeter and compared the observed variations of five days in gravity with water height variations from a tide gauge in Brest and loading predictions from the CSR3.0 model (Eanes 1994). Vey et al. (2002) compared the observed GPS OTL signal of 8 sites with the FES98 (Le Provost et al. 1998) and the GOT00.2 (Ray 1999) ocean tide models over three days and evaluated the impact of OTL signals on the estimated tropospheric zenith delay parameters. Both studies produced preliminary results because their analysis intervals did not allow accurate and robust validations of the OTL predictions.

We cross compare up-to-date OTL GPS observations over a longer time span to a series of predicted OTL estimates from a more recent and larger selection of ocean tide models than the previous studies, and perform accurate OTL validations. Furthermore, we quantify the differences of two OTL algorithms and analyse the GPS high-rate OTL estimates for spurious signals (multipath). Additionally, the geographical distribution of our GPS campaign stations, allows us to study the geographical propagation of the OTL signal further land-inwards from the English Channel and thus validate the OTL models in a larger area than the previous studies.

In section 4.2.1, we briefly review the selected global and local tide models and the two OTL algorithms. We describe the tides and the GPS data used in the study region in

section 4.2.2. In that section, we also discuss our innovative strategy approach for the measurement of GPS OTL displacements and analyze possible systematic errors that may be present in the GPS time-series. Section 4.2.3 presents the comparison of the GPS OTL observations with the model predictions, through the misfits of a root mean square and chi-square statistical indicators, and the evaluation of ocean tide models. Further on sections 4.2.4 , 4.2.5 and 4.2.6 examine the impact of the datum stability on the observed OTL parameters, the influence of OTL on the estimated TZD parameters and finally the aliasing periods of the OTL signatures propagated from 24-hour batch solutions on low-frequency GPS coordinate time-series.

4.2.1 Ocean tide models and ocean tide loading

4.2.1.1 Ocean tide model selection

Subsequent to the launch of the TOPEX/Poseidon (T/P) satellite, the geodetic community has undertaken a huge effort to improve or develop new tidal models, with the objective of attaining a cm accuracy level in tidal prediction, necessary to meet the altimetry product requirements (Lyard et al. 2006, Le Provost et al. 1995). The overall success in improving tidal prediction accuracy is based on the data assimilation of altimetry analysis on one hand and hydrodynamic/assimilation modelling on the other.

There are still however discrepancies between ocean tide models, especially in continental shelf regions with high loading effects like in the northwest European shelf (including Brittany), Japan (Khan and Hoyer 2004), Australia (Penna and Baker, 2002), Canada and northern US (Hudson Bay and Gulf of Alaska) (Schrama 2005, Khan and Scherneck 2003, Lambert et al 1998) as well as Antartica (King and Padman 2005).

In coastal areas, the tidal spectrum can become very complex because the semi-diurnal and diurnal frequencies are mixed with a large number of non-linear, "shallow-water tides", having frequencies within the long-period, diurnal, semi-diurnal, ter-diurnal, and higher bands. These frequencies are consequence of the non-linear interactions between the tidal waves (resonances) and friction phenomena as they propagate in shallow water (Andersen et al. 2006).

In this study, we have used seven ocean tide models as illustrated in **Table 4-1**. These models consist of gridded amplitudes and phases of the eight or even more major tidal constituents such as: M_2, S_2, N_2, K_2, K_1, O_1, P_1, and Q_1. Six of these models are global and one is regional, namely the *North East Atlantic* (NEA) tidal atlas (Pairaud I. personal communication).

GOT00.2 uses 286 cycles of T/P data to adjust to the a priori FES94.1 hydrodynamic model. It also assimilates 81 cycles of ERS-1 and ERS-2 data at latitudes outside the T/P coverage. NAO99.b has 5 years of the MGDRB (Merged Geophysical Data Records generation B) of the cycles 9-198 of T/P and uses an improved hydrodynamic model derived from Schwiderski (1980) by estimating loading effects more precisely (Matsumoto et al. 2000). The CSR4.0 model is based upon 239 cycles (6.4 years) of T/P altimetry which is used to solve for corrections to CSR3.0 orthoweights in 2x3 degree spatial bins (2 deg. lat.). These orthoweight corrections were output on the 0.5° x 0.5° grid of CSR3.0 and then added to the CSR3.0 values to obtain the new model.

TPXO.6.2 uses 324 cycles of T/P data with some small local areas corrected with higher resolution local inverse solutions, while additional data sets were assimilated for the Ross and Arctic Seas. It also incorporates improved bathymetry for the circum-Antarctic seas (King et al. 2005). It best-fits, in a least-squares sense the Laplace tidal equations and the observations. TPXO.7.0 is a more recent version of TPXO.6.2. For the FES2004 atlas, the assimilated data set is composed of 671 tide gauges, plus 337 T/P and 1,254 ERS altimetric crossover points. No ERS1/2 data are assimilated in the FES2004 solution for the S_2 constituent. ERS1/2 data were included (by mistake) in the FES2004 atlas computation for the K_2.

Table 4-1 : Summary of selected Ocean Tide Models

Model	Source	Tide model type[a]	Resolution[b]	Coverage
TPXO.7.0	(Egbert, G. D. and Erofeeva, L, 2002)	H+T/P+ERS+T/G	(0.25° x 0.25°)	Global
TPXO.6.2	(Egbert, G. D. and Erofeeva, L, 2002)	H+T/P+ERS+T/G	(0.25° x 0.25°)	Global
GOT00.2	(Ray R. D., 1999)	H+T/P+ERS	(0.5° x 0.5°)	Global
NAO99.b	(Matsumoto, K., Takanezawa, T. and Ooe, M, 2000)	H+T/P	(0.5° x 0.5°)	Global
CSR4.0	(Eanes R. J., 1994, Eanes and Bettadpur, 1996)	T/P	(0.5° x 0.5°)	Global
FES2004 (cor. K2)[c]	(Letellier T. 2004, Lyard et al. 2006)	H+T/P+ERS+T/G	(0.125° x 0.125°)	Global
NEA 2004	(Pairaud I. personnal communication)	T-UGOm+LSA	(0.016° x 0.016°)	Local

[a] H, Hydrodynamic model; T/P, TOPEX/Poseidon altimetry data assimilated; ERS, ERS altimetry data assimilated; T/G, tide gauge data assimilated; T-UGOm, Toulouse Unstructured Grid Ocean model (follow-up of MOG2D/3D); LSA, loading and self attraction potential.

[b] Latitude x Longitude

[c] cor. K_2, K_2 from FES2002 as advised by Lyard et al. (2006)

Due to the sun-synchronous orbit of ERS1/2, the ortho-tides (or generalized admittance harmonic analysis) for S_2 did not yield sufficient accuracy, especially in the shelf and coastal regions, which apparently had a side effect in the solution for K_2. The recommendation is to use the FES2002 K_2 instead of the FES2004 K_2 tidal elevation solution (Lyard et al. 2006).

4.2.1.2 The NEA2004 model setup

The NEA2004 tidal atlas has been analyzed from a one year-long tidal simulation, carried out with the *Toulouse Unstructured Grid Ocean Model* (T-UGOm) in a 2D barotropic, shallow water mode (Pairaud I. personnal communication). T-UGOm (which is the follow-up of MOG2D/3D a modelled estimate of the sea surface response to both the atmospheric pressure and wind forcing) is based on an unstructured mesh that permits to increase the resolution of the shorelines. It ranges from 20 km over the deep ocean to less than 1 km along the coastlines. Here we use an interpolated regular grid that comes to the highest resolution possible from that mesh.

The boundary conditions in elevation have been extracted from the FES2004 global model, which allows us to nest this high resolution regional grid into the global FES2004 model in order to have a better refinement of the tides, especially near the complex coasts of Brittany, as shown in **Fig. 4-1** for the M_2 tidal wave. The local NEA2004 model covers the area from -20° to 14° in east-longitude and from 30° to 61° in north-latitude, with a 1/60° resolution. It is completed with the FES2004 grid (1/8° resolution) outside the local area in view to cover the whole oceanic surface. This action is necessary since surface displacement variations will not only be sensitive to local tide variations, even if the station is close to the coast, but also to global tides.

4.2.1.3 Computation of OTL displacements

Predicted OTL 3D-displacement amplitudes and phase-lags were computed for each of the GPS stations, using the web-based 'Ocean Tide Loading Provider' facility olfg/olmpp (http://www.oso.chalmers.se/~loading/, accessed December 6 2005) for TPXO.7.0, TPXO.6.2, GOT00.2, NAO99.b, CSR4.0, FES2004, whereas a modified

version called géochargeV3.0 of the load89 OTL program from Francis and Mazzega (1990) was used for FES2004 and NEA2004 (M. Llubes personal communication).

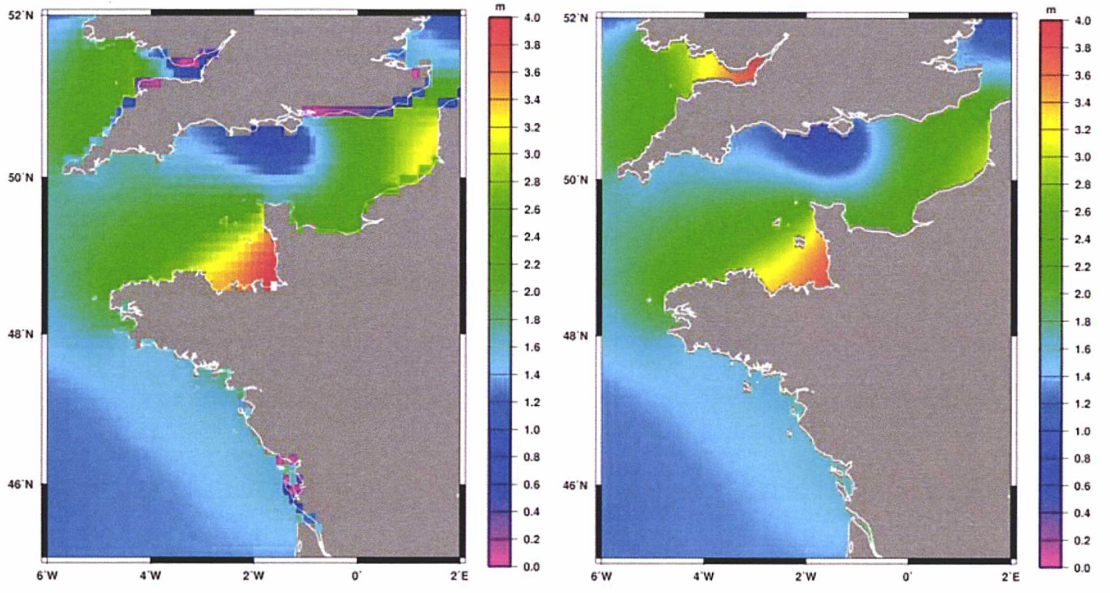

Fig. 4-1 : Effect of the resolution: (left) The M2 surface amplitudes from the FES2004 grids with resolution of 0.125° x 0.125° and (right) the M2 surface amplitudes from the NEA2004 grids with the highest resolution of 0.016° x 0.016°.

Both algorithms are compared with respect to the performances of the FES2004 model for validation purposes. The Olfg/olmpp web-based OTL program convolves each of these tide models with a set of Green's functions based upon the Gutenberg-Bullen Earth model (Farrell 1972). The géochargeV3.0 (modified load89) OTL program formulates the tidal loading based on a set of Pagiatakis's (1990) Green's functions which are enhanced by using the more detailed PREM model (Dziewonski and Anderson 1981).

The complex OTL displacements (amplitude and phase) at every point on the solid Earth's surface, in colatitude and longitude (θ, λ) are computed from **Eq. 4-1**.

Both, the olfg/olmpp and géochargeV3.0 OTL algorithms rely on a point-wise integration of the load tide, which according to Schrama (2005), properly evaluate the tidal heights along a coastal geometry.

4.2.2 The GPS data analysis and estimation of the OTL displacements.

4.2.2.1 The tidal characteristics of the region

The French part of the northwestern European shelf is a region where tides are highly energetic with water height variations in the Bay of Mont St-Michel in excess of 14 m during the equinoxes, as well as important shallow-water tides (Le Provost and Fornerino 1985). The four main semi-diurnal constituents M_2, S_2, N_2, and K_2 provide the most significant contribution to the tide signal and provoke displacements of several cm of the crust along the coasts. The semi-diurnal M_2 constituent is the largest single contributor to the tides in this region. It causes the low-tide high-tide cycle, and its modulation with the mean solar semi-diurnal wave S_2 produces the spring-tide neap-tide cycle. M_2 surface elevation amplitude ranges from 1 m above the abyssal plain to 1.7 m at the Atlantic coasts with a fast increase over the shelf where it reaches 4.3 m in the Mont St-Michel bay (see **Fig. 4-1**).

Furthermore, non-linear semi-diurnal, ter-diurnal and higher bands cannot be neglected, since they can result into OTL displacements of a few mm mostly in the vertical direction. However, given that many of these shallow water constituents have a spectrum very close to the integer multiples of the orbital period of the GPS satellites (K_1, K_2 K_3, K_4, K_5 etc.), their signals cannot be easily distinguished with GPS data, as we will see further on.

The diurnal constituents do not contribute much to the tidal signal over the English Channel which is a typical feature of tides within the Atlantic Basin (Le Provost and Fornerino 1985).

4.2.2.2 GPS data set of the NW-France tide loading campaign

In order to study the intense loading phenomena an experimental multi-technique campaign was organized by the French group G2 (*Géodésie – Géophysique*). The campaign consisted of operating a total of twelve semi-permanent GPS stations during a period of almost four months from March 3 through June 19 2004.

Due to data latency problems, we examined GPS OTL displacement estimates from eight of the twelve campaign stations. The data were collected from the eight GPS stations for the time span of around 104 days, as listed in **Table 4-2**. **Fig. 4-2** and **Fig. 4-3** illustrate the geographical distribution of these eight GPS campaign stations together with the FES2004 predicted vertical displacements for M_2

In order to realize the reference frame in a rigorous and most optimal way, and decorrelate the tropospheric estimates (Vey et al. 2002), these stations are included in a regional network of 14 European stations from the IGb00 reference network (Ferland 2003) , which is presented in **Fig. 4-2.**

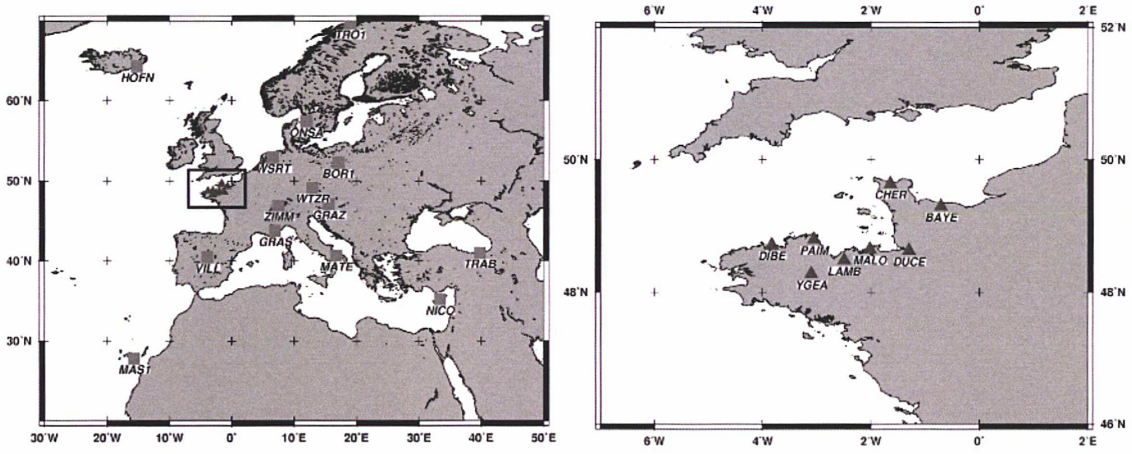

Fig. 4-2 : The IGS and GPS Brittany campaign network

4.2.2.3 Estimation strategy employed

As previously mentioned by King et al. (2005) and Khan and Tscherning (2001), the methods for determining the OTL harmonic constituents of surface displacements using GPS mainly fall into one of two categories. The first consists of determining 1-4 hour batch-sized sub-daily positions using GPS relative positioning techniques, in which the site motion due to OTL is regarded as negligible during each batch solution. Each of the position estimates can then be processed as independent tide gauge measurements from which the harmonic coefficients of OTL displacements can be computed. However, accurate ambiguity fixing and tropospheric zenith delay estimation must be achieved (Melachroinos et al. 2006a, 2006b, King et al. 2003, Vey et al. 2002,

Dach and Dietrich 2001, Dach and Dietrich 2000, Dragert et al. 2000, Blewitt 1989, Melbourne 1985).

GPS station	North-Latitude (°)	East-Longitude (°)	El. Height (m)	Data span (days)
YGEA (Saint Ygeaux)	48.2724914	-3.1041078	257.159	105
DIBE (Le Diben)	48.7104724	-3.8323766	78.780	104
PAIM (Paimpol)	48.7921166	-3.0530512	80.065	103
LAMB (Lamballe)	48.4772429	-2.4999513	125.323	105
MALO (Saint Malo)	48.6433538	-2.0247721	56.912	103
DUCE (Ducey)	48.6228294	-1.2957031	61.157	103
CHER (Cherbourg)	49.6357207	-1.6437806	126.428	105
BAYE (Bayeaux)	49.2904543	-0.7083642	105.777	104

Table 4-2 : The GPS data set of the 8 campaign stations

The second method involves estimating the harmonic displacement constituents and the positions of the GPS stations simultaneously. Although this method offers batch solutions using longer observational periods and therefore more accurate geodetic positioning results, it is more complicated to implement. It requires significant modifications of GPS processing software, as well as longer periods of data in order to effectively de-correlate the OTL displacement parameters (Thomas et al. 2006, King et al. 2005, Allinson et al. 2004).

During my study, an intermediate method which mostly relies on the manipulation of normal equation systems before solving for the final estimates was implemented. In this way, I succeeded in having long enough observational periods for accurately fixing the ambiguity parameters followed by the independent extraction of OTL displacement coefficients. This GPS estimation strategy is similar to that employed in Melachroinos et al. (2006a, 2007). The GPS data were processed and

edited on a site-by-site and day-by-day basis using the latest version (7.1) of the GINS/DYNAMO multi-technique scientific software package of the *Centre National d'Etudes Spatiales* (CNES) and the *Groupe de Recherches de Géodésie Spatiale* (GRGS) (Lemoine et al. 2007).

The general processing scheme consists of two steps: in the first step the positions of the GPS campaign stations in a 24-hour straightforward solution are estimated. At the pre-processing level data editing, cycle slips, clock-drift and millisecond jumps corrections are performed. The synthetic observable of double-difference (DD) baselines of the ionosphere-free (L_3) combination is used. Their formation is based on a common station pass criterion of the GPS satellites. The satellite and receiver clocks are eliminated. We use the IERS 2003 conventions for solid Earth tides, pole tides and the IERS Earth orientation parameters (EOPs). For the stations displacements due to OTL the predicted values from FES2004 are used. The IGS sp3 orbits (Kouba, 2003) are kept fixed. Corrections for relative antenna phase center variations (Mader 1999) according to IGS standards and atmospheric loading from 6-hour gridded (ECMWF) atmospheric pressure data (Biancale and Bode 2006) are applied. The phase observations are weighted with an a-priori sigma of 3.5 mm according to an empirical law. The empirical law is based on an exponential evolution of the DD post-fit residuals as a function of the elevation of the GPS satellites. Outliers are rejected using a three-sigma criterion. Ambiguities are fixed to their integer values with a rate greater than 95 % after the sixth iteration. Tight constraints of 1 mm are applied to the 14 IGS stations for the datum definition. Finally, the estimated geocentric positions for the GPS campaign stations from the 24 h solution are used as a-priori input in the second step.

A new iterative least squares scheme accounts for all the available data in the second step (~104 days). 24-hour batch-solutions are computed including adjusted campaign stations, in the same regional network of the 14 IGS stations for reference frame stabilization, and daily normal equations with hourly-partials for campaign stations positions in a local geodetic system, henceforth called quasi-observables, were calculated subsequently. The entire aforementioned configuration of the main estimation process from the first step is applied. The area of the regional network is large enough that errors introduced into station coordinates are comparable to those of a global stabilization (Tregoning and Van Dam, 2005). In order to obtain a strong

sensitivity of the troposphere estimates from GPS, a cut off angle of 10 degrees was selected (Tregoning et al. 1998). Hourly tropospheric zenith delay parameters using a-priori values from the ECMWF model and a Guo and Langley (2003) Marini-type hydrostatic and wet mapping function are estimated. A sampling interval of 30s is applied and ambiguity fixing is successful after the sixth iteration up to 87 % and more for all daily arcs. The coordinates of the campaign stations are held fixed to their a-priori values from the first step till convergence of the solutions.

The DD L_3 linear observation model up to convergence of the LS-procedure, considering EOPs and the coordinates of GPS satellites and campaign stations fixed, have the following form (here, a simple example of a single DD baseline is presented):

$$\overset{n\times 1}{\begin{bmatrix} \Delta L^{ik}_{_3 AB} \\ \Delta L^{ij}_{_3 AB} \end{bmatrix}} = \overset{n\times(s-r)}{\begin{bmatrix} 1 & 0 & -\lambda_3 & 0 \\ 0 & 1 & 0 & -\lambda_3 \\ \vdots & \vdots & \vdots & \vdots \end{bmatrix}} \overset{(s-r)}{\begin{bmatrix} \Delta T^{ik}_{AB,l} \\ \Delta T^{ij}_{AB,l} \\ \Delta N^{ik}_{_3 AB,p} \\ \Delta N^{ij}_{_3 AB,p} \\ \vdots \end{bmatrix}} + \overset{n\times 1}{\begin{bmatrix} V^{i,k}_{AB} \end{bmatrix}} \qquad \textbf{Eq. 4-5}$$

Where: $\Delta L^{ik}_{_3 AB}$ and $\Delta L^{ij}_{_3 AB}$ are the DD ionosphere-free phase pseudo-range linearized observables in between the A, B stations and *i,k* and *i,j* GPS satellites respectively; λ_3 is the wavelength; $\Delta T^{ik}_{AB,l}$ and $\Delta T^{ij}_{AB,l}$ are the linearized DD tropospheric zenith delay parameters at the selected estimation interval *l*, in the present case one every hour, for the total duration of the 1-day solution; $\Delta N^{ik}_{_3 AB,p}$ and $\Delta N^{ij}_{_3 AB,p}$ are the ionosphere-free DD ambiguities referring to the uninterrupted passage *p* of the satellites *i,k* and *i,j* over the A and B station. When a cycle-slip or a brake is detected in the passage a new ambiguity is created thus a new observation equation; *n* is the total number of observation equations; *s* is the total number of unknowns and *r* in the number of eliminated parameters (clocks, ionosphere etc.); $V^{i,k}_{AB}$ is the DD error-vector that contains everything else that is not modeled, like multipath or noise of the GPS observables.

After convergence, a last iteration is done in order to create the quasi-observables of the station positions at the selected period of one hour. Usually 7 or 8 iterations were necessary to converge to sub-cm residuals. At this stage, the DD ionosphere-free linearized observation equation takes the form given in **Eq. 4-6**:

$$\overset{n\times 1}{\begin{bmatrix}\Delta L^{ik}_{{}_3AB}\\ \Delta L^{ij}_{{}_3AB}\end{bmatrix}} = \begin{bmatrix}(\mathrm{n}^i_B-\mathrm{n}^k_B)^T & \overset{n\times(s-r)}{1} & 0 & -\lambda_3 & 0\\ (\mathrm{n}^i_B-\mathrm{n}^j_B)^T & 0 & 1 & 0 & -\lambda_3\\ \vdots & \vdots & \vdots & \vdots & \vdots\end{bmatrix}\begin{bmatrix}\overset{(s-r)\times 1}{\Delta \mathrm{u}^h_{AB}}\\ \Delta T^{ik}_{AB,l}\\ \Delta T^{ij}_{AB,l}\\ \Delta N^{ik}_{{}_3AB,p}\\ \Delta N^{ij}_{{}_3AB,p}\\ \vdots\end{bmatrix}+\overset{n\times 1}{\begin{bmatrix}V^{i,k}_{AB}\end{bmatrix}} \qquad \textbf{Eq. 4-6}$$

Where: $\mathrm{n}^{i,j,k}_B$ are the *i, j, k* satellite-station B unit-vectors from the station's antenna phase center towards the satellite's antenna phase center in the terrestrial frame; $\Delta T^{ik}_{AB,l}$ and $\Delta T^{ij}_{AB,l}$ are the already linearized (observed – from the previous iterations) DD tropospheric zenith delay parameters after convergence; and $\Delta \mathrm{u}^h_{AB} = \Delta \mathrm{u}^h_B - \Delta \mathrm{u}^h_A$ are the linearized (observed – a-priori) local geodetic position vectors (in East, North, Up) with partials created for every selected interval *h* (in this case one hour); $\Delta N^{ik}_{{}_3AB,p}$ and $\Delta N^{ij}_{{}_3AB,p}$ are real number ionosphere-free DD ambiguities, which represent 10 – 12 % of the remaining non-fixed ambiguities.

Secondly, a final inversion is done using the DYNAMO software. At this stage, all daily normal equation systems are solved independently and the reference frame stabilization is realized through the fixed positions of the GPS satellites and the tight constraints of 1 mm to all IGb00 positions, in a local geodetic system (North, East, Up), of the 14 IGS stations. All IGS site motions have been previously corrected using an a-priori OTL model and atmospheric loading.

Moreover continuity constraints of 3 cm per hour to all campaign stations are applied according to **Eq. 4-7:**

$$\hat{\mathrm{u}}^h_A(h) - \hat{\mathrm{u}}^h_A(h-\Delta t) = 0 \pm 3cm_{continuity} \qquad \textbf{Eq. 4-7}$$

Where: $\hat{\mathrm{u}}^h_A(h)$ and $\hat{\mathrm{u}}^h_A(h-\Delta t)$ are the 3D-coordinate vectors for station A at the time interval *h* and $h-\Delta t$; Δt is the time-length of one hour.

This means adding a side-band (non zero) normal equation in order to connect two consecutive hourly coordinates. This technique allows filtering any remaining outliers from the iterative scheme. Care is taken when this observational equations are added so that the continuity constraint is large enough to allow the station's coordinates

to vary due to the true OTL displacement within an hour, based on the highest OTL modeled amplitude in the region.

After the final inversions of the daily normal equation systems, tidal harmonic coefficients are estimated using standard algorithms (Foreman 1977) and the estimated GPS position time-series are processed as independent tide gauge observations in North, East and Up components.

With regard to the Rayleigh criterion, the duration of the recorded or modeled time, necessary to separate two frequencies f_1 and f_2, must be $\geq \frac{1}{|f_1 - f_2|}$ (Foreman 1977). Therefore, the present study cannot separate all the OTL displacement components as the separation of S_2 and K_2 requires nearly 300 days (Godin 1972). As a consequence, I was able to analyze a set of four major OTL displacement constituents for the region, M_2, S_2, N_2 and K_1.

Constituent	Angular velocity (deg h^{-1})	Period (days)	Period (h)
	Diurnal		
O_1	13.942	1.078	25.819
P_1	14.958	1.003	24.066
K_1	15.041	0.997	23.935
Q_1	13.405	1.119	26.868
	Semidiurnal		
N_2	28.439	0.5271	12.659
K_2	30.082	0.4986	11.967
S_2	30.000	0.4999	12.000
M_2	28.984	0.5175	12.421

Table 4-3 : The main harmonic constituents of the tides in the English Channel (Le Provost and Fornerino 1985)

These four major constituents are sufficient indicators of tide model accuracy (Andersen et al. 1995). For the constituents that are closest in frequency like K_1 and P_1 or K_2 and S_2, I applied the inference technique from Foreman (1977) by excluding P_1 and K_2. This relies on the principal that if the length of a specific tidal record is such that certain constituents cannot be included directly in the analysis, such as K_1 and S_2, they can be estimated by inferring their amplitudes and phases from neighbouring

constituents. Mean values for P_1 and K_2 from all the global ocean tide models are used in this technique. This approach is preferable because the errors of the tide models used will have a minor impact on the constituent analyses.

Furthermore, this will not be the case if the summation, $K_1 + P_1$ or $K_2 + S_2$ is considered, instead of the separation by inference of these waves, which will be significantly more polluted from the GPS noise (especially the one with the smallest amplitude, P_1). Since the K_1 period (see **Table 4-3**) is very close to the GPS constellation repeat period (~23.933 hours), biases are expected to appear in the final constituents estimates, especially at the integer multiples and combinations of this period (King et al. 2005, Allinson et al. 2004).

The diurnal and semi-diurnal constituents are a small subset of tidal constituents. Hence, nodal corrections to each constituent are applied in order to account for the modulating lunar node effect (McCarthy and Petit 2004, Cartwright and Edden 1973, Cartwright and Tayler 1971).

4.2.3 Comparison of GPS estimates with modelled OTL displacement constituents

4.2.3.1 GPS estimates of OTL displacements

The 3D OTL displacement coefficients of GPS estimates are given in **Table 4-4**. These estimates show the significant magnitude of the OTL phenomenon along the coastlines of Brittany and at the eastern entry of the English Channel. We can see that heading from the DIBE (Le Diben) station towards the East along the coastline, the amplitudes of this station for M_2, S_2 and N_2 reach the maximum values of 32.8 mm, 10.35 mm and 7.5 mm in the vertical direction, respectively.

The M_2 OTL wave has its lowest amplitude of 7.0 mm in the vertical, at BAYE (Bayeau), further inside the channel. The K_1 wave has its strongest amplitude of 9.45 mm in the vertical, at YGEA (Saint Ygeaux) which is situated further inland south from PAIM (Paimpol). A quick glance at the geographical variation of the estimated values

for M_2 and S_2 reveals that they are consistent with the distribution of the predicted OTL displacements in the vertical direction as seen from **Fig. 4-3**.

		M_2		S_2		N_2		K1	
GPS-site	***j*[a]**	***A*[b], *mm***	***Φ*[c], *deg***	***A*[b], *mm***	***Φ*[c], *deg***	***A*[b], *mm***	***Φ*[c], *deg***	***A*[b], *mm***	***Φ*[c], *deg***
YGEA	E	7.2	97.5	2.0	118.4	1.6	85.4	0.9	139.1
		(0.2)	(2.2)	(0.7)	(9.1)	(0.3)	(8.8)	(0.2)	(12.5)
	N	6.2	27.3	2.3	52.4	1.3	25.0	0.2	22.9
		(0.2)	(2.2)	(0.2)	(6.0)	(0.2)	(10.4)	(0.2)	(56.4)
	U	23.2	304.6	6.1	16.2	4.6	296.0	9.45	322.55
		(0.7)	(1.6)	(0.6)	(7.2)	(0.8)	(9.4)	(0.7)	(4.2)
DIBE	E	8.6	98.7	2.7	124.2	1.7	74.6	0.5	188.1
		(0.3)	(2.0)	(0.2)	(5.2)	(0.2)	(8.6)	(0.2)	(22.5)
	N	7.1	11.9	2.8	49.4	1.2	10.0	0.7	359.2
		(0.2)	(1.8)	(0.2)	(4.7)	(0.2)	(11.0)	(0.2)	(14.4)
	U	32.8	311.9	10.3	23.5	7.5	296.7	7.9	288.9
		(0.8)	(1.4)	(0.7	(3.8)	(0.8)	(5.5)	(0.6)	(4.5)
PAIM	E	8.0	94.7	2.7	120.8	1.7	74.7	0.4	196.2
		(0.3)	(1.6)	(0.2)	(5.1)	(0.2)	(7.0)	(0.2)	(24.7)
	N	6.9	18.4	2.6	44.8	1.4	19.2	0.1	39.8
		(0.2)	(2.0)	(0.2)	(3.7)	(0.2)	(9.3)	(0.1)	(73.7)
	U	29.3	320.2	8.7	27.0	5.7	308.1	6.69	307.1
		(0.6)	(1.2)	(0.6)	(3.8)	(0.6)	(6.7)	(0.62)	(4.6)
LAMB	E	8.0	109.4	2.0	138.4	1.5	92.1	0.7	155.5
		(0.2)	(1.8)	(0.2)	(6.1)	(0.2)	(8.9)	(0.2)	(15.1)
	N	6.7	21.5	2.4	44.2	1.4	30.1	0.4	124.3
		(0.2)	(1.9)	(0.2)	(4.7)	(0.2)	(7.9)	(0.2)	(23.9)
	U	22.0	314.3	5.9	29.9	5.0	305.3	7.5	333.9
		(0.7)	(1.7)	(0.6)	(6.7)	(0.7)	(8.3)	(0.6)	(4.5)
MALO	E	7.8	151.5	2.7	173.9	1.6	145.7	0.3	31.2
		(0.2)	(1.7)	(0.2)	(4.8)	(0.2)	(9.2)	(0.2)	(28.9)
	N	7.1	55.8	2.8	68.5	1.4	65.1	0.4	146.5
		(0.2)	(2.0)	(0.2)	(4.8)	(0.2)	(9.5)	(0.2)	(27.7)
	U	23.3	357.6	5.8	79.0	5.8	355.7	2.8	187.1
		(0.9)	(2.0)	(0.8)	(7.2)	(0.8)	(8.6)	(0.8)	(15.4)
DUCE	E	8.0	127.8	2.1	157.5	1.5	112.1	1.0	170.6
		(0.2)	(1.4)	(0.2)	(5.3)	(0.2)	(7.9)	(0.2)	(11.7)
	N	4.3	47.7	1.8	61.7	1.0	54.4	0.4	320.9
		(0.2)	(2.6)	(0.2)	(5.9)	(0.2)	(12.1)	(0.2)	(22.5)
	U	14.7	315.9	5.7	45.6	3.1	305.7	4.9	309.1
		(0.6)	(2.2)	(0.6)	(5.7)	(0.6)	(11.4)	(0.5)	(6.8)
CHER	E	10.4	133.3	2.8	173.8	1.9	119.0	0.4	201.1
		(0.2)	(1.21)	(0.2)	(4.6)	(0.2)	(6.2)	(0.2)	(24.6)
	N	3.7	92.3	0.8	165.9	1.0	79.5	0.4	332.7
		(0.2)	(3.0)	(0.2)	(13.2)	(0.2)	(11.0)	(0.2)	(21.2)
	U	15.4	342.7	6.9	60.1	3.2	323.5	6.4	328.7
		(0.7)	(2.17)	(0.6)	(4.9)	(0.7)	(11.2)	(0.5)	(4.8)
BAYE	E	7.6	133.1	2.2	175.0	1.3	115.1	0.6	206.5
		(0.2)	(1.8)	(0.2)	(5.2)	(0.2)	(9.2)	(0.2)	(18.6)
	N	5.1	90.4	1.1	120.7	1.3	86.8	0.4	350.8
		(0.2)	(2.1)	(0.2)	(9.3)	(0.2)	(8.6)	(0.2)	(24.1)
	U	7.0	340.6	4.7	76.9	1.8	346.1	6.1	325.1
		(0.5)	(4.1)	(0.6)	(7.2)	(0.6)	(17.9)	(0.5)	(4.9)

Table 4-4 : GPS OTL displacement estimates. One sigma uncertainties are inside parenthesis

Horizontal amplitudes are not negligible for M_2, S_2, N_2 and K_1. The highest one reaches 10.4 mm at CHER (Cherbourg) for the M_2 wave in the eastward direction. As for the other two major constituents, S_2 and N_2, their maximum horizontal amplitudes are 2.8 mm and 1.9 mm, respectively, situated at CHER in eastward direction. K1 gets it highest horizontal displacement of 1 mm at DUCE (Ducey) in the eastward direction.

Fig. 4-4 displays the GPS OTL time-series for three representative selected stations DIBE, MALO and CHER in north, east and vertical directions. The diurnal and semi-diurnal displacements can reach the maximum of 12 cm, 3 cm and 2 cm peak-to-peak respectively in vertical, easting and northing direction in DIBE, while they decrease when entering the English Channel. The maximal horizontal, in easting and northing, and vertical displacements for MALO and CHER are around 2 cm, 3 cm and 9 cm and 4 cm, 2 cm and 6 cm peak-to-peak respectively.

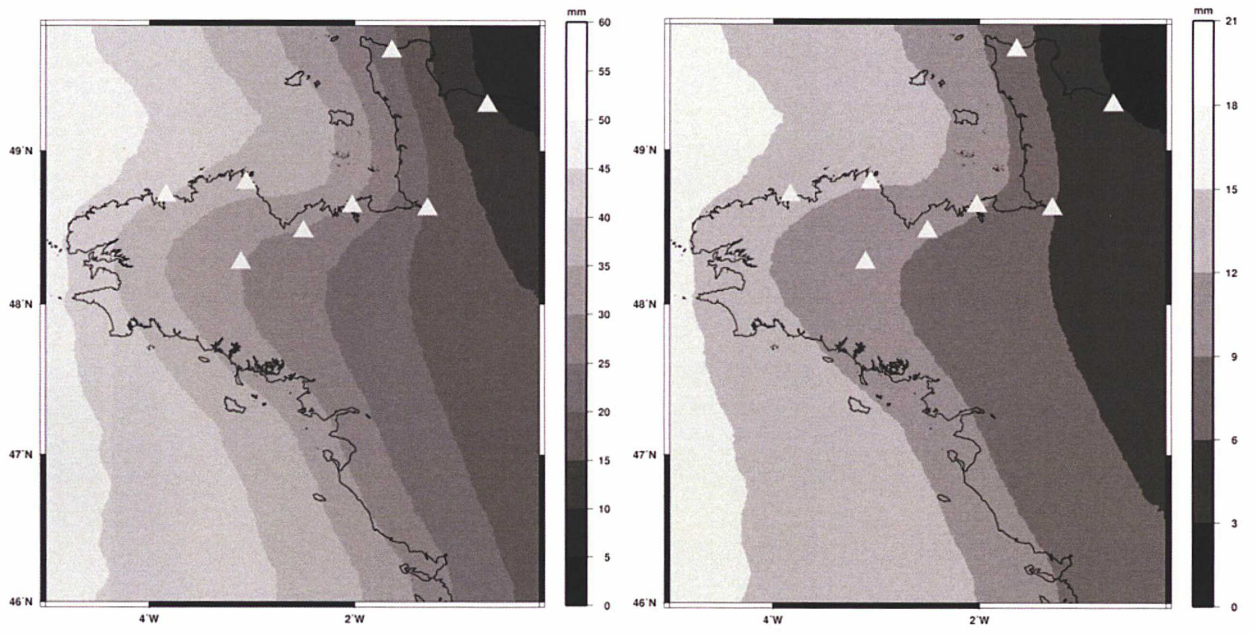

Fig. 4-3 : Amplitudes of the M_2 (left) and S_2 (right) vertical OTL displacement wave over the Brittany shelf and the campaign GPS stations (predictions are from the FES2004 tide model)

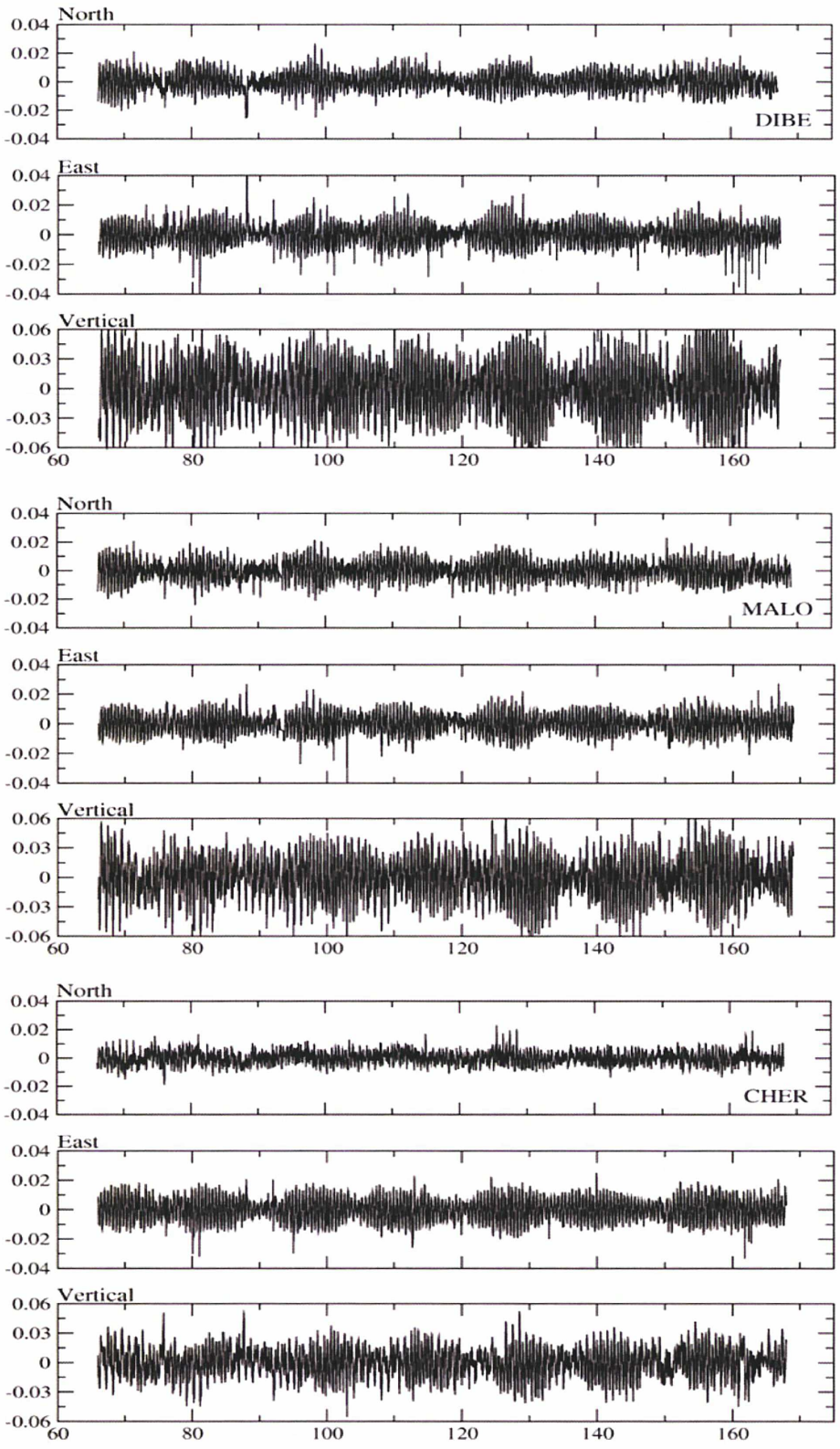

Fig. 4-4 : GPS OTL displacement series in Northing, Easting and Vertical directions for DIBE, MALO and CHER station. Units in y-axis are in meters and in x-axis are in days-of-year (doy).

All stations have almost the same number of days of observations. The K_1 constituent has the largest formal errors for all stations especially in horizontal. This is due to the orbital errors of the GPS satellites and multipath around the monument's environment that propagate at this frequency (Ragheb et al. 2006, Larson et al. 2006, Choi et al. 2004).

Another indication of this relationship between repeatable GPS satellite geometry at a sidereal period and multipath (Larson et al. 2006) is the fact that significant displacement signals appear near the integer multiples of the orbital periods (at $K_1/3$, $K_1/4$, $K_1/5$, $K_1/6$ etc.). By introducing the frequencies of these "fictitious" OTL displacement signals into the harmonic estimates solution significant amplitudes of a few mm as listed in **Table 4-5** for all stations (only shown for the first two frequencies) are calulated. Additionally, **Table 4-5** demonstrates that the amplitudes of these signals are important enough to introduce biases in the signatures of shallow water OTL constituents such as the combinations of SK_3, MK_3, $2MK_5$, $2SK_5$ or constituents very close to them, such as M_3 and M_4.

		K_3	K_4
GPS-site	***j*[a]**	***A*[b], *mm***	***A*[b], *mm***
YGEA	U	4.0 (0.5)	4.0 (0.4)
DIBE	U	5.0 (0.5)	3.0 (0.5)
PAIM	U	3.2 (0.5)	2.1 (0.3)
LAMB	U	1.6 (0.5)	2.0 (0.4)
MALO	U	3.0 (0.6)	2.0 (0.5)
DUCE	U	3.4 (0.3)	2.4 (0.4)
CHER	U	3.2 (0.4)	0.4 (0.4)
BAYE	U	3.0 (0.4)	2.2 (0.4)

Table 4-5 : GPS frequency displacement estimates in integer multiples of the K1 wave

[a] U, Upwards; [b] A, Amplitude

These facts demonstrate an important inconvenience of the GPS technique: shallow water constituents cannot be effectively distinguished due to multipath at higher frequencies, than the semi-diurnal bands. Proper mitigation techniques should be applied in this case.

4.2.3.2 Comparison to modeled OTL displacement constituents

The modeled and estimated constituents of OTL displacements were not corrected for the sub-mm motion of the centre mass of the ocean, which causes a counterbalancing tide in the mass centre of the solid earth. Scherneck et al. (1999) proved that differential frame motion between the GPS stations and the satellite orbits is not affected by the center of mass tide. Nonetheless, an error of 1.5 mm in amplitude and 2° to 4° in phase-lag for the modeled constituents may exist (O. Francis personal communication). That would have been the case if our network of stations was global and not regional, or if our positioning strategy was based on an absolute mode and not a differential one. From the moment that a DD approach was applied on a regional network, the motion of the geocentre induced from the fixed positions of the GPS satellites into the GPS stations time-series will be extremely minimized, if not eliminated, as a common parameter inside the differentiation process of the DD algorithm. Through this approach, a consistent reference frame was achieved for the modeled and the estimated GPS OTL constituents.

Since no error budget is given for the amplitudes and phases of the tide models, we assumed that the modelled derived estimates are error free.

4.2.3.2.1 Spatial variations of OTL displacement

The phasor-diagrams of GPS and model estimates of OTL displacements are formed for the M_2, S_2 semi-diurnal constituents at DIBE station, and going eastwards, at MALO and CHER (**Fig. 4-5** to **4-7**).

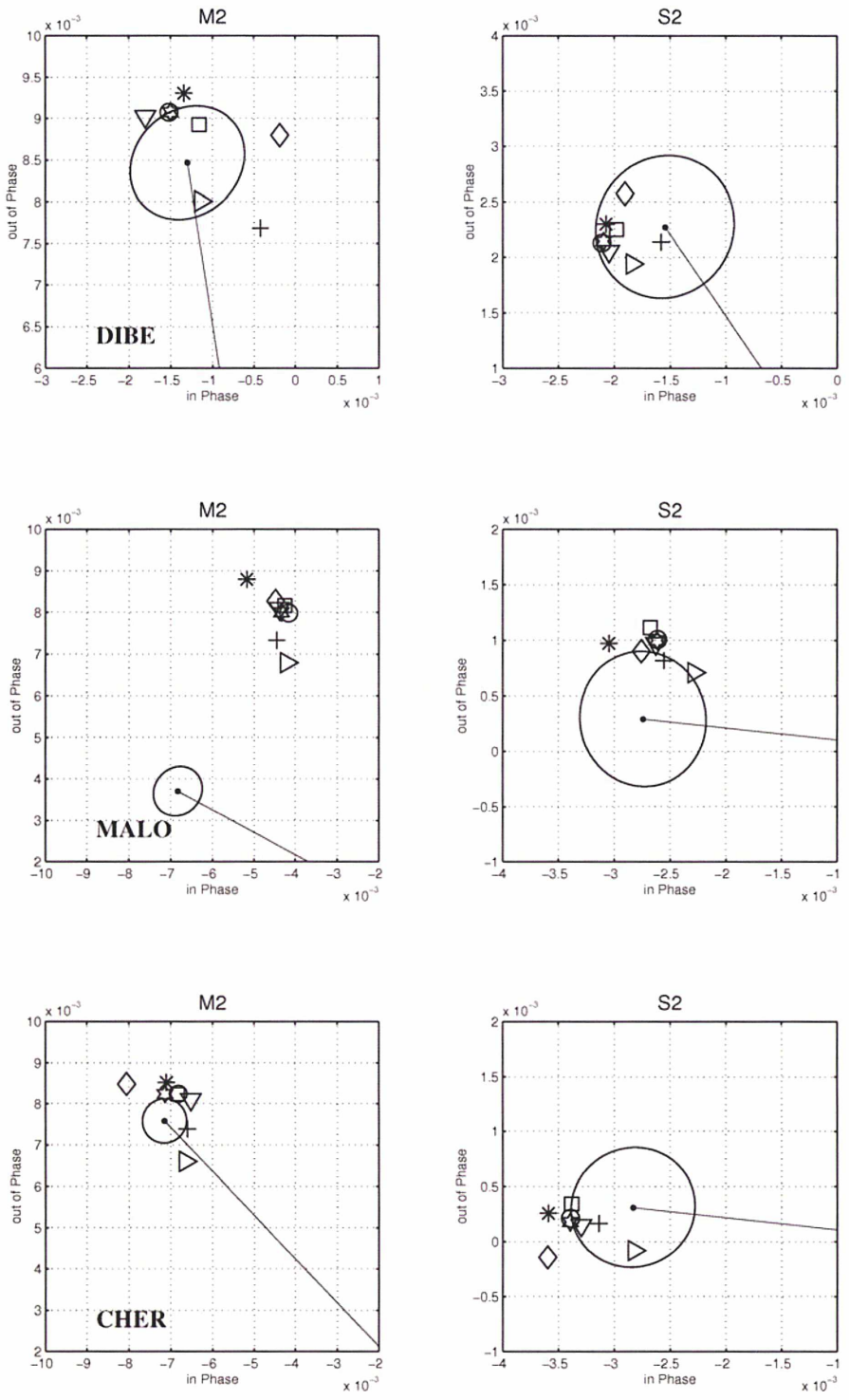

Fig. 4-5 : Phasor diagrams of *eastward OTL* displacements at the three campaign GPS stations. Units are in meters. The GPS estimates are represented by a point sign along with their 95% error ellipse according to the error propagation law in the estimated amplitudes and phases. Olfg/olmpp OTL modelling for : FES2004, *squares*; TPXO.7.0, *diamond*; TPXO.6.2, *downward pointing triangle*; GOT00.2, *hexagram*; NAO99.b, *asterisk*; CSR4.0, *circle*; GéochargeV3.0 OTL modelling for : FES2004, *cross*; NEA2004, right *pointing triangle.*

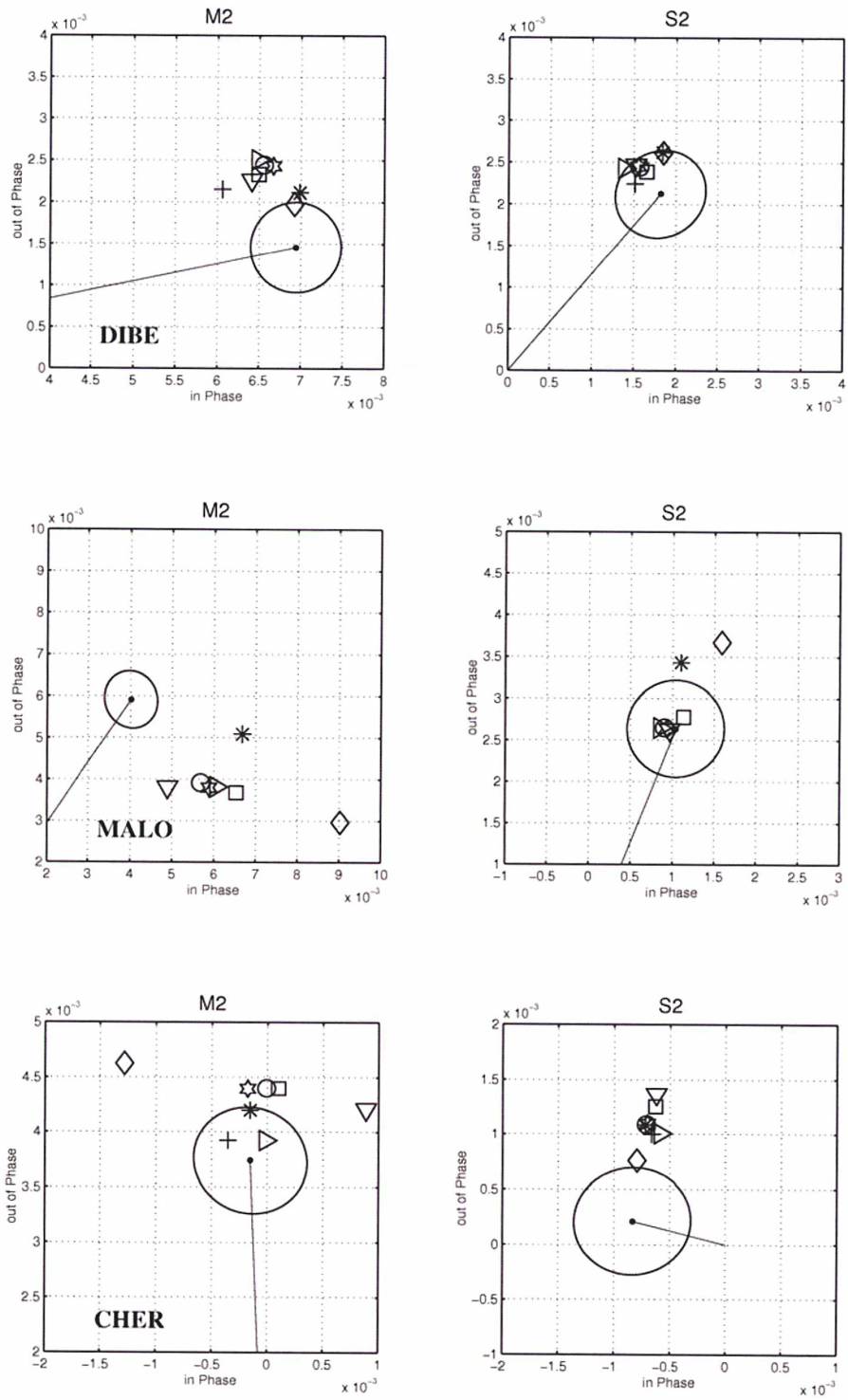

Fig. 4-6 : Phasor diagrams of northward OTL displacements at the three campaign GPS stations. Units are in meters. The GPS estimates are represented by a point sign along with their 95% error ellipse according to the error propagation law in the estimated amplitudes and phases. Olfg/olmpp OTL modelling for : FES2004, squares; TPXO.7.0, diamond; TPXO.6.2, downward pointing triangle; GOT00.2, hexagram; NAO99.b, asterisk; CSR4.0, circle; GéochargeV3.0 OTL modelling for : FES2004, cross; NEA2004, right pointing triangle.

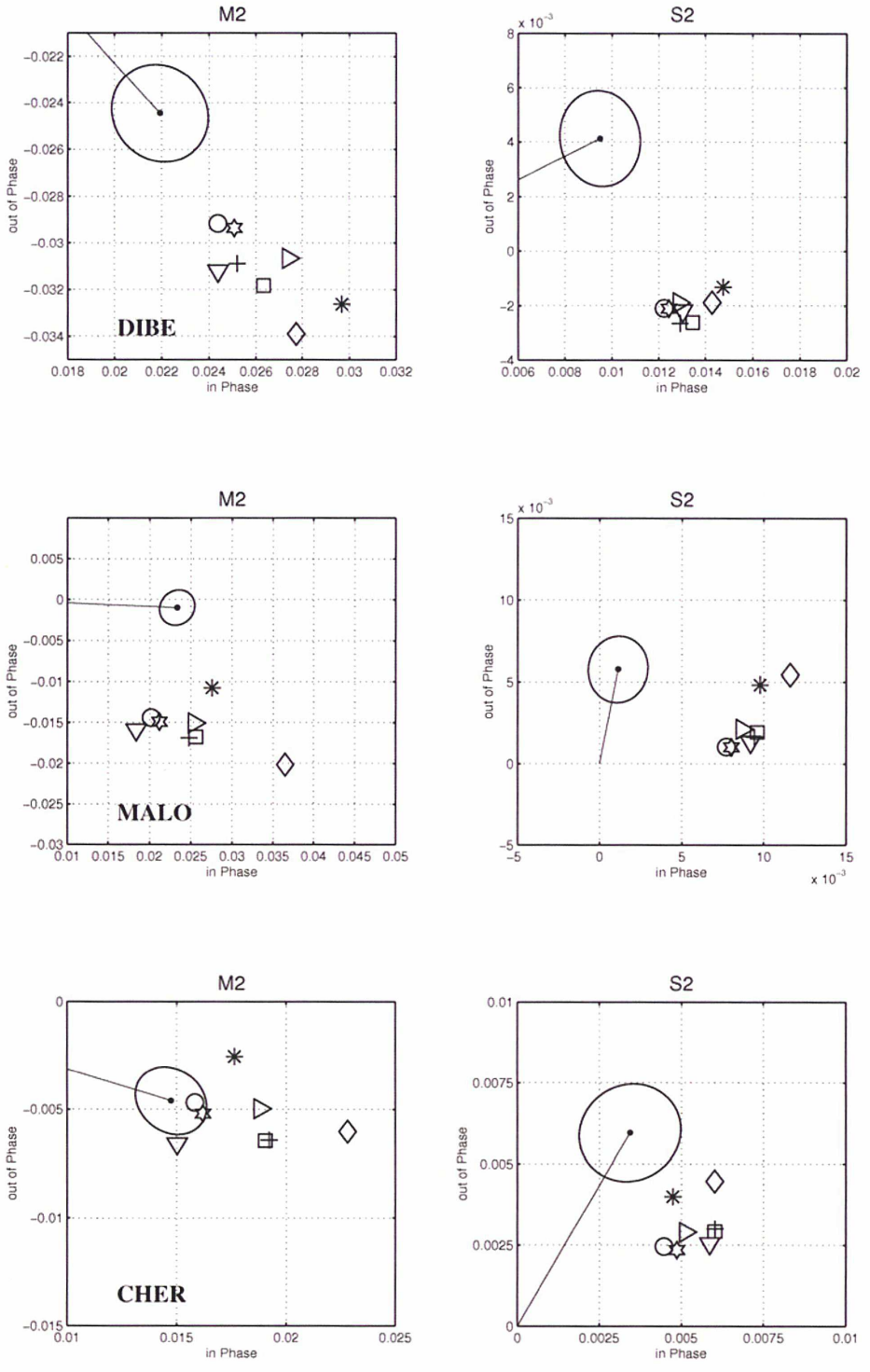

Fig. 4-7 : Phasor diagrams of *up-ward OTL* displacements at the three campaign GPS stations. Units are in meters. The GPS estimates are represented by a point sign along with their 95% error ellipse according to the error propagation law in the estimated amplitudes and phases. Olfg/olmpp OTL modelling for : FES2004, *squares*; TPXO.7.0, *diamond*; TPXO.6.2, *downward pointing triangle*; GOT00.2, *hexagram*; NAO99.b, *asterisk*; CSR4.0, *circle*; GéochargeV3.0 OTL modelling for : FES2004, *cross*; NEA2004, right *pointing triangle.*

From the same plots we observe the spatial longitudinal variation of the OTL displacements at the entry of the English Channel. The tendency is an increased OTL effect for the stations situated at its entry like DIBE and MALO.

The GPS estimates of the horizontal displacements in M_2 are in sub-mm agreement with the models within their 95% error confidence for DIBE and CHER. The observations in vertical displacements are in agreement at the mm-level with the models. The GPS measurements can very well distinguish the M_2 constituents in the vertical component as is already the case for DIBE and CHER. Nevertheless, the observed amplitude at DIBE seems to be smaller by 3-5 mm to the closest in agreement prediction.

The detection of the vertical OTL displacements for S_2 still remains a tricky task. For all three stations the vertical observations precede in the phase-lag all OTL predictions and the discrepancy rises to the mm-level. The northward and eastward estimates for S_2 seem to agree in the sub-mm level at all stations within their 95% error confidence.

At MALO, which concentrates the strongest non-linear semi-diurnal tides of the region the GPS estimates of vertical and horizontal displacements for the M_2 wave have the greatest disagreement in the phase-lag to all models. The S_2 wave follows the same pattern as in the other two stations. There is a sub-mm agreement in the northward and eastward observations and a steady phase-lag advance in the vertical. In order to correctly assess the levels of agreement between the models and GPS estimates, MALO is excluded in the following analysis. I assume that strong un-modeled non-linear OTL interactions in the semi-diurnal band are probably responsible for the models disagreements in the phase-lag with the GPS estimates at this station. Le Provost and Fornerino (1985) have shown that when the M_2 wave propagates through the Mont St-Michel Bay, the local friction and resonance phenomena create localized strong non-linear interactions with some energy transfer towards semi-diurnal ($2MS_2$, $2SM_2$, $2MN_2$, SNM_2, MSN_2, MNS_2, L_2, μ_2, ν_2, λ_2 etc.) or higher bands (such as M4). Nevertheless, this assumption is not definite and more investigation will be done in a future study.

The discrepancy between models seems to vary significantly as well. A sub-mm agreement in the horizontal constituents of S_2 at CHER and DIBE stations is observed. At MALO, the horizontal discrepancies rise up to 1 mm. At the same station, in the

vertical, the differences vary from 2 to 5 mm. For the other two stations, the disagreement reaches up to 2.5 mm. For M_2 the differences become larger since this wave has higher amplitudes than S_2. All models seem to agree worst for MALO in both vertical and horizontal components. The maximum level of disagreement in the vertical rises to 1.5 cm, whereas it is 4 mm in the eastward direction.

4.2.3.2.2 Misfit statistics of GPS/models OTL displacements

In order to assess the level of agreement of the GPS and predicted estimates of OTL displacements, the methods proposed by Thomas et al. (2006), King et al (2005), and Allinson et al. (2004) are followed. We first form the RMS misfits of GPS versus modeled OTL displacements. For $n=1, N$ GPS sites at each component direction j for each tidal loading model k and for the four constituents (M_2, S_2, N_2 and K_1) the root mean square misfit will be:

$$RMS_{misfit}^{k,4} = \sqrt{\frac{1}{N}\sum_{n=1}^{N}\left[\left(A_{GPS}\left(\cos(\Phi_{GPS})+i\sin(\Phi_{GPS})\right)_{j,n} - A_k\left(\cos(\Phi_k)+i\sin(\Phi_k)\right)_{j,n}\right)\right]^2} \quad \textbf{Eq. 4-8}$$

Where A and Φ, stand for the tidal amplitudes and Greenwich phase lag respectively.

The calculated models misfits for the seven selected sites (MALO is excluded) are shown in **Fig. 4-8**. GPS/Model misfits correspond to TPXO.7.0, TPXO.6.2, GOT00.2, NAO99.b, CSR4.0, and FES2004 from olfg/olmpp, and to FES2004, NEA2004 from géochargeV3.0, in bars left (black) to right (white)**.** Note that for all models the K_1 constituent represents the highest disagreement in the vertical and eastward components. This verifies the aforementioned sources of biases at the orbital period of the GPS satellites and is compatible with previous conclusions by Thomas (2006) and Schenewerk et al (2001).

The FES2004 model seems to perform the best in terms of agreement with the GPS estimates. The level of agreement is 0.3 mm for the east, 0.2 mm for the north and 1.8 mm for the vertical component of the M_2 constituent. The two algorithms are performing equivalently with a small exception in the horizontal components of M_2. For this constituent, the géochargeV3.0 OTL predictions for FES2004 seem to be more in

agreement with the GPS estimates. The differences with respect to olfg/olmpp FES2004 predictions are 0.5 mm in east, 0.6 mm in north and negligible in vertical.

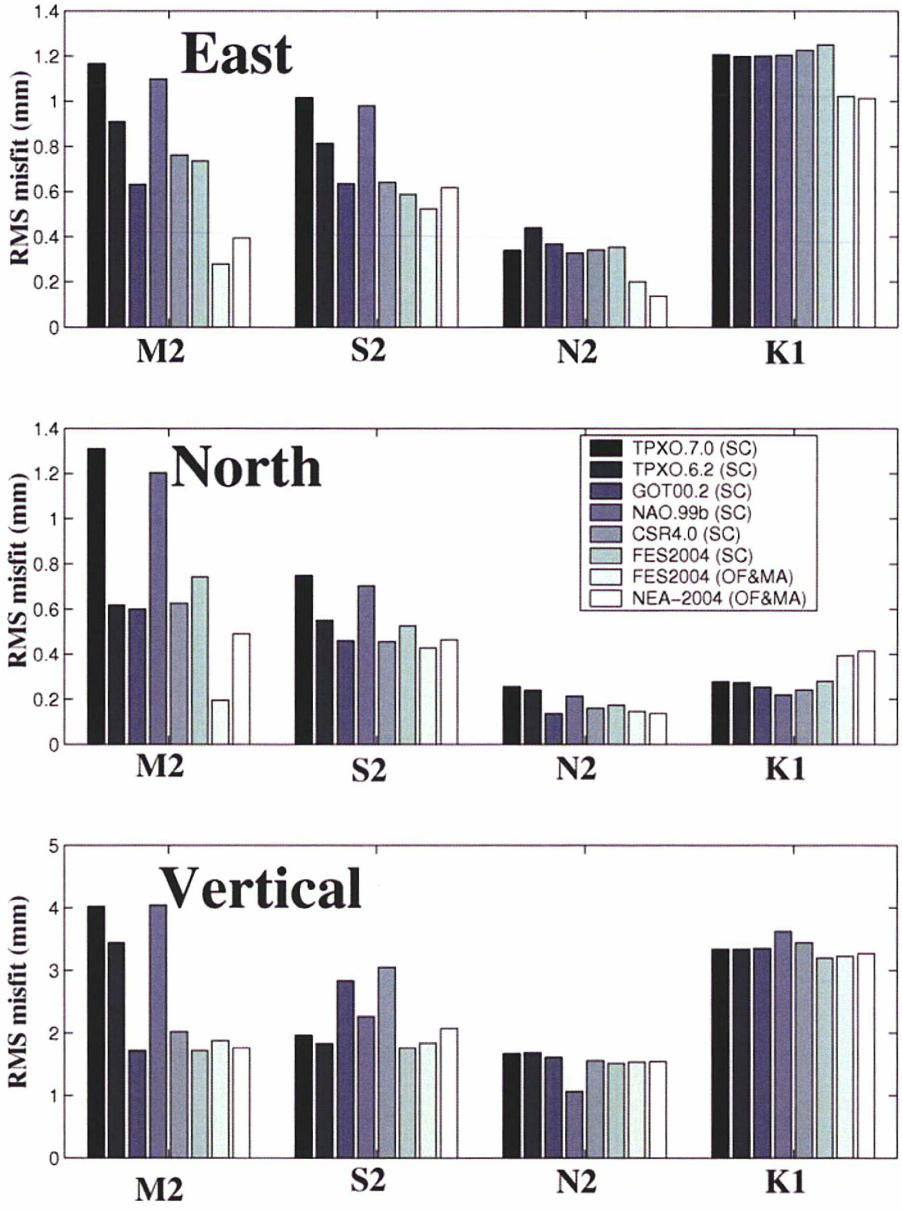

Fig. 4-8 : Misfits of GPS OTL estimates compared to: (SC) Olfg/olmpp OTL modelling for: TPXO.7.0, TPXO.6.2, GOT00.2, NAO99.b, CSR4.0, FES2004; (OF&MA) GéochargeV3.0 OTL modelling for: FES2004, NEA-2004. MALO station is excluded. The misfit bars start respectively from left (black) to right (white).

Table 4-6 : Table Chi-square per degree-of-freedom for GPS estimates of OTL displacements to modelled constituents

	3D
Model	**GPS (fixed ambiguities)** [a]
TPXO.7.0 [b]	3.94
TPXO.6.2 [b]	3.85
GOT00.2 [b]	2.95
NAO99.b [b]	4.74
CSR4.0 [b]	3.43
FES2004 [b]	1.99
FES2004 [c]	1.79
NEA-2004 [c]	2.07

[a] Set of 4 constituents M_2, S_2, N_2, K_1 without St MALO

[b] Olfg/olmpp OTL web service provider

[c] GéochargeV3.0 OTL program

Second in misfit agreement with GPS/models are GOT00.2 and CSR4.0. The models with the highest misfits are TPXO.7.0, TPXO.6.2 and NAO99.b. The local NEA2004 grids are performing almost equivalently with the global FES2004 grids.

In addition to observing the relatively large K_1 GPS/models misfits, I comment that for the models that agree best with the derived GPS estimates (FES2004, GOT00.2, CSR4.0) the misfits for lunar constituents such as M_2 and N_2 compared to the misfits for solar constituents such as S_2 and K_1, seem to be smaller. This effect is due to GPS related systematic errors biasing the constituents (S_2 and K_1) at solar frequencies (Thomas et al. 2006).

Together with the RMS misfits analysed previously, a weighted chi-square statistic for each of the derived sets of GPS estimates using all 7 models, is defined. The uncertainties of the GPS estimates are propagated into the chi-square statistic whereas for the models we adopted an error free assumption (valid for our reference system). The chi-square statistic is:

$$\chi^2 = \sum_{c=1}^{4}\sum_{j=1}^{3}\sum_{n=1}^{N}\left[\frac{\left(A_{GPS}\left(\cos\left(\Phi_{GPS}\right)+i\sin\left(\Phi_{GPS}\right)\right)_{c,j,n} - A_k\left(\cos\left(\Phi_k\right)+i\sin\left(\Phi_k\right)\right)_{c,j,n}\right)}{\sigma_{GPS(c,j,n)}}\right]^2 \quad \textbf{Eq. 4-9}$$

Eq. 4-9 was calculated for a set of seven stations (MALO excluded). We have estimated statistics for a set of 3D parameters in all components and for each component separately. **Table 4-6** describes the results of this comparison. Once again the superior performances of the FES2004 are shown. Second in GPS/models agreement are the NEA2004, GOT00.2, and CSR4.0 while the TPXO.7.0, TPXO.6.2 and NAO99.b have the poorest fit to the GPS estimates. Despite the fact that K_1 observable contains/introduces biases it was not excluded from the analysis.

4.2.4 Checking on the datum stability

In this experiment the influence of the stabilisation sites (the network effect) on the final GPS time-series of a European GPS-network which comports from 16 RGP stations and some IGS-EUREF stations is evaluated in a first place and then to the final OTL estimates of the GPS campaign stations. For this experiment I used the GAMIT/GLOBK software package to analyse data for a period of 80 days in 2004. The

level of consistency between a solution of a selected GPS network aligned to a tightly fixed reference frame of the IGS stations and a solution using the "free-network" approach (Heflin et al. 1992) with looser constraints, is quantified. The impact on the OTL estimates is estimated as well.

For the "free-network" approach I used a global IGS stabilisation network together with a regional, from the EUREF network, and for the "tight constraints" I used the EUREF-IGS network. Both types of networks can be seen in **Fig. 4-9**.

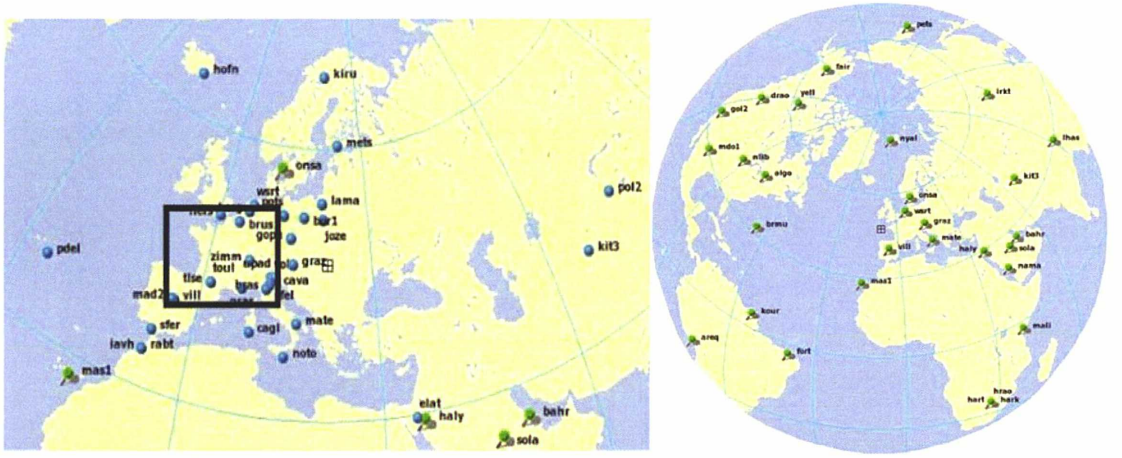

Fig. 4-9 : (left) the EUREF-IGS network together with the estimated GPS stations (Black-box) and (right) the global IGS network used in this experiment.

The quality and accuracy of the estimated time-series in the first stage are determined through two quality factors (Larson and Agnew 1991):

- The Weighted Root Mean Square (WRMS) scatter about the mean of daily estimates. This statistic characterizes the precision of the estimated time-series. Sometimes is called the repeatability :

$$WRMS = \sqrt{\frac{\frac{N}{N-1}\sum_{i=1}^{N}\frac{\left(\hat{x}_i - \bar{x}_i\right)^2}{\sigma_i^2}}{\sum_{i=1}^{N}\frac{1}{\sigma_i^2}}} \qquad \textbf{Eq. 4-10}$$

- The reduced χ^2 statistic defined by the Normalised Root Mean Square (NRMS) of the weighted RMS of the post-fit residuals time-series. A reduced

χ^2 close to 1 indicates that the formal errors agree with the actual scatter in the time-series.

$$NRMS = \sqrt{\frac{\sum_{i=1}^{N} p_i \hat{v}_i^2}{N-m}} \qquad \textbf{Eq. 4-11}$$

Where: N is the total number of data points, m is the total number of estimated parameters, x_i are the estimated parameters, $\overline{x}_i = \sum_{i=1}^{N} \frac{1}{\sigma_i^2} x_i \Big/ \sum_{i=1}^{N} \frac{1}{\sigma_i^2}$ is the weighted mean of the estimated parameters, σ_i are the standard (formal) errors , $p_i = \frac{1}{\sigma_i^2}$ are the weights and $\hat{v}_i^2 = \left(\hat{x}_i - \overline{x}_i\right)^2$ are the post-fit residuals of the positions.

In the following **Fig. 4-10** I present the NRMS and WRMS for the selected GPS network of 6-stations : FJCP (Fanjancouse, RGP, France), WTZR (Bad Koetzting, Germany), TLSE (Toulouse, EUREF-IGS-RGP, France), SJDV (Saint Jean de Vignes, EUREF-RGP, France), MATE (Matera, EUREF-IGS, Italy), MANS (Le Mans, RGP-MANS, France).

From the same **Fig. 4-10** we can observe that the solutions with "tight constraints" (in red) on the positions of a set of IGS-EUREF stabilisation sites give results (in terms of precision and accuracy) for the selected 6-GPS network of stations equivalent to the "loose constraints" approach of the global set of IGS-stabilisation sites which makes use of a similarity transformation of 7 parameters for the datum definition. The regional "loose constraint" stabilisation approach seems to perform less well in precision and accuracy with respect to the two others strategies. In general terms the consistency of the three solutions does not surpass the discrepancy of 1 mm in the WRMS indicator, with the exception of MATE station. The discrepancy in this station reaches the maximum level of 6 mm for the loose solution of the regional IGS stabilisation network. In terms of accuracy the NRMS indicator does not differ by more than 10 %.

Coming back to the problems in terms of OTL determination, during the collaboration with the scientific teams mentioned in paragraph § **3.2.1,** I applied the same experimental aforementioned approach on the determination of the position time-series of the Brittany GPS campaign sites. In this case in Vergnolle et al. (2007) we

compared the results of a regional IGS-network with "tight constraints" to the results of a "loose constraints" approach of the same regional IGS-network ("free network" approach). Theoretically the "tight-network" approach might be influenced by the errors in the a-priori positions and velocities of the IGS-stabilisation sites which are errors induced during the implementation of the IGS (aligned to ITRF) reference system itself.

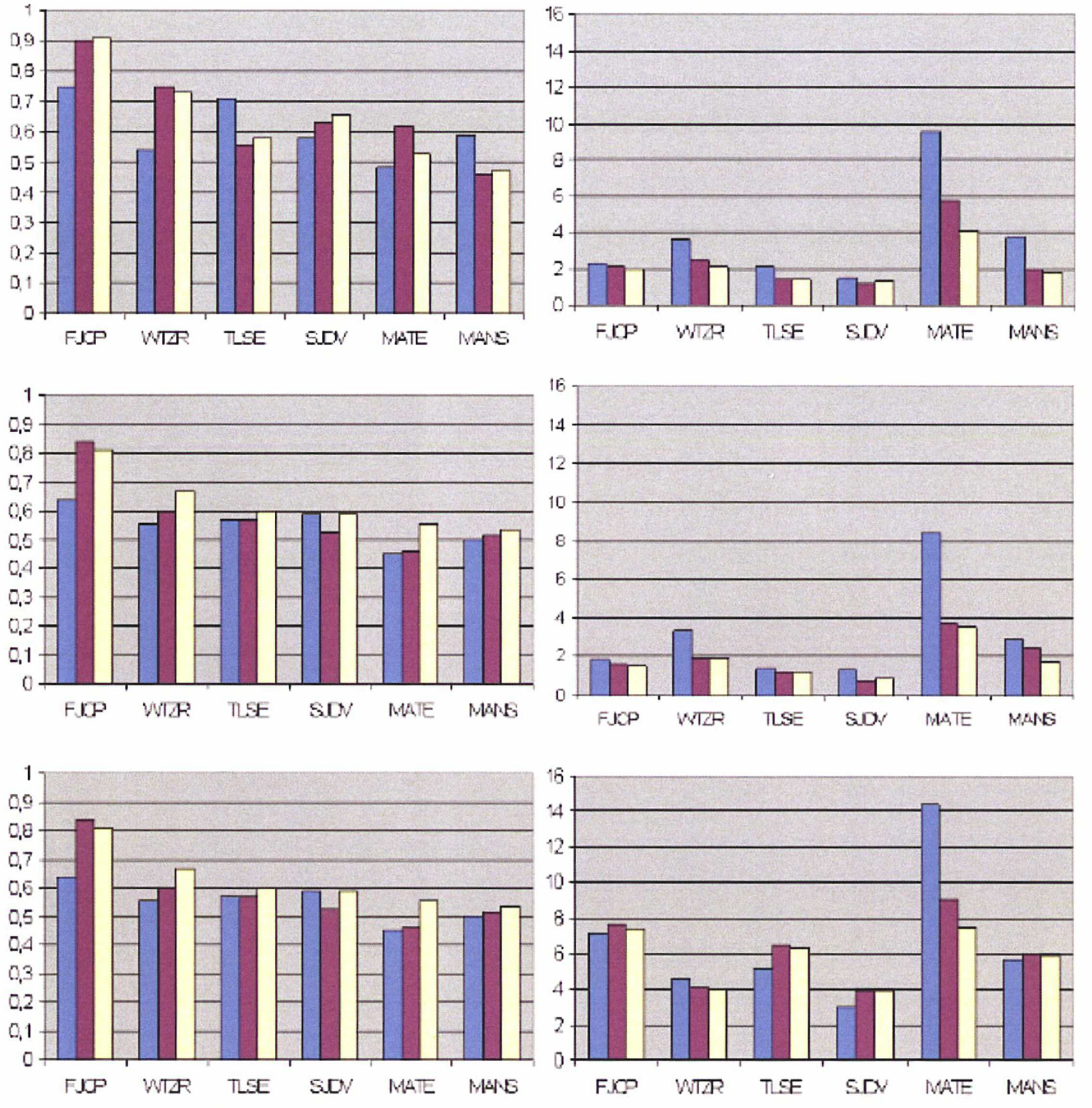

Fig. 4-10 : Left column: Up-to-bottom, **NRMS** of the post-fit residuals in East, North and Vertical respectively; Right column: Up-to-bottom **WRMS** of the post-fit residuals in East, North and Vertical respectively of the position time-series of the 6 selected GPS stations. In blue are the GPS-network solutions with "loose constraints" on a regional IGS-EUREF stabilisation network through a 7-transforamtion parameters datum definiton, in red are the solutions with "tight constraints" on the IGS-EUREF stabilisation network, and in white are the solutions with "loose contraints" on the global IGS stabilisation network and a datum alignement approach through a set of 7-Helmert transformation parameters.

Nevertheless, the drawback of the "loose constraints" approach is that a strong correlation exists between the free network solution and the a-priori positions of the GPS stations. The constraints applied must be loose enough so as not to bias the intermediate network results. Especially the GPS campaign stations can strongly influence the solution due to their erroneous a-priori non-adjusted coordinates. This correlation is observed for every IGS-stabilisation site and increases for the remote sites located at the edge of the network. In this case we applied different sets of a-priori constraints. We observed that in the present case with 5/10 cm constraints on the IGS stations (horizontal and vertical respectively) and 10/20 cm on the campaign stations (horizontal and vertical respectively) and by taking into account different sets of IGS stabilisation sites (remote stations removed) this behaviour was not reproduced anymore. The datum definition was established by the application of a 7-parameter Helmert transformation between the individual coordinates of our network and the global reference frame defined by the IGS stabilisation sites.

The two approaches were evaluated by comparing the resulting WRMS of the differences of the two solutions with respect to the mean standard deviation of the time-series. The WRMS differences were of the order of 3.4 mm, 4.0 mm and 9.4 mm in North, East and Vertical and the mean formal errors for the "tight" and "loose" approach were respectively in North, East and Vertical: 6.1 mm 3.3 mm, 9.7 mm and 3.0 mm, 2.8 mm, 10.4 mm. The overall consistency between the two approaches is at the mm level. Their differences are not significant because they are below the formal errors of the final position estimates.

From the consistent results of the "tight" and "loose" solutions I conclude that for the time-span of the current campaign both approaches give equivalent results in terms of precision and accuracy.

In the current study I applied the "tight" constraints approach on set of selected IGS stabilisation sites.

4.2.5 Influence of vertical displacements on TZD parameters

The high correlation between the troposphere parameters and the vertical site displacements is very well known. Meteorological applications of GPS-derived *Precipitable Water Vapor* (PWV) require that these parameters are estimated with an accuracy of 1 mm or better. An error of 8 mm in the TZD parameters will result in an

error of about 1.2 mm of PWV according to the rule of thumb from Bevis et al. (1992). An un-modelled sub-daily OTL effect may seriously affect the estimated troposphere parameters. Previous studies from Dach and Dietrich (2000), Dragert et al. (2000), Vey et al. (2002) and Urschl et al. (2005) have demonstrated the impact of OTL on the ZTD estimated parameters.

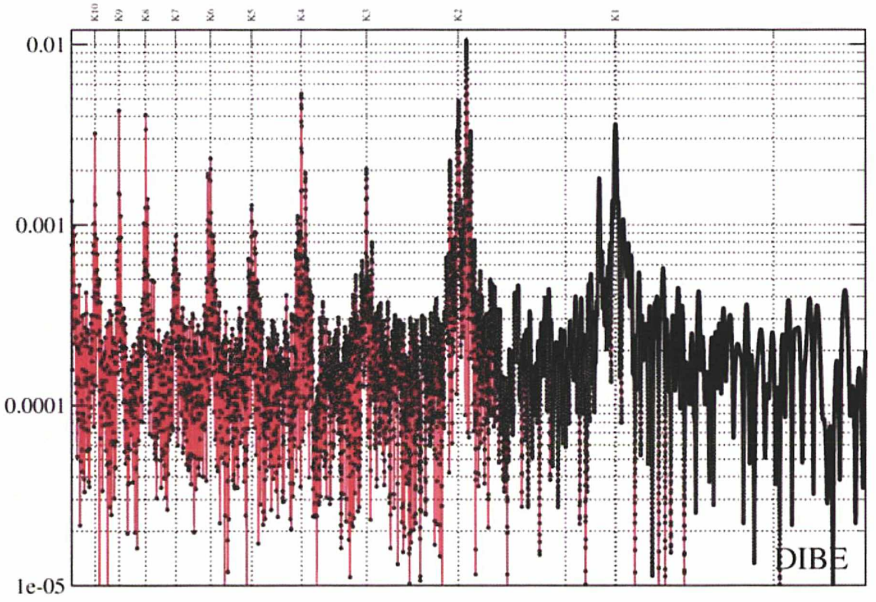

Fig. 4-11 : Power spectra of the TZD time-series from 24-h solutions where OTL is corrected. Units in x-axis are in log (days-of-year) and in y-axis in log (m).

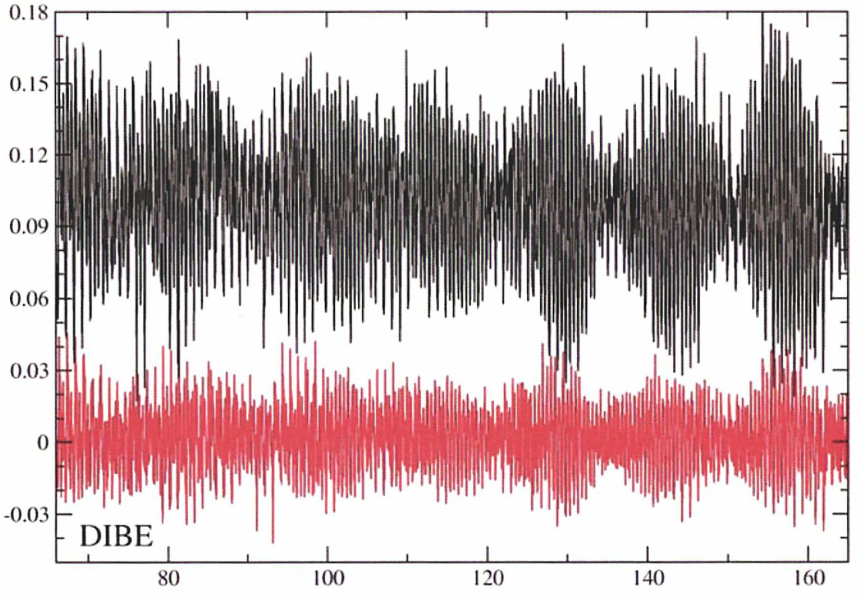

Fig. 4-12 : Vertical GPS time-series (in black) versus the TZD time-series (in red) obtained with ocean loading and without ocean loading corrections. Units are in (m) in y-axis and days-of-year in x-axis.

In order to better investigate the influence of the tidal loading on the zenith path delay parameters I computed the differences of hourly estimated TZD parameters from a solution where OTL predictions were applied to the GPS stations from the FES2004 model and from the ones obtained without OTL corrections. This operation removes everything that is of non-tidal and origin common to the two TZD time-series, such as multipath. The latter propagate into the TZD time-series due to the correlations with the vertical component. In **Fig. 4-11** the TZD time-series in the case were OTL displacements are applied for all tidal waves to all GPS sites, is illustrated. Peaks in the power spectrum of spurious signals are located at multiples of the repeat orbital period of the GPS satellite (K_2, K_3, K_4 etc.). It is obvious that such correlations introduce erroneous estimates in the TZD parameters that can reach several mm as seen in **Fig. 4-11**. The largest of those is 5 mm detected in the K_4 frequency, equivalent, according to the rule of thumb, to 0.8 mm of PWV.

Fig. 4-12 shows the time-series of the TZD differences (OTL corrected – no OTL) (in red) estimated for DIBE and the vertical GPS displacement time-series due to OTL (in black). Both time-series are correlated indicating that an important part of the un-modelled OTL displacement is absorbed by the TZD parameters.

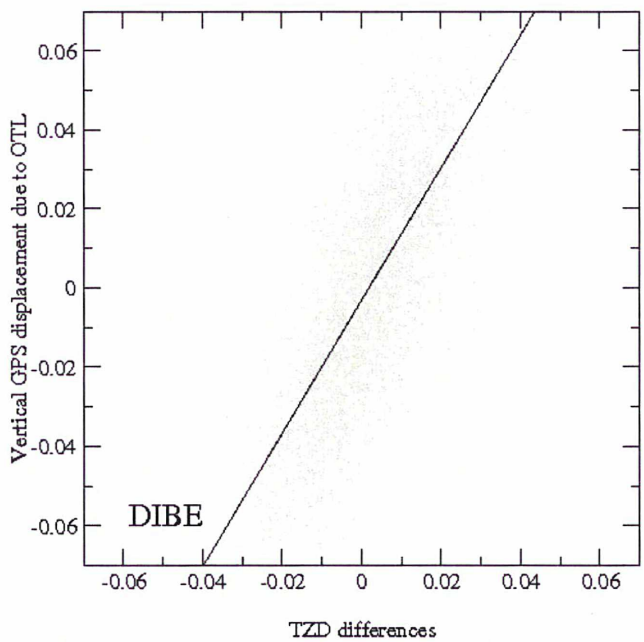

Fig. 4-13 : Correlation diagram of the observed vertical site displacements due to OTL and of the differences of TZD parameters estimated. Units are in (m).

Furthermore, **Fig. 4-13** demonstrates the correlation diagram for DIBE in order to quantify the quasi-linear relation between the differences of the TZD and the vertical site displacements. The correlations for the other sites show the same quasi-linear behaviour. For DIBE a scaling factor (ratio) of the vertical displacements versus TZD of the order of 2.94 ± 0.03 and a correlation of 75.9 % is obtained. At MALO the ratio is 2.70 ± 0.02 and the correlation is 65.2 %.

The results here show that TZD parameter estimates can be significantly biased if ocean loading effects are not accounted for properly. Additionally there is a strong propagation of multipath effects due to the high correlation with the vertical site's coordinates which will bias the final TZD estimates at the order of some mm if we do not consider proper mitigation techniques.

4.2.6 Aliased OTL signatures

GPS satellites have a repeat orbital period almost of one sidereal day, 23.93447192 hours (23 hours 56 min 4.1 s), which is insufficient enough to adequately sample semi-diurnal and diurnal tidal constituents. Penna and Stewart (2003) have shown that aliasing effects of the ocean tides are also present in the GPS data due to un-modelled residual OTL effects. Stewart et al. (2005) demonstrated that the combination of a moving reference point and un-modelled periodic displacements at the unknown point of interest (due to OTL) results in an output coordinate time-series containing long-wavelength periodic terms when zero and first-order Taylor expansion terms are used in the linearization of the functional model.

The aliasing to longer wavelengths will strictly depend on the sampling rate of the discrete output solutions which may beat each other to cause additional spurious effects in the GPS height time-series (Penna et al. 2007).

As such, I repeated the previous experiment of the Brittany OTL campaign by processing 24-hours non-overlapping solutions. To create the mismodeling scenarios, seven GPS height time-series were generated per site, using all available data (**Table 4-2**). The procedure and options are the same as in the 24-hours straightforward solution of described in **§ 4.2.3.1**. First, corrections were applied for all eight principal constituents M_2, S_2, N_2, K_2, K_1, O_1, P_1, and Q_1 as well as for Mf, Mm and Ssa. This

procedure was then repeated except all principal OTL constituents were modelled but M_2 and N_2. The 24-hours solutions in which all eleven principal tidal constituents were modelled to obtain GPS height time-series per site were used in order to check the total remaining long wavelength signal arising from ocean tide model errors. The OTL predictions for each site were effectuated with géochargeV3.0 and FES2004. Next the height time-series resulting from the solution with all predicted OTL displacement constituents but M_2 and N_2 were used in order to evaluate the level of admittances (ratio of amplitude of spurious long-wavelength output signal in the height time-series to amplitude of predicted periodic displacement).

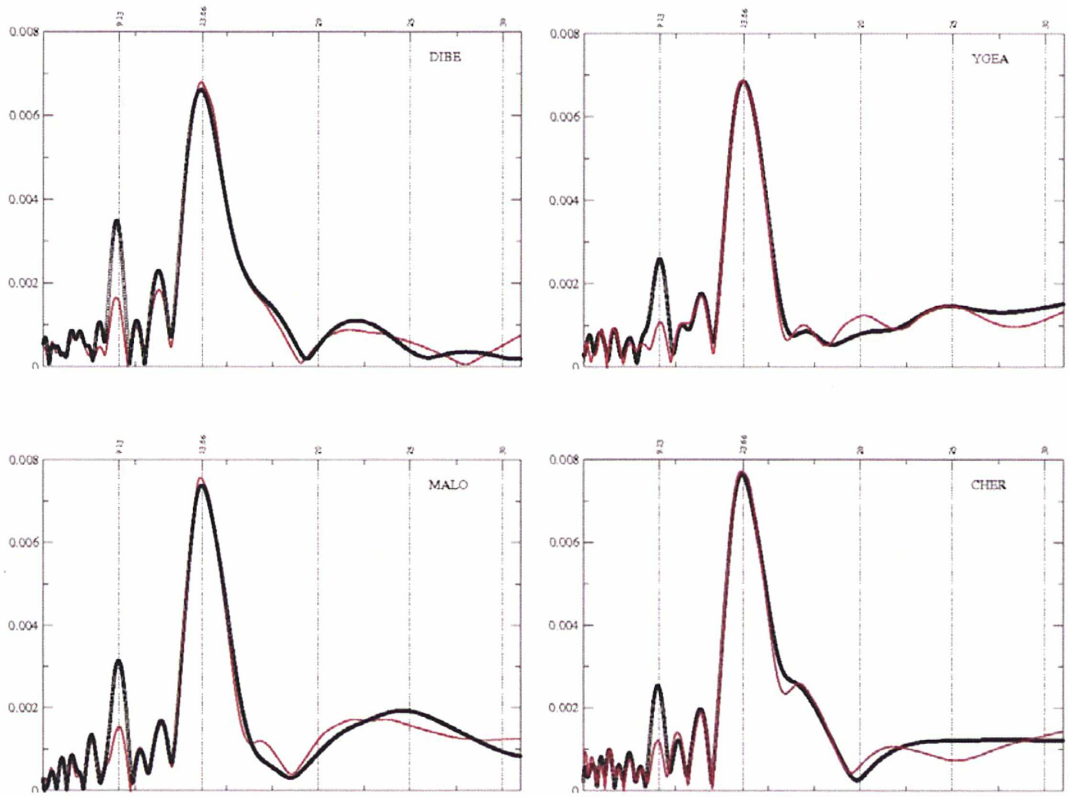

Fig. 4-14 : The least squares spectral lobs of the GPS height time-series for four representative stations. In black are the harmonics from a solution were the M_2 and N_2 predictions were not applied. In red is a solution were all the OTL predictions were applied but M_2. Units are days (x-axis) and metres (y-axis).

In order to extract the propagated long-wavelength amplitudes from the GPS height time-series a least squares spectral analysis was established (G. Balmino personal communication). The aliasing periods used in these scenarios were two: the 13.66 days beat-period for M_2, and the 9.13 days beat-period for N_2. The later were chosen according to the conclusions from Penna and Stewart (2003), Stewart et al. (2005) and

Penna et al. (2007). The time interval covered by the data set did not allow performing the experiment for the second important solar OTL constituent S_2 (second after M_2). The dominant aliasing period for S_2 yields a signal at 182.63 days. Additionally, M_2 should yield a secondary spectral peak at 14.77 days which is the aliasing period obtained from the equation according to Jacobs et al. (1992):

$$f' = abs\left[f - \frac{1}{\Delta}\mathrm{int}\left(f \cdot \Delta + 0.5\right)\right] \qquad \textbf{Eq. 4-12}$$

Where: f' is the aliased frequency; f is the original frequency; Δ is the sampling interval. Again in this case, due to the limited time-span of the data-set this peak will not be easily separated from the dominant 13.66 days signal.

With the present scenario we can also not examine the aliasing signals for the less important diurnal OTL waves of O_1 and K_1 (with period close to the GPS orbital revolution) at 14.19 days and 364.26 days respectively.

Harmonics of the GPS height time-series spectral analysis are presented in **Fig. 4-14** for four representative campaign stations: DIBE, YGEA, MALO and CHER. For all stations the dominant aliasing periods of M_2 and N_2 yield signals with amplitudes of several millimetres. Considering first M_2, the prominent spectral peak at 13.66 days and most probably the one at 14.76 days are detected since the lobs are rather large in that band. Similarly N_2 shows a pronounced spurious signal around 9.13 days period which is detected for all sites.

The above results stress the importance of modelling all periodic systematic errors as accurately as possible.

Site	~13.6 Day Period (M_2)			~9.13 Day Period (N_2)		
	Input Amplitude mm[a]	Output Amplitude and Formal Errors, mm	Admittance %	Input Amplitude mm	Output Amplitude and Formal Errors, mm	Admittance %
DIBE	35.5	6.7 ± 0.4	18.8	7.1	3.3 ± 0.8	46.5
YGEA	27.6	6.8 ± 0.4	24.6	5.5	2.6 ± 0.5	47.3
PAIM	31.6	7.4 ± 0.5	23.4	6.2	3.2 ± 0.9	51.6
LAMB	25.5	7.2 ± 0.4	28.2	5	2.9 ± 0.8	58.0
MALO	26.7	7.5 ± 0.4	28.1	5.1	3.1 ± 0.8	60.8
DUCE	17.9	6.5 ± 0.4	36.3	3.5	2.8 ± 0.8	80.0
CHER	19.6	7.6 ± 0.5	38.8	3.8	3.4 ± 0.6	89.5

[a]Input Amplitudes from FES2004 ocean tide model

Table 4-7 : Periods, Amplitudes and Admittances of the Long Wavelength Signals arising from unmodelled M_2 and N_2 3D OTL

Table 4-7 shows the level of admittances with which the un-modelled M_2 and N_2 displacements propagate into the GPS height time-series. The predicted OTL displacements are not applied to all three directions in order to provide a more realistic assessment of the spurious effects in the real data. It is obvious that the un-modelled periodicities are significant and cannot be ignored. For example in DIBE the input height amplitude for M2 is 35.5 mm and the spurious effect of un-modelled 3D OTL displacements of around 6.7 mm propagates with an admittance of 18.8 %. At CHER, the unmodeled 3D OTL effect propagates at 13.66 days with a 7.6 mm height signal and an admittance of 38.8 %. The N_2 un-modelled 3D effect can be substantial as well. At YGEA the unmodeled amplitudes result in a spurious signal of 2.6 mm in height at ~9.13 days period with an admittance of 47 %. At CHER the spurious signal of unmodeled OTL results in an amplitude of 3.4 mm propagated with an admittance of 89.5 %. It is obvious that the admittance, with which the unmodeled OTL constituents propagate into the GPS height time-series of the campaign sites, grows for stations with smaller input vertical amplitude. This demonstrates that there is a significant propagation of spurious signals also from the horizontal unmodeled OTL constituents which usually have amplitudes considerably less (often by a factor of 3) than the height amplitudes.

While the 13.66 and 9.13 days signatures are apparent for all stations **Table 4-8** demonstrates the effect if FES2004 or TPXO.7.0 (from olfg/olmpp) OTL model predictions are applied.

	~13.6 Day Period (M_2)		**~9.13 Day Period (N_2)**	
Site	**FES2004 (mm)**	**TPXO.7.0 (mm)**	**FES2004 (mm)**	**TPXO.7.0 (mm)**
DIBE	0.5 ± 0.3	4.55 ± 3.0	0.5 ± 0.8	4.2 ± 2.9
YGEA	0.9 ± 0.4	4.2 ± 3.1	0.3 ± 0.8	4.0 ± 3.0
PAIM	0.2 ± 0.4	5.7 ± 3.0	0.6 ± 0.5	4.4 ± 3.0
LAMB	1.4 ± 0.4	3.4 ± 3.1	0.5 ± 0.4	5.5 ± 3.0
MALO	1.3 ± 0.4	1.3 ± 0.4	0.6 ± 0.3	5.8 ± 3.0
DUCE	1.4 ± 0.4	3.6 ± 3.2	0.5 ± 0.4	5.5 ± 3.1
CHER	1.4 ± 0.4	4.4 ± 3.1	0.2 ± 0.4	5.2 ± 3.0

Table 4-8 : Amplitudes of the long-wavelength signals arising from the FES2004 and TPXO.7.0 OTL displacement modelling errors.

The periodicities at which significant peaks are expected for M_2 and N_2 where simultaneously estimated using the GPS height time-series corrected from all eleven OTL constituents. The harmonic analysis estimation was effectuated by least squares. As seen in **Table 4-8** there are significant reductions to the amplitudes and admittances of the 13.66 and 9.13 days spurious signals with respect to **Table 4-7** when the FES2004 model predictions are applied. Looking at **Table 4-8** the remaining spurious amplitudes due to errors in the TPXO.7.0 tide model are much more significant compared to those from FES2004. Moreover the N_2 level of admittances with which these spurious signals propagate, is close to 100 % in some cases, indicating that N_2 OTL effects are not being accurately modelled by the TPXO.7.0 model. This fact indicates that FES2004 is modelling OTL displacements more accurately than TPXO.7.0 which agrees with the previous conclusions from § **4.2.3**.

So by comparing the amplitudes at the predicted periodicities arising when the OTL predictions are applied thus provide an alternative mean to test the validation of ocean tide models. A limitation of this method for testing OTL displacement estimates is that the method cannot discern between M_2 and O_1 model quality if substantial amplitudes are present for O_1 for example. Fortunately this is not the case for this region.

4.3 Summary

The capacity of GPS to determine OTL displacement coefficients in one of the world's coastal areas with the highest and most complex OTL phenomena was demonstrated.

Our strategy of GPS OTL extractions is based on 24-hour period observations for robust ambiguity resolution. An inversion scheme of final normal equations systems based on tight constraints to IGS stations for the datum definition and continuity constraints on hourly coordinates of the GPS stations in a local geodetic system, was implemented. After solving in daily batches, the estimated GPS time-series were processed as independent tide gauge measurements in the harmonic analysis. The amplitudes and Greenwich phase-lags for four of the major OTL displacement coefficients in Brittany and Contentin were estimated. Thus, we have implemented a new GPS processing strategy to calculate OTL constituents.

Limited by the duration of the GPS campaign we were only able to extract GPS OTL coefficients for four of the most energetic tidal constituents, namely M_2, S_2, N_2 and K_1. We have shown that the GPS technique is capable of distinguishing between the modeled OTL displacements at 95 % confidence level in all three directions for all campaign stations.

Nevertheless, in the vertical direction GPS had the weakest performance in distinguishing the OTL displacement constituents of K_1. We believe that this is mostly related to multipath effects (for the waves close to the repeat period of the GPS satellites) and errors in the GPS orbits.

Multipath effects propagated to frequencies equal to the integer multiples of the GPS orbital repeat period were found. Hence "fictitious" signals at these periods can bias GPS tidal loading coefficients of shallow water constituents. This effect shows the drawbacks of the GPS technique in distinguishing OTL displacements of the shallow water interactions (like SK_3 or S_4). Multipath mitigation techniques could be tested in our case. These effects are mainly due to the 2:1 commensurability of the orbital period of the GPS satellites and the sidereal day where the partial tides K_1 and K_2 are highly correlated with the orbital period (Urschl et al. 2005). Therefore this situation could also be improved by using data from GLONASS (repeat period 22.434-h) or the future Galileo (repeat period 28.158-h) and Compass (repeat period 25.682-h) satellites in a

combined GNSS data processing scheme because their revolution period is outside the 2:1 commensurability.

Nevertheless, highly energetic shallow water and non-linear interactions in the semi-diurnal and higher band in the region of St-Malo are assumed to be the reason for significant differences in the Greenwich phase-lag and amplitudes of modeled and predicted OTL constituents. These effects are contained in the M_2 GPS OTL displacement estimates as seen from the phasor-plots of **Figs 4-5 to 4-7**. In the same figures the large discrepancies of M_2 between predicted OTL constituents verify the same assumption. Previous studies refer to the significance of the extremely localized non-linear semidiurnal and higher (such as M_4) interactions in the region (Le Provost and Fornerino 1985). As such, in areas like Mont St-Michel bay, non-linear and shallow water OTL displacement cannot be ignored. A suggestion for the ocean tide modeling solutions would be the assimilation of these kinds of observed OTL constituents into the LSA terms, which could help to constrain the non-linear part of the local loading coefficients in Brittany.

By calculating an RMS misfit and a chi-square statistic of the complex differences, for the four major constituents M_2, S_2, N_2 and K_1 between the OTL displacement estimates from GPS and model grids, we conclude that FES2004 is the most accurate model for the region. Second in accuracy are the NEA2004, GOT00.2 and CSR4.0 models. The NEA2004 grids are in good agreement with the GPS estimates but from the present results they do not seem to offer more information despite the higher resolution of its grid. The TPXO.7.0, TPXO.6.2 and NAO99.b have the poorest performances in terms of agreement with the GPS estimates. Therefore, we recommend to exclude them from further use in the region.

Furthermore, we have evaluated and validated the performance of the updated load89 (Francis and Mazzega 1990) géochargeV3.0 OTL program, by cross-comparing to the OTL estimates of Onsala's web-based olfg/olmpp algorithm with respect to the FES2004 model and to the GPS estimates. All predicted OTL constituents have a good agreement in height with the GPS estimates and sub-mm agreement in the horizontal. Their 3D differences, which are given in **Table 4-6** for FES2004, reach 5.2 %. Possible causes are the interpolation scheme applied and the use of a different set of Green's functions. Onsala's web-based olfg/olmpp algorithm uses the Gutenberg-Bullen Earth model (Farell 1972) while in géochargeV3.0 we used the input set of Pagiatakis (1990)

Green's functions based on the PREM Earth model (Dziewonski and Anderson 1981). The olfg/olmpp refines the tide model in a 3° x 3° box centered on the station. Since in this region the FES2004 model has relatively high resolution grid cells (0.125° x 0.125°), we forced the géochargeV3.0 to use the nearest grid value. The 5.2 % relative difference in the chi-square factor of the GPS/model OTL predictions from the two OTL programs is consistent with the conclusions from Bos and Baker (2005) concerning OTL software discrepancies due to the integrated Green's functions (~0.2 %) and the nearest grid value instead of bilinear interpolation (~7 %).

The impact of the network effect on the final OTL estimates was tested. From the consistent results of the "free network" – "loose constraints" and "tight constraints" experiments I conclude that for the current campaign both approaches give equivalent results in terms of precision and accuracy.

The resulted TZD parameters were found to contain spurious signals due to multipath present at the multiples of the repeat period of the GPS satellites. Furthermore the impact of un-modelled OTL signals on the PWV estimations was quantified.

Spurious signals were found in the long-period time-series of the GPS campaign stations of 24-hours solutions corrected for all OTL waves but M_2 and N_2. The latter were examined using a least squares harmonic spectral analysis. The most predominant periods are those of ~13.66 days and ~9.13 days. These signals propagate in the 24-hours GPS time-series with admittances that vary from 18 % through 39 % for the M_2 ~13.66 day signal and 46 % through 90 % for the N_2 ~9.13 day spurious signal. Then OTL displacement predictions from FES2004 and TPXO.7.0 were accounted for all tidal waves including M_2 and N_2. The comparison of the remaining amplitudes of spurious signals at the same periods demonstrated that a validation method using the 24-hours GPS time-series is possible. Again the most accurate emerging from this comparison is FES2004.

I finally conclude that GPS is capable of measuring OTL displacements with high accuracy and precision in 3D, and it constitutes an accurate and efficient technique for evaluating ocean tide models in complex regions like Brittany.

I own my gratitude to N. Florch and M. Llubes the PIs of the ocean tide loading Brittany campaign performed in 2004, as well as the GDR G2 (Geodesy-Geophysics) that financed the campaign. The valuable contribution from P. Collard, J. Kieffer

(Montpellier University), and J. Cali (ESGT/L2G) for the installation of the GPS sites must be mentioned.

This research project was greatly supported by my PhD fellowship award of the French Minister of Superior Education, and Research (MESR).

5 Kinematic GNSS technique to measure ocean surface dynamic topography, sea-state, and derived parameters.

This part of my Thesis embraces two domains of the Earth Sciences, geodesy and oceanography.

It first involves a complex geodetic GPS technique to provide a precise real-time 3D positioning of a floating tracer (e. g. boat, buoy) with respect to distant fixed reference geodetic points. This technique was used and demonstrated previously but over close distances to fixed reference stations, especially in the altimetric calibration sites of Senetosa in Corsica (Bonnefond et al 2003), Bass Strait, in Australia (Watson et al. 2004), the T/P California off-shore platform in the US (Haines et al. 2003), the most recent one on the Gavdos island of Crete in Greece (Pavlis and Merticas, 2007) and in the mean sea-level studies in the Aegean and Black sea (Müller et al 2006, Tziavos et al. 2004).

In the present case such a technique is extended to a larger area, the Drake Passage. It is used to determine the absolute sea surface *Dynamic Topography* (DT), the

Sea Surface-Height (SSH) and derived geostrophic current and transport in this region which is a key place to observe the strong *Antarctic Circumpolar Current* (ACCt) and its variability. The latter will form the second part of my research project.

For the ACCt observation the required quantity is the absolute DT which is the sea-level relative to the geoid:

$$DT = MDT + SLA \qquad \textbf{Eq. 5-1}$$

Where: MDT is the mean dynamic topography and SLA is the sea-level anomaly which is the residual component of the SSH and the Mean SSH (MSSH).

Precise estimation of the MDT and SSH is needed. A good way to evaluate a high resolution, highly accurate MDT is to estimate the difference between the MSSH (computed from altimetry and kinematic GPS) all along the DRAKE passage and the geoid or the gravity anomalies in the area:

$$DT = MSSH - geoid \qquad \textbf{Eq. 5-2}$$

The latest gravimetric missions such as CHAMP and GRACE have allowed great improvements of our knowledge of the geoid. Nonetheless, the resolution of the latest geoid models like EIGENGL04S (~400 km) not being sufficient enough for our purposes, additional absolute gravimetric observations were effectuated all along the passage.

The three main objectives foreseen for this project are:

- To validate with respect to altimetric data such a kinematic GPS technique for measuring the sea-state and the sea-surface topography over a baseline of few hundreds kilometres in an especially rough area;
- To combine the GPS derived sea-level data with altimetric and gravimetric data to determine in the Drake passage the ACCt geostrophic mean current, its variability and associated absolute transport, and to validate these results with respect to climatology, model outputs and in-situ data when available;
- To give recommendations for improving the demonstrated GPS technique in order to use it more systematically in many other regions during further dedicated or opportunity campaigns.

5.1 Background of the DRAKE GPS campaign

The ACCt is one of the most important current in the world in terms of volume, transport (around 135 Sv $=135 \cdot 10^6 m^3/s$) and extension (up to 3000 km). It is freely moving around the Antarctic continent, conveying heat, salt and particles from one ocean to the other, affected by the ice melting and exchanging a lot of energy with the atmosphere during its circumpolar trip. Thus, its role is essential in the climate system. The Drake Passage is the place where the ACCt becomes the narrowest (around 700 km) making thus its observation and/or monitoring more easy as seen in the black box of **Fig. 5-1**.

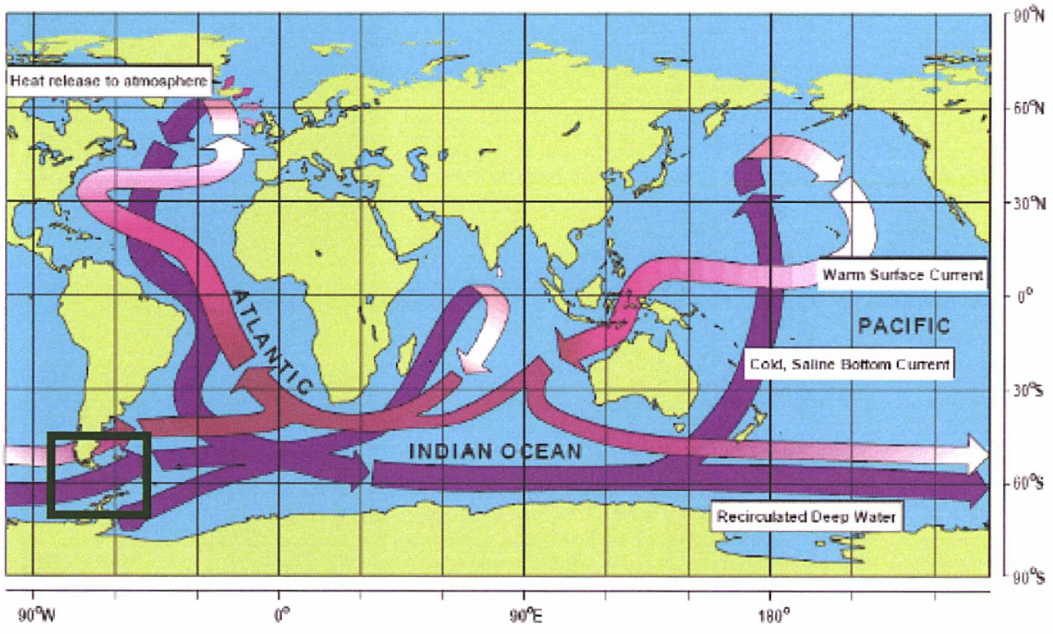

Fig. 5-1 : Schematic representation of the global circulation pathways, the 'conveyer' belt, image courtesy CLIVAR (after W. Broecker, modified by E. Maier-Reimer) available at http://www.windows.ucar.edu/tour/link=/earth/Water/thermohaline_ocean_circulation.html

The first DRAKE campaign (**Fig. 5-2**) from January 14 through February 8, 2006 (C. Provost project manager LOCEAN, http://www.locean-ipsl.upmc.fr), was a unique opportunity to know more about this strong and influent current which is not so well known even if several studies and campaigns have been conducted previously. The objectives of the Drake campaign were essentially to measure through the Drake passage the magnitude and variability, from intra-seasonal to inter-annual, of the ACCt transport, based on two years long moorings, dense hydrographic stations, and

coincident repetitive altimetric sea-level profiles for more than 15 years. To complete this multi- sensors observatory, an additional innovative GPS technique was tentatively proposed to collect sea-level measurements with respect to geodetic reference stations along the southward and northward trajectory of the "Polarstern" vessel (Ménard et al. 2005).

The kinematic GPS survey provided a lot of independent sea level measurements. High frequency (1 s sampling) GPS receivers (Trimble and Ashtech) installed on-board the research vessel "Polarstern" have generated continuous in-situ measurements along the Jason-1 altimeter ground-track 104 followed by the vessel. Additionally, a number of GPS buoys were deployed in the harbour of Puntas Arenas, in Jubany and O'Higgins on the Antarctic Peninsula, and during open-sea sessions to measure the on-board GPS antenna positions with respect to the sea-level, referred as the *Floating Line* (FL) henceforth.

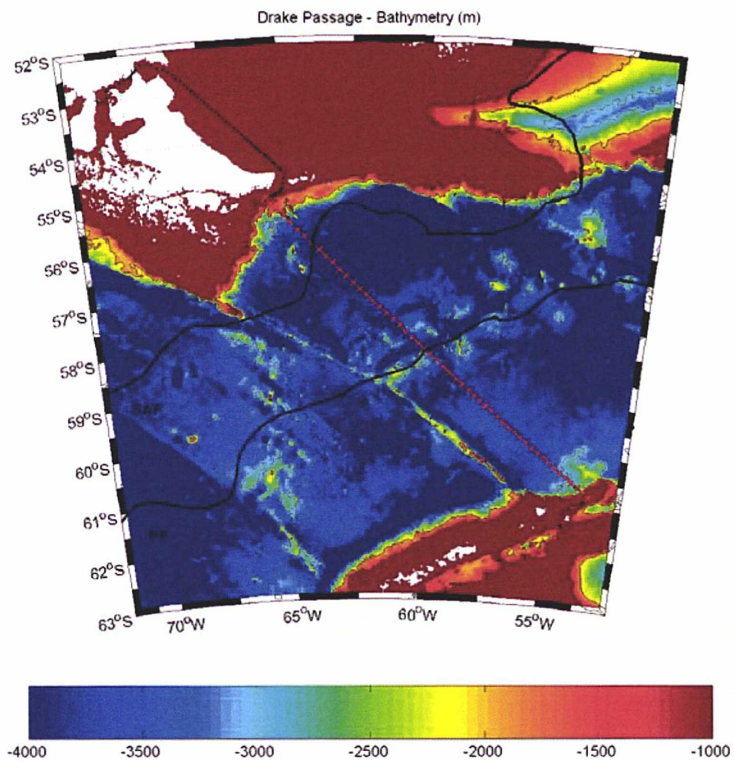

Fig. 5-2 : The "Polarstern's" trajectory on Jason's-1 104 ground path (in red pointed line) and the bathymetry variations along the DRAKE Passage in (m)

5.2 Data collection and editing

The 1 Hz GPS data sets from a total of 50 buoy-ship sessions have a mean duration of 2 hours each. The configuration of each one of them is using one antenna on a GPS wave-rider buoy and three other antennas on the research vessel "Polarstern". The receivers on the vessel were collecting data in a continuous mode all along the passage.

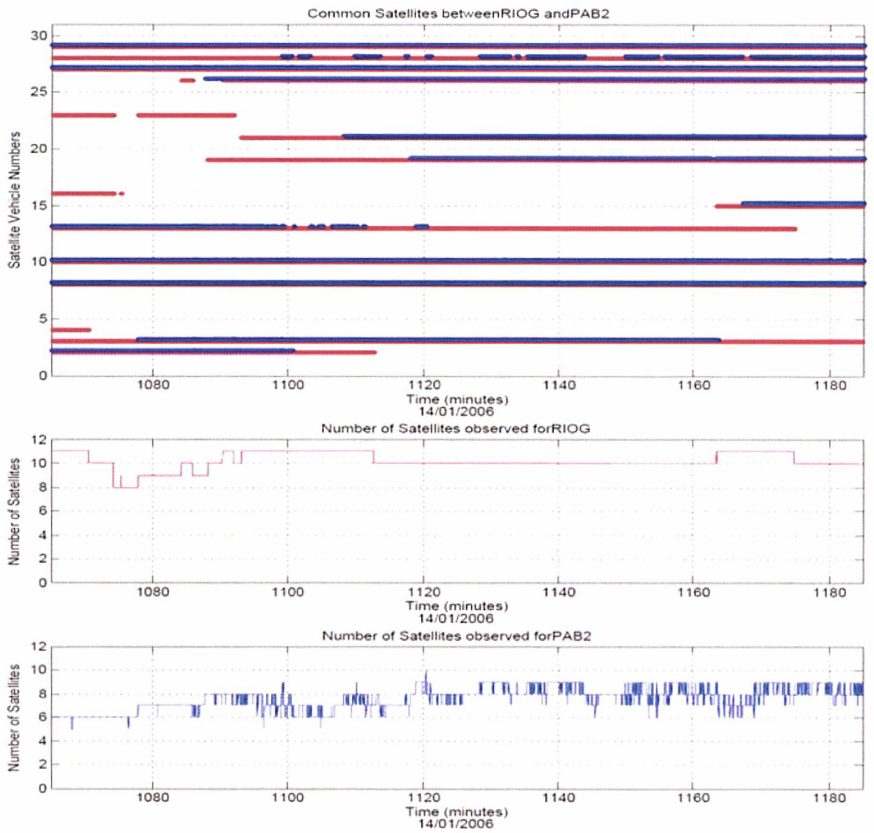

Fig. 5-3 : Satellite visibility for a reference station (in red) and a GPS buoy (in blue) at the bottom and middle panels respectively. The number of common passages of the baseline formed is shown in the upper panel.

Due to high sea-state dynamics for both the ship and the buoy, a checking for data gaps was first performed as well as cycle-slips detection and corrections caused by bad oscillators of clock-jumps. Since DD observations are used, the estimated number of common satellites seen by each pair of stations forming the baselines gives a first indication on the feasibility of a geometrically robust solution. The higher the number of common visible satellites and longer the duration of such simultaneous observations between the two baselines stations, the better the performance of the solution. This kind

of a qualitative analysis was carried out for all the baselines involved when determining a solution. An example of visualisation of the common passes between a GPS reference station and a buoy is given in **Fig. 5-3.**

5.2.1 GINS software adaptation and testing

To compute dynamic solutions for the buoy and the ship receivers, 1 s RINEX observations have been processed with the GINS scientific package. The software has been used to obtain epoch-by-epoch semi-kinematic solutions for sites of the Brittany OTL campaign (see **Chapter 4**). For the DRAKE GPS experiment, GINS has been modified in order to derive solutions at the second level necessary for *Significant Wave Height* (SWH) and SSH estimation.

5.3 Preliminary results - Calibration and validation of the floating line

This part of the project forms the preliminary work which has been conducted to test the GINS adapted software and to calibrate, based on the GINS processing strategy, the exact position of the FL of the antenna-receivers on-board the research vessel above the MSSH.

An accurate calibration of the vessel's FL is first required in order to use the on-board GPS stations for measuring the SSH in a consistent reference frame, ITRF2000 in this case, before cross-comparing these independent GPS sea-level data with the coincident altimeter data along the 104th Jason-1 ground-track. The definition of the FL of the research vessel "Polarstern" is defined through the GPS on-board antenna and the antenna of the wave-rider buoy as below:

$$\mathrm{FL} = h_{se} - h_{be} + b \qquad \textbf{Eq. 5-3}$$

Where: h_{se} is the ellipsoidal height of the Ashtech Receiver antenna on-board "Polarstern"; h_{be} is the ellipsoidal height of the GPS buoy; b is the height of the GPS buoy *Antenna Reference Point* (ARP) with respect to the mean sea surface.

The calibration campaigns were performed at the two terminals (Asmar and Gas terminals) near the Punta Arenas harbour (**Fig. 5-4**). The two places where vessel and co-located GPS-buoy water level measurements have been simultaneously realized are described in **Table 5-1**.

Fig. 5-4 : The Puntas Arenas calibration campaign

These observation periods are henceforth referred to as the 1st and 2nd calibration periods. Independent positions were determined for the buoy and ship receivers during these two calibration periods. These solutions were subsequently used to derive the floating lines.

GPS Station Description	Code Name	Duration	
		From	To
Dock station, Punta Arenas, Asmar Terminal	PAFX	13/01/06 21:08	14/01/06 13:31
Dock station, Punta Arenas, Gas Terminal	PGFX	14/01/06 16:27	14/01/06 21:49
Buoy session, Punta Arenas, Asmar Terminal	PAB1	13/01/06 21:37	14/01/06 13:17
Buoy session, Punta Arenas, Gas Terminal	PAB2	14/01/06 16:41	14/01/06 21:46
Polarstern Ashtech Receiver, Asmar Terminal	POLA	13/01/06 15:23	13/01/06 18:00
Polarstern Ashtech Receiver, Gas Terminal	POLB	13/01/06 23:19	14/01/06 23:26
Polarstern Trimble Receiver, Gas Terminal	POLT	14/01/06 19:40	15/01/06 18:05

Table 5-1 : The GPS stations-buoys and code names used during the 1st and 2nd calibration campaigns.

During the second calibration period I also evaluated the position time-series for 2 antennas on-board the Polarstern in order to analyze the correlation in motion between

them. Attitude variations observed in the ship's positions may generate a significant noise in the final position estimates (see § **5.3.3**).

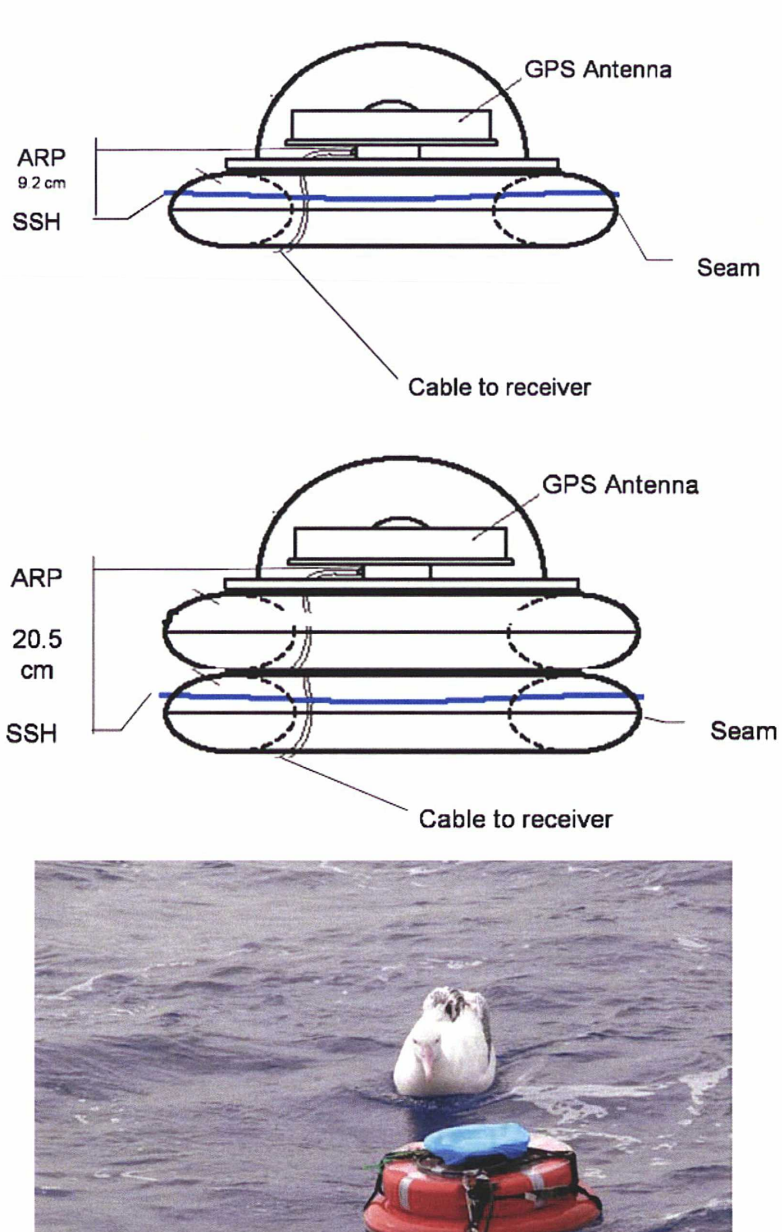

Fig. 5-5 : Schematic view of the two configurations for the wave-rider GPS buoy, with the ARP above the mean SSH. (The graph was modified from the one of Watson 2005. The photograph was taken by Y. Menard)

5.3.1 Antenna Height Determination

The ARP above the mean SSH was calibrated in a basin at the location of the Observatory of Midi-Pyrenees for two configurations of the buoy. Though, as the fresh water of the basin does not have the same density with sea-water (33.2 psu), we accept a mm-level error in the height estimate. For the first configuration we found a position of 9.2 cm above the mean SSH for the case where one life preserver is used. In the open ocean, where two life preservers were used, the position of the ARP above the SSH was 20.5 cm. This simple design of wave-rider buoys is inspired from the altimetry calibration campaigns at the Harvest platform (Key et al. 1998) and at the Corsica site undertaken in 1996/97 (Exertier et al. 1998).

The two geometric representations of the wave-rider GPS boy used during the two calibration periods of the FL inside the port and at the sessions in the open sea are illustrated in **Fig. 5-5**. In the first configuration the GPS antenna platform is placed on a unique life preserver. This configuration was used during the calibration periods in the Port of Puntas Arenas. In the second configuration the antenna platform is placed on a double life preserver used in the open ocean and at the O'Higgins sessions.

5.3.2 Working at the cm-level during the calibration periods

A common strategy is used to estimate the position of a moving target during the calibration periods. Here a moving target refers to either the GPS buoy or the ship's antennas. The key steps of the positioning strategy are listed below:

1. Two stable reference stations are used (RIOG and PARC) to form independent baselines with the moving targets and also in between them. So three baselines are formed to estimate the dynamic position of the moving station as indicated below:
    a. RIOG – moving target (buoy or ship)
    b. PARC – moving target (buoy or ship)
    c. RIOG – PARC (between reference stations)

    The two independent baselines (*a* and *b*) with the moving station provide redundant solutions for the moving target. The third baseline (were ambiguities are fixed) between the two reference stations provides not only redundant, but more accurate

solutions for parameters like TZD. When the individual solutions are cumulated, these more accurate estimations from the baseline between the reference stations positively influence the solutions for the other baselines. This configuration increases the accuracy and robustness of the solution. **Fig. 5-6** gives the conceptual idea of the baselines involved. **Fig. 5-7** shows the map of GPS stations involved during the 1st and 2nd Calibration Periods.

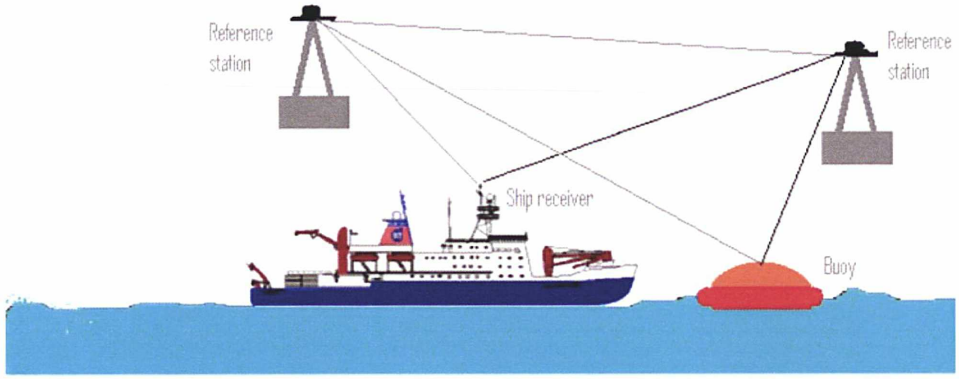

Fig. 5-6 : The basic principle of position determination during the DRAKE campaign

2. Each of the baselines is independently processed in order to form the normal equations (partials of the positions) at a selected time-step of 3 s and define the SWH period. The ambiguities are not fixed for the baselines with the moving targets, while they are fixed for the baseline between the two stable reference stations.

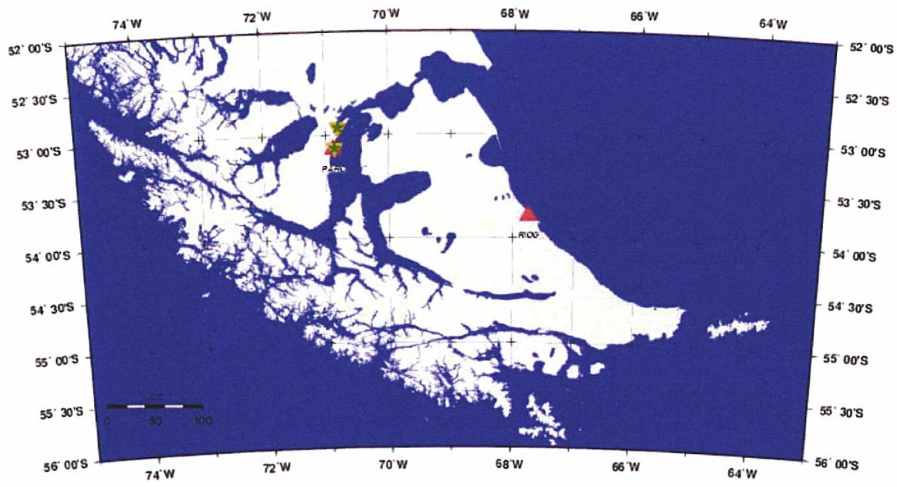

Fig. 5-7 : The GPS network of the 1st and 2nd calibration periods. In red are the two reference stations and in yellow the campaign stations.

3. The three sets of normal equations formed for the three independent baselines are then combined using DYNAMO, to get the stacked normal equations. These normal equations are then simultaneously inverted to get the final position time-series. Tight constraints are applied to the ITRF 2000 coordinates of the IGS stations PARC and RIOG for each independent baseline.

5.3.2.1 Results of the 1st calibration period

The estimated SSH time-series of a total duration of 75 min for the buoy (PAB1) and the "Polarstern" antenna connected to the Ashtech receiver (POLA) are shown in **Fig. 5-8** and **Fig. 5-9** respectively. The mean uncertainties on the positions of the moving targets are illustrated in **Table 5-2**. All time-series are relative to ITRF2000 and expressed in the GRS80 ellipsoid (semi-major axis 6378137 m and inverse flattening of 278.25722210).

RMS error (mm)			
Moving targets	North	East	Up
PAB1	9.4	9.3	10.6
POLA	9.6	7.7	10.1

Table 5-2 : RMS errors for PAB1 and POLA at 3s time-steps

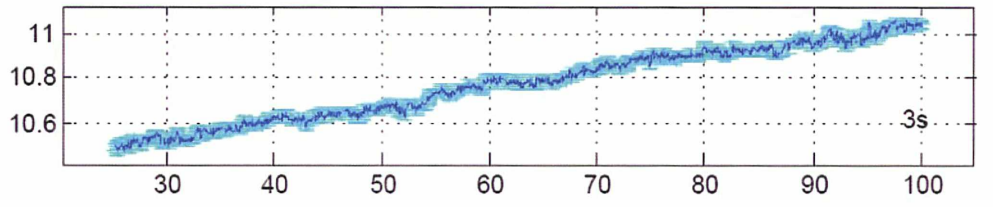

Fig. 5-8 : SSH time-series of the 1st calibration period at 3s time-steps for PAB1. Y-axis units are in meters and x-axis units are in minutes of day

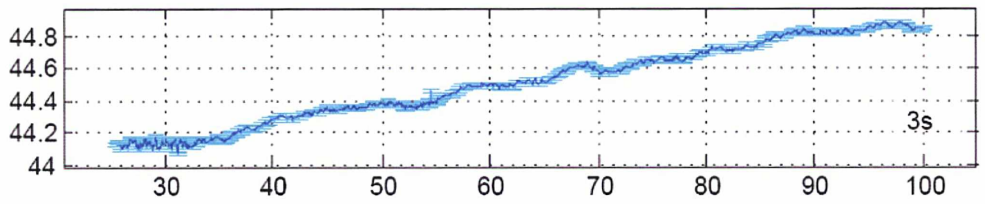

Fig. 5-9 : SSH time-series of the 1st calibration period at 3s time-steps for POLA. Y-axis units are in meters and x-axis units are in minutes of day

From **Fig. 5-8** and **Fig. 5-9** the buoy and the ship's GPS antenna show a similar gradient in the height dimension. I attribute this trend in height due to the local tide movement. It was my intention to validate this interpretation with a local tide model. However at the time of this report, I still do not have accurate information regarding the local tides. Till today there are no tide models publicly available for the Magellan's straits where Puntas Arenas is situated.

By performing the differences of the two SSH time-series the FL of the vessel during the 1st Calibration period is calculated. From **Fig. 5-10** we understand that the ship's mean FL is ~33.8 m ± 14.6 mm below the GPS antenna phase center.

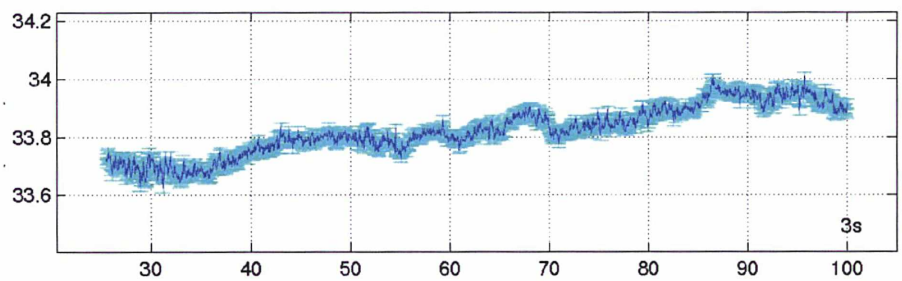

Fig. 5-10 : The FL of the 1st Calibration at Asmar Terminal. The RMS error is 14.6 mm. Y-axis units are in meters and x-axis units are in minutes of day

From the same **Fig. 5-10** we see that the FL is rather constant with the exception of small trends between 20 min after the beginning of the session and 20 min before the end of the session. There is also high-frequency variations coupled with the gradual increase of the FL. This increase in the floating line could be attributed to the offloading of equipment at the Asmar terminal during the 1st Calibration period which suggests a decrease in the weight of the ship. Finally the FL is determined with an RMS error of less than 1.5 cm.

5.3.2.2 Results of the 2nd calibration period

The common duration of the buoy and the ship observations in the second calibration is 30 minutes (**Table 5-1**), which is significantly smaller compared to the first calibration period. The main reason for this is that the GPS buoy during this period suffers from frequent loss-of-lock events, and long durations of adequate satellite visibility were difficult to obtain. Coupled with this, the Ashtech receiver has important data-gaps in the RINEX raw files attributed to the more rough conditions during this period.

RMS error (mm)			
Moving targets	North	East	Up
PAB2	24.0	85.2	41.3
POLB	5.4	11.7	8.5

Table 5-3 : RMS errors for PAB2 and POLB at 3s time-steps

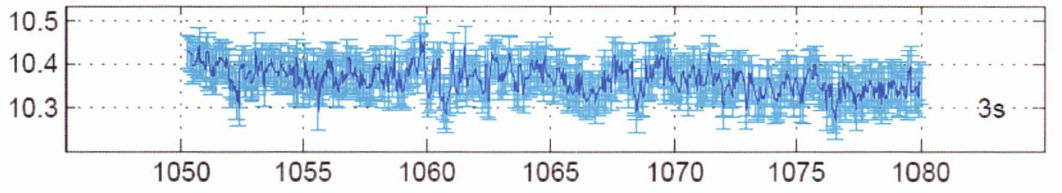

Fig. 5-11 : SSH time-series of the 2nd calibration period at 3s time-steps for PAB2. Y-axis units are in meters and x-axis units are in minutes of day

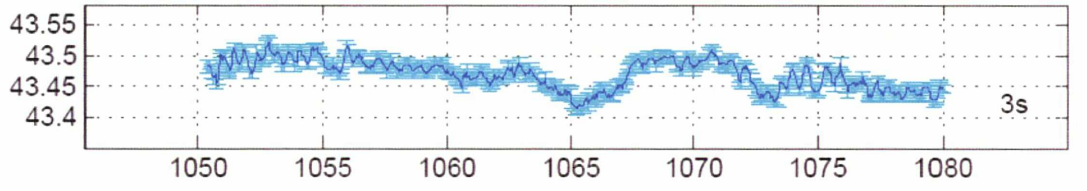

Fig. 5-12 : SSH time-series of the 2nd calibration period at 3s time-steps for POLB. Y-axis units are in meters and x-axis units are in minutes of day

The SSH time-series for the buoy (PAB2) and the on-board antenna connected to the Ashtech receiver (POLB) are shown in **Fig. 5-11** and **Fig. 5-12** respectively. The mean

uncertainties on the positions of the moving targets are illustrated in **Table 5-3.** The 3D-RMS error in the determination of the buoy's position rises to 97 mm, whilst 15 mm for the ship's position.

From **Fig. 5-13** we understand that the movement of the buoy is much more dynamic in the second session than in the first. This is clearly seen by comparing **Table 5-2** with **Table 5-3** were the RMS error is remarkably higher for PAB2.

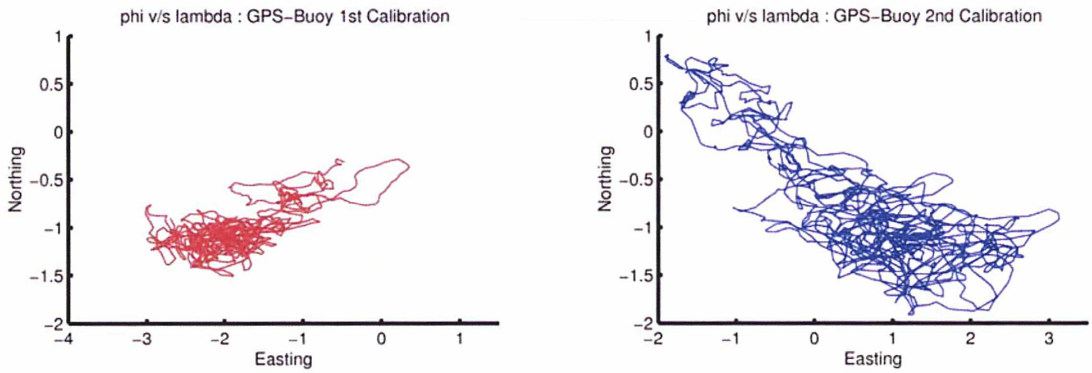

Fig. 5-13 : Horizontal motion of the buoy during the 1st Calibration period (left) versus the 2nd Calibration period (right). Units are in metres

During the first period the buoy moved in an almost E-W direction of 3 m and 1 m in the N-S direction within 75 min. In the second session the buoy moved within a bigger area of 9 m in E-W and 3 m in N-S within 30 min. This is an indication of the fact that PAB1 shows significantly less dynamic movement than PAB2. This could also explain the numerous loss-of-lock events associated with PAB2. As the buoy's dynamic state gets rougher, smaller time steps will produce results with better precision but nonetheless our processing scheme in GINS needs further improvements for the high-state dynamic cases especially in the open ocean.

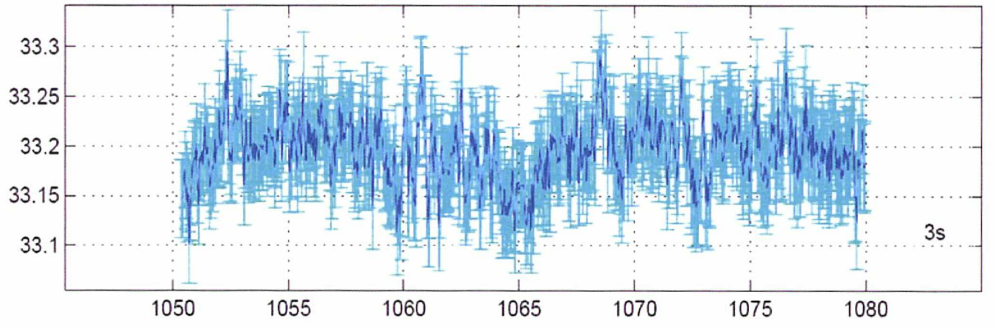

Fig. 5-14 : The FL of the 2nd Calibration period at Gas Terminal. The RMS error is 42.2 mm. Y-axis units are in meters and x-axis units are in minutes of day

The 2nd FL is determined in **Fig. 5-14** by differentiating the two SSH time-series for the buoy and the ship. The FL shows high-frequency variations, but compared to the first calibration does not show a long-term gradual change. We observe that the FL is now at 33.2 m ± 42.2 mm about 60 cm less than the FL of the 1st Calibration period. This implies that the weight of the vessel has increased, which is entirely possible as the ship was fuelled of the Gas terminal at the time of the second session.

5.3.3 The Vessel's attitude determination

The ultimate aim of the GPS positioning is to realize globally referenced coordinates of the vessel's GPS antennas in the ITRF2000. Additionally, the gravimetric observations are a product of accelerations sensed from the accelerometers of a *Strapdown Inertial Measurement Unit* (SIMU) on-board the "Polarstern". The heart of the SIMU is the *Dynamic Reference Unit* (DRU) of the *Marine Inertial Navigation System* (MINS, http://www.l-3klein.com). The *Inertial Sensor Assembly* (ISA) of the DRU is built up of 3 HONEYWELL production-model GG1342 Ring Laser Gyros (RLGs) and 3 Sundstrand QA2000 accelerometers with associated electronics and high voltage power supply.

The GPS antennas will serve as constraints for the determination and re-calibration of the IMU's accelerations all along the Drake Passage. Prior to this installation the offsets (lever-arms) between the IMU and the GPS ARP need to be known with sub-mm precision in order to avoid systematic perturbations of the *Lever-*

Arm Effect (LAE) (Melachroinos 2004). These offsets may have any value from 0 to 150 m. The longer the offset the bigger will be the LAE.

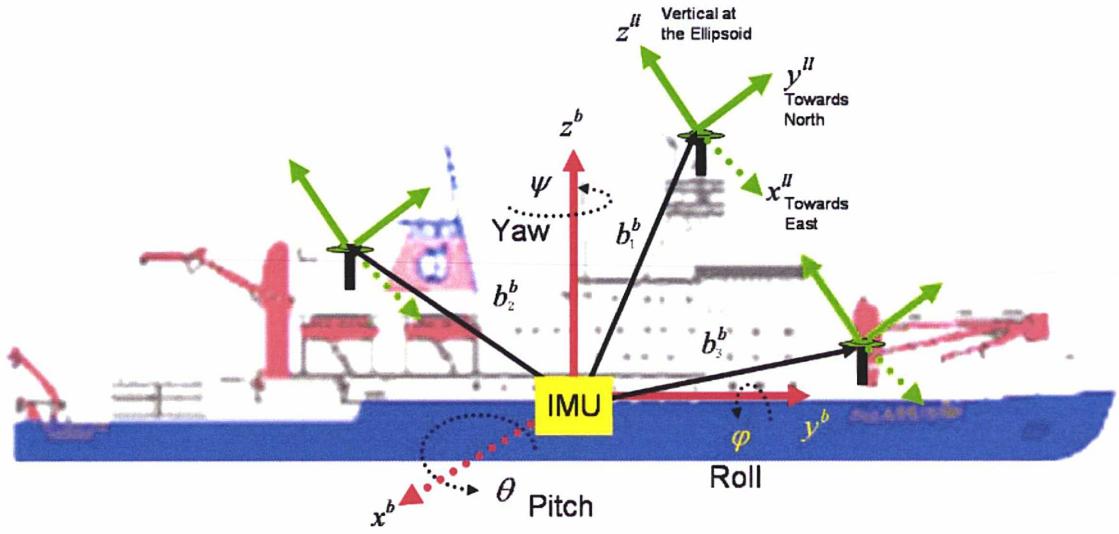

Fig. 5-15 : The Polarstern's GPS and IMU configuration in the b-body and *ll*-navigation frame

In **Fig. 5-15** the different frames are illustrated that participate in the ship's position, velocity and acceleration determination. The *b*-frame represents the body-frame centred either at the strapdown platform of the IMU or at the vessel's zero reference point (sometimes both are the same): y^b is the axis parallel to the keel and positive forward; x^b abeam and positive to port; z^b positive up. The *ll*-frame represents the navigation or local-level geodetic frame which is defined as the tangent local frame to the ellipsoid centred at the strapdown platform of the IMU or at the phase center of one of the GPS antennas: y^{ll} axis is pointing towards the geodetic north; x^{ll} points positive towards the East; z^{ll} is normal to the ellipsoid and positive up.

The navigation frame is the frame in which we will reference the GPS SSH observations. As such, and since the GPS antennas on-board the "Polarstern" participate in the vessel's rough movements in the open ocean, the attitude variations should be propagated according to equation 5-4 (Melachroinos 2004):

$$\mathrm{x}^{ll}_{GPS_{mov}} - \mathbf{C}^{ll}_{b} \cdot \mathrm{b}^{b}_{GPS} = \mathrm{x}^{ll}_{GPS_{cor}} \qquad \textbf{Eq. 5-4}$$

Where: $\mathbf{C}_b^{ll} = \mathbf{R}_3(-\psi)\mathbf{R}_1(-\theta)\mathbf{R}_2(-\varphi)$ is the rotation matrix of the *b*-frame to the *ll*-frame; b_{GPS}^{b} is the lever-arm vector in the *b*-frame centered either at the GPS antenna phase center or at the reference center of the IMU; $x_{GPS_{mov}}^{ll}$ is the 3-D vector of the antenna's position in the *ll*-frame (previously transformed from the Earth fixed *e*-frame) containing the attitude perturbation; $x_{GPS_{cor}}^{ll}$ will be the 3-D vector of the antenna's position in the *ll*-frame.

The attitude variations could be determined by the measured angles of roll-φ, pitch-θ and yaw-ψ of the IMU's RLGs gyroscopes.

As far as it concerns the propagation of the b-frame in the observed accelerations, there are terms that will be measured by the gyros that do not represent true body motion. The tangent *ll*-frame will rotate as the vehicle moves over the elliptical Earth, and although this term is small, it is felt by the gyros. The earth's rotational rate will also be felt by the gyros, and is included in the body frame propagation as well.

The final errors in the GPS SSH time-series can reach 5-15 cm due to the perturbations induced from attitude variations.

A case where the effect of the attitude perturbations on the GPS antenna final coordinates will be amplified due to the LAE is given in **Fig. 5-16**.

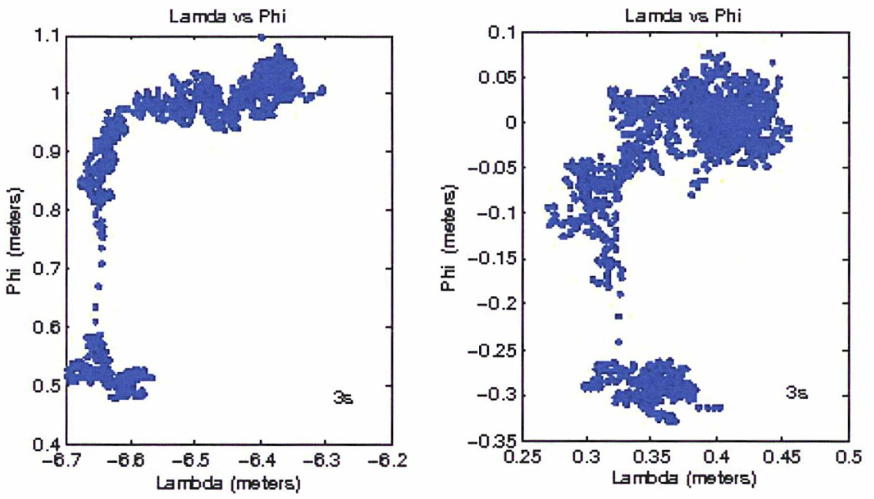

Fig. 5-16 : (Left) The long-lat time-series from POLB (antenna connected to the Ashtech receiver) and (right) the long-lat time-series from the POLT (antenna connected to the Trimble receiver).

In **Fig. 5-16** the long-lat time-series of POLB and POLT antennas on-board the "Polarstern" are illustrated. POLB is 12.65 m higher than POLT. The ship at the moment of this experience is docking at Gas terminal. The variations of POLB's position are within 65 cm in N-S and 40 cm in E-W. The equivalent variations for POLT are 35 cm in N-S and 15 cm in E-W. Despite their correlated motion, the horizontal motions of the two antennas do not cover the same area. Small un-modelled yaw and pitch rotations, during the vessel's docking, is one of the plausible causes. Additionally, since POLB is further from the vessel's centre of equilibrium (considering that this is the centre of the *b*-frame) the length of the lever arm will add an amplified effect on the variations of the coordinates projected on the *ll*-frame, namely the LAE (Melachroinos 2004). In this case the corrections according to **Eq. 5-4** should be applied.

5.4 Validations of the current GPS kinematic method

Part of the validation of the implemented GPS kinematic approach was accomplished externally by the use of an independent data-set, under more or less the same calm environmental conditions, from two GPS-buoy campaigns at Spring Bay in Tasmania (many thanks to C. Watson from the University of Tasmania and to J.-M. Lemoine from the CNES for providing me with the data). During this empirical validation process I compared two GPS-buoys SSH time-series with a collocated Tide Gauge (TG) for about 7 hours. This comparison is illustrated in **Fig. 5-17**. The two GPS SSH time-series (in blue and green) compared to the TG SSH time-series (in red) show a significant correlation. Their maximal and minimal differences are around 70 mm and 20 mm respectively. Consequently, the current GPS kinematic epoch-by-epoch approach reaches the relative accuracy of 20-70 mm compared to the TG SSH time-series. As such the same accuracy applies to the SSH time-series of the two sessions during the calibration of the vessel's FL.

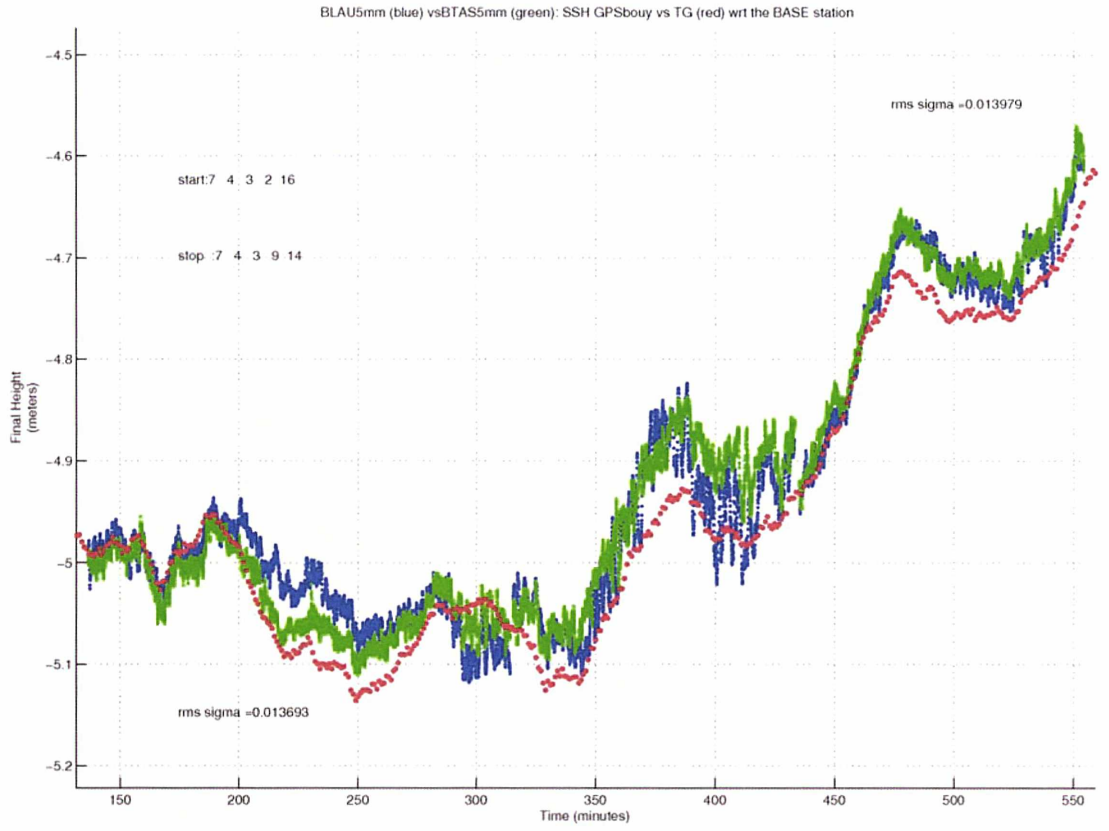

Fig. 5-17 : The two GPS-buoy SSH (3 s) time-series (in blue and in green) against the collocated TG SSH (1 min) time-series (in red) at Spring Bay, Tasmania.

5.5 Summary and perspectives

During this preliminary phase I had the opportunity to develop for the first time in the GINS scientific software package the capacity to process GPS kinematic data. An epoch-by-epoch mode procedure for the calibration of the vessel's FL and the determination of the GPS-buoy MSSH under calm conditions was established with a minimum and maximum precision of 15 mm and 45 mm respectively. The relative accuracy of the current implementation is 20-70 mm compared to an independent TG SSH data set. The 1st and 2nd calibration periods with the current modifications have shown that "reasonable" GPS MSSH can be achieved depending on the dynamic states of the buoy and the ship. Valuable experience was earned since for the first time in GRGS we dealt with this kind of problem.

The next steps in this research project are already planned:

1. The kinematic GPS processing will be extended to the whole DRAKE data set (in the open sea and at the Jubany and O'Higgins Antarctica bases for further validation). This part will be divided into two tasks. The first task will be to upgrade the GINS GNSS software for addressing the ambiguity resolution issue in high dynamics state environments. Then I will define the best strategy for a long-baseline precise estimation of the coordinates of the GPS antennas fixed on the buoy and on the research vessel Polarstern. Tropospheric zenith delay parameters will be constrained through the combinations of independent baselines of permanent IGS stations and the use of ECMWF model. The second task is related to the evaluation of the impact of the ship's attitude variations, mostly in roll, pitch and yaw, through the use of the attitude law given by the inertial measurement unit on-board the ship. Here again necessary software modifications and algorithm developments of the Eq. 5-4 in the observational model will be implemented and validated. The software package TRACK developed at MIT (Herring 2002) will be used to re-process all ship and buoy sessions for the empirical internal validation. TRACK is a kinematic software initially developed by Chen (1998) for the use in airborne laser altimetry.
2. Once all software modifications are implemented and validated I will be ready to proceed with the determination of the ship's position at every second of its southward and northward cruise. Thus, GPS sea-level profiles (SSH) will be determined all along the Polastern's trajectory and the Jason-1 104 ground track. SWH parameters will be extracted.
3. Next, collocated SSH, MSL and SWH altimetric profiles from Jason-1, ENVISAT (and GFO) will be cross-compared with the coincident GPS derived SSH, MSL and SWH profiles and analyzed in order to interpret the differences in terms of errors (as for instance the impact of the sea state bias SSB in the altimetric SSH profiles or in the GPS results). Additional comparisons with in-situ SWH observations during the campaign and with sea-state models will be performed. By these comparisons I will be able to finalize a complete error budget including a study of the impact of a multi-GNSS (GPS+GLONASS+GALILEO) constellation on the kinematic solution. Then recommendations to improve the error budget for further projects (The Drake campaign of 2009) will be given.

   From the current experiences an error budget of the GPS SSH estimations can be formed in **Table 5-4.**

Error Budget component on GPS-buoy SSH	Quantified uncertainty (under calm conditions)	Expected uncertainty
GPS buoy ARP height determination	still to be quantified	< 1 mm accuracy (Watson 2005)
Lever arm effect	~ 100 mm	< 10 mm
Vessel's attitude	still to be quantified	< 10 mm
Ambiguity on long baselines	still to be quantified	< 20 mm
Tethering techniques	-	no significant impact (Watson 2005)
Reference system effect	10 mm	< 5 mm
Geoid error over a 100 m distance ship-buoy	still to be quantified	< 2 mm (Watson 2005)
Kinematic solution	15 – 45 mm up to ~200 km	< 30 mm at baselines up to ~2000 km
Phase center variations due to dome	still to be quantified	< 3 mm
Totality of $\sqrt{\sum_{i=1}^{n}\sigma_i^2}$	~120-150 mm	~50 mm

Table 5-4 : Error budget of the GPS SSH observations in Puntas Arenas. Expected uncertainties are referring to all sessions including the whole cruise in the open ocean and the Antarctic buoy sessions.

4. The estimated geoid profile (or gravity anomaly profile) from GPS MSSH estimates will be cross-compared:
   - with the altimetric and gravimetric measurements collected during the campaign;
   - with the GRACE geoid models EIGEN-GL05S (200 km resolution) and the more refined model EIGEN-GL05C (55km resolution) gravity model (Lemoine et al 2007);
   - if possible, with the first GOCE observations after its launch in spring 2008.
   - Interpretations of the different results will be the desired outcome.

5. The computation of the ACCt's sea-level signature will be the final goal together with derived parameters and their variability based on altimetry, GPS and on the estimated geoid profiles used as references. For validation purposes, additional comparisons with climatology, in-situ known estimates and model outputs (e.g. Mercator) will be realized.

The anticipated results will bring a fully validated GINS version for processing GPS data in a kinematic mode which we intend to promote in the international community for Cal/Val and oceanographic activities.

The knowledge and experience gained will be used for extending this kind of GPS survey to other regions through dedicated campaigns or opportunity campaigns.

Recommendations resulting from the present study will be applied for the next DRAKE campaign scheduled for the beginning of 2009 in order to improve the technique, reduce the error budget and consolidate the 2006 DRAKE scientific results.

Altimetry Cal/Val issues will benefit from our experience in validating altimetry data off-shore and over large distances from the coasts minimizing radiometer errors (absence of large pollution in the altimeter's footprint at ~40km from the coasts).

Problems like ambiguity resolutions and multi-GNSS constellation combinations over long baselines for the determination of high precision coordinates in GPS kinematic mode and at high dynamics state, which remain nowadays a challenging part of geodesy, will be studied.

Finally benefits from our geodetic approach for oceanography in regions like the Drake Passage that are suffering from a lack-of-data and model uncertainties, will be significant.

I would further like to express my gratitude to Dr. Y. Menard and PEng. M. Faillot for giving me this opportunity to work and develop this project into a Post-Doc contract.

6 Conclusions – Perspectives

6.1 Realized work

The work realized during the last three years was coordinated with the efforts of the CNES/GRGS group to improve and to promote the GINS software package in the geodetic community by producing valid scientific results.

Through the guidance and plans of my supervisors these efforts were divided into two main parts: 1) the first part was oriented towards the development and validation of the software; 2) and the second part was aiming at the scientific interpretation of observations from dedicated campaigns of terrestrial and maritime GNSS networks.

6.1.1 Software Development and Validation (Part 1)

More specific in matters of development and improvements of the software's capacities I concentrated in:

- the development of a unified geodetic coordinate system more suitable for geophysical studies to an already implemented geocentric system ;
- the possibility to create time dependent partials of the station's positions for high-frequency positioning ;
- the possibility to process high-frequency GPS kinematic data of 1 Hz ;
- the development of new processing schemes that would allow me to proceed in my geodetic studies;
- the implementation of a new B-W SRP model for the GPS satellites as well as for the GIOVE-A, the first satellite of the Galileo constellation,
- paving the way of integration of the Galileo radio observables in the software.

All modifications were then evaluated against a series of validation tests:

- The comparisons of the estimated GPS stations' high-frequency coordinate time-series with respect to the ones originating from other well-established GNSS software in the geodetic community such as : GAMIT 10.21, GIPSY/OASIS II, Bernese 5.0 ;
- The 3D-RMS misfit overlaps of GINS' POD of the GPS satellites to the precise IGS sp3 orbits ;
- The evaluation of the SLR POD precision of the first Galileo satellite, GIOVE-A;

The GINS' estimated GPS high-frequency position coordinate time-series comparisons were made using the observational set of 9 GPS dedicated campaign stations used in order to study OTL in Brittany. The linear correlations of more than 80 % with respect to the other solutions and the agreement in the periodicities of the high-frequency time-series indicated the high level reliability of GINS' results. During the POD validations more emphasis was put on the newly modified B-W SRP model for the GPS satellites. The GINS' GPS orbit tests were based on internal and external comparisons to the IGS sp3 orbits. The internal 3D-RMS misfits were found to be 5 cm with the inclusion of periodical terms in the solar oriented or orbital plane directions. The external 3D-RMS misfit compared to the IGS orbits varied between 5 cm and 10

cm. Histograms of SLR range residuals and biases were also compared. The SLR observed range for both GPS 35/36 satellites were computed from a series of GINS and IGS GPS 35 and 36 microwave orbits. The respective biases obtained were: -2.9 cm from GINS and -3.7 cm from IGS. The mean SLR station RMS range residuals with respect to the GINS' microwave orbits were found to be about 4 cm. These were less dispersed to those calculated with the IGS orbits of 4.5 cm. Finally the B-W SRP parameterization in a solar-oriented attitude referential was selected as the ideal configuration.

Furthermore, the precision of the SLR-only POD of the GPS 35/36 satellites was found to be 2 cm to 3 cm radially and the SLR network effect affected the orbits' reference frame up to 4 cm – 6cm in the z-shift and 0.1 cm – 1.6 cm in scale, for the two orbits (from June 6 to 16 2006 of the experiment) respectively. The SLR-only POD for GIOVE-A was realized for a period from June 5 through November 25 2006 and the radial precision was evaluated to 5-10 cm.

6.1.2 Geodetic interpretation of observations from dedicated campaigns of terrestrial and maritime GNSS networks (part 2)

For the first time in the GRGS research activities, these types of studies were performed using a modified GINS GNSS software package.

The capacity of GPS to determine OTL displacement coefficients at 95 % confidence level in all three directions and evaluate ocean tide models in one of the world's coastal areas with the highest and most complex OTL phenomena was demonstrated and an original method was implemented. The loading signals for M_2, S_2, N_2 and K_1, were extracted from the GPS observations of a dedicated campaign that took place for about 104 days from March through June 2004. These observed GPS OTL constituents were compared to the predicted OTL estimates from seven ocean tide models TPXO.7.0, TPXO.6.2, GOT00.2, NAO99.b, CSR4.0, FES2004 and the regional NEA2004. Phasor plots of the GPS and predicted M_2 OTL coefficients have demonstrated strong discrepancies in the vertical in the area of St-Malo, around 20° for the phase-lag and ~1.5 cm for the amplitude. These were attributed to strong non-linear

effects of the sub-diurnal band mapped onto the GPS time-series, which according to le Provost and Fornerino (1985) are the highest in the region at this location. As such, it was proposed, that a good way to constrain these non-linear effects in the assimilation of the loading and self attraction terms for the ocean tide models, is to include the GPS observed OTL constituents. Furthermore, the ter-diurnal and higher frequencies of the GPS OTL spectrum, seems to suffer from unmodeled multipath effects that propagate in periods of the integer multiples of the repeat orbital period of the GPS satellites around the K_1 frequency. As such, the order of the multipath effect on the GPS OTL estimates was quantified that maps into these frequencies with amplitudes of ~5 mm and can seriously bias estimated shallow water GPS OTL constituents. In this case multipath mitigation techniques should be tested. In parallel the differences between the predicted FES2004 OTL coefficients from two OTL programs, olfg/olmpp and géochargeV3.0, with respect to the GPS observed OTL constituents were quantified. These differences were found to be of the order of ~5 % and agree with previous studies in discrepancies between OTL software (Bos and Baker 2005). The causes are mostly located in the different set of Green's functions and interpolation scheme used. From the RMS and chi-square statistical indicators it was derived that the most accurate model for the region is the FES2004. From the consistent results of a "free network" – "loose constraints" and "tight constraints" solution the impact of the network effect on the final OTL estimates was tested. It was concluded that for the current campaign both approaches gave equivalent results in terms of precision and accuracy. Furthermore, an estimated set of TZD parameters was found to contain spurious signals of ~9 mm in amplitude at the multiples of the repeat period of the GPS satellites mainly due to multipath effects originating from the correlations with the vertical component of the GPS stations. Furthermore, the impact of un-modelled OTL signals on the PWV estimations was quantified. When accounting for all OTL predictions except for M_2 and N_2 in a set of 24-hour solutions during the whole campaign period, spurious signals were found at fortnight periods in the GPS campaign-stations time-series. The latest were examined using a least squares harmonic spectral analysis. The most predominant periods found are those of ~13.66 days and ~9.13 days which are in agreement to previous studies from Penna and Stewart (2003), Stewart et al. (2005) and Penna et al. (2007) about aliasing effects on 24-hours GPS solutions of un-modelled OTL displacements. These signals propagate in the 24-hours GPS time-series with

admittances that vary from 18 % through 39 % for the M_2, ~13.66 day signal and 46 % through 90 % for the N_2, ~9.13 day spurious signal larger than those found in Penna et al. (2007). When OTL displacement predictions from FES2004 and TPXO.7.0 accounted for all tidal waves including M_2 and N_2, the remaining amplitudes of spurious signals at the same periods verified again that the most accurate model for the region is FES2004.

Finally, a study for the ACCt variability and absolute transport using the GPS – ship – buoy and gravity data set from the 2006 DRAKE campaign was initialised. During this preliminary phase an epoch-by-epoch mode procedure was developed designated to calibrate the vessel's FL and determine the MSSH from a GPS-buoy combination under calm conditions. The minimum and maximum precision reached in the estimation of the FL were 45 mm and 15 mm respectively. The relative accuracy of the current implementation is between 20 mm to 70 mm compared to an independent TG and GPS-buoy collocated SSH data set from Spring Bay in Tasmania. The 1st and 2nd calibration periods with the current modifications have shown that "reasonable" GPS MSSH determination can be achieved depending on the dynamic states of the buoy and the ship.

As a general conclusion, during these 3 years I managed to modify and validate new software designated to be used in studies of local and regional GNSS networks. The scientific objectives concerning the studies of a deformable network due to ocean tide loading have been reached. I proved that GPS can be used as a validation technique for ocean tide models in complex areas like Brittany at the N-W part of France very efficiently and not only. These GPS derived OTL estimates could be used for the further improvement of ocean tide models accuracy in the region. This study enters into the nonlinear, temporal, geophysical and stochastic approaches for the establishment of Global Reference Frames through the direct observation of the displacements which relate the regularized positions of reference points to their instantaneous positions as referred in Chapter four and seven of the IERS 2003 conventions (McCarthy and Petit 2004). Additional software modifications have allowed me to develop for the first time at GRGS, a GPS kinematic processing scheme designated to embrace two domains of the Earth' sciences, geodesy and oceanography. The final objective is the observation of the Antarctic Circumpolar Current through a purely geodetic combination technique of GNSS maritime networks, spatial gravimetry and altimetry.

6.2 Perspectives

My future perspectives in function with the experiences earned during the last three years of my PhD are concentrated around: 1) The further development of the GNSS kinematic technique dedicated to observe the ACCt; 2) Collocated TG networks with GNSS stations for the determination of *Vertical Land Motion Rates* (VLMR) and the calibration of the altimeters' *Global Sea Level Rise* (GSLR).

The first completes what has been initiated in the last chapter of this Thesis. It consists of:

- Extending the kinematic GPS processing to the whole DRAKE data set;
- Updating the GINS Global Navigation Satellite Systems (GNSS) software for addressing the ambiguity resolution issue in high state dynamics environment;
- Determining GPS sea level profiles all along the "Polarstern" trajectory and so along the Jason-1 104 ground track. Parameters, including instantaneous Sea Surface Height (SSH), significant wave height (SWH) and the mean sea level (MSL) will be extracted;
- Comparing collocated SSH, MSL and SWH altimetric profiles from Jason-1, ENVISAT (and GFO) with coincident GPS derived SSH, MSL and SWH profiles and analyzing the differences in terms of errors. Additional comparisons with in-situ SWH observations noted during the campaign and with sea-state models will be performed as well as with the future altimetry mission of Jason-2;
- And finally, estimating the ACCt sea-level signature and derived parameters and their variability based on altimetry, GPS and on the derived geoid profiles from : a) GPS MSL estimates; b) altimetric and gravimetric measurements collected during the campaign; c) from Grace geoid models EIGEN-GL05S (200 km resolution), the more refined model EIGEN-GL05C (55km resolution) gravity model and the future GOCE.

The second project proposes to use a global set of TG collocated with GPS and DORIS techniques in a consistent TRF. The set of TG sites will be carefully chosen. Emphasis

will be given to TG situated in areas with strong geological and geophysical interest such as Polar Regions, Alaska and Greenland.

The TG observations corrected from any vertical motion will be used for the calibration/validation of T/P, Jason-1 and Envisat drifts and GSLR estimations in the next step. The implemented procedure will be applied on Jason-2 which will be launched in 2008. Finally a calibrated and validated value of the GSLR will be the beneficial outcome.

Both projects should hopefully be financed by Post-Doc grants.

Bibliography

Allinson C.R., Clarke P.J., Edwards S.J., King M.A., Baker T.F., Cruddace P.R., 2004, Stability of direct GPS estimates of ocean tide loading, Geophys Res Let, 31, L15603, doi:1029/2004GM020588

Altamimi Z., Collilieux X., Legrand J., Garayt B., Boucher C., 2007, ITRF2005: A new release of the International Terrestrial Reference Frame based on time-series of station positions and Earth Orientation Parameters, J Geophys Res, (in press)

Altamimi Z., Boucher C., Gambis D., 2005, Long-term stability of the terrestrial reference frame, Adv in Space Res, 36 342-349, doi: 10.1016/j.asr.2005.03.068

Altamimi Z., Sillard P., Boucher C., 2002, ITRF2000: A new release of the International Terrestrial Reference Frame for earth science applications, J Geophys Res, vol. 107, no. B10, 2214, doi:10.1029/2001IJB000561

Andersen, O. B., P. L. Woodworth, R. A. Flather, 1995, Intercomparison of recent ocean tide models, J. Geophys. Res., 100(C12), 25,261-25,282

Appleby G., and Otsubo T., 2000, Comparison of SLR measurements and orbits with GLONASS and GPS microwave orbits, in Proceedings of the 12th International Workshop on Laser Ranging Matera Italy, 13-17 November 2000

Baker T. F, Curtis D. J., Dodson A. H., 1995. Ocean tide loading and GPS, GPS world, vol. March, pp. 54-59

Baker, T. F. and M. S. Bos, 2003, Validating Earth and ocean tide models using tidal gravity measurements, Geophys. J. Int., 152, 468-485

Baker, T. F., D. J. Curtis, and A. H. Dodson, 1996, A new test of Earth tide models in central Europe, Geophys. Res. Lett., 23, 3559-3562

Bar-Sever Y. E., 1996, A new model for GPS yaw attitude, J Geod, 70:714-723

Bar-Sever Y. E., Bertiger W. I., Davis E.S., Anselmi J.A., 1996, Fixing the GPS Bad Attitude: Modeling GPS satellite Yaw During Eclipse Seasons, J Instit Nav, vol. 43 (1), Spring 1996, USA

Bar-Sever Y., and Kuang D., 2004, New empirically derived solar radiation pressure model for Global Positioning System Satellites, IPN Progress report 42-159, Nov 15

Bar-Sever Y., Bertiger W., Byun S., Desai S., Haines B., Hajj G., 2005, Calibrating the GPS satellites transmit antenna, Advances in GPS data processing and modelling, 9-10 November, London

Bar-Sever Y.E., Kroge P.M., Borjesson J.A., 1998, Estimating horizontal gradients of tropospheric path delay with single GPS receiver, J Geophys Res, vol. 103(B3), pp. 5019-5035

Bassiri S., and Hajj G.A., 1993, Higher-order ionospheric effects on the global positioning system observables and means of modelling them, Manuscripta Geodaetica, 18:280-289

Bastos L., Landau H., 1988, Fixing cycle slips in dual-frequency kinematic GPS-applications using Kalman filtering, Manuscripta Geodaetica, vol. 13, no. 4, pp. 249-256

Bevis M., Businger S., Herring T. A., Rocken C., Anthes R.A., Ware R.H., 1992, GPS meteorology : remote sensing of the atmospheric water vapor using the global positioning system. J Geophys Res 97 (D14) : 15.787-15.801

Biancale et al. , 2007, Towards a new strategy for mutli-technique combined series of EOP and TRF, American Geoscience Union, Spring meeting, Accapulco, Mexico

Biancale R., 1997, Report on Diademe, CSTG SLR/LLR Sub-Comission meeting, Maratea, June 13

Biancale R., and Bode A., 2002, Mean Annual and Seasonal Atmospheric Tide Models Based on 3-hourly and 6-hourly ECMWF Surface Pressure Data, Scientific Technical Report STR06/01, (ed.) GeoForchungsZentrum, Potsdam, ISSN 1610-0956

Blewitt G., 1989, Carrier Phase Ambiguity Resolution for the Global Positioning System Applied to Geodetic Baselines up to 2000 km, J Geophys Res, vol. 94 (B8), pp. 10.187-10.203

Blewitt G., 1989, Carrier Phase Ambiguity Resolution for the Global Positioning System Applied to Geodetic Baselines up to 2000 km, J. Geophys. Res., 94(B8), 10, 187-10, 203

Blewitt G., 1990, An automatic editing algorithm for GPS data, Geophys Res Lett, vol. 17 (3), pp. 199-202

Blewitt G., Self-consistency in reference frames, geocenter definition, and surface loading of the solid Earth, J Geophy Res, vol. 108 (B2), 2103, doi:10.1029/2002JB002082

Boehm J., Schuh H., 2007, Troposphere gradients from the ECMWF in VLBI analysis, J Geod, 81:403-408, doi:10.1007/s00190-007-0144-2

Boehm J., Niell A., Tregoning P., Schuh H., 2006b, The global mapping function (GMF): a new empirical mapping function based on data from numerical weather model data. Geophys Res Lett 33:L07304, doi:10.129/2005GL025546

Boehm J., Niell A.E., Schuh H., Tesmer V., Tregoning P., Mapping functions for atmospheric delay modelling in GNSS analysis, IGS Workshop 2006, Darmstadt, Germany

Boehm, J., and Schuch H., 2004, Vienna mapping fucntions in VLBI analyses, Geophys Res Lett, 31, L01603, doi:10.1029/2003GL018984

Bonnefond, P., P. Exertier, O. Laurain, Y. Menard, E. Jeansou, A. Orsoni, B.J. Haines, D.G. Kubitschek and G. Born, 2003, Levelling Sea Surface using GPS-Catamaran, Mar. Geod., 26: 319-334

Bos M.S., and Baker T.F., 2005, An estimate of the errors in gravity ocean tide loading computations, J Geod, 79:50-63, doi:10.1007/s00190-005-0442-5

Boucher C., Altamimi Z., 2001, ITRS, PZ-90 and WGS 84: current realizations and the related transformation parameters, J Geod 75: 613 - 619

Boucher C., Altamimi Z., Feissel M., Sillard P., 1996, Results and analysis of the ITRF94, IERS Tech Note 20, Obs de Paris

Boucher C., Altamimi Z., Sillard P., 1998, Results and analysis of ITRF96, IERS Tech Note (24), Obs de Paris

Boucher C., Altamimi Z., Sillard P., 1999, The 1997 International Terrestrial Reference Frame (ITRF97), IERS Tech Note (27), Obs de Paris, Paris

Bouillé F., Cazenave A., Lemoine J.M., Crétaux J.F., Geocentre motion from the DORIS space system and laser data to the Lageos satellites : comparison with surface loading data, Geophys J Int, 143, 71-82

Brockman E., 1997, Combination of Solutions for Geodetic and Geodynamic Applications of the GLobal Positioning System (GPS), vol. 55, Geodätisch-geophysikalische Arbeiten in der Scweiz, Zurich

Carrère L., and Lyard F., 2003, Modelling the barotropic response of the global ocean to atmospheric wind and pressure forcing - comparisons with observations, Geophys Res Lett, vol. 30(6), 1275, doi:10.1029/2002GL016473

Cartwright D. E., Edden A. C., 1973, Corrected Tables of Tidal Harmonics, Geophys. J. Roy. Astr. Soc., 33, pp. 253-264

Cartwright, D. E., Tayler R. J., 1971, New Computations of the Tide-Generating Potential, Geophys. J. Roy. Astr. Soc. 23, pp. 45-74

Chen G., 1998, GPS Kinematic Positioning for the Airborne Laser Altimetry at Long Valley, California, submitted to the Dept. of Earth, Atm. and Planet. Sc. in partial fulfilment of the requirements for the degree of Doctor of Phil. in Geophysics, Massachusetts Institute of Technology, Nov. 1998, US

Choi K., A. Bilich, K. M. Larson, P. Axelrad, 2004, Modified sidereal filtering: Implications for high-rate GPS positioning, Geophys. Res. Let., 31, L22608, doi: 10.1029/2004GL021621

Collin F., and Warnant R., 1995, Application of the wavelet tranform for GPS cycle slip correction and comparison with Kalman filter, Manuscripta Geodaetica, vol. 20, no. 3, pp. 161-172

Comp J. C., Axelrad P., 1998, Adaptive SNR-Based Carrier Phase Mutlipath Mitigation Technique, IEEE Transactions on Aerospace and Electronic Systems vol. 34, No. 145

Coulot D., Berio P., Laurain O., Féraudy D., Exertier P., Lebail K., 2005, Analysis of 12 years (1993-2004) of Satellite Laser Ranging data, European Geoscience Union, Vienna, Austria

Crisci M., Hollreiser M., Falcone M., Spelat M., Giraud J., La Barbera S., 2006, GIOVE Mission Sensor Station receiver performance characterization: preliminary results, Proceedings of the 3rd ESA Workshop on Satellite Navigation User Equipment Technologies NAVITEC '2006, ESTEC, Noordwijk, The Netherlands

Dach R., R. Dietrich, 2000, Influence of the ocean loading effect on GPS derived precipitable water vapor, Geophys. Res. Let., 27(18), 2953-2958

Dach R., Hugentobler U., Fridez P., Meindl M., 2007, Bernese GPS software version 5.0, Astronomical Institute, University of Bern

Dach R., R. Dietrich, 2001, The Ocean loading effect in the GPS Analysis: A case study in the Antarctic Peninsula Region, Marine Geodesy, 24(1), 13-25

Davis J. L., Herring T. A., Shapiro I. I., Rogers E. E., Elgered G., 1985, Geodesy by radio interferometry : Effects of atmospheric modelling errors on estimates of baseline length, Radio Sci., 20(6), 1596-1607

Davis J.L., Elgered G., Niell A.E., Kuehn C.E., 1993, Ground-based measurements of the gradients in the wet radio refractivity of the air, Radio Sci 28(6): 1003-1018

Dermanis A., 1985, Optimisation Problems in Geodetic Network with Signals, 3rd Course of the International School of Advanced Geodesy "Optimization and Design of Geodetic Networks", Ettore Majorana, Centre for Scientific Culture, Erice, Sicily, In Grafarend E. and Sanso F. (eds.): "Optimization and Design of Geodetic Networks", Springer Verlag, pp. 221-256

Dermanis A., 2001a, Global Reference Frames, Connecting Observation to Theory and Geodesy to Geophysics, IAG 2001 Scientific Assembly "Vistas for Geodesy in the New Millenium", 2-8 Sept. Budapest, Hungary

Dermanis A., 2006, The ITRF beyond the linear model choices and challenges, VI Hotine-Marussi Symposium of Theretical and Computational Geodesy : Challenge and Role of Modern Geodesy, May 29 - June 2, Wuhan, China

Dobler D., 2006, Amélioration des modèles de pression de radiation solaire au sein du logiciel GINS de calcul d'orbite pour les satellites des constellations GPS et Galileo, Projet fin d'étude, Ecole Nationale Supérieure d'Ingénieurs en Construction Aéronautiques

Dong D., and Bock Y., 1989, Global Positioning System Network Analysis With Phase Ambiguity Resolution Applied to Crustal Deformation Studies in California, J Geophys Res, vol. 94 (B4), pp. 3949-3966

Dong D., Dickey J.O., Chao Y., Cheng M. K., Geocenter variations caused by atmosphere, ocean and surface ground water, Geophys Res Lett, vol. 24, no. 15, pp. 1867-1870

Dong D., Yunck T., Heflin M., 2003, Origin of the International Terrestrial Reference Frame, J Geophy Res, vol. 108 (B4), 2200, doi:10.1029/2002JB002035

Dow J and Neilan R., Meeting the Challenge : How can the International GNSS Service (IGS) Contribute to the Global Geodetic Observing System (GGOS), 2006, IGS 2006 Workshop, Darmstadt, Germany

Dragert H., T.S. James, A. Lambert, 2000, Ocean loading corrections for continuous GPS: a case study at the Canadian coastal site Holberg, Geophys. Res. Let., 27(14), 2045-2048, doi: 10.1029/2000GL011536

Duha J., Bruno Afonso G., Danilo L., Ferreiraet D., 2006, Thermal re-emission effects on GPS satellites, J Geod, 80:665-674, doi:10.1007/s00190-006-0060-x

Dziewonski A. M., D. L. Anderson, 1981, Preliminary reference Earth model, Physics of the Earth and Planetary Interiors, 25, 297-356

Eanes R. J, 1994, Diurnal and semidiurnal tides from TOPEX/POSEIDON altimetry, Eos Trans., AGU, 75(16), 108

Eanes R. J., S. V. Bettadpur, 1996, The CSR3.0 global ocean tide model: Diurnal and semi-diurnal ocean tides from TOPEX/Poseidon altimetry, Tech. Memo. CSR-TM-96-05, Univ. of Tex. Cent. For Space Res., Austin

Egbert G. D., S. Erofeeva, 2002, Efficient modeling of barotropic ocean tides, J. Atmos. Oceanogr. Technol., 19, 183-204

Estey L. H., and Meertens C. M.,1999, TEQC: The Mutli-Purpose Toolkit for GPS/GLONASS Data, GPS solut, vol. 3(1), pp. 42-49

Exertier P., Bonnefond P., Laurain O., and Barlier F., 1998, Calibration of Radar Altimeters in the Corsica Area: Recent Improvements in View of Jason-1 Mission, in TOPEX/Poseidon Science Working Team (SWT) Meeting, Poster Presentation, October 13-15, Keystone, Colorado, USA

Farell W.E., 1972, Deformation of the Earth by Surface Loads, reviews of Geophys. And Sp. Phys., vol. 10, No. 3, pp. 761-797

Feigl K. L., King R. W., Herring T. A., 1991, A scheme for reducing the effect of selective availability on precise geodetic measurements from the global positioning system, Geophys Res Lett, vol. 18 (7), pp. 1289-1292

Ferland, R., 2003, IGSMail 4748, 4758 and 4666, available at http://igscb.jpl.nasa.gov/mail/igsmail/2003/maillist.html.

Fliegel H.F., Gallini T.E., Swift E.R., 1992, Global Positioning System radiation force model for Geodetic Applications, J Geophys Res, vol. 97(B1), pp. 559-568

Fliegel H.F., and Gallini T.E.,1996, Solar Force Modelling of Block IIR Global Positioning System Satellites, J Spacecr Rock, vol. 33 (6), November-December . 117

Foreman, M. G. G., 1977, Manual for tidal heights analysis and prediction, in Inst. Oc. Sc., Pacific Marine Sc. Rep. 77-10

Francis O., Mazzega P., 1990, Global charts of ocean tide loading effects, Journal of Geophysical Research, 95(C7), 11411-11424

Fritsche M., Dietrich R., Knöfel C., Rülke A., Vey S., Rothacher M., Steinberger P., 2005, Impact of higher-order ionospheric terms on GPS estimates, Geophys Res Lett, vol. 32, L23311, doi:10.1029/2005GL024342

Gambis D., 2004, Monitoring Earth Orientation using space-geodetic techniques : state-of-the-art and prospectives, J Geod, 78:295-303, doi: 10.1007/s00190-004-0394-1. 67

Ge M., Gendt G., Dick G., Zhang F.P., Reigber Ch., 2005, Impact of GPS satellite antenna offsets on scale changes in global network solutions, Geophys Res Lett, 32(6), L06310, doi:10.1029/2004GL022224

Gendt G., 2005, Status of the IGLOS/GLONASS combined products, IGSMAIL-5118, available at http://igscb.jpl.nasa.gov/mail/igsmail/2005/

Gendt G., Fang P., Ferland R., Ray J., Romero I., Steigenberger P., 2007, IGS activities for improving its contribution to ITRF, European Geoscience Union 2007, session G1, Vienna

Gendt G., Söhne W., Rothacher M., and the GGSP Prototype team, 2007, GGSP: Realisation and Maintenance of the Galileo Terrestrial Reference Frame, Proceedings

on the First Colloquim on Scientific and Fundamental Aspects of the Galileo Program, Toulouse, France

Godin G., 1972, The analysis of tides. University of Toronto Press, Toronto

Grafarend E.,and Schaffrin B.,1973, Unbiased free net edjustement, Survey Review 171:200-218

Grelier T., Dantepal J., Delatour A., Ghion A., Ries L., 2007, Initial Observations and Analysis of Compass MEO satellite signals, Inside GNSS, vol. 2 (4), pp. 39-43

Guo J., and Langley R. B., 2003, A new tropospheric propagation delay mapping function for elevation angles to 2°, Institute of Navigation Proceedings in GPS

Haines B., D. Dong, G. Born and S. Gill, 2003, The Harvest experiment: Monitoring Jason-1 and TOPEX/POSEIDON from a California off-shore platform. in Marine Geodesy, vol. 26, no. 3-4, pp. 228-260

Hahn H. J., Powers D. E., 2005, Implementation of the GPS to Galileo Time Offset (GGTO), 0-7803-9052-0/05, IEEE

Han S., 1997, Carrier phase-based long-range GPS kinematic positioning, UNISURV S-49, School of Geomatic Enginnering, The University of New South Wales, pp. 185

Heflin M., Argus D., Jefferson D., Webb F., Zumberge J., 2002, Comparison of a GPS-defined global reference frame with ITRF2000, GPS Solutions, vol. 6, pp. 72-75

Heflin M., Bertiger W., Blewitt G., Freedman A., Hurst K., Lichten S., Lindqwister U., Vigue Y., Webb F., Yunck T., and Zumberge J., 1992, Global Geodesy Using GPS without fiducial sites, Geoph. Res. Let., vol 19, No 2, pp. 131-134

Hein G., 2006, GNSS Interoperability: achieving a Global System of Systems or "Does Everything Has to be the Same?", Inside GNSS, working papers, January-February 2006, vol. 1 (1), pp. 57-60

Hein G., Avila-Rodriguez J.-A., Eisssfeller B., Pany T., Wallner S., Hartl P., 2007, Envisioning a Future GNSS System of Systems, Part 1, Inside GNSS, working paper, vol.2 (1), pp. 58-67

Hernandez, C., Catalan C., Fernandez M. A., Gavin A. J., Srdon E., Martin J. R., 2006, GALILEO Integrity : The Ground Segment Computation Algorithm Perspective, Proceedings of the ION GNSS 19th International Technical Meeting of the Satellite Division, Fort Worth, TX, US

Herring T., 2005, Connections between atmospheric modelling and vertical motions estimation and models, Advances in GPS, COMET, London

Herring T., 2007, Impact of Absolute Phase Center Models on GPS Reference Frames, European Geoscience Union 2007, session G1, Vienna

Herring T.A., 2002, "TRACK GPS Kinematic Positioning Program." Version 1.13, Massachusets Institute of Technology, Cambridge, MA.

Hothem L., 2006, GPS Modernisation Program Current Status and Plans, National Space-Based PNT Coordination Office, IGS Workshop 2006, Darmstadt, Germany

Hugentobler U., Ineichen D., Beutler G., 2003, GPS satellites: Radiation Pressure, Attitude and Resonance, Adv Space Res, vol. 31(8), pp. 1917-1926, doi:10?1026/S0273-1177(03)00174-1

Hugentobler U., Schaer S., Fridez P., Bernese GPS software Version 4.2, Astronomical Institute, University of Berne, Switzerland, Berne, February 2001

Hugentobler U., van des Marel H., Springer T., 2006, Identification and Mitigation of GNSS Errors, IGS workshop, session ERRO, ESA/ESOC Darmstadt, Germany

Hujsak R.S., Gilbreath G.C., 1998, Sequential Orbit Determination for GPS 35 and GPS 36 using SLR data from NRL@SOR, SPIE Proceedings, 3380 (32), April

Jacobs G. A., Born G. H., Parke M. E., Allen P. C., 1992, The global structure of the annual and semiannual sea surface height variability from Geosat altimeter data, J. Geophys Res., 103, 30.231-30.244

Khan S. A., C. C. Tscherning, 2001, Determintation of semi-diurnal ocean tide loading constituents using GPS in Alaska, Geophys. Res. Lett. 28(11), 2249-2252, doi : 10.1029/2000GL011890

Khan S. A., J. L. Hoÿer, 2004, Shallow-water loading tides in Japan from superconducting gravimetry, J. Geod., 78(4-5), doi:10.1007/s00190-003-0391-

Khan S. A., Scherneck H.-G, 2003, The M2 ocean tide loading wave in Alaska: vertical and horizontal displacements, modeled and observed, J. Geod. , 77 (3-4) : 117-127, doi: 10.1007/s00190-003-0312-y

King A. M., L. Padman, 2005, Accuracy assessment of ocean tide models around Antarctica, Geophys. Res. Let., 32, L23608, doi: 10.1029/2005GL023901

King A. M., N. T. Penna, P. J. Clarke, 2005, Validation of ocean tide models around Antarctica using onshore GPS and gravity data, J. Geophys. Res., 110, B08401, doi: 10.1029/2004JB003390

King M., Coleman, R., Nguyen L. N., 2003, Spurious periodic horizontal signals in sub-daily GPS position estimates, J. Geod., 77 (1-2) : 15-21, doi:10.1007/s00190-002-0308-z

King R.W., and Bock Y., 2005, Documentation for GAMIT GPS analysis software, Release 102, Mass Inst of Techol Cambridge, MA 2005

Kleusberg A. Y., Georgiadou F., van de Heuvel, 1993, "GPS data preprocessing with DIPOP 3.0", internal technical memorendum, Departement of Geodesy and Geomatics Engineering), University of New Brunswick, Fredericton, pp. 84

Kogure S., Sawabe M., Kishimoto M., ION GNSS 19th International Technical Meeting of the Satellite Division, 26-29 September, Fort Worth, TX, US

Kouba J. A, 2003, A guide to using international GPS service (IGS) products, International GNSS service, February

Lambert A., S.D. Pagiatakis, A.P. Billyard, H. Dragert, 1998, Improved ocean tide loading corrections for gravity and displacement: Canada and nothern United States, J Geophys Res, 103, B12, 30.231-30.244

Larson K, Bilich A, Axelrad P, 2006, Improving the precision of high-rate GPS, J. Geophys. Res., 112, B05422, doi: 10.1029/2006JB004367

Larson K.M., Agnew D.C., 1991, Application of the Global Positioning System to Crustal Defrormation Measurement 1. Precision and Accuracy, J Geophys Res, vol. 96(B10), pp. 16.547-16.565

Lavallée D., van Dam T., Blewitt G., Clarke J. P., 2006, J Geophys Res, vol. 111 (B05405), doi:10.1029/2005JB003784

Le Provost C., and Fornerino M., 1985, Tidal spectroscopy of the English Channel with a Numerical Model, Journal of Physical Oceanography 15(8) : 1009-1031

Le Provost C., Bennett AF, Cartwright D.E., 1995, Ocean tides for and from TOPEX/POSEIDON. Science, vol. 267, no. 5198, pp. 639-642, doi: 10.1126/science.267.5198.639

Le Provost C., Lyard F., Genco M.L., Rabilloud F., 1998, A hydrodynamic ocean tide model improved by assimilation of a satellite altimeter-derived data set., J. Geophys. Res. 103(C3):5513-5529

Lemoine J.M., Bruisna S., Loyer S., Biancale R., Marty J.-C., Perosanz F., Balmino G., 2007, Temporal gravity field models inferred from GRACE data, J Adv Space Res, doi:10.1016/j.asr.2007.03.062

Letellier T., 2004, Etude des ondes de marée sur les plateaux continentaux, hèse doctorale, Université de Toulouse III, Ecole Doctorale des Sciences de l'Univers, de l'Environnement et de l'Espace, pp. 237

Lichtenegger H., and Hofmann-Wellenhof B., 1990, "GPS-data preprocessing for cycle-slip detection." Global Positioning System: an overview. Y.Bock and N. Leppard (Eds), International Association of Geodesy Symposia 102, Edinburgh, Scotland, 2-8 August, 1989, pp. 57-68

Llubes M., N. Florsch, M. Amalvict, J. Hinderer, M.-F. Lalancette, D. Orseau, B. Simon, 2001, Observation gravimétrique des surcharges océaniques : premières expériences en Bretagne, C. R. Acad. Sci. Paris, Earth and Planetary Sciences, 332, 77-82

Lyard F., F. Lefevre, T. Letellier, O. Francis, 2006, Modelling the global ocean tides: modern insights from FES2004, Ocean Dynamics, 56, 394-415, 2006, doi: 10.1007/s10236-006-0086-x

Lynch D.R., and Gray W.G., 1979, A wave equation model for finite element tidal computations, Computer and fluids, 7, 207-228

Mader G.L., 1999, GPS antenna calibration at the National Geodetic Survey, GPS Solutions, 3(1), 50-58

Marini, J. W., 1972, Correction of satellite tracking data for an arbitrary tropospheric profile, Radio Sci, 7(2), 223-231

Matsumoto, K., T. Takanezawa, M. Oee, 2000, Ocean tide models developed by assimilating TOPEX/Poseidon altimeter data into hydrodynamical model: A global model and a regional model around Japan, J. Oceanogr. 56, 567-581

McCarthy D. D., G.Petit, 2003, IERS Conventions 2003, IERS technical Note No.32

Melbourne, W.G., 1985, The Case For Ranging in GPS Based Geodetic Systems, in Proceedings 1st International Symposium on Precise Positioning with the Global Positioning System, edited by Clyde Goad, pp. 373-386, U.S. Department of Commerce, Rockville, Maryland

Melchior P., 1983, The tides of the Planet Earth, 2nd Ed.,pp. 641, Elsevier, New York

Menard Y., M; Faillot, F. Boldo, Sea level and sea-state measurements by GPS, FS POLARSTERN, expeditions program Nr. 74, October 2005

Menge F., Seeber G., Voelksen C., Wübenna G., Schmitz M., 1998, Results of absolute field calibration of GPS antenna PCV, in Proc. ION GPS-98, Nashville, TN, pp. 31-38

Montenbruck O., Günter C., Graf S., Garcia-Fernandez M., Furthner J., Kuhlen H., 2006, GIOVE-A initial signal analysis, GPS Solut , doi: 10.1007/s10291-006-0027-7

Morel L. and P. Willis, 2005, Terrestrial reference frame effects on the global sea level rise determination from TOPEX/Poseidon altimetric data, Adv Space Res, 36, 358-368

Moore P., Wang J., 2003, Geocentre variation from Laser tracking of LAGEOS1/2 and loading data, Adv Space Res, vol. 31 (8), pp. 1927-1933, doi : 10.1016/S0273-1177(03)00170-4

Moudrak A., Furthner J., Hammesfahr J., Bourga C., 2005, Timing Performance of Galileo Mission Segment (GMS), Proceedings of the ION GNSS 19th International Technical Meeting of the Satellite Division, Fort Worth, TX, US

Munk W.H., MacDonald G. J. F., 1960, The Rotation of the Earth. A Geophysical Discussion, Cambridge University Press

A. Müller, B. Bürki, P. Limpach, H.-G. Kahle, V.N. Grigoriadis, G.S. Vergos and I.N. Tziavos, 2006. Validation of marine geoid models in the North Aegean Sea using satellite altimetry, marine GPS data and astrogeodetic measurements. Proceedings of the 1st International Symposium of the International Gravity Field Service "Gravity Field of the Earth", August 28 – September 1, 2006, Istanbul, pp. 90-95.

Navaro-Reyes D., 2007, Galileo program status and on going experimentation, EGU General Assembly, Vienna

Niell A. , 2005, Interaction of Atmosphere modelling and GPS Analyses Strategy, Advances in GPS, COMET, London

Niell A. E., 1996, Global mapping functions for the atmosphere delay at radio wavelengths, J Geophys Res, vol. 101 (B2), pp. 3227-3246

Niell A. E., 2000, Improved atmopsheric mapping functions for VLBI and GPS, Earth Planets Space, 52, 699-702

Oehler V., Luongo F., Boyero J.-P., Stalford R., Trautenberg H. L., Hahn J., Amarillo F., Crisci M., Schlarmann B., Flamand J. F., 2004, The Galileo Integrity Concept, Proceedings of the ION GNSS 17th International Technical Meeting of the Satellite Division, Long Beach, CA, US

Pagiatakis, S. D., 1990, The response of a realistic earth to ocean tide loading, Geophys. J. Int., 103, 541-560

Paimblanc P., Macabiau C., Lobert B., Van den Bossche M., 2006, Impact of SISMA Computation Algorithm on User Integrity Performance, Proceedings of ION NTM, Monterey, CA, US

Pavlis E.C., 1995, Comparison of GPS S/C orbits dermined from GPS and SLR tracking data, Adv Space Res, vol. 16(12), pp. 1255-1258

Pavlis E. and S. Métricas, 2007, JASON-1 Absolute Calibration Results from the Eastern Mediterranean GAVDOS Project in OSTST meeting, Hobart 12-15 March, Poster CV-16 Cal/Val session

Penna, T. N., M. A. King, and M. P. Stewart, 2007, GPS height time-series: Short-period origins of spurious long-period signals, J. Geophys. Res., 112, B02402, doi:10.1029/2005JB004047

Penna, T. N., M. P. Stewart, 2003, Aliased tidal signatures in continuous GPS height time-series, Geophys. Res. Let., 30(23), 2184, doi:10.1029/2003GL018828

Penna T. N., Baker F. T., 2002, Ocean loading considerations for GPS processing around Australia, Geomatics Res. Aus., 77, pp. 1-26

Piriz R., Fernandez V., Auz A., Tavella P., Sesia I., Cerretto G., Falcone M., Navarro D., Hahn J., Gonzalez F., Tossaint M., Gandara M., 2006, The Galileo System Test Bed V2 for Orbit and Clock Modeling, Proceedings of the ION GNSS 19th International Technical Meeting of the Satellite Division, Fort Worth, TX, US

Ragheb A. E., P. J. Clarke, S. J. Edwards, 2006, GPS sidereal filtering: coordinate-and carrier-phase-level strategies, J. Geodesy, doi:10.1007/s00190-006-0113-1

Ramillien G., Frappart F., Cazenave A., Günter A., 2005, Time variations of land water storage from an inversion of 2 years of GRACE geoids, Earth Plan Sci Lett, 235, 283-301

Ray J., and Senior K., 2005, Geodetic techniques for time and frequency comparisons using GPS phase and code measurements, Metrologia 42, pp. 215-232, doi:10.1088/0026-1394/42/4/005

Ray J., van Dam T., Altamimi Z., Collilieux X., 2006, Anomalous Harmonics in the Spectra of GPS Position Estimates, American Geoscience Union Fall Meeting, Poster G43A-0985, San Francisco

Ray, R. D., 1999, A global ocean tide model from TOPEX/Poseidon altimeter: GOT99.2, NASA Tech. Memo., TM-209478, pp. 58

Reigber Ch., 2000, GLONASS Pilot Project, IGSMAIL-2722, available in http://igscb.jpl.nasa.gov/mail/igsmail/2000/

Rochat, P., Droz F., Waller P., Hahn J., Navarro D., Gonzalez F., 2007, Orbit and Clock Characterisation RAFS Assessment and Lessons Learned, Galileo one year in orbit Workshop, 2 March 2007, ESA/ESTEC

Rothacher M., 1992, Orbits of Satellite Systems in Space Geodesy, vol. 46, Geodätisch-geophysikalische Arbeiten in der Schweiz, Oberwagen

Rothacher M., Schmid R., 2006, ANTEX: The Antenna Exchange Format Version 1.3, available at ftp://igscb.jpl.nasa.gov/pub/station/general/

Rothacher M.,and Mader G., 2003, Receiver and satellite antenna phase center offsets and variations, in Proc. IGS 2002 Network, Data and Analysis Center Workshop, eds. P. Tetreault, R. Neilan, and K. Gowey, pp. 141-152, Ottawa, Canada

Schenewerk, M. S., J. Marshall, and W. Dillinger, 2001, Vertical ocean loading deformations derived from a global GPS network, J. Geod. Soc. Jpn., 47(1), 237-242

Scherneck H.-G., Haas R., Webb F.H., 1999, Ocean loading tides in space techniques and implications for mass center variations, in Jonsson B. (ed.) Proceedings of the 13th General Meeting of the Nordic Geodetic Comission, Gaüle, Sweden, 25-29 May 1998. LMV rapport : 12, National Land Survey of Sweden

Schmid R., and Rothacher M., 2003, Estimation of elevation-dependent satellite antenna phase center variations of GPS satellites, J Geod, 77 (7-8), 440-446

Schmid R., Gendt G., Steigenberger P., Ge M., Rothacher M., Gäde A., 2006, Generation of igs05.atx-status quo, IGS workshop 2006, May 8-11, Darmstadt

Schmid R., Rothacher M., Thaller D., Steingenberger, 2005a, Absolute phase center corrections of satellite and receiver antennas: Impact on global GPS solutions and estimation of azimuthal phase center variations of the satellite antenna, GPS solutions, doi:10.1007/s10291-005-0134-x

Schrama J. O. E., 2005, Three algorithms for the computation of tidal loading and their numerical accuracy, J Geod 78:707-714, doi: 10.1007/s00190-005-0436-3

Schuh H., and Boehm J., 2004, VMF and IMF mapping functions based on data from ECMWF, in Celebrating a Decade of the International GPS service Workshop and Symposium, 1-5 March 2004, Bern, Switzerland, edited by M. Meindel, Astron. Inst., Univ of Bern, Bern, Switzerland

Schwiderski E.W., 1980, Ocean tides, II, a hydrodynamic interpolation model, Mar. Geod. 3(1-4):219-255

Sillard P., Altamimi Z., Boucher C., The ITRF96 realization and its associated Velocity field, Geophys Res Let, vol. 25(17), pp. 3223-3226

Sillard P., Boucher C., 2001, A review of algebraic constraints in terrestrial reference frame datum definition, J Geod 75(2-3): 63-73

Simsky A, 2006, Three's the charm, triple-frequency combinations in future GNSS, Inside GNSS, vol. 1(5), pp. 38-41

Simsky A., Sleewaegen J.-M., De Wilde W., Wilms F., 2005, Galileo Receiver Development at Septentrio, ENC GNSS 2005, Munich, Germany, 19-22 July

Slabinski V. J., 2004, Observed Outgassing Acceleration of GPS Blobk IIR Spacecraft, American Astronom Soc, DDA meeting 38, 14.01, abstract

Slater J, 2003, Timely rapid and final GLONASS orbits available from CODE analysis center, IGSMAIL-4771, available at http://igscb.jpl.nasa.gov/mail/igsmail/2003/

Slater J., 2000, International GLONASS Service Call for Participation, IGSMAIL-2860, available at http://igscb.jpl.nasa.gov/mail/igsmail/2000/

Söhne W., Gendt G., Rothacher M., 2007, GGSP: Realisation of the Galileo Terrestrial Reference Frame, EGU General Assembly, Vienna

Springer T. A., 2000, Modeling and Validating Orbits and Clocks using the Global Positioning System, Vol. 60, Geodätisch-geophysikalische Arbeiten in der Scweiz, Zürich, ISBN 3-908440-02-5

Stewart M. P., N. T. Penna, and D. D. Lichti, 2005, Investigating the propagation mechanism of unmodelled systematic errors on the coordinate time-series estimated using least squares, J Geod 79:479-489, doi: 10.1007/s00190-005-0478-6

Tesmer V., Boehm J., Heinkelmann R., Schuh H., 2007, Effect of different tropospheric mapping functions on the TRF, CRF and position time-series estimated from VLBI, J Geod 81:409-421, doi: 10.1007/s00190-006-0126-9

Thomas D. Ian, Matt A. King, Peter J. Clarke, 2006, A comparison of GPS, VLBI and model estimates of ocean tide loading displacements, J Geod, 81:359-368, doi:10.1007/s00190-006-0118-9

Traveset-Ventura J., Gauthier L., Toran F., de Lesthievent C., Bedu J. Y., 2005, EGNOS Status, performances and Planned Evolutions (2006 - 2010), Proceedings of the European Navigation Conference, Munich

Tregoning P., Boers, R. & O'Brien, D., 1998, Accuracy of absolute precipitable water vapor estimates from GPS observations, J. Geophys. Res., 103, D22, 28,701-28,710

Tregoning, P., T. van Dam, 2005, Effects of atmospheric pressure loading and seven-parameter transformations on estimates of geocenter motion and station heights from space geodetic observations, J. Geophys. Res., 110, B03408, doi: 10.1029/2004JB003334

Tziavos I.N., V. Kotzev, G.S. Vergos and L. Pashova, 2004: Mean sea level and sea surface topography studies in the Black Sea and the Aegean. International Association of Geodesy Symposia, Vol. 129, Jekeli C, Bastos L, Fernandes J (eds.), Gravity Geoid and Space Missions 2004, Springer – Verlag Berlin Heidelberg, pp. 254 - 259.

Urschl C., Beutler G., Gurtner W., Hugentobler U., Ostini L., Ploner M., 2007, Assessing the quality of GNSS orbit models using SLR, European Geoscience Union, G1-session, Vienna

Urschl C., Beutler G., Gurtner W., Hugentobler U., Schaer S., 2006, Validation of GNSS orbits using SLR observations, IGS workshop, ESA-ESOC, Darmstadt, Germany

Urschl C., Dach R., Hugentobler U., Schaer S., Beutler G., 2005, Validating ocean tide loading models using GPS, J Geod, 78: 616-625, doi: 10.1007/s00190-004-0427-9

vanDam T.M., and Herring T.A., 1994, Detection of atmospheric pressure loading using very long baseline interferometry measurements, J Geophys Res, vol. 99(B3), pp. 4505-4517

Vey S., Dietrich R., Fritsche M., Rülke A., 2006, Influence of mapping function parameters on global GPS network analyses: Comparisons between NMF and IMF, Geophys Res Lett, vol. 33, L01814, doi:10.1029/2005GL024361

Vey S., E. Calais, M. Llubes, N. Florsch, G. Woppelmann, J. Hinderer, M. Amalvict, M. F. Lalancette, B. Simon, F. Duquenne, J. S. Haase, 2002, GPS measurements of ocean loading and its impact on zenith tropospheric delay estimates: a case study in Brittany, France, J Geod 76:419-427, doi: 10.1007/s00190-002-0272-7

Watkins M.M.,and Eanes R.J., 1997, Observations of Tidally coherent diurnal and semidiurnal variations in the geocenter, Geophys Res Lett, vol. 24, no. 17, pp. 2231-2234

Watson C. , 2005, Development of GPS buoy technology for satellite atimeter calibration and validation, PhD Thesis for the fulfilment of the requirements for the

Degree of Doctor of Philosophy, Centre for Spatial Information Science, University of Tasmania, March 2005

Watson C., Tregoning P., Coleman R., 2006, Impact of solid Earth tide models on GPS coordinate and tropospheric time-series, Geophys Res Lett, vol. 33, L08306, doi:10.1029/2005GL025538

Watson, N. White, R. Coleman, J. Church, P. Morgan, R. Govind, TOPEX/Poseidon and Jason-1 Satellite Altimeters : Absolute Calibration in Bass Strait, Australia (2004). in Marine Geodesy 27 (1-2).

Willis P., 1998, GLONASS observation campaign (IGEX-98), IGSMAIL-1906, available in http://igscb.jpl.nasa.gov/mail/igsmail/1998

Wu J. T., Wu S.C., Hajj G.A, Bertiger W.I., Lichten S.M., 1993, Effects of antenna orientation on GPS carrier phase, manuscripta geodaetica, 18:91-98

Wübenna G., 2007, New GNSS Signals and Ambiguity Resolution, European Geoscience Union General Assembly, Vienna, Session G6

Wübenna G., Schmitz M., Boettcher G., 2006, Absolute GNSS Antenna Calibration with a Robot : Repeatability of Phase Variations, Calibration of GLONASS and Determination of Carrier-to-Noise Pattern, IGS workshop 2006, May 8-12, Darmstadt

Xu G., 2003, GPS Theory, Algorithms and Applications, Springer-Verlag Berlin Heidelberg Ed., New-York, ISBN 3-540-67812-3

Zhu S.Y., Massmann F.-H., Yu Y., Reigber Ch., 2003, Satellite antenna phase center offsets and scale errors in GPS solutions, J Geod, 76:668-672

Ziebart M., Adhya S., Sibthorpe A., Edwards S., Cross P., 2005, Combined radiation pressure and thermal modelling of complex satellites: Algorithms and on-orbit tests, Adv Space Res, 36, 424-430, doi:10.1016/j.asr.2005.01.014

Zumberge J.F., Heflin M.B., Jefferson D.C., Watkins M.M., Webb F.H., 1997, Precise Point Positioning for the efficient and robust analysis of GPS data from large networks, J Geophys Res, 102(B3), 5005-5017

Glossary

AAC- .....Associate Analysis Centers
ACC- ..... Analysis Center Coordinator
ACCt- ..... Antarctic Circumpolar Current
ACs- ..... Analysis Centers
AHM- .....Active Hydrogen Maser
AIUB- ..... Astronomical Institute, University of Bern
ARGN- .....Australian Regional GPS Network
ARNS- ..... Aeronautical Radio Navigation Service
ARP- ..... Antenna Reference Point
AT- .....Atomic Time
B-W- ..... Box-and-Wing
CASTC- ..... China's Aerospace Science and Technology Corporation
CB- .....Central Bureau
CDMA- .....Code Division Multiple Access
CNES- ..... Centre National des Etudes Spatiales
CODE- .....Center for Orbit Determination in Europe
CORS- .....Continous Operationg Reference Stations
CRC- .....Combination Research Centers
CRS- ..... Celestial Reference System
CS- .....Commercial Service
DD- .....Double Differences
DoF- ..... Departement of Defense
DORIS- .....Doppler Orbitography by Radio positioning Integrated on Satellite
DoS- ..... Department of State
DRU- ..... Dynamic Reference Unit
DSN- ..... Deep Space Network
DT- .....Dynamic Topography
ECMWF- .....European Center for Medium-Range Weather Forecasts
EGNOS- .....European Geostationary Navigation Overlay Service
EGSA- .....European GNSS Supervisory Agency
EOPs- .....Earth Orientation Parameters

EPN- ..... European Permanent Network
ESA- ..... European Space Agency
EUREF- ..... EUropean REference Frame
FA- ..... False Alarm
FDMA- ..... Frequency Division Multiple Access
FL- ..... Floating Line
FM4- ..... Flight Model 4
FM5- ..... Flight Model 5
FOC- ..... Full Operational Capability
GB- ..... Governing Board
GCC- ..... Galileo Control Centers
GDF- ..... GINS' Directory-File
GTER- ..... Galileo TEst Receiver
GFZ- ..... GeoForschungsZentrum
GGSP- ..... Galileo Geodetic Service Provider
GGTO- ..... Galileo-GPS Time Offset
GINS- ..... Géodésie par Integrations Numériques Simultanées
GIOVE-A- ..... Galileo In Orbit Validation Element - A
GJU- ..... Galileo Joint Undertaking
GLF- ..... GINS' Listing-File
GMS- ..... Galileo Mission Segment
GNSS- ..... Global Navigation Satellite Systems
GPS- ..... Global Positioning System
GRGS- ..... Groupe de Recherche de Géodésie Spatiale
GRSP- ..... Galileo Reference Service Provider
GSFC- ..... Godard Space Flight Center
GSLR- ..... Global Sea Level Rise
GSPM.97- ..... GPS Solar Pressure Model 1997
GSS- ..... Galileo Sensor Stations
GST- ..... Galileo System Time
GSTBV-1- ..... Galileo System Test Bed Version 1
GTER- ..... Galileo TEst Receeiver
GTRF- ..... Galileo Terrestrial Reference Frame

GTSP- ..... Galileo Time Service Provide
GUS- ..... Galileo Uplink Stations
IDS- ..... International DORIS Service
IERS- ..... International Earth Rotation Service
IGEX98- ..... International GLONASS Experiment
IGLOS-PP- ..... International GLONASS Service – Pilot Project
IGN- ..... Intitute Geographique National
IGS- ..... International GNSS Service
ILRS- ..... International Laser Ranging Service
INRiM's - ..... stituto Nazionale di Ricerca Metrologica
IOC- ..... Initial Operational Capability
IOV- ..... In Orbit Validation phase
IPF- ..... Integrity Processing Facility
IPGS- ..... Institute de Physique du Globe de Strasbourg
ISA- ..... Inertial Sensor Assembly
ISB- ..... Inter-Station Bias
ITRF- ..... International Terrestrial Reference Frame
IVS- ..... International VLBI Service
JPL ..... Jet Propulsion Laboratory
L2G- ..... Laboratoire de Géodésie
LAE- ..... Lever-Arm Effect
LAREG- ..... LAboratoire de REsearch en Géodésie
LEO ..... Low Earth Orbit
LLR- ..... Lunar Laser Ranging
LRR- ..... Laser Retro Reflector
MCS- ..... Master Control Station
MDT- ..... Mean Dynamic Topography
MEO- ..... Medium Earth Orbit
MINS- ..... Marine Inertial Navigation System
MIT- ..... Massachusetts Institute of Technology
MSSH- ..... Mean Sea Surface Height
NCEP- ..... National Center for Environmental Prediction
NGS- ..... National Gedetic Survey

NOAA- ..... National Oceanic and Atmospheric Administration
NRC- ..... Natural Resources Canada
NRMS- ..... Normalised Root Mean Square
OCS- ..... Operational Control Segment
ODSF- ..... Orbit Determination and Synchronization Facility
ODTS- ..... Orbit Determination & Time Synchronization
OS- ..... Open Service
OTL- ..... Ocean Tide Loading
PCVs- ..... Phase Center Variations
PEng- ..... Professional Engineer
PGR- ..... Post Glacial Rebound
PNT- ..... Positioning, Navigation and Timing policy
POD- ..... Precise Orbit Determination
PPP- ..... Public Private Partnership
PPS- ..... Precise Positioning Service
PRS- ..... Public Regulated Service
PTF- ..... Precision Timing Facility
PWV- ..... Precitable Water Vapor
QIF- ..... Quasi Ionosphere Free
QZSS- ..... Quasi-Zenith Satellite System
RAFS- ..... Rubidium Atomic Frequency Standards
RF- ..... Reference Frequency
RLG- ..... Ring Laser Gyros
RNSS- ..... Radio Navigation Satellite Services
SD- ..... Single Differences
SIMU- ..... Strapdown Inertial Measurement Unit
SINEX- ..... Software INdependent EXchange
SIO- ..... Scrippts Institution of Oceanography
SISE- ..... Signal-in-Space-Error
SIS-ICD- ..... Signal-In-Space Interface Control Document
SISMA- ..... Signal-in-Space-Monitoring-Accuracy,
SLA- ..... Sea Level Anomaly
SoL- ..... Safety-of-Life

SPS- ..... Standard Positioning Service
SRP- ..... Solar Radiation Pressure
SRS- ..... Search and Rescue Support
SSH- ..... Sea Surface Heights
SV- ..... Satellite Vehicle
SWH ..... Significant Wave Height
TCAR- ..... Three Carrier Ambiguity Resolution
TG- ..... Tide Gauge
TEC- ..... Total Electron Content
TOA- ..... Time Of Arrival
TRF- ..... Terrestrial Reference Frame
TRS- ..... Terrestrial Reference System
TSP- ..... Time Service Provider
TZD- ..... Tropospheric Zenith Delay
UCL- ..... University College of London
URE- ..... User Range Error
USNO- ..... US Naval Observatory
UTC- ..... Universal Time Coordinated
VLMR- ..... Vertical Land Motion Rates
WAAS- ..... Wide Area Augmentation System
WRMS- ..... Weighted Root Mean Square
WVR- ..... Water Vapor Radiometers
ZHD- ..... Zenith Hydrostatic Delay
ZPD- ..... Zenith Path Delay
ZTD- ..... Zenith Tropospheric Delay